THE ANALYSIS OF AEROSPACE ADHESIVELY BONDED ALUMINIUM PLATES USING ELECTROMAGNETIC ACOUSTIC TRANSDUCERS (EMATs)

by

Steven Dixon

A thesis submitted for the degree of Doctor of Philosophy

University of Warwick

Department of Physics

September 1994

TABLE OF CONTENTS

	Page no.
List of Illustrations	v
Acknowledgements	xvi
Declaration	xvii
Summary	xviii
Chapter 1 , Introduction	1
1.1 Background	1
1.2 Common techniques used in testing adhesively bonded structures	2
1.3 Defect types	5
1.4 Proceeding chapter outlines	6
Chapter 2 , Basic theory and Review	8
2.0 Introduction	8
2.1 Simple theory of ultrasound	8
2.1.1 Ultrasonic wave propagation	10
2.2 Phase and group velocity calculations	11
2.3 Transmission of ultrasonic waves through layered media	14
2.4 Ultrasonic methods for testing adhesive bonds	16
2.4.1 Wave modes	16
2.4.2 Bulk waves at normal incidence	16
2.4.3 Bulk waves at oblique incidence	17
2.4.4 Guided waves	18
2.5 Ultrasonic transduction	20
2.5.1 Laser generation and detection	20
2.5.2 Electromagnetic acoustic transducers (EMATs)	21
2.6 Summary	22

Page no.

Chapter 3 , Description of the EMAT systems and their characteristics 23

3.0 Introduction 23
3.1 The EMAT system 23
3.1.1 Basic properties of the EMAT 24
3.1.2 Waveforms obtained using EMATs 27
3.1.3 The EMAT as a velocity sensor 28
3.1.3a Generation 28
3.1.3b Detection 31
3.1.4 EMAT-sample stand-off considerations 33
3.1.5 EMAT electrical impedance 34
3.2 Ultrasonic field generated by the radially polarised EMAT 36
3.2.1 Theoretical field and waveforms 38
3.3 Pre-amplifier response - gain and phase relations 39
3.4 Signal modulations of EMAT waveforms 40
3.5 Summary 41

Chapter 4 , EMAT operation on aluminium plates 42

4.0 Introduction 42
4.1 EMAT operation on isotropic and anisotropic polycrystalline metals 43
4.2 Theory of acoustic birefringence of grain aggregates 44
4.3 Modulation of birefringent waveforms 47
4.4 Variation of acoustic birefringence in aluminium plate with applied stress 47
4.5 Comparison of single crystal and textured polycrystalline aluminium 50
4.6 C-scan detection of flat bottomed holes in aluminium plate 51
4.7 Summary 53

Page no.

Chapter 5 , Adhesive bond analysis and experiments 54

5.0 Introduction 54
5.1 Description of adhesive bonds examined 54
5.1.1 Geometry of the bonds 54
5.1.2 Different bond and sample types investigated 55
5.2 Characteristics of isolated bond components 56
5.2.1 Aluminium plates 56
5.2.2 Epoxy adhesive 57
5.3 Experimental procedure 59
5.3.1 Basic setup 59
5.3.2 Ultrasonic signals within adhesive bonds 59
5.3.3 The ultrasonic measurements employed 60
5.4 Through transmission (TT) and send-receive (SR) 62
5.4.1 Detailed explanation and justification of the techniques 62
5.4.2 Analysis employed 63
5.4.3 Results derived from EMAT scans of the adhesive bonds 64
5.4.4 General considerations for results obtained in scanning bonded samples 67
5.5 Some specific sample scan results 69
5.5.1 Voided sample 69
5.5.2 Release film containing sample 70
5.5.3 Silicon grease contaminated adherent sample 70
5.5.4 Defective wedged sample 72
5.6 Summary 74

Chapter 6 , Waveform analysis and simulation 76

6.0 Introduction 76
6.1 Modelling waveforms 76
6.2 Phase and group velocity 82
6.2.1 Phase velocity in aluminium 82
6.2.2 Phase velocity in the epoxy adhesive 84
6.3 Summary 87

Page no.

Chapter 7 , Adhesive curing experiments 88

7.0 Introduction 88
7.1 Justification of the technique 88
7.2 Structural changes within a curing epoxy 89
7.3 Basic experimental setup 90
7.4 Shear wave pulse amplitude measurements 91
7.5 Waveform and Fourier analysis 94
7.6 Shear wave phase velocity changes in the curing adhesive 95
7.7 Theoretical fit to phase velocity data 96
7.8 Shear wave group velocity changes in the curing adhesive 97
7.9 Summary 97

Chapter 8 , Conclusion 98

Appendices

A: Viscoelastic model derivation 103
B: Construction of adhesive bonds 105

Bibliography 107

List of Illustrations

Chapter 1

1.1 Schematic of defect types encountered when adhesively bonding aluminium samples.

Chapter 2

2.1 Calculated phase for a shear wave pulse in various positions within a window prior to the FFT.

2.2 Comparison of magnitude FFTs of EMAT through transmission waveforms on a bonded sample with identical 3mm thick aluminium adherents and on a blank 3mm thick aluminium adherent.

2.3 Schematic of pitch catch ultrasonic technique in adhesive bond analysis.

2.4 Ultrasonic displacement of a radially polarised shear wave.

Chapter 3

3.1 Cross sectional diagram of the radially polarised EMAT

3.2 Through transmission, send-receive and double coil EMAT experimental geometries

3.3 The EMAT current driver circuit.

3.4a The effect on electrical impedance of adding a 1000pF capacitor in parallel with the EMAT coil for operation on mild steel and aluminium.

3.4b Comparison of send-receive waveforms on aluminium with and without the addition of a 2200pF capacitor in parallel with the EMAT coil.

3.5 Electrical impedance and phase shifting characteristics of the radially polarised EMAT used in this project for various EMAT-sample separations.

3.6 Hypothetical annulus of charge motion due to the Lorentz interaction.

3.7 The direction of motion and displacement of the ultrasonic shear wave generated by the radially polarised shear wave EMAT.

3.8 Demonstration of the relationship between ultrasonic displacement and ultrasonic velocity associated with that displacement.

3.9 Variation in the signal amplitude with increased EMAT stand-off from the sample surface.

3.10a &b Predicted variation in signal amplitude with EMAT-sample stand-off and relevant calculated parameters.

3.11 Electrical impedance and phase shifting characteristics of the radially polarised EMAT used in this project operating on aluminium, mild steel and in the absence of any sample.

3.12 Experimental setup of the EMATs used in investigating the ultrasonic field generated by the radially polarised EMATs.

3.13a Arrival time of the shear wave pulse maxima generated by the radially polarised EMAT and observed by a linearly polarised in-plane-motion EMAT.

3.13b&c Waveform demonstrating that the shear wave pulse peak-peak reverberation separation is constant over a long total transit distance in a polycrystalline sample (b) and a single crystal sample (c).

3.14 Calculations of the shear wave amplitude generated by the radially polarised EMAT for various radial positions from the coil axis in a plane 5mm away from the plane of the coil.

3.15 Calculations of the shear wave displacement velocity associated with the shear waves generated by the radially polarised EMAT for various radial positions from the coil axis in a plane 5mm away from the plane of the coil.

3.16 EMAT preamplifier phase and gain response for circuit designs used in send-receive and through transmission.

3.17 Observed and calculated EMAT signals generated and detected in through transmission.

Chapter 4

4.1 Calculated shear pulse minimum-maximum signal amplitude modulation arising due to the birefringent nature of an aluminium sample.

4.2 Amplitude decay of the two horizontally polarised shear wave polarisations observed using the radially polarised EMAT on a birefringent aluminium sample.

4.3 EMAT through transmission waveform obtained on a birefringent aluminium sample.

4.4 Schematic of textured aluminium tensile test samples.

4.5a&b Temporal splitting of the two shear wave polarisations for the 12th shear wave echo within the tensile sample for tensile stress applied along the rolling direction (a) and perpendicular to the rolling direction (b).

4.6a&b Velocity dependance on applied tensile stress in an aluminium sample for the two shear wave polarisations.

4.7 EMAT generated radially polarised shear waveform in two different crystallographic directions in a single crystal of aluminium.

4.8 Topological and cross sectional view of the range of flat bottomed holes milled into a 13mm thick aluminium plate.

4.9 C-scans of flat bottomed holes in a birefringent aluminium plate using an EMAT send-receive system with scanning axes parallel and perpendicular to the rolling direction.

4.10 C-scans of flat bottomed holes with scanning axes parallel and perpendicular to the rolling direction (A) , and at 45^0 to the rolling direction.

4.11 C-sacn of a transversely isotropic aluminium plate (cross sectional cut from an extruded aluminium bar of diameter 150mm) using an EMAT send-receive system. The flat bottomed hole was 20mm in diameter and 3mm in depth into a plate 13.5mm thick.

Chapter 5

5.1 Cross-sectional diagram of adhesively bonded samples investigated in this project.

5.2a Sample construction, defect location and location of strips prepared for tensile testing from the sample.

5.2b Test geometry for destructively testing regions of bonded samples.

5.3 Ultrasonic waveforms obtained using Nd:YAG laser generation / radially polarised EMAT detection, EMAT send-receive and through transmission on a blank 4.8mm aluminium adherent.

5.4 EMAT waveforms obtained on a sample of adherent backed by a layer of cured Redux 312 adhesive with carrier.

5.5 Nd:YAG generation / Michelson interferometer detection of ultrasound in a cured ingot of Redux 312 epoxy.

5.6 Experimental setup of EMATs for scanning adhesive bonds.

5.7 Schematic of adhesive bond scanning system hardware.

5.8 EMAT waveforms from two adhesive bonds, one a plain epoxy adhesive layer , the other bonds' epoxy adhesive layer contained a fabric carrier.

5.9 EMAT send-receive and through transmission waveforms and measurements on adhesively bonded samples.

5.10 EMAT through transmission waveform obtained on adhesively bonded sample with identical adherents.

5.11a EMAT through transmission waveform obtained on adhesively bonded sample with adherents of thickness 3.3mm and 4.8mm.

5.11b Identification of defective (grease contamination) adhesive-adherent interface by a simple pulse amplitude comparison.

5.12 EMAT send-receive waveform obtained on adhesively bonded sample with one adherent-adhesive interface contaminated by a smear of silicon grease.

5.13 Adhesive thickness variation across the wedged adhesive layer samples represented as a temporal measurement.

5.14 Attenuation of shear wave pulse amplitude in the defective wedged adhesive layer sample and the defect free wedged layer sample.

5.15 Schematic of shear wave bond reverberation broadening due to the wedged nature of an adhesive layer.

5.16 EMAT through transmission waveform obtained on two adhesive bonds of identical average adhesive layer thickness over the area of the EMAT face, one a wedged adhesive layer the other nominally parallel faced.

5.17 Comparison of EMAT generated shear wave transit time (or temporal 'thickness') measurement of an adhesive layer and a micrometer thickness measurement of that layer as a function of position.

5.18 Demonstration of shear wave coupling through a totally unbonded adhesive-adherent interface with the application of compressive stress to the interface.

5.19a&b Radially polarised shear wave EMAT through transmission scan of an adhesive bond containing a void , of the shear wave pulse amplitude (a) and temporal adhesive 'thickness' (b).

5.20a&b Radially polarised shear wave EMAT send-receive scan of an adhesive bond containing a void, of the back reflected pulse amplitude from the 4.8mm adherent side (a) and the 3.3mm (b) adherent side.

5.21a,b&c Radially polarised shear wave EMAT send-receive scan of an adhesive bond containing release film on the 3.3mm adherent-adhesive interface of the amplitude of the first principal pulse (a) , the bond layer echo pulse amplitude (b) and the temporal 'thickness' of the adhesive layer.

5.22a&b Radially polarised shear wave EMAT through transmission scan of an adhesive bond containing release film on the 3.3mm adherent-adhesive interface, of the shear wave pulse amplitude (a) and temporal adhesive 'thickness' (b).

5.23a&b Radially polarised shear wave EMAT through transmission scan of an adhesive bond containing a silicon grease smear on the 3.3mm adherent-adhesive interface, of the shear wave pulse amplitude (a) and temporal adhesive 'thickness' (b).

5.24a,b,c&d Radially polarised shear wave EMAT send-receive scan of an adhesive bond containing a silicon grease smear on the 3.3mm adherent-adhesive interface, of the back reflected principal pulse amplitude from the 3.3mm adherent side (a), the back reflected principal pulse amplitude from the 4.8mm adherent side (b), the back reflected adhesive layer echo pulse amplitude from the 4.8mm adherent side (c), and the temporal adhesive 'thickness' (d).

5.25 Cross sectional representations of the silicon grease contaminated adhesively bonded sample.

5.26a&b Radially polarised shear wave EMAT through transmission scan of an adhesive bond with a defect free wedged adhesive layer , of the shear wave pulse amplitude (a) and temporal adhesive 'thickness' (b).

5.27a&b Radially polarised shear wave EMAT through transmission scan of an adhesive bond with a defective wedged adhesive layer , of the shear wave pulse amplitude (a) and temporal adhesive 'thickness' (b).

5.28 Radially polarised shear wave EMAT send-receive scan of an adhesive bond with a defect free wedged adhesive layer, of the back reflected principal pulse amplitude from the 4.8mm adherent side (a), the back reflected first adhesive layer echo pulse amplitude from the 4.8mm adherent side (b), the back reflected second principal pulse amplitude from the 4.8mm adherent side (c), and the temporal adhesive 'thickness' (d).

5.29 Adhesive layer frequency dependant shear wave attenuation over the defective region of the wedged sample, and over a defect free region of the wedged sample of identical wedge angle and thickness.

Chapter 6

6.1 Send-receive EMAT waveform showing the temporal location of the shear wave pulse amplitudes that were monitored in a c-scan.

6.2 C-scan measured amplitude of first principal shear wave pulse.

6.3 C-scan measured amplitude of second principal shear wave pulse.

6.4 C-scan measured amplitude of first shear wave adhesive echo pulse.

6.5 C-scan measured amplitude of second shear wave adhesive echo pulse.

6.6 Illustration of how higher order reverberations within the adhesive structure can significantly interfere with the larger amplitude dominant signals present in the waveform.

6.7 Simulated EMAT send-receive waveforms in an adhesively bonded sample for a 150μm and 200μm thick adhesive layer.

6.8 Shear wave phase velocity in a 12.5mm thick polycrystalline aluminium disc shaped sample.

6.9 Shear wave phase velocity in the aluminium adherents used in the adhesively bonded samples calculated from measurements performed in both send-receive and through transmission geometries.

6.10 Shear wave phase velocity in the (100) direction of a single crystal aluminium sample.

6.11a&b Shear wave phase velocity (a) and shear wave group velocity (b) in the epoxy adhesive layer.

6.12a&b Schematic representations of viscoelastic behavior using a spring and dashpot combination.

6.13 Elastic moduli as a function of frequency for the simple Voigt model and the improved viscoelastic model.

6.14 Calculated shear wave phase velocity in the epoxy adhesive layer from EMAT send-receive, through transmission and two separate through transmission waveforms.

6.15 Calculated fit to phase velocity in the epoxy layer from the improved viscoelastic model.

Chapter 7

7.1 Schematic of experimental setup in monitoring the cure of a two component epoxy adhesive.

7.2 Cross-section of the cell containing the curing adhesive and the position of the EMATs used to ultrasonically monitor the cure.

7.3a&b Peak-peak amplitude of shear waves in send-receive (a) and through transmission (b) as a function of time.

7.3c Normalised shear wave attenuation coefficient of epoxy as a function of time.

7.3d&e Peak-peak amplitude of shear waves in send-receive (d) and through transmission (e) as a function of time for a quick setting two component epoxy adhesive.

7.4 Change in shear wave pulse maximum arrival time in through transmission.

7.5 Reflection coefficient at adherent-adhesive interface as a function of time.

7.6 Send-receive EMAT shear wave pulses recorded at various cure times (a) with the corresponding magnitude FFTs (b).

7.7 Through transmission EMAT shear wave pulses recorded at various cure times (a) with the corresponding magnitude FFTs (b).

7.8 Shear wave attenuation in the curing epoxy for a number of specific frequencies as a function of time.

7.9 Calculated shear wave phase velocity at a number of various times during the adhesive cure.

7.10 Fitting parameters to the improved viscoelastic model for various times during the adhesive cure.

7.11 Calculated shear wave group velocity at a number of various times during the adhesive cure.

Chapter 8

8.1a&b&c&d Shear wave pulse amplitude through transmission measurements taken on scanning an adhesive bond that had an adherent treated with release agent prior to construction.

Acknowledgement

This research was wholly funded by the Materials and Structures Department of DRA (Aerospace Division). I would like to thank the people involved in the collaboration for the financial support and samples that I received, particularly my industrial supervisor Stephen Shaw and especially Martin Stone who constructed the samples that were essential to the project.

At Warwick I would like to thank my supervisor Stuart Palmer for taking me on in the first place, and who has had to correct some of the worst English grammar ever encountered in the Western world. The biggest source of expertise and assistance with this work was Chris Edwards, to whom I am extremely grateful for his ideas, patience, friendship and coffee. Thanks also to Don Paul for help with the Macintosh, and to the 'Solid State Boys' who have made my PhD more enjoyable both in and outside the department. The project involved many trips to the mechanical workshop, help and advice was freely given by Pat Beechcraft and John F Reed who was always ready to assist with a cheery smile. In the Engineering Dept ., Dave Hutchins and Duncan Billson also provided help and loan of equipment.

A big thanks for support and patience must also go to Anna (my bird), whose cheeky little chirps and flapping kept me going. Lastly and most importantly I would like to thank my parents who have always encouraged and supported me in whatever I have wanted to do. For what its worth, this thesis is dedicated to them.

Declaration

The material presented in this thesis is my own work except where specifically stated as otherwise. The work was carried out in the Department of Physics, the University of Warwick, in the period from October 1991 to September 1994. No part of this work has been submitted previously to the University of Warwick, nor any other academic institution, for admission to a higher degree. Some of the work has already appeared in the form of publications which are listed in the bibliography section.

Summary

This Thesis describes techniques used in the analysis of aerospace adhesively bonded sandwich joints using radially polarised shear wave EMATs, together with an analysis of the general performance of the EMAT systems used in the investigation.

It is generally accepted that to date there is no satisfactory technique for the detection of defect types commonly encountered in adhesively bonded aerospace samples. This has limited the use of adhesives for joining components on critical parts, where no additional fixing techniques are used. Consequently, if a test procedure could be developed to accurately monitor post production defects and in-service degradation then there would be great benefits in terms of weight saving and strength in joined components which were held together by adhesive bonds alone. Ultrasonics is a technique commonly applied to the assessment of bond quality and readily lends itself to the probing of media which support the propagation of acoustic waves. The principal is that the propagation of sound through a medium gives some indication of the mechanical properties of that medium, and in terms of an adhesive layer could measure the strength of the adhesive bulk itself - cohesion. The efficiency of propagation of sound from one medium to another depends on the physical properties of each medium, and possibly on how well the surfaces of each medium are joined together - adhesion. Adhesion is the more difficult property to monitor as it is not just a case of mechanically keying one medium to another on a nanometre scale, but other interactions occur between the media similar to a Van der Walls type force that also contribute to adhesion.

It has been extensively reported in the literature that the most sensitive ultrasonic wave to use would be a shear wave at normal incidence to the adherent-adhesive interface. Radially polarised shear wave EMATs have been used to generate the shear waves that induce a shear stress at an adherent-adhesive interface. Some of the work involved in this project has concentrated on the design, construction and characterisation of these EMATs and the supporting hardware such as current pulser circuits and the necessary low noise-high bandwidth preamplifiers. The experimental work is presented in chapters 3-7. Chapter 3 covers the performance of the EMAT systems, chapter 4 discusses the EMAT operation on birefringent aluminium plates, chapters 5 and 6 cover the results and analysis used in the adhesive bonds and chapter 7 describes a technique to monitor adhesive cure using EMATs which monitor changes at an adherent-adhesive interface and within the adhesive bulk itself.

Chapter 1

Introduction

1.1 Background

It is generally accepted that to-date, there is no satisfactory probe for testing the integrity of adhesively bonded samples. The technique presented here is not offered as a complete solution to the problem, but as a complementary method to those already in existence. The project concentrated on one particular type of joint, a sandwich structure joint (sometimes called a long bond). This was to be investigated in the form of two adhesively bonded aluminium plates.

Unfortunately, the technology needed to non-destructively test adhesive bonds has lagged behind the advances in adhesives themselves. The most common adhesives in use today are epoxy adhesives. These have been around for about fifty years and throughout that time have been developed for a variety of specific applications. The main attraction of using an epoxy adhesive is their high strength, low weight, ability to adhere to a wide range of materials and their low shrinkage factors. The main fields concerned with adhesively bonding metals are the aerospace and automotive industries. There is of course more cause for concern in the integrity of aerospace structures as failure here would be far more catastrophic. Adhesive bonds are only exclusively used on the internal structure of aircraft, where failure of a joint would not greatly impair the performance of the aircraft. In regions where the structural integrity is paramount, the structure is adhesively bonded and joined using metal fasteners (rivets). In some ways the presence of these fasteners, undermines the reasons behind constructing adhesive bonds in the first place. The actual preparation of the bonded samples is obviously done under strictly controlled conditions. Both the adherents (aluminium plate) and adhesive (an epoxy) must be carefully prepared prior to bonding, and the curing process itself must be performed within specific technical margins. A more detailed description of the bonding and pre-treatment process is given in the Appendix B.

The impetus behind using an adhesive is the reduced weight of the structure as a whole, and the fact that a relatively large area can be joined, while spreading the stress fairly evenly over the total area: a well prepared bond is undoubtedly one of the best ways to join two plates together, with the only real mechanical threat to the joint coming from the plates peeling away from each other. Fasteners not only increase overall weight, but the holes they are located in act as points of stress concentration, and the whole process of 'riveting' damages the adhesive bonding to varying degrees. Quite often when an adhesive bond fails on such a structure, it fails around the riveted area. And of course, from a testing point of view, the presence of metal fasteners in the plate make the process of checking bond integrity more complicated. This is true from the actual scanning of a bond, to the analysis that will have to be performed on the signal. Apart from the potential defects introduced in manufacture, there will also be degradation of the aircraft structure as a whole, while in service. Joints are constantly being stressed, and problems may develop in regions that were initially well constructed. The main threat to an adhesively bonded structure is the ingression of water into the joint. In order to protect the exposed areas of bond lines the structure is painted. Any practical technique for testing bonds 'in-service' should therefore not damage the paint layer, let alone require its removal.

1.2 Common techniques used in testing adhesive bonded structures

There are several review papers concerned with the general topic of techniques for testing composite structures. The reader is referred to four papers which give a good background to the topic.[1,2,3,4].

X-ray techniques [5,6] can be used in some adhesively bonded structure examinations. They are better suited to carbon fibre composite type joints, as in metal joints, the interaction with the metal is by far the most dominant process. The only tests of any use direct theX-ray down the less absorbing adhesive layer itself, giving a measure of the amount of material in the bondline. Even if the metal were extremely thin, examination through the entire bulk

of the bond is futile as x-rays 'measure' the amount and density of the material present. Quite often in a structure, all the material required for bonding may be present but unbonded.

Neutrons can be used in checking bond integrity [7,8], as they have the advantage of interacting with both the metal and the adhesive. In fact, neutrons will preferentially interact with hydrogen containing compounds. This is a good technique to highlight the presence of moisture in a bond, at the interface or within the adhesive bulk. The main disadvantage here is that neutron sources are expensive (in terms of beam time), immobile and not remotely suitable for testing large constructions.

Thermography or thermal imaging uses heat waves to measure the degree of thermal, and thus mechanical coupling across an interface [9,10]. Thermal imaging falls into two categories, active (where heat waves are produced by stressing the sample) and passive (heat waves applied to sample). This is not a particularly sensitive technique and if it is to be used on metal-metal bonds, the metal must be thin so that some appreciable amount of heat can propagate to the adherent-adhesive interface.

A metal-metal adhesive bond can behave as a capacitor, and this geometry can lend itself to a dielectric based test of the bond [11]. An AC signal is applied across the bonded structure and the impedance and losses can be studied as a function of frequency. When moisture traps itself inside a bond it can either be bound to the adhesive molecules in the form of hydroxyl groups, or just sit free at the adhesive-adherent interface. The relaxation phenomena for free and bound water occur at very different frequencies (approximately 1MHz for 'bonded' , 20GHz for 'free'). Thus, in theory it is possible to detect the presence and type of moisture contamination in the bondline.

Eddy current testing has been successfully implemented in the NDT of aircraft structures [12]. However, the test does not check adhesive bond integrity, but the condition of the metal fasteners and metal around these fasteners (for problems such as cracks or corrosion). The eddy currents are trapped within an electromagnetic skin depth and the thinnest of metal-metal bonds are too thick to allow any probing of the adhesive layer.

The ideal setup for testing a bond would have the ability to test without the test probe making contact to the sample, while maintaining a sensitive probe to adhesive bulk and

interface properties. One of the most obvious techniques that satisfies this criterion is non-contact ultrasound. The main types of non-contact generators/detectors are lasers, air coupled transducers, capacitance transducers, eddy current probes and electromagnetic acoustic transducers (EMATs). The latter two are closely related to each other, but strictly speaking fall into their own categories. The experiments that will be described in this thesis mainly employ broadband, radially polarised shear wave EMATs. Simple ultrasonic theory shows that plane shear waves should be more sensitive to variations in the impedance mismatch at a bond interface than a longitudinal plane wave, especially where liquid or liquid-like media are present. This will be discussed in more detail in chapter 2. The easiest EMAT to construct which is also the most efficient (in terms of ultrasonic mode generated) is the radially polarised shear wave EMAT, which was the type used in the experiments. These EMATs have been designed, built and developed at Warwick University during the course of this project, and have been under continuous development. Thus, some of the thesis is concerned with EMAT characteristics and general performance. The use of EMATs in ultrasonics has been well documented and they have been used in acoustic measurements for around 20 years [13,14]. They are commercially available, and as with other fields of technology, they have become smaller and more efficient as the components of the system have improved: mainly the strong permanent magnet used and the electronics that amplify the signal. Advances in signal processing have also helped make the EMAT a more versatile instrument, perhaps the most useful being the ability to quickly average digitised waveforms using equipment that is relatively inexpensive. The EMAT is effectively a sensitive RF signal receiver, and as such is susceptible to electromagnetic noise, making the ability to average signals imperative if accurate amplitude values of specific pulses are to be measured.

A sensible route to take when analysing the physical properties of a bonded structure is to measure the physical properties of the individual isolated components that constitute the bond. Characterisation experiments were conducted on both aluminium plate and the cured epoxy adhesive. At its simplest level, the bonded structure can be envisaged as 3 distinct layers. In reality the most simple bond is multi-layered, with the layers having no

distinct boundaries on a nanometre scale, but rather a graduated change in composition and thus physical properties. It is the sudden change in the acoustic properties at the boundary of two media that gives rise to reflection of a sound wave [15,16]. Where the change in acoustic properties are not 'sudden', then the impedance mis-match is reduced, and thus more of the energy of the ultrasonic wave is coupled across the boundary.

Fortunately, the system can almost always be treated as a 3 layer system for most ultrasonic investigations. Basic wave theory shows that in order to observe an object, the wavelength of the wave that interacts with it must be less than the size of the object. In other words, if the feature is a layer of thickness say D, and the incident ultrasound has wavelength L, then the layer cannot be observed if D>>L. This is the case for the interfacial and primer layers when using the EMAT, as the smallest significant wavelengths present in the broadband pulse are the order of 300μm (corresponding to 10MHz SH wave in aluminium), while the interfacial layers are usually no more than 1μm thick in total.

1.3 Defect Types

There are several types of defect that are commonly found in adhesive bonds produced during manufacture, which are shown in fig 1.1 [1,2,3,4]. The composition of an adhesive gives it the required strength, both adhesive and cohesive and its other physical properties. The correct composition also requires the appropriate curing conditions. Contaminants and incorrect composition will give rise to a defect type that in general will not be localised, as the adhesive will have been mixed. Contaminants can be introduced from the preparation processes, as these will often use volatile degreasing and cleaning agents. Atmospheric moisture and air can also be trapped in the bondline prior to cure. This will give rise to porosity within the adhesive and also at the adherent-adhesive interface, giving reduced internal strength and interface coupling. When there is a high degree of porosity, a complete void may form, though voids are more commonly formed by trapped air, or a localised lack of adhesive. Cracking of the epoxy layer during manufacture is only

really observed in brittle high temperature adhesives. Defects that occur at the interface between adhesive and adherent are most commonly caused by oils, release agents or loose oxide layers on the metal surface. This can result in the cured epoxy touching the metal adherent, but not actually being stuck to it. This is usually referred to as a kissing bond or zero volume disbond, and is difficult to detect using conventional testing procedures. The adhesive used in the bonds in this project is manufactured as a film which is protected on each side by a thin plastic 'peel-ply'. This is removed prior to bonding, but situations can arise where a small portion is left on the adhesive surface, preventing any adhesion to the surface. In situations where the bonding process takes place at high temperature, some types of contaminants can be dissolved into the adhesive, reducing the problem of poor interface coupling.

Defects introduced in-service are mainly caused by attack of aggressive chemicals, moisture, and both thermal and mechanical cycling. Mechanical cracking of the adhesive is obviously a very serious threat, as once a crack has been formed it takes relatively little energy to encourage it to propagate. Cracks also increase susceptibility to attack from other agents, but fortunately this type of defect is one of the easier types to detect.

1.4 Proceeding chapter outlines

Chapter 2 gives an introduction to ultrasound with the emphasis on aspects relative to this study, and as a summary and review of some of the relevant work in the field of both EMAT and adhesive bond analysis.

Chapter 3 describes the EMAT systems used and developed during the course of this project, including both supporting circuitry and the transducers themselves. The non-contact generation and detection processes are discussed in more detail. Some theoretical calculations are also presented and compared with the experimental observations.

Chapter 4 deals with the phenomena of acoustic birefringence. This effect arises due to the anisotropic nature of a sample. Despite the fact that aluminium plate is polycrystalline, it does have anisotropy. This is brought about by the process of working the metal. The mechanism and nature of this anisotropy is described, extending the basic equations

presented in chapter 2. Experiments were performed studying the birefringence as a function of applied stress, and c-scans were performed on a range of flat bottomed holes which also revealed the anisotropic nature of the aluminium plate.

Chapter 5 describes the general results and considerations that are required when ultrasonically scanning adhesively bonded samples such as those investigated in this project. The through transmission and send-receive techniques are discussed for the specific case of the EMATs used and the results from these experiments are presented. The basic properties of the isolated components that constitute the bonded samples are individually examined. Finally, some specific scan results from different samples are explained from both the send-receive and through transmission techniques.

Chapter 6 is a more detailed investigation of the ultrasonic signals observed in the adhesive bonds and the aluminium plates. Some simple waveform simulation is performed and the results used to explain why certain features manifest themselves in particular situations. A number of calculations are presented on phase and group velocity using the procedure outlined in chapter 2. The viscoelastic behaviour of the epoxy adhesive is also examined and a single relaxation frequency model has been used to determine certain physical parameters from the experimentally obtained phase velocities.

Chapter 7 is a brief description of the study of an adhesive bond cure using EMATs in send-receive and through transmission simultaneously. The adhesives used in the experiments were 2 part air cure epoxy adhesives. Basic measurements on transmitted and reflected shear wave amplitude measurements are presented with more detailed work performed in the frequency domain. Once again, the results are fitted to a single relaxation frequency viscoelastic model and the results compared with those obtained by other workers.

Chapter 8 is the conclusion and discussion, and a summary of the implications that arise as a result of the work presented in this thesis.

Ch.1 References

1 J.A.G. Temple , Inspection of adhesive joints :a review , AEA Industrial Technology (march 1992) AEA-intec-0828

2 R.D. Adams and P. Cawley , A review of defect types and non-destructive testing techniques for composites and bonded joints. , NDT international , vol 21 , No.4 , 1988 , pp208-222

3 C.C.H. Guyott , P. Cawley and R.D. Adams , The non-destructive testing of adhesively bonded structure: a review , J. Adhesion , vol.20 , 1986 , pp129-159

4 E. Segal , J.L. Rose , Nondestructive techniques for adhesive bond joints, Research Techniques in Nondestructive Testing, 4 , Ed. R.S. Sharpe, Academic Press, London and New York , 1980 , pp275-316

5. D.E.W. Stone , Non-destructive inspection of composite materials for aircraft structure applications, Brit. Jour. NDT , 20 , 1986, pp 65-75

6. D.E.W. Stone and B. Clarke, Non-desturctive evaluation of composite structures - an overview, Proc ICCM VI/ECCM II, Ed. F.L Mathews, N.C.R. Buskell, J.M. Hodginson and J. Morton, Elsevier Applied Science , 1987 , pp1.28-1.59

7. E. Sandcaktar, Nondestructive examination of adhesive bonds with neutron radiography, Int Jour Ahesion and Adhesives , 1(6) , 1981, pp329-330

8. H.U. Mast, T. Brandler and R. Richter , Various industrial applications of neutron radiography , Neutron Radiography (3) , Osaka (Japan) , Ed. S. Fujine, K. Kanda, G. Matsumoto and J.P. Barton , 14-18 May , 1989 , Kluwes Academic Publishers , pp 645-651

9. W.N. Reynolds and G.M. Wells, Video-compatible thermography, Brit. Jour. NDT, 26, 1984 , pp40-44

10. W.N. Reynolds , Inspection of laminates and adhesive bonds by pulse-video thermography, NDT Int. , Vol. 21, No.4 , 1988, pp229-232

11. S.B. Joshi, R.A. Pethrick and D. Hayward , Aspects of theoretical modeling for high frequency dielectric studies of adhesively bonded structures , Brit. Jour. of NDT , vol 35, No.3 , 1993 , pp494-498

12. D.E. Bray and D. McBride, Eddy current testing of materals : in Nondesructive Testing Techniques , Ch.18 , John Wiley &Sons , pp503-527

13. H.M. Frost , Electromagnetic-ultrasonic transducer : principles, practice and applications in: Physical Acoustics XIV , (Ed. WP Mason and RN Thuston), Academic Press, New York , pp179-275

14. P.K. Larsen and K. Saermark , Helicon excitation of acoustic waves in aluminium , Phys. Lett. , 1967 , A24 , pp375-375

15. J.D. Achenbach , Wave propagation in elastic solids , North-Holand 1973

16. V.A. Shultilov, Fundametal physics of ultrasound , (trans. M.E. Alferieff) , Gordon and Breach Science Publishers , 1988

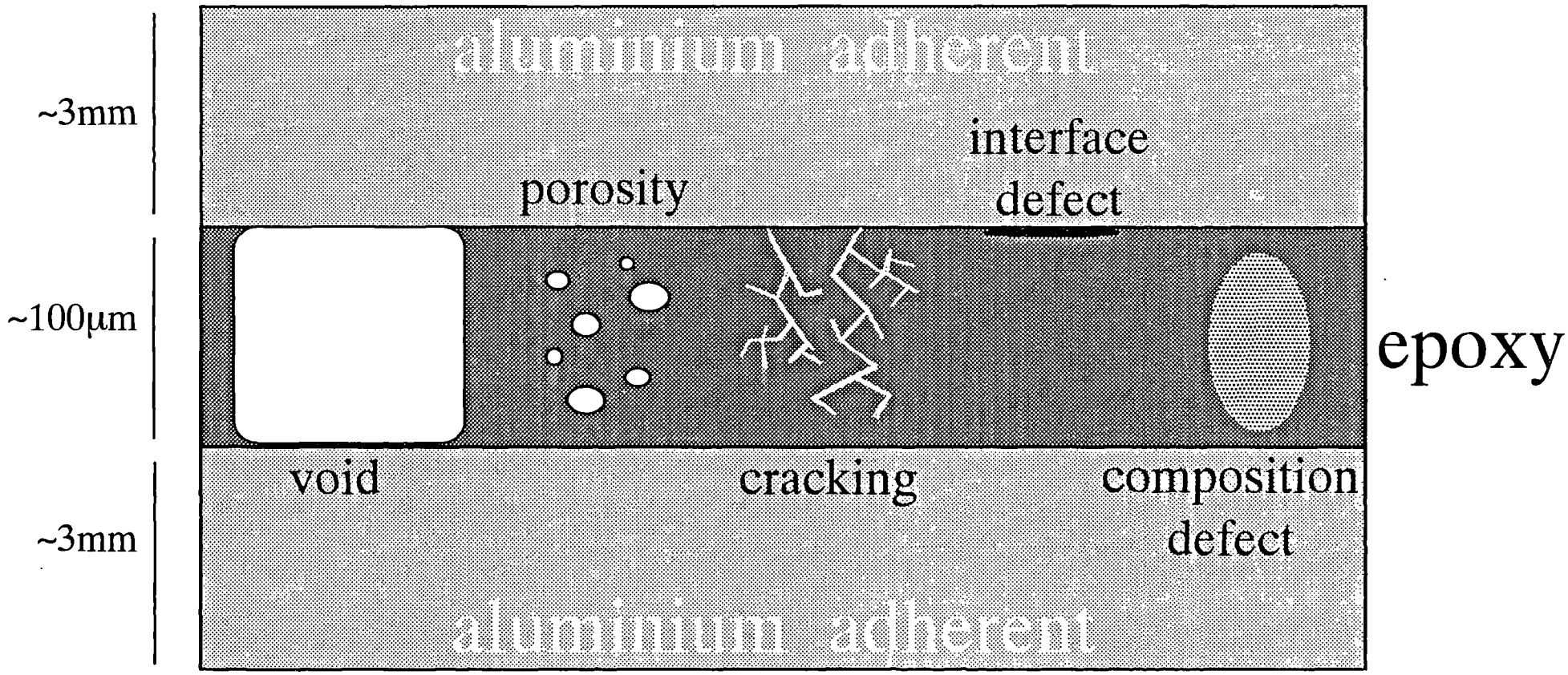

Fig 1.1

Schematic diagram of defect types encountered when adhesively bonding aluminium samples.

Chapter 2

Basic Theory and Review

2.0 Introduction

The aim of this chapter is to provide background knowledge to the proceeding experimental chapters, and some justification for the techniques used. A brief recap of simple ultrasonic theory is given, with more detailed theory being presented in the relevant chapter as required. Once having established the basic wave equation, the equipment and mechanisms for generating the ultrasonic modes described later in the thesis are discussed. The second part of the chapter is a review and comparison of some theory and experiments performed by other workers in the field of adhesive bond analysis.

2.1 Simple theory of ultrasound

Wave propagation in an elastic medium [1,2,3,4] is most easily derived in terms of the relationship between the stress in that medium and the strain at the same point in that medium. Here stress is denoted by the tensor σ_{ik} and strain by e_{ik}.

The stress tensor is given by,

$$\sigma_{ik} = \begin{pmatrix} \sigma_{11} & \sigma_{12} & \sigma_{13} \\ \sigma_{21} & \sigma_{22} & \sigma_{23} \\ \sigma_{31} & \sigma_{32} & \sigma_{33} \end{pmatrix} \qquad 2.1$$

and can be separated into the sum of a symmetric part (corresponding to a pure linear operating force), and an anti-symmetric part (corresponding to a pure rotational force or torque).

The strain tensor can also be separated into a symmetric part (corresponding to pure displacement) and an anti-symmetric part (corresponding to a pure rotation). As the pure displacement and the pure linear force terms are only required, the stress and strain tensors can be written,

$$\sigma_{ik} = \begin{pmatrix} \sigma_1 & \sigma_6 & \sigma_5 \\ \sigma_6 & \sigma_2 & \sigma_4 \\ \sigma_5 & \sigma_4 & \sigma_3 \end{pmatrix} \qquad 2.2$$

$$e_{ik} = \begin{pmatrix} e_1 & e_6 & e_5 \\ e_6 & e_2 & e_4 \\ e_5 & e_4 & e_3 \end{pmatrix} \qquad 2.3$$

In the limit of small deformations, the stress and strain are related by the equation,

$$\sigma_{ij} = C_{ijkl}\, e_{kl} \qquad 2.4$$

Taking the pure displacement and pure linear force components of stress and strain, as both σ_{ij} and e_{kl} consist of 6 independent components rather than 9, the modulus of elasticity tensor has 36 independent components.

By consideration of the energy associated with a deformation, the components of the modulus tensor are related by,

$$C_{ijkl} = C_{klij} \qquad 2.5$$

The modulus tensor is therefore symmetric with 21 independent components, and for a general anisotropic system (with an centre of inversion - a type of symmetry condition) the stress - strain relationship can be written as :

$$\begin{pmatrix}\sigma_1\\ \sigma_2\\ \sigma_3\\ \sigma_4\\ \sigma_5\\ \sigma_6\end{pmatrix} = \begin{pmatrix}C_{11} & C_{12} & C_{13} & C_{14} & C_{15} & C_{16}\\ C_{12} & C_{22} & C_{23} & C_{24} & C_{25} & C_{26}\\ C_{13} & C_{23} & C_{33} & C_{34} & C_{35} & C_{36}\\ C_{14} & C_{24} & C_{34} & C_{44} & C_{45} & C_{46}\\ C_{15} & C_{25} & C_{35} & C_{45} & C_{55} & C_{56}\\ C_{16} & C_{26} & C_{36} & C_{46} & C_{56} & C_{66}\end{pmatrix} \bullet \begin{pmatrix}e_1\\ e_2\\ e_3\\ e_4\\ e_5\\ e_6\end{pmatrix} \qquad 2.6$$

The symmetry operators that describe a particular crystal structure put extra constraints on the above equation, and can thus make certain components of the matrix null, or equal in magnitude, reducing the number of independent elastic constants. For example, a system with triclinic symmetry would have 36 independent constants, an orthorhombic system will (generally) have 9, a cubic 3 and an isotropic medium 2 independent elastic constants.

2.1.1 Ultrasonic wave propagation

The wave equation effectively relates the dynamic response of a medium to an applied force. This is introduced via the stress, as the stress is a force and force is related to acceleration via F=ma. Thus combining stress and strain into a general wave equation we can write,

$$\frac{d^2u}{dx^2} = \frac{1}{v^2}\frac{d^2u}{dt^2} \qquad 2.7$$

The preceding wave equation describes a plane wave in an infinite elastic medium and its solution can be written in the form given by Christoffel [3] as ,

$$\det\left|\Gamma_{ik} - \rho v^2 \delta_{ik}\right| = 0 \qquad 2.8$$

where the tensor Γ_{ik} comprises the directional wave normal cosines in quadratic form, and v is a real phase velocity.

The solutions to the above equation for the phase velocity are dependant on wave propagation direction and the acoustic wave polarisation direction.

When ultrasound is generated by transduction, the wave generated has a spatial and time dependant form. The calculation of the ultrasonic displacement produced by a real transducer can be performed via the use of a Greens function [5,6,7]. The ultrasound generated by the radially polarised EMATs used in the project described here was broadband in frequency. This means that there was a range of frequencies present in the pulse, which makes the pulse spatially sharper than would be obtained if the EMAT was driven by a resonant single frequency toneburst. In real media, the physical behaviour will deviate from ideally elastic with the result that the phase velocity is a function of frequency. In order to measure the phase velocity, the analysis must be performed in the frequency domain, as described in the next section.

2.2 Phase and group velocity calculations

Following the notation and derivation of the formula suitable for phase and group velocity calculation presented by Sacshe et al [8], the wave equation for ultrasonic displacement can be written as,

$$u(x,t) = A\exp[i(\omega t \pm k x + \varepsilon)] \qquad 2.9$$

where k is the ω is the angular frequency of the ultrasound, k the wavenumber and ε

a phase shift or difference. In the next step, either the frequency or the wavenumber can be chosen to be a complex number. Taking the wavenumber to be complex, such that

$$k = \beta + i\alpha \qquad 2.10$$

and substituting into the wave equation yields,

$$u(x,t) = A\exp(-\alpha x).\exp[i(\omega t \pm \beta x + \varepsilon)] \qquad 2.11$$

The phase velocity V_p , and group velocity V_g are defined as,

$$Vp = \frac{\omega}{\text{Real}[k]} = \frac{\omega}{\beta} \qquad 2.12 \qquad\qquad Vg = \frac{\partial\omega}{\partial\beta} \qquad 2.13$$

The fast Fourier transform (FFT) used in the present work yielded the transform in the format of a real component and an imaginary component. This procedure does not directly give the phase for a particular frequency. It is the ratio of the imaginary component to the real component that gives the arctan value of the phase angle. In order to obtain the phase relationship, which in effect shows the relative position of each frequency component in phase space, a polar co-ordinate system was used in the complex notation. This form of the polar notation is $Re^{i\theta}$, where R is the magnitude of the frequency component, and θ is the relative phase of the frequency component. As the computer algorithm used did not return values of phase (arctan) outside $+\pi$ or $-\pi$ (as doing so would be ambiguous), the values obtained need 'unwrapping' , or extrapolating such that the phase continuously varies, either increasing or decreasing. The slope of the phase component is completely arbitrary, depending of the position of the waveform in the transform window, prior to the transform operation. This point is illustrated in fig2.1 showing a pulse in 3 different positions, with the 3 corresponding phase relations. Note that the phase information is only plotted up to values of 10MHz as there is no frequency information in the observed EMAT

pulses at frequencies higher than this (evident in the magnitude FFT). This is a general consideration for the frequency information from the broadband ultrasound used in the experiments described in this thesis.

In order to put any absolute meaning on the value of phase a reference phase is required, from a reference ultrasonic pulse. Thus, a minimum of 2 ultrasonic pulses are necessary if any quantitative measurements are to be made in the frequency domain. In the phase and group velocity calculations, the expressions obtained are shown below.

The phase velocity can be calculated from the equation,

$$V_p(f) = \frac{2\pi f L}{[\phi(f) - \phi_0] + 2\pi f \tau_s} \qquad 2.14$$

and the group velocity from

$$V_g(f) = \frac{2\pi L}{\left(\frac{\partial\phi_0}{\partial f} - \frac{\partial\phi(f)}{\partial f}\right) + 2\pi\tau_s} \qquad 2.15$$

where ϕ_0 is the phase relationship from the reference pulse, $\phi(f)$ is the phase derived from the pulse that has traversed a distance L through the medium under investigation and f is the frequency of the ultrasound. The term τ_s is a correction that can be used where one pulse has been shifted towards the other. In general the pulses are shifted closer together in windowing capture techniques making the term τ_s a positive quantity.

2.3. Transmission of ultrasonic waves through layered media

Classical acoustic theory predicts that at the interface of 2 elastic halfspaces, the reflection coefficient r and transmission coefficient t are given by,

$$r = \frac{Z_1 - Z_2}{Z_1 + Z_2} \qquad 2.16$$

$$t = \frac{2Z_2}{Z_1 + Z_2} \qquad 2.17$$

where Z_1 is the acoustic impedance (velocity * density) of the medium that contains the incident and reflected waves, and Z_2 is impedance of the medium that contains the transmitted wave only. Where one of the media significantly deviates from elastic behaviour the above expressions for the reflection or transmission coefficients will be modified, in general being frequency dependant.

At a simple level, the structures studied in this thesis which comprise the adhesively bonded aluminium plates can be considered as three-layered. A further simplification is to model the adherents as semi-infinite half spaces, with a finite adhesive layer between the 2 adherents. The boundary conditions (of continuity of particle velocity and pressure) that need to be satisfied give rise to a frequency dependant transmission function for ultrasonic waves propagating through the joint. The intensity plane wave transmission coefficient at normal incidence for such a system is given by [9,10],

$$T_i = \frac{Z_1}{Z_3} \cdot \frac{1}{\frac{1}{4}\left(1+\frac{Z_1}{Z_3}\right)^2 \mathrm{Cos}^2(k_2L) + \frac{1}{4}\left(\frac{Z_2}{Z_3}+\frac{Z_1}{Z_2}\right)^2 \mathrm{Sin}^2(k_2L)} \qquad 2.18$$

The above equation will hold for the case of bonded aluminium plates where the ultrasonic wavelength is much shorter than the adherent thickness, which is approximately the case in the experimental samples in this project. It must still be bourn in mind however that the ultrasonic field generated by the EMAT will not be a plane wave in the limit of the aluminium adherent thickness.

The transmission coefficient equation can be expressed in matrix form ,

$$\begin{bmatrix} A_1 + B_1 \\ A_1 - B_1 \end{bmatrix} = \begin{bmatrix} \text{Cos } k_2L & i\frac{Z_2}{Z_3}\text{Sin } k_2L \\ i\frac{Z_1}{Z_2}\text{Sin } k_2L & \frac{Z_1}{Z_3}\text{Cos } k_2L \end{bmatrix} \times \begin{bmatrix} A_3 \\ A_3 \end{bmatrix} \qquad 2.19$$

where A_1 is the amplitude of the incident wave, B_1 is the wave amplitude reflected from the first interface and A_3 is the amplitude of the wave transmitted into the far adherent halfspace. This representation can be expanded to an nth layered structure such that the amplitude coefficients in only the first halfspace and the second final halfspace are denoted.

The bonded structure as a whole has a number of mechanical resonances, associated with the propagation of ultrasound through the structure, and is therefore in essence a low frequency technique. Several workers have adopted the frequency domain analysis approach [11,12,13] to investigate the 'cohesive' properties of the adhesive layer, or rather the thickness for a known ultrasonic velocity within the adhesive or vica versa. The technique is better suited to adhesively bonded structures where the adherents are much thinner than in the samples used in this project, as for thick adherents the geometry of the adherents dominate the frequency response [14]. This is illustrated by the FFT of the waveform in through transmission in an adhesively bonded sample consisting of two identical 3.00mm plates and a 100μm adhesive layer, compared with the FFT of a waveform in a 3.00mm blank plate, shown in fig 2.2(a). The spectra appear nominally identical and the repeat frequency corresponds to the reverberations within an aluminium adherent.

Features in the spectrum can be made clearer by selectively transforming certain regions of the waveform. This is also shown in fig 2.2(b) where instead of taking the FFT of the entire displayed waveform, the window is chosen to include only the bond reverberations and the first principal pulse. It is quite evident that the repeat frequency in this magnitude FFT corresponds to the adhesive layer reverberations

(or adhesive thickness / ultrasonic shear velocity). In the first FFT (fig 2.2(a)) of the entire waveform this magnitude information is lost, or rather hidden due to the dominant nature of the ultrasound trapped within the much thicker aluminium adherents.

2.4 Ultrasonic methods for testing adhesive bonds

2.4.1 Wave modes

Ultrasound is usually the favoured means of non-destructively testing the condition of a bonded structure. Within the field itself there are many different techniques applied to the testing of adhesive bonds. This thesis however is concerned with both the techniques, and the physical properties that such measurements can reveal. The three main methods using ultrasonic waves are discussed below.

2.4.2 Bulk waves at normal incidence

Longitudinal and shear waves which propagate at normal incidence to a sample surface are the easiest and most basic ultrasonic modes to generate. Theory shows that for the majority of conceivable cases, the most sensitive probe of an interface should generate a shear stress at the interface and this fact has been pointed out in the literature [15,16,17,18]. A basic approach is to take a simplified case where mechanical coupling at the adhesive-adherent interface is modelled via connecting tangential and normal spring components of variable stiffness, which is akin to allowing a certain degree of slip between the two planes at the interface. This will be discussed further in chapter 5.

An SH wave at normal incidence to the interface will induce the purest shear stress component at the boundary. Conventional piezoelectric shear wave transducers are contact devices, and require a very viscous couplant to transmit the ultrasound into the sample. This makes any scanning technique extremely problematic. The shear wave piezoelectric transducer generates a linearly polarised shear wave which could lead to further complications

if the aluminium plate adherent is birefringent. This will be discussed in more detail later in chapter 4. Due to the difficulties encountered with shear wave generation, experimenters using longitudinal transducers dominate the literature. This is still a contact method, and the transducers require an acoustic couplant such as water, oil or a dry couplant such as rubber coupled to the transducer face [19] (but these transducers are currently relatively insensitive). Typical scanning techniques are performed using water jet coupled transducers, immersion tank scans and spot measurements. While the coupling and scanning requirements can be achieved in this fashion, the techniques are far from ideal. For example, it is always desirable to ensure that moisture does not attack aerospace adhesive bonds, but this is one of the most common coupling media, while the acoustic gel used for spot-type measurements is actually corrosive if not properly removed. Longitudinal waves are less sensitive to interface coupling than shear waves, particularly solid-liquid interfaces, but are by far the most commonly used ultrasonic mode for adhesive bond analysis.

The signals observed using ultrasonic transducers never consist of a pure shear or pure longitudinal wave displacements due to the finite size of the source (where the source is the active area of the transducer). This general phenomena has been discussed in the case of electromagnetic acoustic transducers by Kawashima [20].

2.4.3 Bulk waves at oblique incidence

An alternative way of generating a shear stress at an interface rather than actually using a shear wave transducer is to send longitudinal waves at an oblique angle to the interface. Simple plane wave theory predicts that a fraction of the longitudinal wave energy will mode convert to a shear wave depending on the angle of incidence. There is an optimum angle for generating a shear wave in such a geometry, dependant on the acoustic characteristics of the transducer face and the test specimen. In general, the ultrasound entering the medium will consist of both longitudinal and shear waves.

The second point to note is that when a pure longitudinal wave impinges on a boundary at some oblique angle there are stress components generated both normal to and along the boundary. This situation can again give rise to some mode conversion [2,4,20]. Thus there are typically four principal wave modes to consider in such a technique. These are ;-

1) longitudinal wave into adherent, longitudinal wave off interface LL

2) longitudinal wave into adherent, shear wave off interface LS

3) shear wave into adherent, shear wave off interface SS

4) shear wave into adherent, longitudinal wave off interface SL

These modes are not as sensitive as a shear wave at normal incidence, but at least posses some shear component parallel to the adhesive-adherent boundary[21,22]. This technique is sometimes called pitch-catch (see fig 2.3) and while it can be carried out from one side of the sample only, it requires two transducers. One transducer generates the ultrasound , while the other has to be aligned in the correct position to detect the wave reflected from the boundary

2.4.4 Guided waves

A potentially powerful technique for measuring the quality of a bondline is to use waves that are guided along the bondline. The main attractive feature of this technique is that in theory, a large bond area can be analysed in a single pulse. It would of course be quite a difficult task to determine defect type and location from the raw data, but most practical applications would only require a pass/fail criterion.

The waveguiding within a particular layer occurs since there is typically a very large impedance mismatch at the adherent-adhesive boundary of the order of 80-90%. The main portion of the ultrasonic energy within a particular layer will then tend to remain within that layer. Guiding a wave down the adherents may yield some measure of the interface condition/s but sending the ultrasound through the adhesive layer itself should be far more

sensitive to the adhesive properties. The problem with this method is that the adhesive is highly attenuative to ultrasonic waves, cutting off frequencies above 2MHz very sharply. Thus as the guided wave is attenuated the acoustic information needed to investigate adhesive properties is lost.

Classically a surface bound non-dispersive Rayleigh wave arises in 'thick' samples where the acoustic wavelength is much smaller than the samples thickness, as the wave penetrates to a depth the order of magnitude of the wavelength. Rayleigh waves have been used in adhesive bond analysis [23], usually by generating the wave on the blank adhesive-side face of a lap-type joint. The problem here is that once the wave interacts with the adhesive layer it is no longer really a Rayleigh wave. The presence of the adhesive strongly attenuates frequencies above about 2MHz, and it is very difficult to observe differences between different surface loadings.

Lamb wave type modes occur where the thickness of the sample is comparable in size or less than the wavelength components present in the ultrasonic pulse. In the extreme limit that the sample is much thinner than the ultrasonic wavelengths, there are two basic zero order Lamb wave modes, antisymmetric and symmetric [24]. The symmetric mode is non-dispersive and small in amplitude, while the anti-symmetric mode is highly dispersive and large in amplitude. In general, there are many possible higher order Lamb wave modes making the system complicated to analyse. The dispersion relations for Lamb waves in a bonded structure are dependant on the combination of properties of all the individual components present in the bonded structure [25,26]. Plate adherent thicknesses used in this project were approximately 3mm and 5mm, so that wavelengths significantly larger than this would be well within the Lamb wave criterion (frequency< 1MHz). A Lamb wave analysis technique is better suited to adhesively bonded structure much thinner than those used in this project.

2.5 Ultrasonic transduction

Ultrasonic transduction simply refers to the conversion of some form of energy into acoustic energy. With most transducers this is the conversion of electrical energy into acoustic energy. For the reasons outlined in the preceding sections it was decided that the most promising method to use would be to generate and detect ultrasound in a non-contact regime. The majority of measurements taken this project were performed using electromagnetic acoustic transducers, imparticularly the radially polarised shear wave EMAT. Some measurements were also performed using lasers in both the generation and detection of ultrasound.

2.5.1 Laser generation and detection

A pulsed Nd:YAG laser was used to generate broadband ultrasonic waves in a sample of epoxy ingot. The generation mechanism used was in and energy regime between pure thermoelastic and ablative [27]. The laser generates both longitudinal and shear waves simultaneously, and the directivity and general source characterisation is now well established. Ideally, the laser would be used to generate pure shear wave modes in the thermoelastic regime, but the energy densities required are so low that the ultrasonic amplitude is also very low. Thus the signal may need to be averaged in order to obtain a satisfactory signal to noise ratio. Ensuring that the source does not change and the repetition rate is fast enough to permit the averaging required within a scan is the limiting factor governing the feasibility of such a technique.

A modified Michelson interferometer was used to detect the out-of-plane component of the ultrasonic waves generated by the pulsed laser. This is a totally remote non-contact detection mechanism with a bandwidth of roughly 80MHz. The obvious problem with using this technique in adhesive bond analysis is that the set-up alignment is difficult to automate and only the out-of-plane component is detected.

2.5.2 Electromagnetic acoustic transducers (EMATs)

The basic mechanism of EMAT operation is the Lorentz force [28]. The requirement is that charge carriers must somehow be induced to move in a static magnetic field, and in doing so experience a force (Lorentz force) mutually perpendicular to the carrier velocity and static magnetic field. The static field can be provided by an electromagnet, or a permanent magnet. With recent advances in permanent magnet technology, field strengths for reasonably sized magnets are approaching those available for small electromagnet supplies. Permanent magnets also greatly simplify design, construction and transducer practicality.

On an aluminium plate, the charge carrier current generation is achieved by pulsing current through a coil near to the aluminium surface. The current generated in thesurface skindepth of the aluminium is an image current. In the case of the radially polarised EMAT, the coil is a flat spiral 'pancake' type. The image current motion in the static magnetic field (provided by a NdFeB magnet behind the coil), gives rise to a radial acceleration of the electrons and thus of the atoms in the metal (see fig 2.4). This then generates the radially polarised stress field. This process is discussed in more detail in chapter 3.

EMATs have been used by other workers in the analysis of adhesive bonds. Hutchins et al [29] investigated the integrity of a titanium diffusion bond using a pulsed Nd:YAG laser to generate the ultrasound and an EMAT to detect ultrasound. The laser generation was performed in a thermoelastic regime, directed through the centre of a radially polarised shear wave EMAT with a hole in its centre. The defect identified was a total disbond between the two metal sheets. The EMAT used was operated in a narrowband regime, so signals were temporally quite large (approximately 10μs long resonant pulses). These pulses would be much broader than those required in the analysis described in this thesis. The system will also suffer from variation in laser pulse energy and will emit a large amount of electromagnetic noise. If any averaging is required, the scanning speed of such a system would be primarily limited by the repetition rate of the laser (typically less than 100Hz).

EMATs were also used by He et al [30] to analyse adhesively bonded low carbon steel plates. Both bulk and Lamb waves were used in the analysis. The systems used were not

pulse echo systems - a separate generation and detection EMAT was required. The generation EMAT was designed to be solely an efficient generator, and similarly for the detection EMAT. The net result was that the whole system was quite resonant and the EMAT pulses were typically over 10μs wide in the time domain.

2.6 Summary

This chapter has dealt with the basic theory needed for a background understanding of the preceding chapters. Some of the techniques generally used in adhesive bond investigation have been described and compared to that used in this project. This has hopefully given the reader some insight as to why the particular techniques and analysis methods used in this project were chosen in preference to the alternatives available.

Ch.2 References

1 A.E.H. Love , The mathematical theory of elasticity , 4th ed. New York, Dover Publications , Inc. , 1944

2 J.D. Achenbach , Wave propagation in elastic solids , North-Holand 1973

3 M.J.P. Musgrave , Crystal acoustics , Holden-Day , 1970

4. V.A. Shultilov, Fundametal physics of ultrasound , (trans. M.E. Alferieff) , Gordon and Breach Science Publishers , 1988

5. H. Seki, A. Granato and R. Truell , Diffraction effects in the ultrasonic field of a piston source and their importance in the accurate measurement of attenuation , J. Soc. Am. , 28 , 1956 , pp230-238

6. K. Kawashima , Theory and numerical calculations of the acousic field produced in metAl by an electromagnetic ultrasonic transducer, J. Soc. Am. , 60 , 1976 , pp1089-1099

7. L.F. Bresse and D. Hutchins , Transient generation by a wide thermoelastic source at a solid surface , J. Appl. Phys. **65** , 1989 , pp1441-1447

8. W. Sachse and Y. Poa , On the determination of phase and group velocities of dispersive waves in solids , J. Appl. Phys. 49(8) 1978

9. L.M. Brekhovskikh , Waves in layered media , New York , Academic Press 1960

10. W.M. Ewing, W.S. Jardetzky and F. Press , Elastic waves in layered media , 1957 , McGraw-Hill , New York

11. J. L. Rose and P.A. Meyer , Ultrasonic procedures for predicting adhesive bond strengths , Mat. Eval. , 31, 6 , 1973, pp109-114

12. P.A. Meyer and J.L. Rose , Ultrasonic attenuation effects associated with the physical modelling of adhesive bonds , J. Appl. Phys. , 48, pp 3705-3712

13. C.C.H. Guyott and P. Cawley , Evaluation of the cohesive properties of adhesive joints using ultrasonic spectroscopy , NDT International Vol **21** , No.4 , 1988 , pp233-239

14. P.N. Dewen and P. Cawley , An ultrasonic scanning technique for the quantitiative determination of the cohesive properties of adhesive joints , Rev. of Prog. in QNDE, (Ed. D.C Thompson and D.E. Chimenti) Plenum Press New York, 1992 , pp1253-1260

15. S.I. Rokhlin M. Hefets and M. Rosen , An ultrasonic interface wave method for predicting the strength of adhesive bonds , J. Appl. Phys. **52** 1981 pp2847-2851

16. A. Pilarski and J.L. Rose , A transverse wave ultrasonic technique for interfacial weakness detection in adheive bonds, J. Appl. Phys. , 63 , pp300-307

17. A.C. Smith and H. Yang, Ultrasonic study of adhesive bond quality at a steel-to-rubber interface by using quadrature phase detection techniques, Mat. Eval. , 47 , 1989 , pp1396-1400

18. H.G. Tattersall , The ultrasonic pulse echo technique as applied to adhesion testing , J. Phys. D: Applied Physics , Vol 6 , no.7 , 1973 , pp819-832

19. J. Szilard , Review of conventional testing techniques , in:Ultrasonic testing (Ed. J. Szillard) , John Wiley & Sons , New York , 1982 pp25-52

20. K. Kawashima , Experiments with two types of electromagnetic ultrasonic transducers, J. Soc. Am. **60** , No.2 , 1976 , pp365-373

21. S.I. Rohklin , Interface properties characterisation by interface and Lamb waves , Rev. of Prog. in QNDE , (Ed. D.C Thompson and D.E. Chimenti) ,Vol. 5B , Williamsburg, 1986, pp1301-1308

22. S.I. Rokhlin and D. Marom, Study of adhesive bonds using low frequency obliquely incident ultrasonic waves , J. Soc. Am. , 80 , 1986 , pp585-590

23. A.C. Bushell , The application of laser-generated ultrasound to the study of aluminium-epoxy bonded systems, University of Warwick Ph.D. Thesis , 1993

24. H. Lamb , Waves in an elastic plate , Proc. R. Soc. A **93** , 1917 , pp114-128

25. S.I. Rokhlin , Lamb wave interaction with lap-shear adhesive joints: Theory and experiment , J. Acoust. Soc. Am. **89** , 1991 , pp2758-2765

26. P.B. Nagi and L.Adler , Ultrasonic characterisation of dissimilar bonds, Rev. of Prog. in QNDE, (Ed. D.C Thompson and D.E. Chimenti) Plenum Press New York, Vol. 8B, 1989, pp3205-3213

27. R.J. Dewhurst , D.A. Hutchins , S.B. Palmer and C.B. Scruby , Quantitative measurements of laser-generated acoustic waveforms , J Appl. Phys. **53** 1992 , pp4064-4071

28. H.M. Frost , Electromagnetic-ultrasonic transducer : principles, practice and applications in: Physical Acoustics XIV , (Ed. WP Mason and RN Thuston), Academic Press, New York , pp179-275

29. D.A. Hutchins , M.D.C. Moles , GS TAylor and S.B. Palmer , Non-contact ultrasonic inspection of diffusion bonds in titanium , ,Ultrasonics **29** ,1991 , pp294-301

30. F. He , S.I. Rokhlin and L. Adler , Application of SH and Lamb wave EMATs for evaluating adhesive joints , Rev. of Prog. in QNDE , (Ed. D.C Thompson and D.E. Chimenti) ,Williamsburg, 1987 , pp911-918

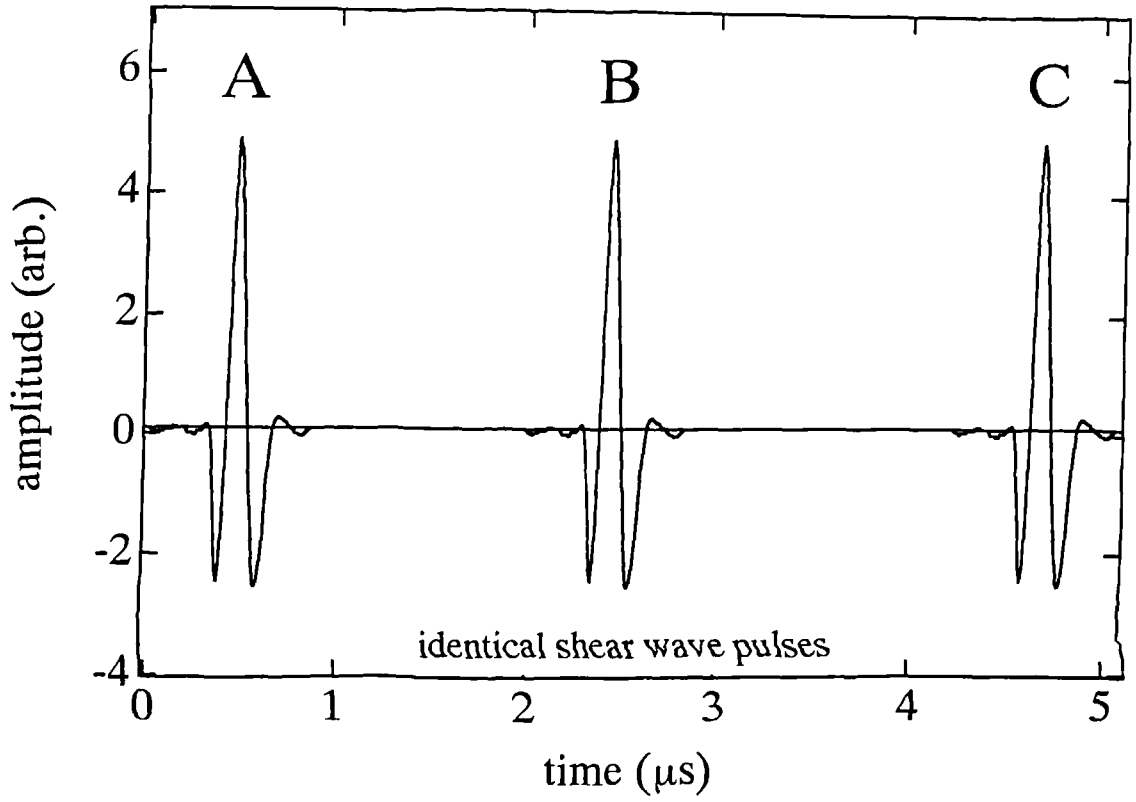

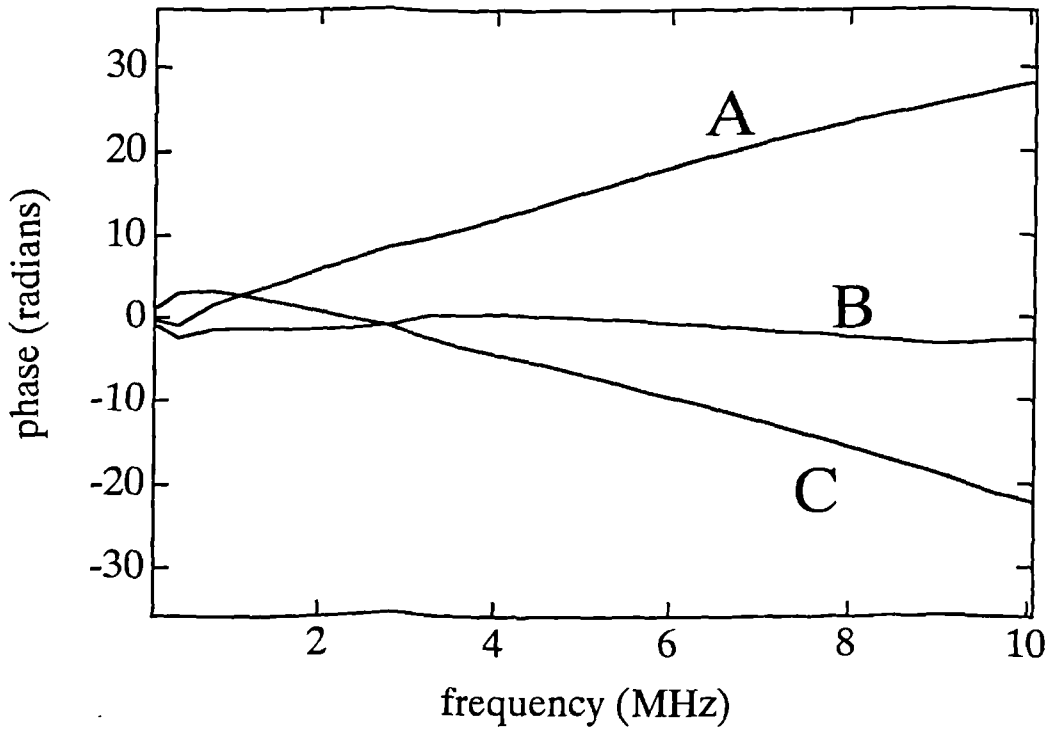

Fig 2.1

Calculated phase for a shear wave pulse in various positions within a window prior to the FFT.

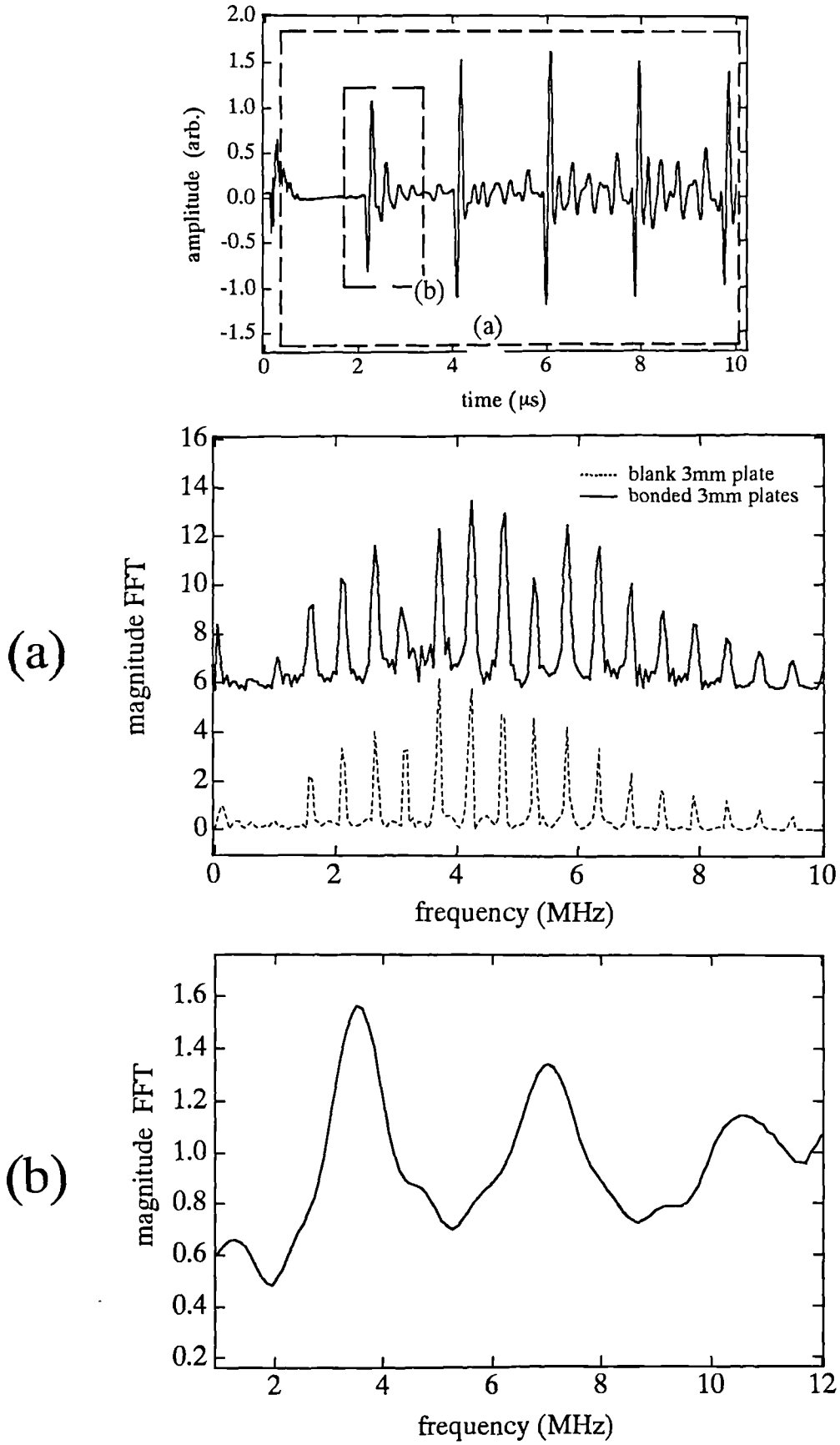

Fig 2.2

Comparison of magnitude FFTs of EMAT through transmission waveforms on a bonded sample with identical 3mm thick aluminium adherents and on a blank 3mm thick aluminium adherent.

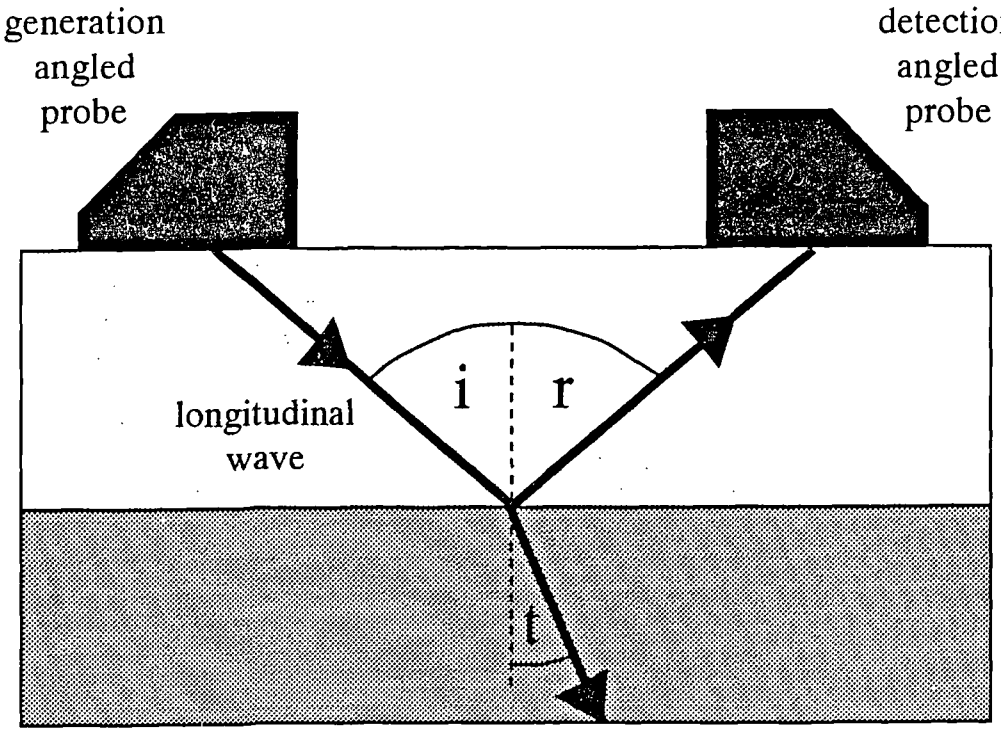

i=r

i - angle of incidence
r - angle of reflection
t - angle of transmission

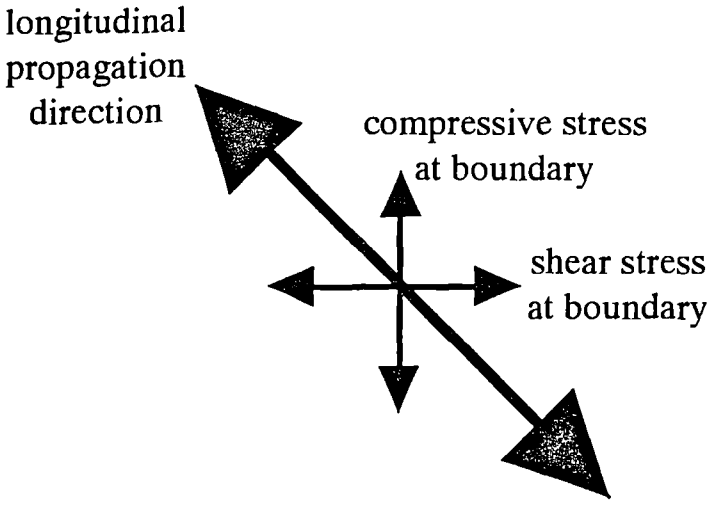

Fig 2.3

Schematic diagram of pitch catch ultrasonic technique in adhesive bond analysis.

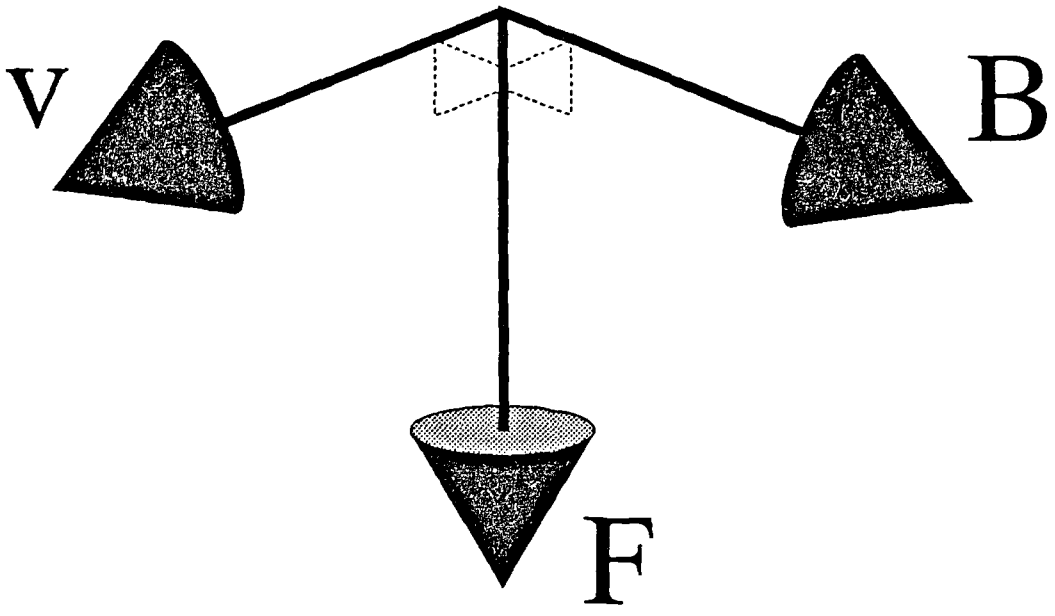

$$F = -q\,\underline{v} \times \underline{B}$$

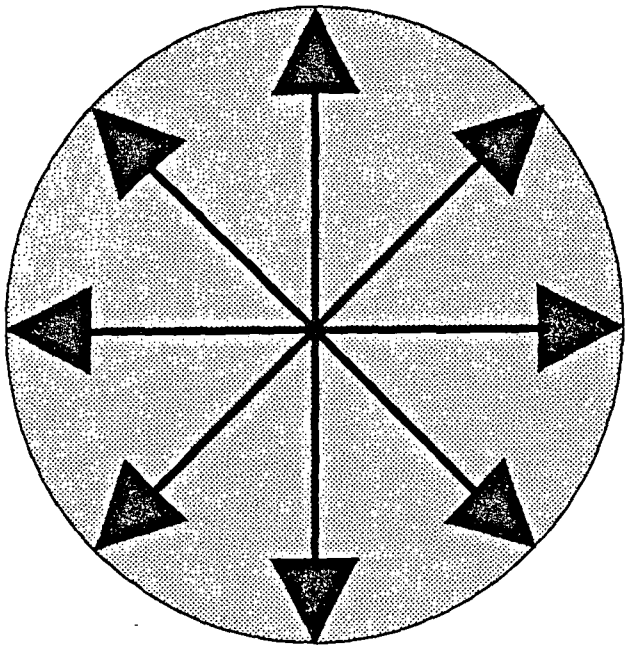

The stress field generated by the spiral coil EMAT is a radial force acting within the relevant electromagnetic skindepth of the metal surface.

Fig 2.4

Ultrasonic displacement of a radially polarised shear wave.

Chapter 3

Description of the EMAT systems and their characteristics

3.0 Introduction

EMAT systems employed in this project have a wide range of applications by virtue of the fact that radially polarised shear waves are generated in a non-contact regime. The analysis of adhesively bonded aluminium plates is a specific application where this type of EMAT is ideally suited to investigate the integrity of the bond. In order to gain a deeper understanding of both the transducer and supporting electronic circuitry, a range of characterisation experiments have been performed, such as preamplifier response and the EMAT electrical properties. The ultrasonic field generated by the EMAT has also been investigated, and compared with the results from simple theoretical models.

3.1 The EMAT system

The basic principals of EMAT operation have already been explained. In this section, results illustrating the properties of the specific EMAT systems used are described. This study was necessary because before absolute measurements (such as ultrasonic displacement) can be calculated, the response and characteristics of the system as a whole must be known.

In chapter 2 the construction of an EMAT was outlined. A more detailed cross-sectional diagram is shown in fig 3.1. The magnetic field is provided by a cylindrical disc shaped NdFeB permanent magnet (Magnetic Developments Ltd) of 7mm thickness and 25mm diameter. This is backed by a steel disc to decrease the demagnetising factor [1], providing an increase in the normal component of the static magnetic field from 0.3T (without the steel backing) to 0.35T (with the steel backing) at the surface of the magnet.

The field drops from 0.35T at the surface to 0.25T at a distance 1.1mm away from the surface. This distance is significant because it is equal to the thickness of the printed circuit board (PCB) , onto which the coil is etched.

The three main EMAT systems used are the single coil send-receive, the double coil send-receive and the through transmission setup of one EMAT generating and the other EMAT receiving. Schematics for these 3 methods are shown in fig 3.2 , where the arrows indicate the ultrasonic propagation directions for the shear waves that are detected by the EMAT. Where the EMAT is discussed in the proceeding sections, it is the single spiral coil etched onto PCB that is being referred to unless otherwise stated.

3.1.1 Basic properties of the EMAT

In terms of electronics the EMAT is basically an inductive component. There is of course a resistive element (of approximately 2 ohms), and a small stray capacitance, which can be measured. The generation of broadband ultrasound requires a sharp driving pulse (i.e. broadband) of current through the EMAT coil. The amplitude of the shear waves generated is proportional to the magnitude of the current pulse. Therefore looking at the EMAT as a generator, it is desirable to have a low impedance for a fixed voltage drive, as more current can be driven through the EMAT. At the same time as maintaining the low impedance, the coil should induce image currents within the metal sample surface. A larger image current gives rise to a larger stress amplitude. Thus, from one view point, the coil should have a low number of turns to maintain low inductance, but a high number of turns for generating the stress field. If the coil is also to be used as a detector, then the impedance of the coil should preferably be high, as the induced signal is proportional to the number of turns on the coil. As a result of these considerations the EMATs were constructed with these compromising factors in mind. It should also be noted that the amplifier input impedance should match that of the EMAT and both impedances should be close to 50 ohms for signal transmission down standard coaxial cable.

The EMAT and driving circuitry is shown schematically in fig 3.3. The EMAT is not a tuned circuit for the main frequency present in the driving current pulse: this is because efficiency (electrical to acoustic energy) is sacrificed for the acoustic broad bandwidth. The EMAT could be made into a more resonant circuit by the addition of a suitable capacitor across the coil. The value of the capacitor depends on the inductance of the coil and should be tuned to the main frequency present in the driving current pulse. The coil inductance in turn is modified by the electromagnetic properties of the metal surface in which the ultrasound is generated and also the standoff of the coil from this surface. The effect on impedance and phase of adding a 1000pf capacitor in parallel with the coil (against the metal surface) can be seen in fig 3.4a , on aluminium and steel. The resonant frequency and width of the resonant peak are quite different for the two different metals. The resonant frequency for aluminium is approximately 8.5MHz, higher than the most dominant frequency present in the drive pulse (6MHz), or the maxima in the preamplifier gain (5MHz). By adding a 2200pF capacitor in parallel with the EMAT coil, the EMAT was made more resonant, and the waveforms for this experiment are shown in fig 3.4b. Note that the 'tuning' of the EMAT yields larger amplitude signals. The disadvantage here is firstly that the electronic dead time at the front of the waveform is much longer and larger in amplitude - the drive pulse component picked up by the preamp was not being sufficiently damped. This is a problem commonly associated with tuned amplifier circuits. Secondly, the actual width of the pulse has increased, more than doubling. This is because the oscillations in the pulse are far from critically damped, so it is a larger number of oscillations, rather than actual pulse broadening.

The combination of inductance and capacitance in parallel (tuned EMAT) has a resonant maximum impedance. The larger the impedance of the coil, the higher will be the voltage signal is picked up by that coil, and from a fixed voltage drive source there will be a larger proportion of voltage over that coil compared to other impedance sources present in the circuit. The system is more complicated than may at first appear and needs to be considered as a whole for both generation and detection.

The impedance and phase variation with standoff for a single coil EMAT is shown in fig 3.5 , where the measurements have been taken for a frequency of 5MHz. It should be remembered that there is also an additional standoff not corrected for here due to the PCB thickness (reducing the static magnetic field) and the EMAT face cover (reducing both static and dynamic field).

The single EMAT coils were produced by etching a 16mm diameter spiral coil of 18 turns onto PCB. This was done to ensure reproducibility of the EMATs and durability of the coil. A PCB track coil is more efficient than a wire coil of equal resistance and length due to the tracks being much broader than they are thick on the PCB. At the frequencies present in the ultrasonic pulse (approximately 1-10MHz), the skin depth in the current carrying wire becomes an important consideration as ac current will only flow within the skin depth. Thus a flat strip of conductor is more efficient ac conductor than a round thicker wire of equal dc resistance, as the flat coil has a larger surface area to volume ratio. The rear of the PCB was left unetched to provide an electromagnetic field screen between the coil and the magnet, reducing unwanted ultrasonic generation in the magnet as it is an electrical conductor. For scanning samples in the lab, the coil faces were protected by a 100μm thin layer of plastic sheet. If the EMATs were to be used in more hostile environments of for example, high temperature, then materials such as a thin ceramic disc or mica have been employed in protecting the EMAT face.

The double coil EMATs were produced by winding two coplanar, concentric coils, on the copper free side of unetched single sided PCB. (Wire was used as the manufacture of two concentric coils with connections on PCB was too problematic without using specialist techniques and equipment). The inner coil has a radius of 5mm of 18 turns. The outer coil has 11 turns and an inner radius of 5mm and an outer radius of 8mm. The particular gauge of wire used (0.2mm diameter) proved to give good performance in both detection and generation modes. The coils shared a common earth and were fixed onto unetched single sided PCB. The coil was wound on the bare face of the PCB, with the copper plane again on the rear face providing an electromagnetic shield between coils and magnet. Coils were also wound directly onto thin copper foil (100μm thick), in an attempt to reduce

standoff of the static magnetic field. It was found that this significantly reduced the EMAT sensitivity, despite the fact that permanent magnet - coil separation was reduced. The reason for this was that more energy from the drive pulse was lost in generating eddy currents in the copper foil. The advantage of the double coil is that it can be used in conjunction with most ultrasonic flaw detector units, if the signal from the detection coil is boosted by a pre-amplifier.

3.1.2 Waveforms obtained using EMATs

Waveforms obtained in send-receive, through transmission and with the double coil send-receive EMATs are shown in figs 3.6a, 3.6b and 3.6c respectively. All the waveforms show 3 characteristic mode converted signals between the larger shear wave pulses. These arise as initially, the EMAT generates a small longitudinal component along with the larger shear component, and on subsequent echoes the ultrasound can mode convert at a free surface(see section 2.4.2). The send-receive waveform has a much longer paralysis time than through transmission at the front of the waveform since the same coil is used in generation (roughly 800V pulsed the across coil), and in detection (roughly 10μV across the coil). The double coil waveform also suffers from a paralysis of approximately a 2.5μs as detection and generation coils are in close proximity. The waveform was recorded with and without a bandpass filter on the output of the preamplifier. The filter serves as to take off the low frequency droop at the front of the waveform, but as can be seen makes the system slightly more resonant. The through transmission waveform has a paralysis time of less than 0.25μs, and typically much better signal to noise characteristics. This is however the most impractical of the 3 techniques requiring access to both sides of the sample and accurate central alignment.

3.1.3 The EMAT as a velocity sensor

The EMAT operates via a Lorentz mechanism. At first glance, it may seem obvious that the EMAT is a velocity sensor, but care is needed for a complete understanding. Authors will generally talk about eddy currents generating ultrasound, and while this is not untrue, it is inaccurate. An ultrasonic wave in a metal is the result of coherent displacements of the atoms (or ions), in the metal. In the following argument, it is useful to think of a nearly free electron model, where the electrical properties of the metal are due to the Fermi electrons, and these interact with the lattice 'ions' via a Coulomb force.

The first point to note is that the velocity of the electrons responsible for 'current' is the Fermi velocity $\sim 10^6$ ms^{-1}. This is much faster than any ultrasonic velocity, and thus it is not possible to ultrasonically induce a net uneven charge distribution (considering both positive ions and electrons). Thus, both the electrons and the lattice 'ions' (or atoms) must be considered in any argument pertaining to the operation mechanism of an EMAT. Bearing this mind, generation and detection are discussed separately, making suitable approximations in the mathematical derivations. Both these processes can in theory be described in one general argument, as they are in effect reciprocal processes. A more thorough derivation of the general case would yield the same results, and this has been shown by Dobbs [2]. The following arguments are specific to the EMATs used (operating on isotropic metals), but can readily be adapted to other EMAT geometries.

3.1.3 a) Generation - The process of generation of ultrasound using an EMAT must have the end result of inducing a force on the positive ions (or atoms) in the metal, as 'ultrasound' is the coherent motion of these ions. In generation, the coil is pulsed with a current spike. Electrodynamic boundary conditions must be preserved (Maxwells equations), so as the coil is close to the surface of the metal, a resultant image current is generated in the surface of the metal. This current will be effectively contained within a range of electromagnetic skin depths, as there is a range of frequencies present in the driving current pulse.

The skin depth, δ is given by,

$$\delta^2 = \frac{2}{\omega \mu \sigma}$$

where ω is the angular frequency of the electromagnetic wave incident on the metal, μ is the relative permeability of the metal, and σ the conductivity of the metal. For aluminium $\mu=1$ and $\sigma=4 \times 10^7\ \Omega^{-1}m^{-1}$. The frequency of the electromagnetic radiation corresponds to either the frequency of ultrasound incident at the surface in detection, or the frequency of the driving current pulse through the EMAT coil in generation. As the EMATs used here generate / detect broadband ultrasound, then there is a range of frequencies and thus skin depths to consider.

In aluminium, for frequencies of 1MHz the skin depth and shear wave wavelength are 0.089μm and 3.1mm respectively, and at 10MHz are 0.028μm and 0.31mm respectively. It can be seen that over the range of frequencies present within the ultrasonic pulse, the skin depth is much less than the ultrasonic wavelength for that particular frequency (<1% at 10MHz). Thus, the generation processes effectively take place on the surface of the metal - it is not a buried source. This is also the case when pulsed lasers are used to generate ultrasound in metals (via a similar skin depth argument) [3].

The image current in the metal is due to a spiral, or approximately circular electric field line. The 'free' electrons and the metal cations experience the same force (assuming there is one 'free' electron per atom), in opposite circular directions. Ions having much more inertia however, are not accelerated as greatly as the electrons, resulting in the only significant motion of charge (+ or -) being that of the electron eddy current. The ions do however experience a torque, which will generate a weak torsional shear wave component. The circular movement of the electrons does not change the net charge density within any region, but this motion in a perpendicular magnetic field gives rise to a radial force on the electrons. The radial force on the ions due to their relatively low velocity is negligible. The electrons are therefore accelerated radially. It is this radial motion of the electrons that

induces radial stress in the sample via a Coulomb interaction, as it is affected in such a way as it attempts to change the net charge density.

Considering the annulus of current shown in fig 3.7a. The current density is the same for any size of annulus over the area covered by the coil. As the Lorentz force on the electrons accelerates the electrons radially (say outwards), then the electron charge density decreases in the skin depth. If the initial radius of the annular element was ' r_0' prior to pulsing the current, and at some time later the annulus has radius 'r' then the drop in the free electron density would be a factor of 'r/r_0' . This change in charge density sets up a radial electric field and thus induces a radial force on the ions via a Coulomb force. The radial displacement of the electrons is counteracted by the Coulomb force in the opposite direction to the Lorentz force. The radial stress generated in this process generates a radially polarised shear wave where the plane of vibration is perpendicular to the direction of propagation as shown in fig 3.7b.

The resulting ultrasonic field distributions for with the thermoelastic laser source - a good means of generating shear waves has been calculated [10] using a Greens function. The stress field generated by the EMAT, is not the same as would be generated by a finite thermoelastic laser source. The net resultant force for a laser source of constant energy density profile is a ring of force at the beam edge, while the EMAT induces a (roughly) uniform radial force over the area covered by the coil. The calculation of a ring force in the Greens function is a more straightforward calculation than the uniform EMAT induced radial stress. The field generated by an EMAT spiral coil has been specifically calculated by Kawashima [4] - a very involved mathematical derivation, and as such there is little point in reproducing the formula here. It is worth noting that this detailed analysis did predict the mode conversion for the shear wave mode to a longitudinal mode at normal incidence, as seen experimentally.

3.1.3 b) Detection - Consider the situation where a radially polarised shear wave has been generated by some means, and it is to be detected using an EMAT. As the wave propagates, there is a motion of the atoms in the lattice normal to the direction of propagation. The ions or atoms, have much more momentum than the electrons. The displacement of the ions causes changes in the local ion density. The Coulomb interaction 'drags' the electrons along, so as to keep the net charge density in any region constant. Thus, the electrons can cause a damping of the ultrasound, which is discussed in the general case by [6]. The electrons are therefore moving in phase with the ions. When this motion occurs in a static magnetic field parallel to the direction of shear wave propagation, both the electrons and ions experience a torque of opposite polarity. The ions have much more inertia (due to mass and interatomic forces) than the electrons, so that only the electrons give rise to a circular eddy current. The motion of this current once again, can occur without any change in local electron density, and is not impeded by a Coulomb interaction. It is this current that is detected by the EMAT coil. The actual signal induced in the coil can be thought of as an image current as described above in the generation process, or by considering the amount of magnetic flux from the eddy current that cuts the coil, inducing an E.M.F. Both these viewpoints are of course simply different approaches to exactly the same phenomena.

The mathematical proof that the EMAT is a velocity sensor has been demonstrated by Kawashima [6], using Fourier analysis to integrate the cw single frequency components into a broadband signal for a specific coil geometry. The same proof can be applied to a general case if a simple approximation is made. Using the notation of Kawashima -

The displacement , s , of the ultrasound wave propagating in the direction of increasing z is given by the standard equation,

$$S_{(t,z)} = S_0 e^{i(\omega t - kz)} \qquad 3.1$$

the displacement at the free surface of the metal ξ is,

$$\xi = S_0(e^{-ikz} + e^{ikz})e^{i\omega t} \quad 3.2$$

the current density at the surface J can be written,

$$J(z) = \sigma \frac{\delta \xi}{\delta t} B_0 \quad 3.3$$

$$J(z) = i\omega\sigma S_0(e^{ikz} + e^{-ikz})e^{i\omega t} \quad 3.4$$

as the current flows within the skin depth δ for a particular frequency,

$$z \leq \delta \quad 3.5$$

giving the condition below, where k is the wavenumber of the ultrasound wave,

$$k\delta << 1 \quad 3.6$$

by expanding the exponential terms $(e^{ikz} + e^{-ikz}) \approx 2$ 3.7

yielding the equation,

$$J \approx \sigma i\omega \times 2S_0(t,0)e^{i\omega t} \quad 3.8$$

and finally re-writing as :-

$$J \approx \sigma \frac{\delta}{\delta t}(S_0(t,0)) \quad 3.9$$

thus demonstrating that the EMAT is a velocity sensor. This result hinges on the fact that the spatial extent of the observation window of the ultrasonic arrival (the skin depth), is

much smaller than the wavelength of the shear wave in the direction of propagation. The measurement is effectively a point measurement on the waveform in velocity terms, rather than a section of the waveform.

Now that the idea of the EMAT being a velocity sensor has been established, the shape of the observed signals can be explained. Both amplifier and EMAT response need to be considered. For the present argument amplifier response is neglected. The voltage induced in the EMAT coil is the differential of the displacement at the metal surface. If a Gaussian form for the inplane displacement is assumed, the observed signal should be its differential, as shown in fig 3.8. If the displacement and velocity signals are then Fourier transformed, the ratio of these transforms is a linear relationship. This can be explained by considering one frequency component of the displacement, of the form say $A\cos(\omega t)$, for which the differential or velocity component is therefore $-A\omega\sin(\omega t)$. In terms of the FFT magnitude, the velocity has the higher frequencies enhanced by the factor ω.

3.1.4 EMAT - sample stand-off considerations

EMAT standoff characteristics have been studied by Maxfield et al [7] and Alers et al [8], on both aluminium (which is non-magnetic) and ferromagnetic steel . The theory for the standoff on steel is much more complicated than that on aluminium due to the magnetic properties of steel. Experimental stand-off measurements were made using two transducers, one fixed, the other free to move on epicentre on the other side of an aluminium sample. The drop in amplitude with increased stand-off is exponential (see fig 3.9) , as theory predicts . If one transducer is used in send-receive, the stand-off decay follows that seen in the through transmission experiment, except the decay factor is doubled (ie decay rates go from e^{-ax} goes to e^{-2ax}, where a is a constant and x distance). Thus, it can be seen that a small change in standoff can greatly affect the signal amplitude. In a lab environment, the standoff can be carefully controlled, the most easily implemented situation being 'zero', or rather minimum standoff. This is the easiest consistent setup to maintain, while of course having the advantage of maximising the signal. In a general 'on-site' situation however, the

transducer - sample separation may not remain constant. Obviously, this can be accounted for by monitoring the relative signal amplitudes in a waveform, rather than monitoring the absolute amplitude of one particular ultrasonic pulse. An alternative approach would be to measure the inductance of the EMAT and use it to normalise any acoustic amplitude measurements. This requires calibration for the particular metal type and EMAT, but has the advantage that it yields a measure of the standoff completely independent of the acoustic measurements.

Another factor that will be influenced by standoff is the sensitivity variation across the coil. Simple theoretical models were used to calculate the sensitivity and these are shown in fig 3.10a with their corresponding equations. The dynamic or pulsed magnetic field was approximated by two adjacent 2-dimensional current strips with the current running anti-parallel in each. The static field was modelled by the monopole assumption and the function obtained was numerically evaluated on a PC. Thus the theoretical variation in coil sensitivity was derived and is also plotted fig 3.10a. Specific dynamic and static field theoretical characteristics are shown in figs 3.10b and 3.10c.

Fig 3.10a indicates that increasing the standoff should have the effect of making a point of the coil between the centre and the edge more sensitive than the centre or edges of the coil. In absolute terms of course it will be less sensitive for increased stand-off, and the coil will always have some degree of standoff via the protective face. Results obtained from scanning small diameter flat bottomed holes would seem to indicate that the predicted sensitivity is observed (see chapter 4), but due to the complex nature of scattering from such a geometry, the measurements presented are qualitative.

3.1.5 EMAT electrical impedance

EMAT signal amplitude will decrease with increased stand-off, as both the normal static magnetic field and the dynamic field at the surface of the sample will decrease. There is also the question of the electronic characteristics of the EMAT coil to consider. The presence of a conducting body near to an inductive load will change the inductance of the

coil - a metal detector operates on this principle. Thus, the frequency spectrum generated by the EMAT, and the efficiency due to inductive changes must be considered. There will always be some trade-off between signal amplitude and frequency content. In this project the EMAT system has been designed for its broadband nature rather than the increased ultrasonic sensitivity that would be obtained with resonant electrical signals. The reason that the frequency content of an observed ultrasonic signal is dominated by a particular frequency is due to the natural resonance of the current discharge circuit and the frequency dependant gain of the preamplifier circuit. Thus, the ultrasonic signal is bound to have a dominant frequency corresponding to the resonance of the drive circuit. As the impedance is larger for higher frequencies, it is easier to drive the lower frequency pulses through the coil and thus generate the lower ultrasonic frequencies.

The frequency dependent phase and impedance of the coil were measured using an impedance meter. The EMAT impedance was found to vary approximately linearly from 0.5-20MHz (see fig 3.11). This first of all shows that the load is almost entirely inductive (gradient of $2\pi L$) below 20MHz, which gives a corresponding coil inductance of about 1.1μH for an isolated EMAT and 0.56μH against an aluminium plate. Calculating the stray capacitance of the coil by fitting to the impedance and phase shift data would give a very inaccurate value. Measuring the resonant frequency of the EMAT gives a value of capacitance of 8.2pF +/- 2pF for both EMAT locations. Most of this stray capacitance when connected to the driver/receiver circuitry is due to capacitive effects between adjacent coils in the EMAT, but some will come from the capacitance of the coaxial cable that connects the EMAT to the current driver. It has been observed that the length of coaxial cable used can affect the amplitude of the ultrasonic signals.

The EMAT could be made much more efficient by driving it with a resonant tone burst pulse, and this is how the earlier EMAT systems were driven. This can be best achieved by the addition of an appropriate capacitor in parallel with the coil in the EMAT. This maximises EMAT impedance for the particular driving frequency used. Even by driving the coil with the broadband pulse, significant signal amplitude increases (and signal broadening) can be obtained by tuning the EMAT to the dominant frequency present in the broadband

pulse. Tuning effects could be employed in situations where the signal amplitude is more critical than the broadband nature of the ultrasonic pulse, but this is not the case in the analysis of adhesive bonds, where it is desirable to have sharp, broadband pulses in order to resolve acoustically thin bondlines.

3.2 Ultrasonic field generated by the radially polarised EMAT

Measurement of the acoustic field produced by a shear wave EMAT is considerably more difficult than measuring the field produced by a longitudinal source [4]. Ideally, the transducer used to map out the field should be point like and measure the in plane shear component only. In principal it would be possible to measure the out-of-plane component associated with the shear wave arrival and work back to the shear wave field from the stress free boundary condition at the surface. This would be a mathematically and computationally involved procedure and is beyond the scope of this thesis, and probably its author. So, the measurement was limited to the shear wave component. Suitable transducers for such an experiment include the shear wave piezoelectric transducer and linearly polarised EMAT or an appropriate interferometer [9] that detects in plane motion. An EMAT can be easily apertured using metal foil, reducing the coil area and therefore signal, but increasing the spatial resolution. A small shear wave piezoelectric transducer could be used but would have a resonant bandwidth, and be subject to coupling considerations. Whichever transducer is used, the deconvolution for the transducer shape, size and frequency response would not be trivial. A horizontally polarised EMAT was apertured {3mm coil length, 10 turns within a coil width of 1mm} and fixed to the surface, while the radially polarise EMAT was scanned along a line across the centre of.the linearly polarised EMAT as shown in fig 3.12. The amplitude of the observed signal was corrected using simple trigonometry to take account of the fact that the ultrasonic field was circular while the measuring transducer was a linearly polarised device.

The absolute shear wave amplitude was not directly measurable using this method, but this measurement is useful in showing (within experimental accuracy) that the EMAT produces an effectively plane wavefront in terms of the acoustic arrival time (see fig 3.13a) , over the area covered by the coil. The discontinuity in the experimentally recorded arrival time on crossing the centre of the radial EMAT field reflects the polarity change in the observed ultrasonic signal: the ultrasonic displacement are in opposite directions either side of the centre of the radial EMAT. The uniform arrival time across the wavefront ensures that the peak-peak separations in the EMAT obtained waveforms are constant (in non-disperive media) This is illustrated in the waveform (in a 12.50mm thick isotropic aluminium disc) of fig 3.13b, where the peak-peak separation is constant. The shape of the pulse does change however and this could be due to either dispersion in the aluminium or some geometrical effect. A single crystal of aluminum was examined using an EMAT, generating in the (100) plane. The waveform is shown in fig 3.13c with the two pulses taken from extreme ends of the waveform, which appear much closer in shape, suggesting that it is dispersion giving rise to the differing pulse shapes of fig 3.13b.

From the measurements made on the EMAT acoustic field, the approximate ultrasonic displacement has been estimated. Dobbs [2] gave an expression for the theoretical displacement that could be generated by a pulse of current. In calculating the displacement, Dobbs neglected the fact that the ultrasound would be generated by a finite size transducer, subject to a time dependant current pulse. Once again, a thorough treatment would involve finding solutions to Greens functions. Nevertheless, the theory demonstrates the factors that influence the magnitude of displacement. The theoretical displacement field calculated as described in section 3.2.2 is shown in fig 3.14.

The equation for the displacement is shown below,

$$|\xi| = \frac{\sigma B B_0}{\rho v \omega} \cdot \frac{1}{\sqrt{1+\beta^2}} \qquad 3.10$$

where β is given by,

$$\beta = \left(\frac{\omega}{v}\right)^2 \cdot \frac{\delta^2}{2} \qquad 3.11$$

In the above v is the ultrasonic wave velocity, ω the angular frequency, ρ the density of the metal, δ the electromagnetic skin depth of the metal B the magnitude of the dynamic magnetic field at the sample surface and B_0 the magnitude of the static magnetic field at the sample surface.

In calculating the displacement, Dobbs neglected the fact that the ultrasound would be generated by a finite size transducer, subject to a time dependant current pulse. Once again, a thorough treatment would involve finding solutions to the appropriate Greens functions. Nevertheless, the theory demonstrates the factors that influence the magnitude of displacement. The displacement obtained from the above equation using suitable values corresponding to those used in the experiments here yields a value of ultrasonic displacement of 4nm .

The values used here were ,

1) a peak current through the coil of 20A, at a distance of 200μm from the sample giving a peak dynamic magnetic field of 0.02T (using Amperes law).

2) a static magnetic field of 0.3T (measured using a Hall probe)

3) an electrical conductivity of $4 \times 10^7\ \Omega^{-1}m^{-1}$, and skin depths of 0.09μm at 1MHz and 0.03μm at 10MHz in aluminium.

3.2.1 Theoretical field and waveforms

The estimation of the ultrasonic field generated by a radially polarised EMAT required the Greens function solution to time and spatial response of the EMAT. The turns on the EMAT coil can be considered to be a number of concentric rings of force. A thermoelastic laser source behaves as a single ring of force when the laser beam has uniform intensity. The solution to the ultrasonic in-plane displacement generated by such a source

was calculated by Bresse and Hutchins [10] with a Heaviside time dependance for the laser pulse. The first approximation to obtaining the displacement solution for the EMAT is to take a finite number of ring sources to describe the stress field generated by the EMAT. A total of 8 ring sources were used, with radii increasing successively by 1mm from 1mm to 8mm. The waveform response within the bulk was then calculated as a function of radial displacement at a distance of 4.8mm from the surface on which the generation occurs. The experiment measured the dynamic response at a free surface 4.8mm normal distance from the source (the blank adherent plate thickness).This measurement will slightly differ to that in a bulk medium 4.8mm away from the source, which is what is really being calculated by the theoretical approximation used.

The waveforms thus obtained were then differentiated once, to obtain the response from a delta function as oppose to a Heaviside step. This was then FFT'd and convolved with a function that approximately described the frequency content of the ultrasonic pulse. The convolved waveforms were then inverse FFT'd and then differentiated to yield velocity signals. The waveforms show some spurious features, arising from the numerical calculation and differential routines. The main pulse is clearly visible (see upper plot of fig 3.15) and demonstrates that the arrival time of the pulse maximas are constant, which is consistent with the experimental maxima arrival data in fig 3.13a. Experimentally measured and theoretically estimated signal amplitudes are shown in the lower graph of fig 3.15. Theory and experiment show reasonable agreement, but the most noticeable difference is the extended 'tail' on the theoretically obtained plot. This could possibly be due to the fact that the theory takes no account of the random background noise that is observed on the experimentally obtained plot (at a level of about 0.5 units - 1/5 of the maximum amplitude).

3.3 Pre-amplifier response - gain and phase relations

It is necessary to cover the subject of pre-amplifier response in order to provide a more complete investigation. Once the preamplifier and EMAT responses are known , the shape of the detected signals can be calculated and explained. The phase and gain characteristics of the amplifiers used are shown in figs 3.16. The first preamplifier type is that used in a

through transmission geometry, while the second is that used in the send-receive system. Both these pre-amps use the same low noise, wide bandwidth operation preamplifier chips, but are configured differently, due to the different operating conditions. The graphs show that the pre-amp used for the send-receive EMAT has the larger phase shifting response. Taking a pulse obtained in plain aluminium plate, and correcting for the effects of amplification, yields the pulse shown in fig 3.17. This shows directly how the signals observed in through transmission and send receive would roughly correspond to a bipolar velocity signal, and thus to Gaussian form for the displacement generated by the EMAT.

3.4 Signal modulation of EMATs waveforms

Waveforms on the send-receive system are subject to a modulation that deviates from the expected exponential decay. In send-receive, this envelope is associated with the partial preamplifier paralysis towards the beginning of the waveform, directly after the generating pulse. The modulation is shown on a plain aluminium plate, identical to those used in the bonded samples. Some of the modulation present in the waveform is due to energy loss during mode conversion, coupled with the predicted exponential decay. Fitting later pulse amplitudes in the waveform yields an exponential decay. This decay is different from the pure decay due to propagating a finite distance due to the mode conversion contribution.

By inducing a continuous 5MHz wave into the 'free running' send-receive EMAT and driver / amplification circuit, a more detailed modulation envelope can be measured. As the bulk of the acoustic energy is around 5MHz, and amplifier responses do not have large variations around this frequency, it is assumed that the modulation envelope for a waveform is the same as that observed in the 5MHz cw case. The envelope is shown in fig 3.18, along with the relevant amplitude modulation.

Taking a waveform directly from the amplifier, then deconvolving with the modulation function yields the waveform shown in the lower plot of fig 3.18. This appears to account for some of the observed modulation, but is still not exponential. Some of the modulation is probably due to the inhomogeneous nature of the plane wave front generated by the EMAT.

3.5 Summary

Any system that is to be used to obtain quantitative experimental measurements requires a thorough understanding of its characteristic behaviour. The results presented in this chapter indicate that the ultrasonic field generated by the EMAT is not plane-wave-like over the area covered by the transducer. The field profile has been established, and the observed velocity signal amplitude appears to correlate well with that obtained theoretically. Correcting for the amplifiers response, and examining the EMAT signals would suggest that the induced ultrasonic displacement is roughly Gaussian. It has also been demonstrated how the EMAT bandwidth can be sacrificed for sensitivity simply by tuning the EMAT to the dominant frequency present in the drive pulse.

Ch. 3 References

1 J. Crangle , Solid State Magnetism , Edward Arnold 1991 pp157-158

2 E.R. Dobbs , Electromagnetic generation of ultrasonic waves in: Physical Acoustics X , (Ed. WP Mason and RN Thuston), Academic Press, London , pp127-189

3 J.D. Jackson , Classical Electrodynamics , John Wiley & Sons, New York 1962 pp296-298

4 K Kawashima , Theory and numerical calculation of the acoustic field produced in metal by an electromagnetic ultrasonic transducer , J. Acoust. Soc. Am. **60** , 1976 , pp1089-1099

5 N.W. Ashcroft and N.D. Mermin , Solid State Physics , Holt ,Rinehart and Winston, 1976

6 K. Kawashima , Quantitative calculation and measurement of longitudinal and transverse ultrasonic wave pulses in solids , IEEE Trans. Sonics Ultrason. **SU-31** , No.2 , 1984 , pp83-94

7 B.W. Maxfield , A. Kuramotot and J.K. Hulbert , Evaluating EMAT designs for selected applications, Materials Eval. **45** , No.10 , 1987 , pp 1166-1183

8 G.A. Alers and L.R. Burns , EMAT designs for special applications , Materials Eval. **45** , No.10 , 1987 , p 1184-1189

9 J.-P. Monchalin , Optical detection of ultrasound , IEEE Trans. Ultrasonics , Ferroelectrics and Frequency Control , **UFFC-33** , 1986 , pp485-499

10 L.F. Bresse and D. Hutchins , Transient generation by a wide thermoelastic source at a solid surface , J. Appl. Phys. **65** , 1989 , pp1441-1447

EMAT Cross Section

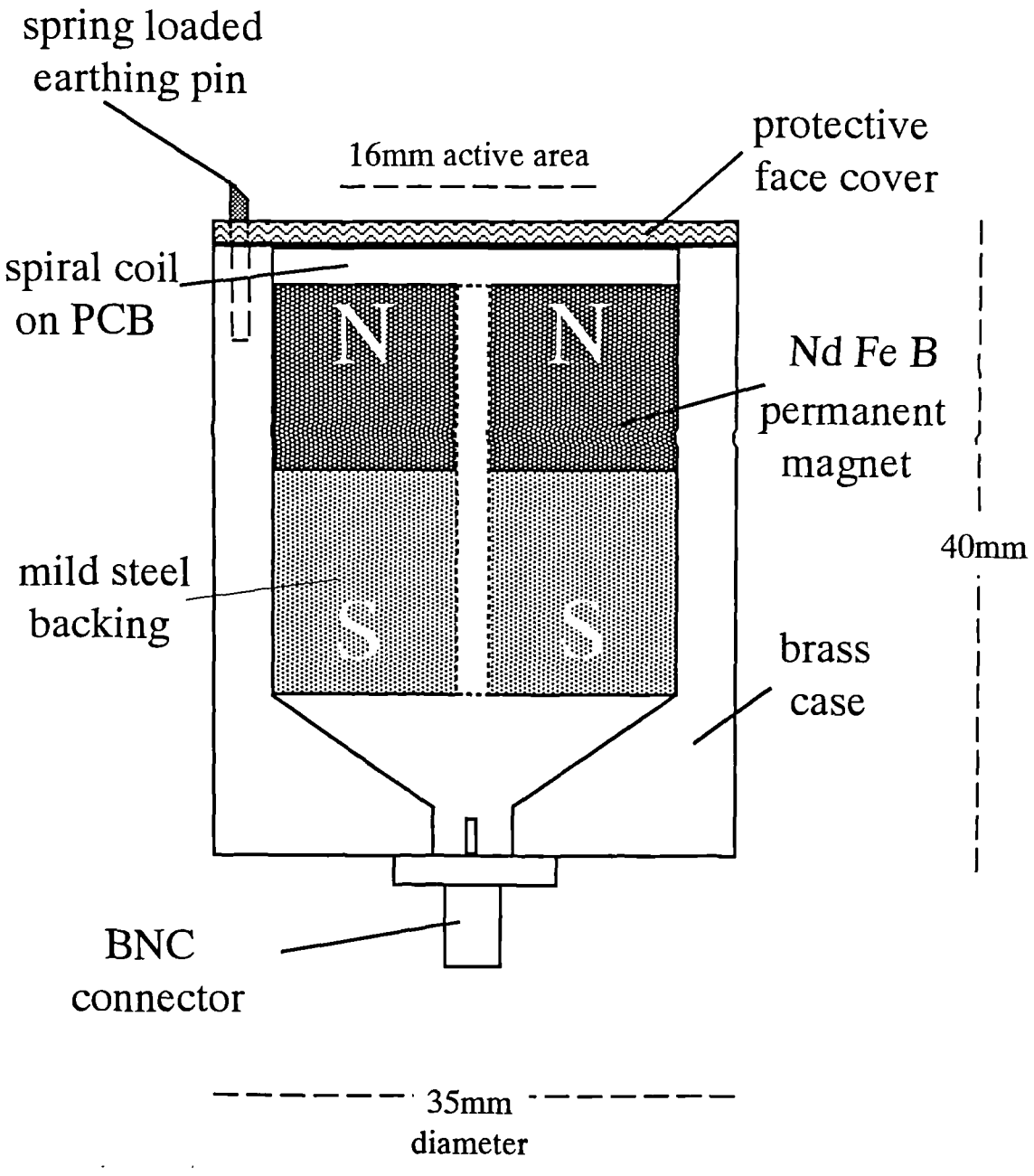

Fig 3.1

Cross sectional diagram of the radially polarised EMAT.

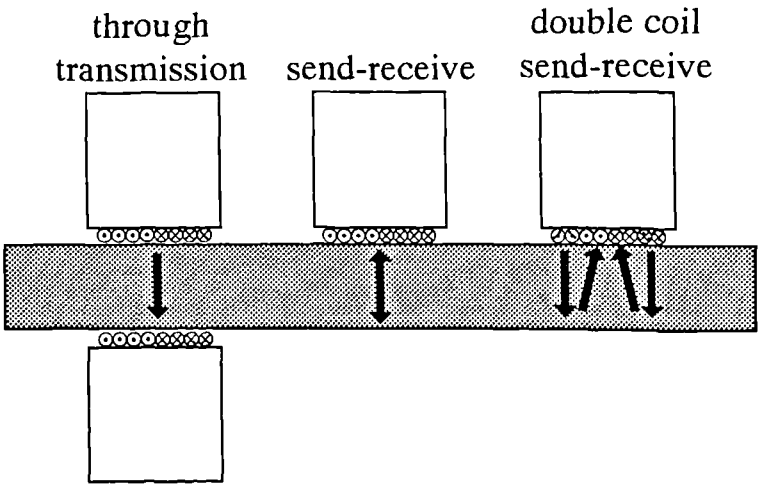

Fig 3.2

Through transmission, send-receive and double coil EMAT experimental geometries.

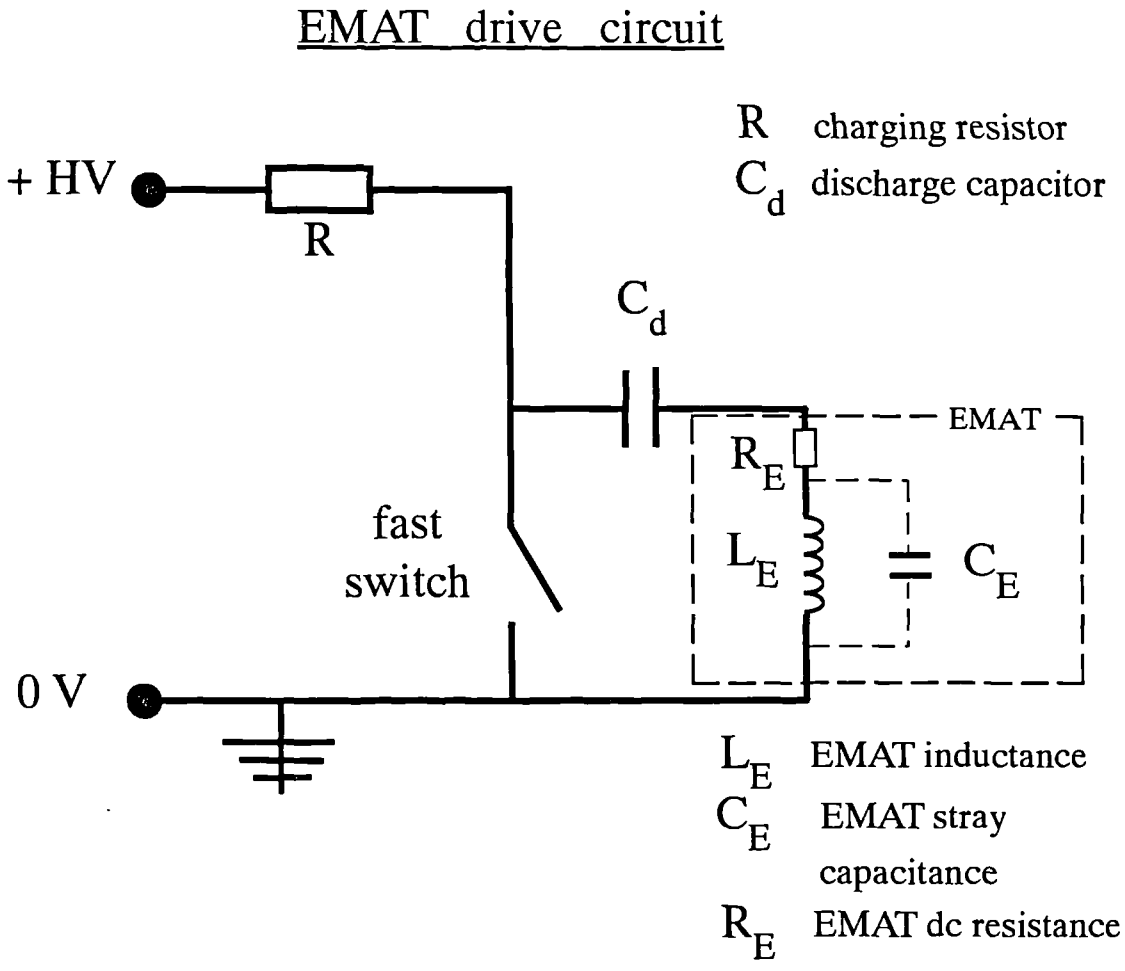

Fig 3.3

The EMAT current driver circuit.

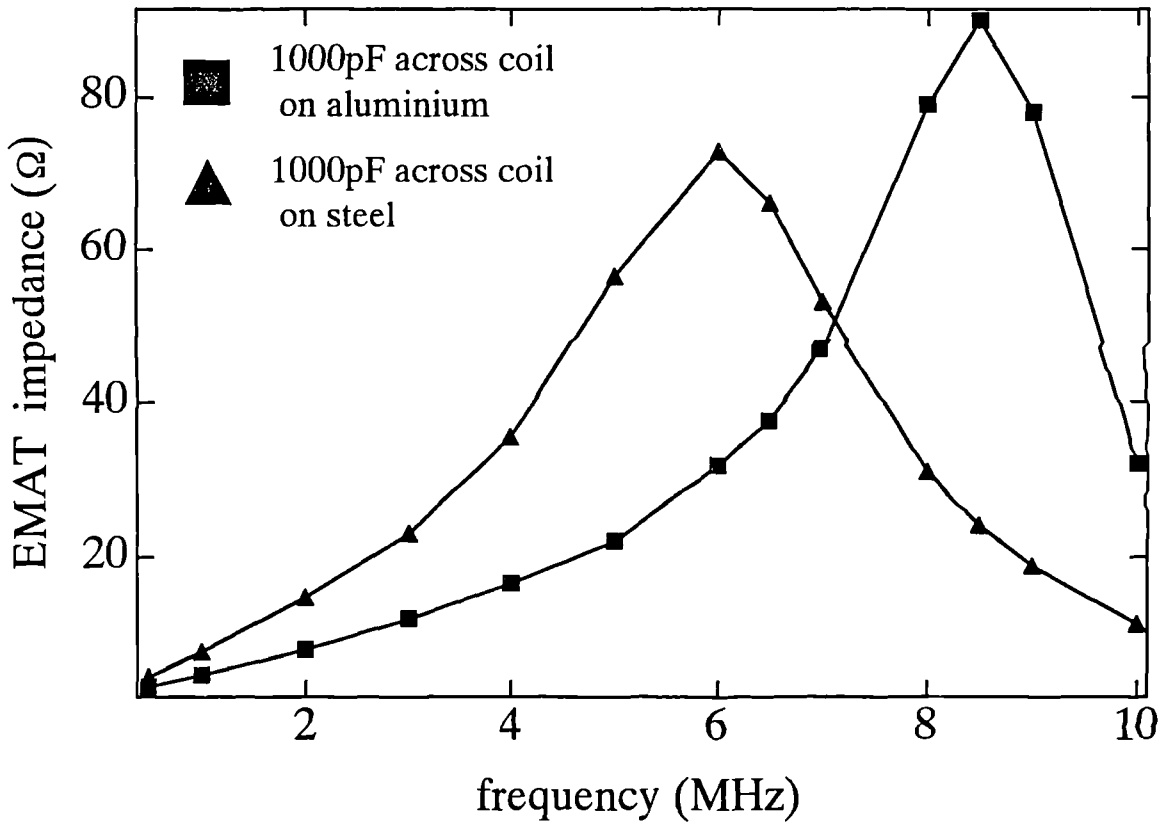

Fig 3.4a

The effect on electrical impedance of adding a 1000pF capacitor in parallel with the EMAT coil for operation on mild steel and aluminium.

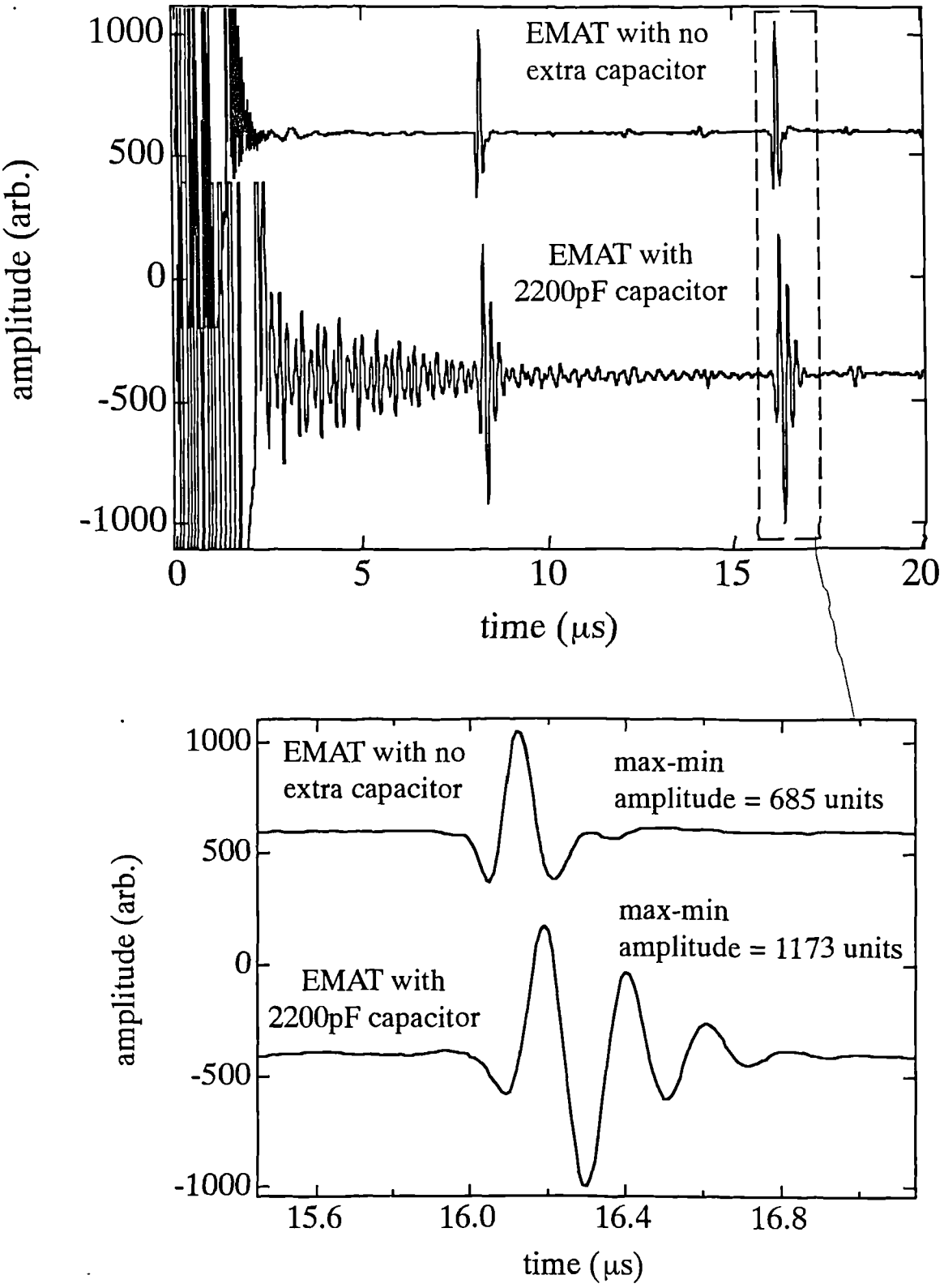

Fig 3.4b

Comparison of send-receive waveforms on aluminium with and without the addition of a 2200pF capacitor in parallel with the EMAT coil.

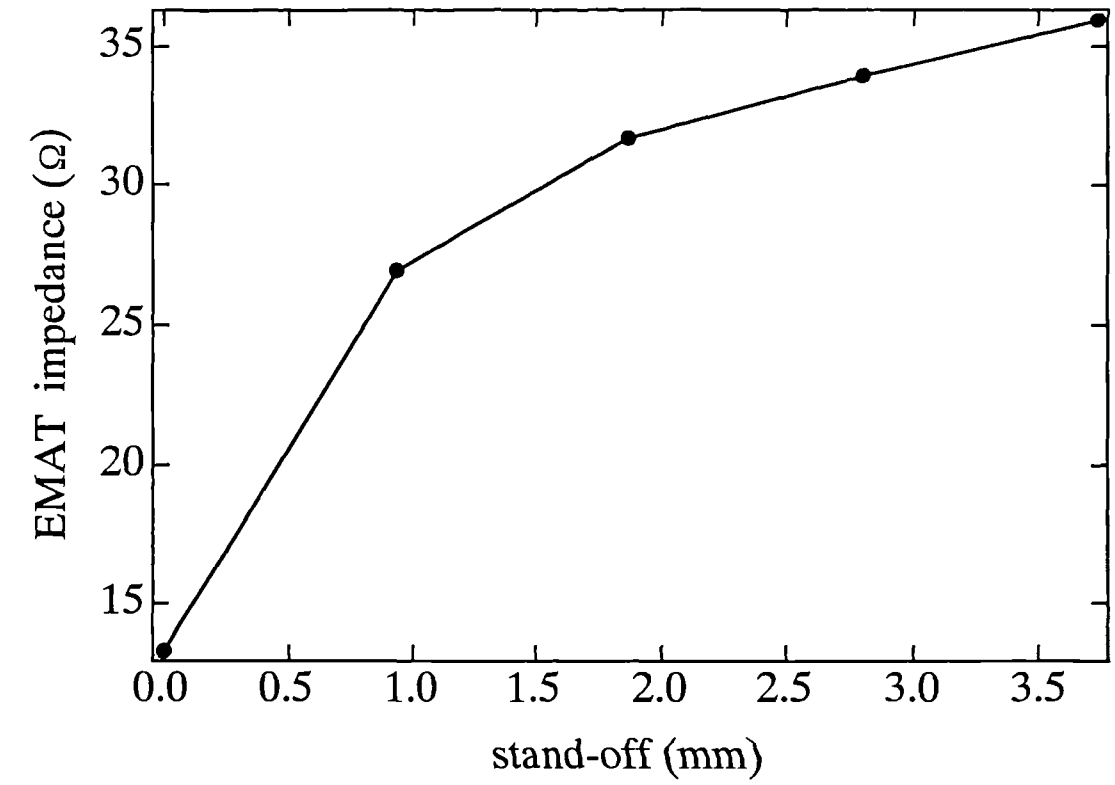

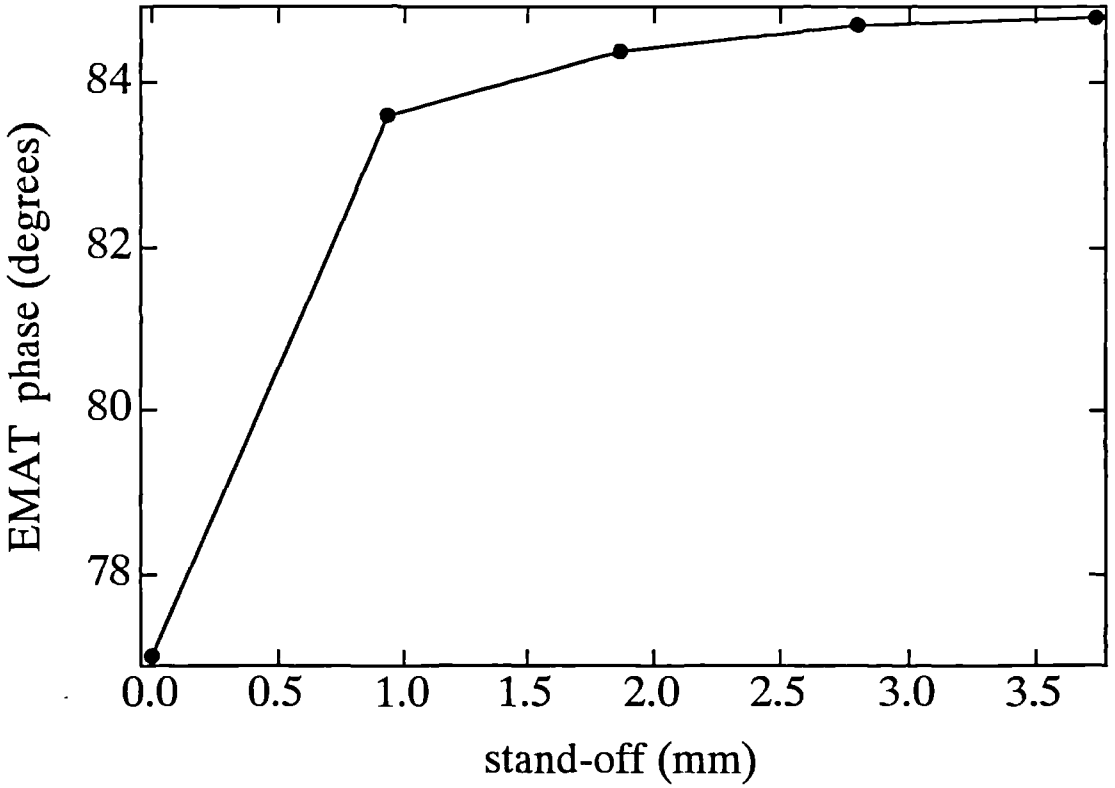

Fig 3.5

Electrical impedance and phase shifting characteristics of the radially polarised EMAT used in this project for various EMAT-sample separations.

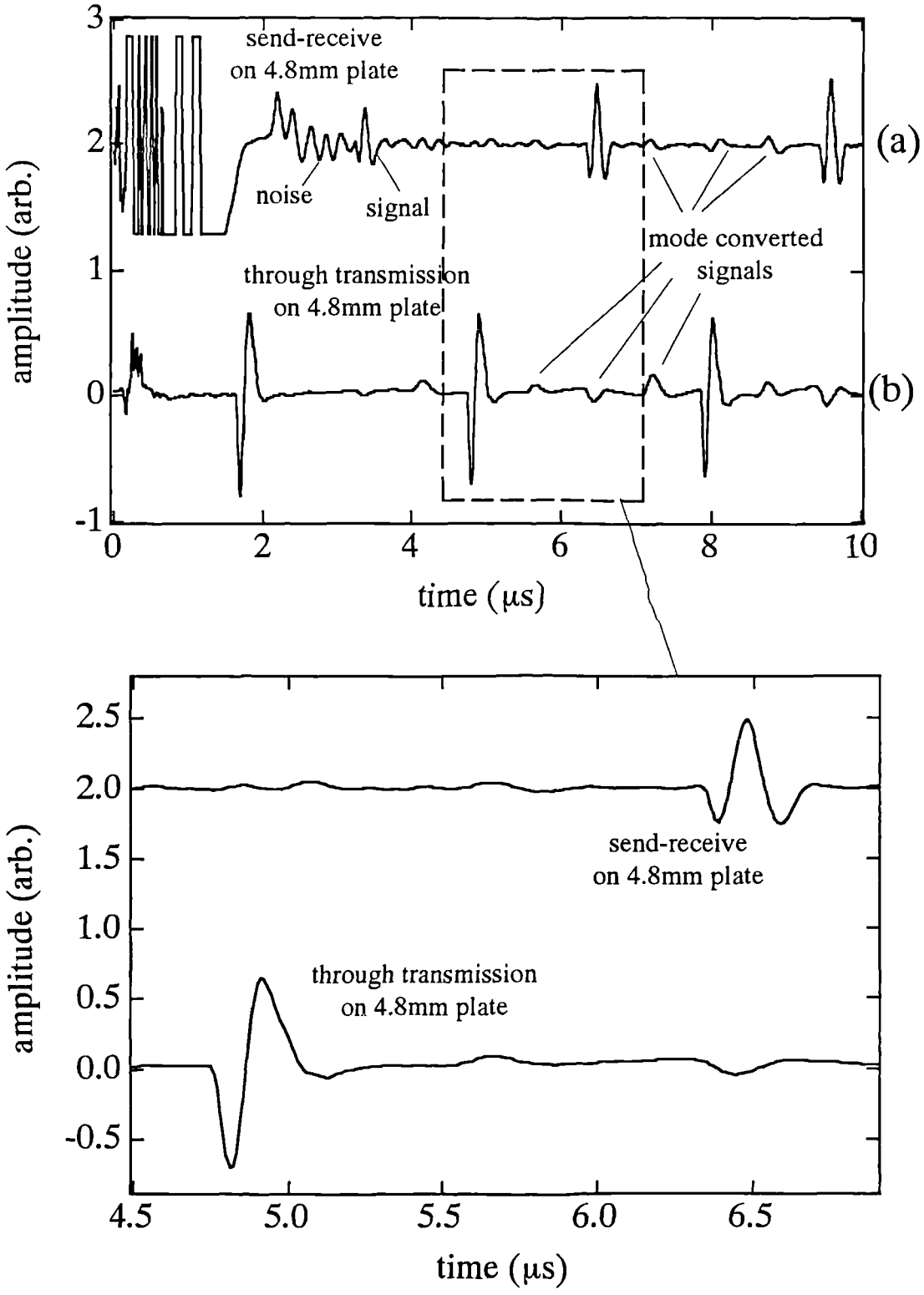

Fig 3.6 (a) &(b)

Waveforms obtained using radially polarised shear wave EMATs on a 4.8mm aluminium plate (blank adherent - BL156), in a send-receive geometry and a through transmission geometry.

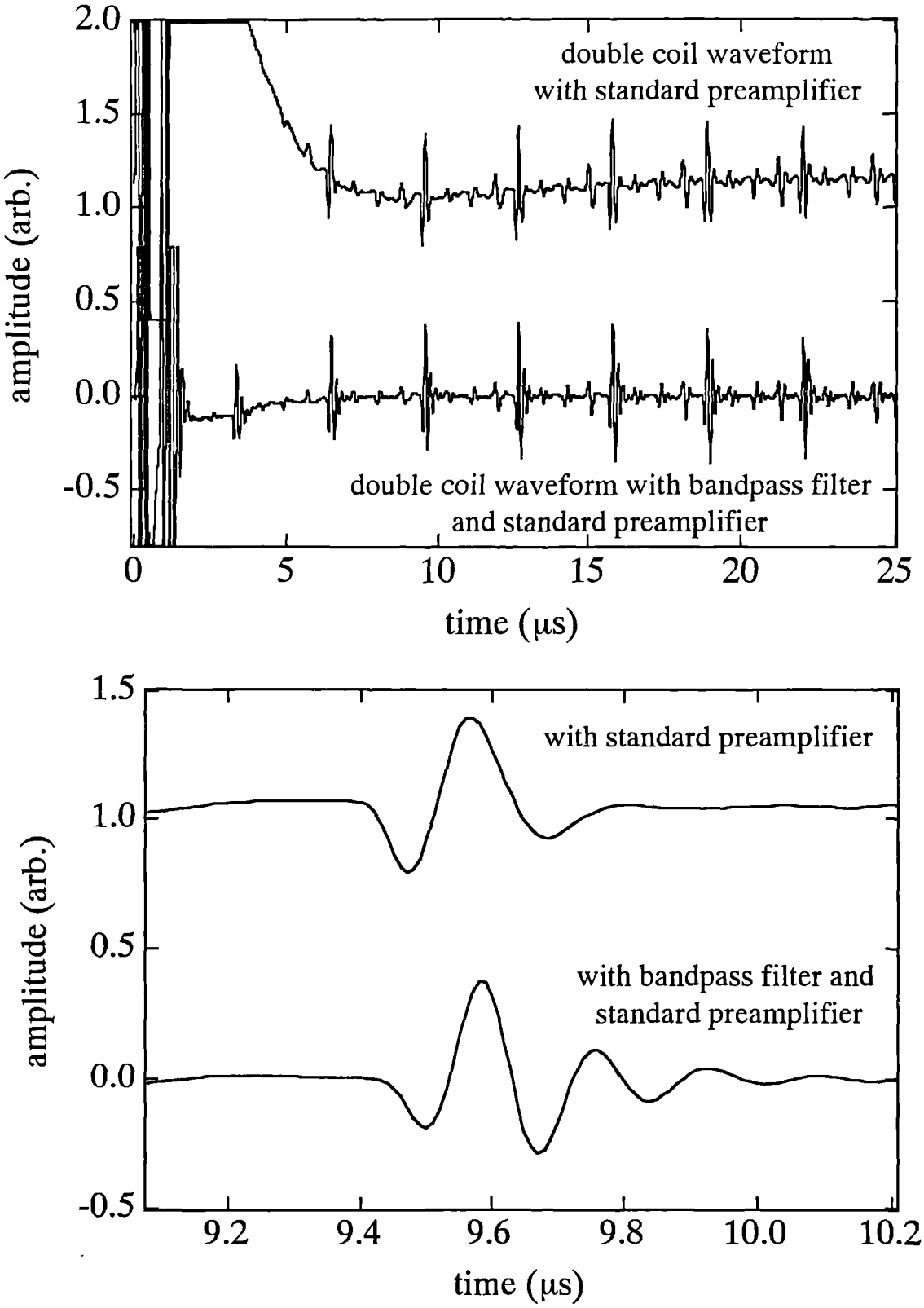

Fig 3.6c

Wavefoms obtained with a double coil EMAT.

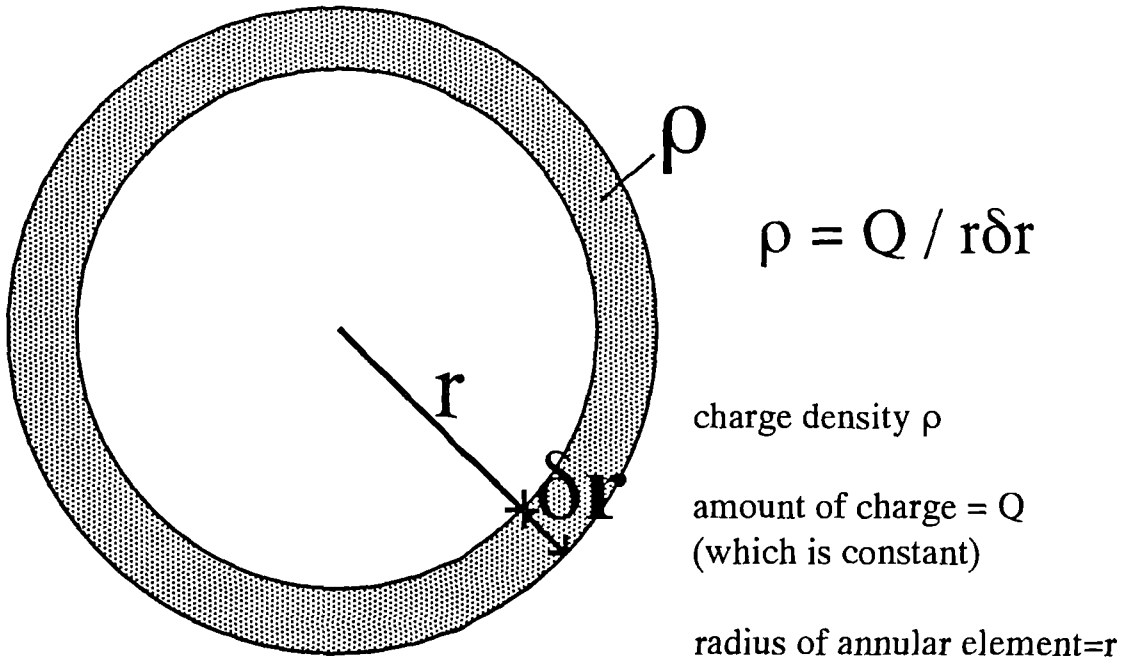

Fig. 3.7a

Annulus of electrons expanding outwards.

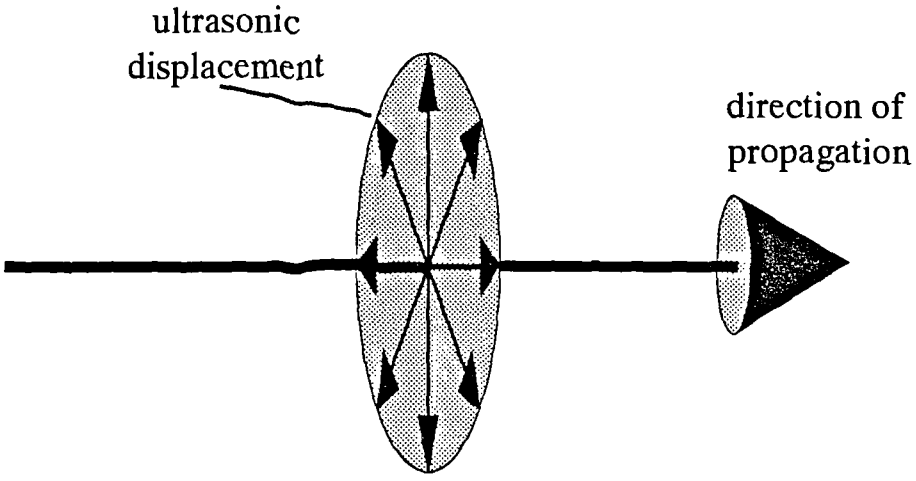

Fig 3.7b

The direction of motion and displacement of the ultrasonic shear wave generated by the radially polarised shear wave EMAT.

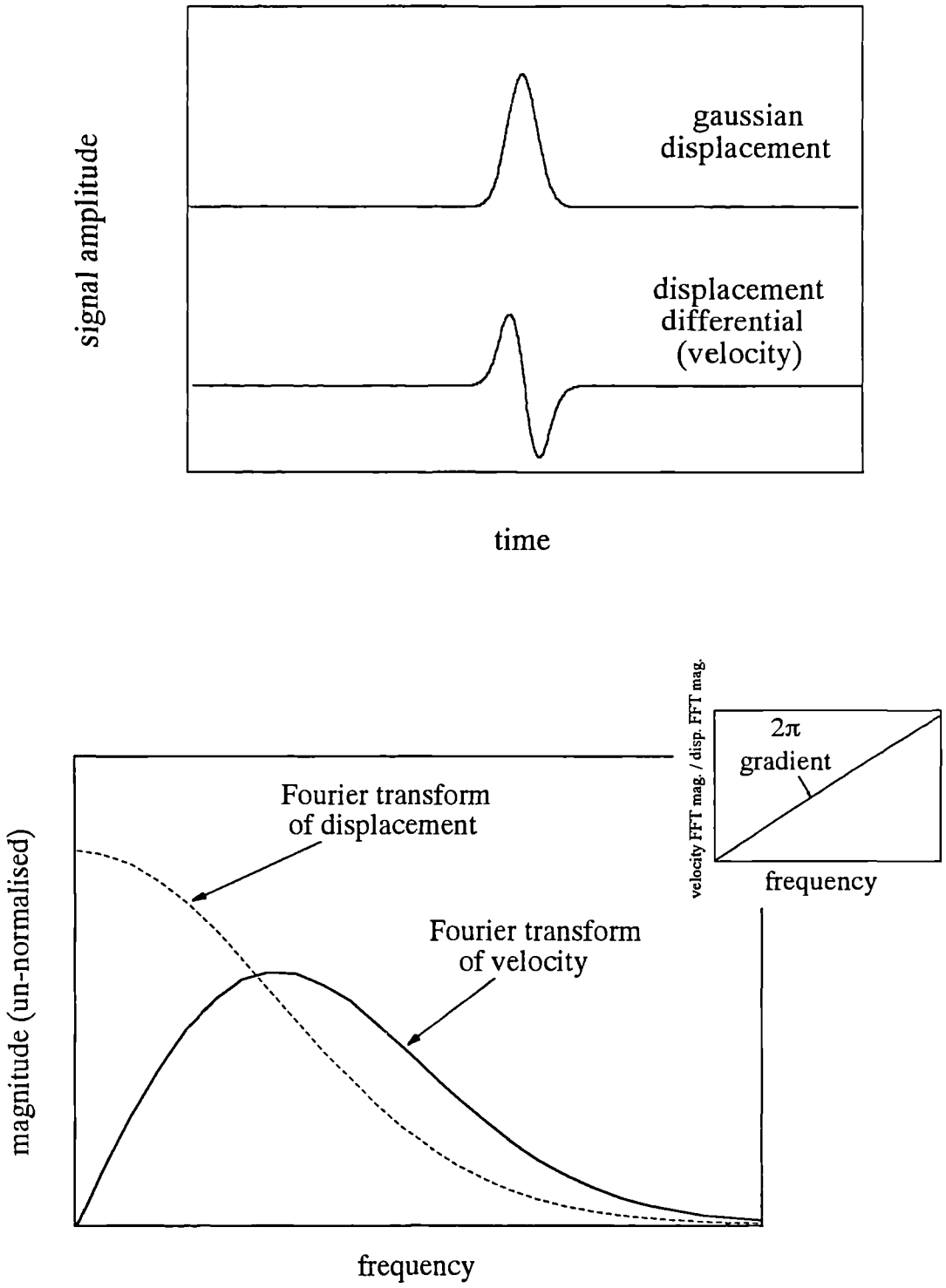

Fig 3.8

Demonstration of the relationship between ultrasonic displacement and ultrasonic velocity associated with that displacement.

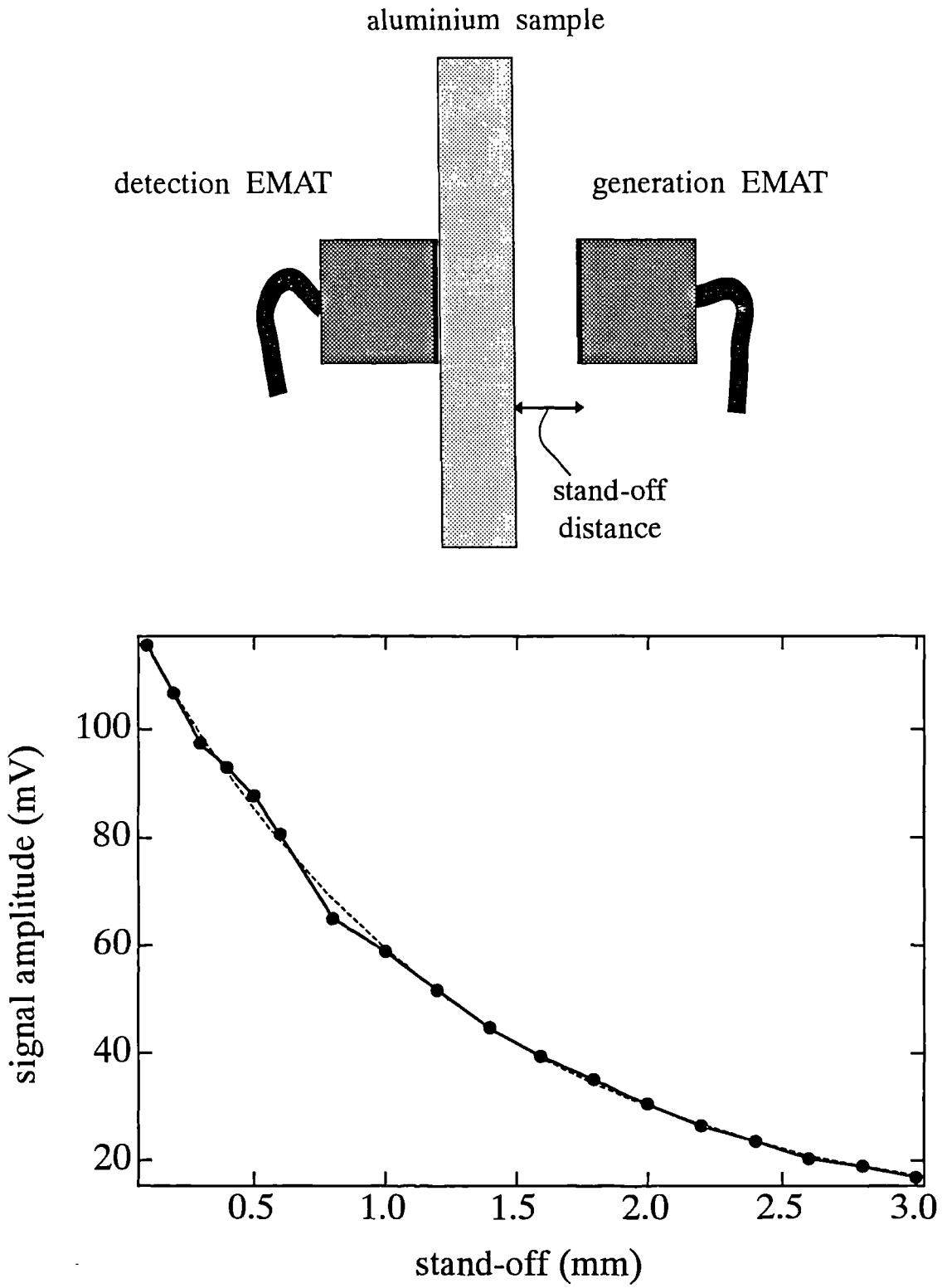

Fig 3.9

Variation in the signal amplitude with increased EMAT stand-off from the sample surface.

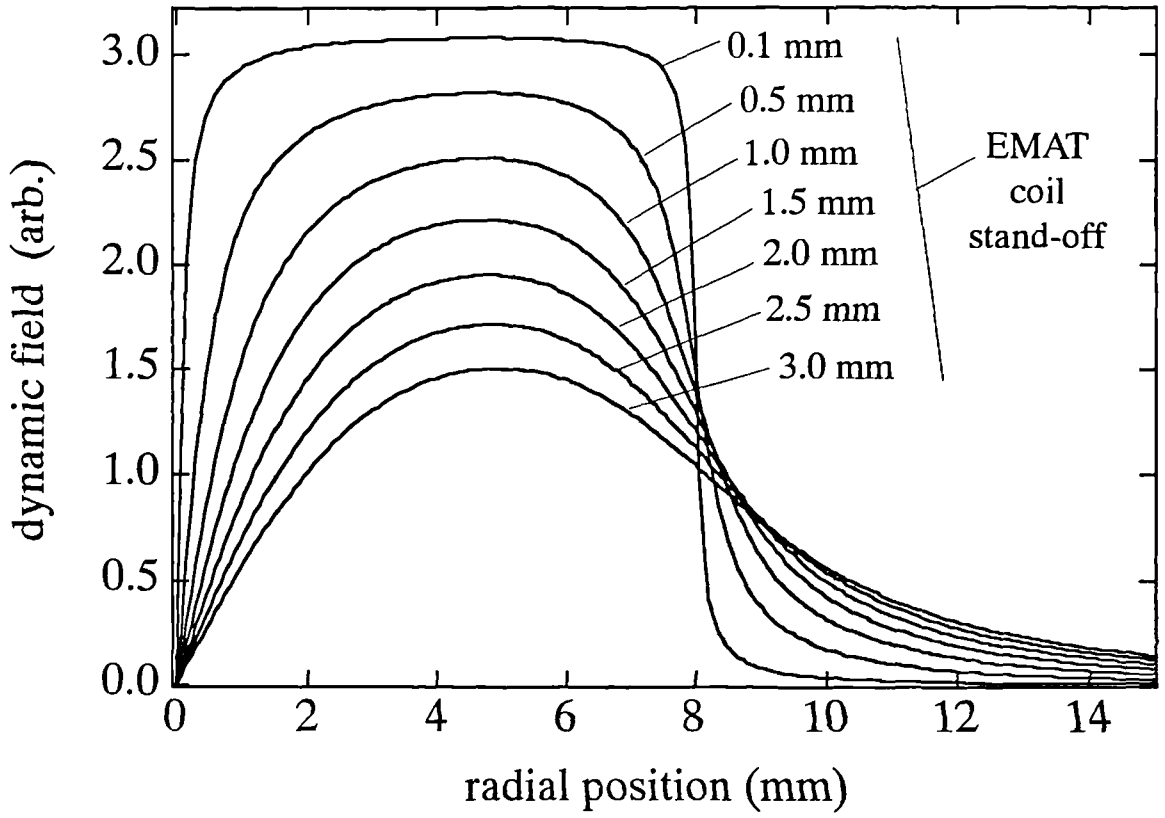

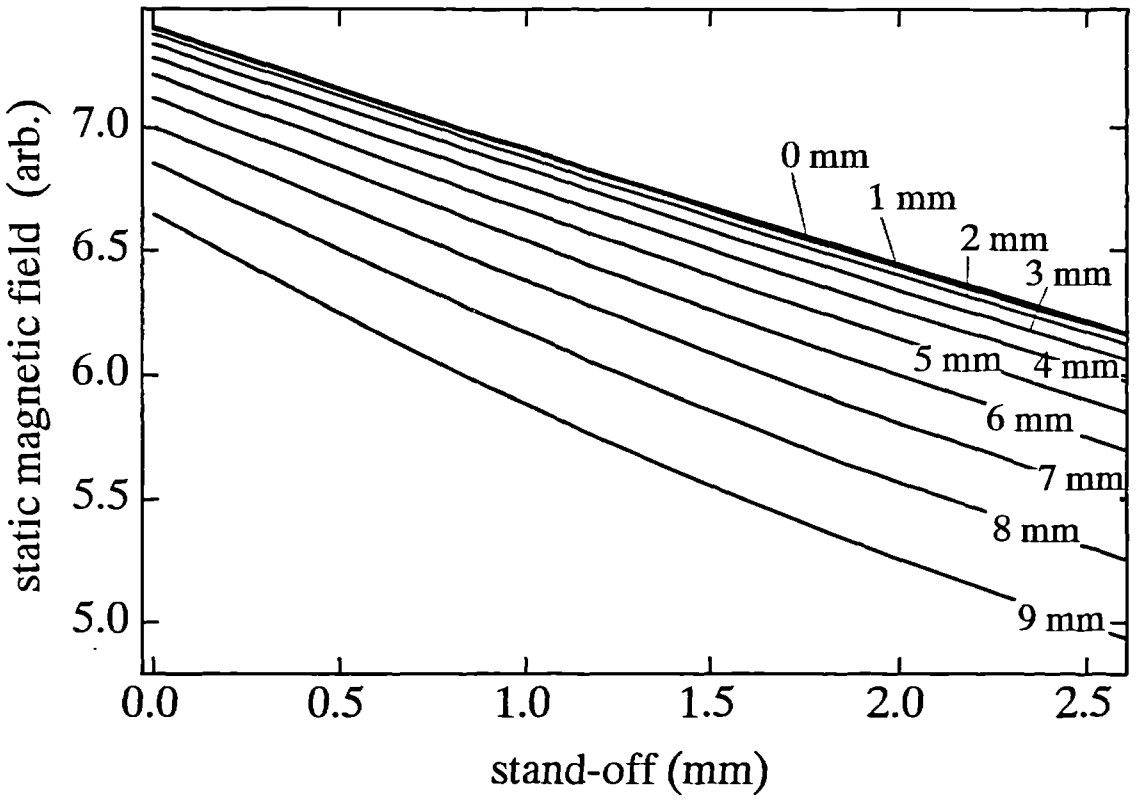

Fig 3.10a(i)

Predicted variation in static and dymanic magnetic fields with EMAT-sample stand-off.

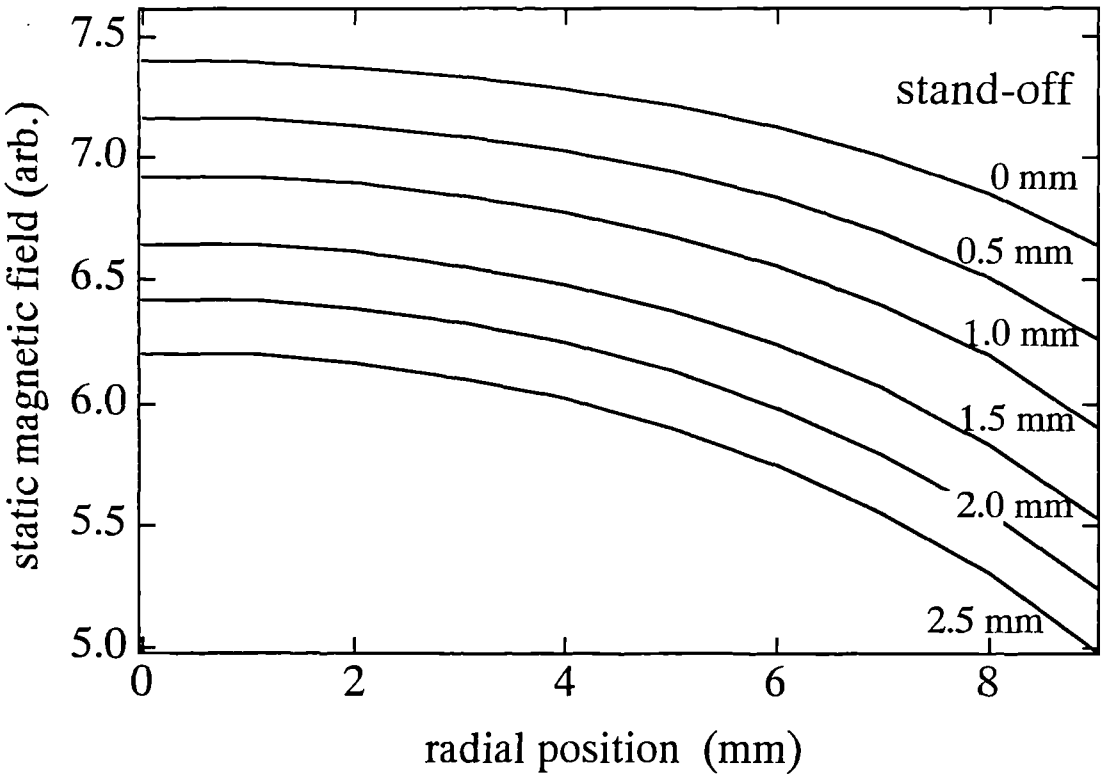

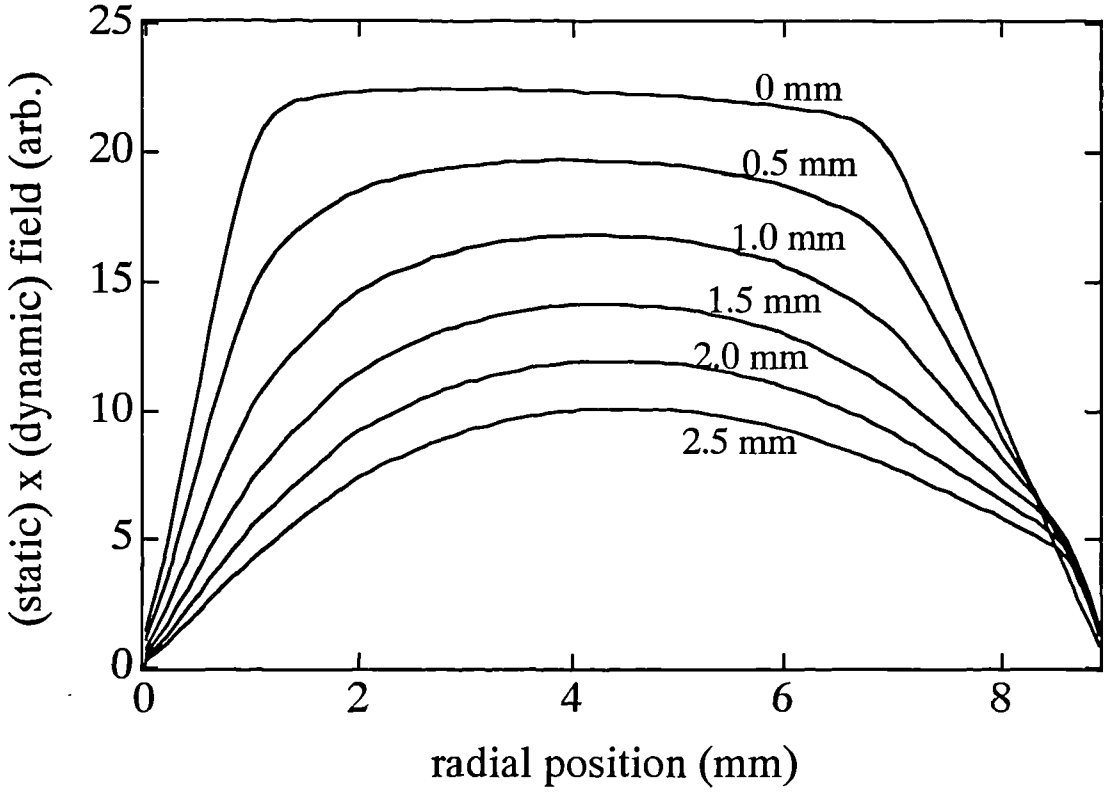

Fig 3.10a(ii)

Predicted variation in staic magnetic fields and signal amplitude with EMAT-sample stand-off.

2D sheet current approximation, where each strip of uniform current is 8mm wide (a = the EMAT coil radius), and has infinite length.

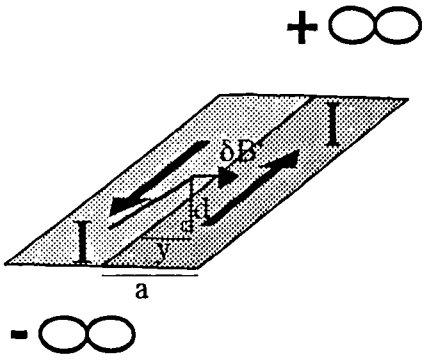

$$B' = \arctan\left(\frac{a-y}{d}\right) + \arctan\left(\frac{-(a+y)}{d}\right) - \arctan\left(\frac{-y}{d}\right)$$

where a is the width of the current strip, y is the displacement from the centre in the plane of the strip and d is the stand-off distance from the strip.

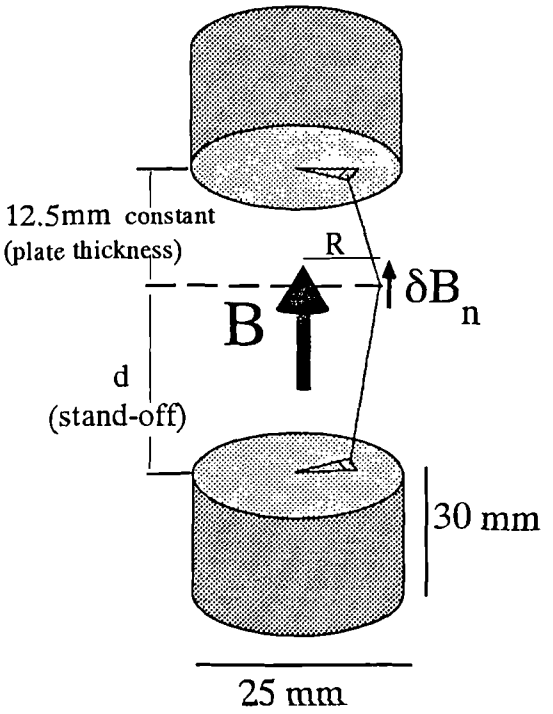

$$B = r\{(d^2+(R-r)^2)^{-1/2} + ((z-d)^2+(R-r)^2)^{-1/2} + ((d+c)^2+(R-r)^2)^{-1/2} - ((z+c-d)^2+(R-r)^2)^{-1/2}\}$$

The diagrams above show the models used in the calculation of EMAT signal amplitude variation with stand-off. The dynamic and the static magnetic field calculations are shown on the left and right respectively.

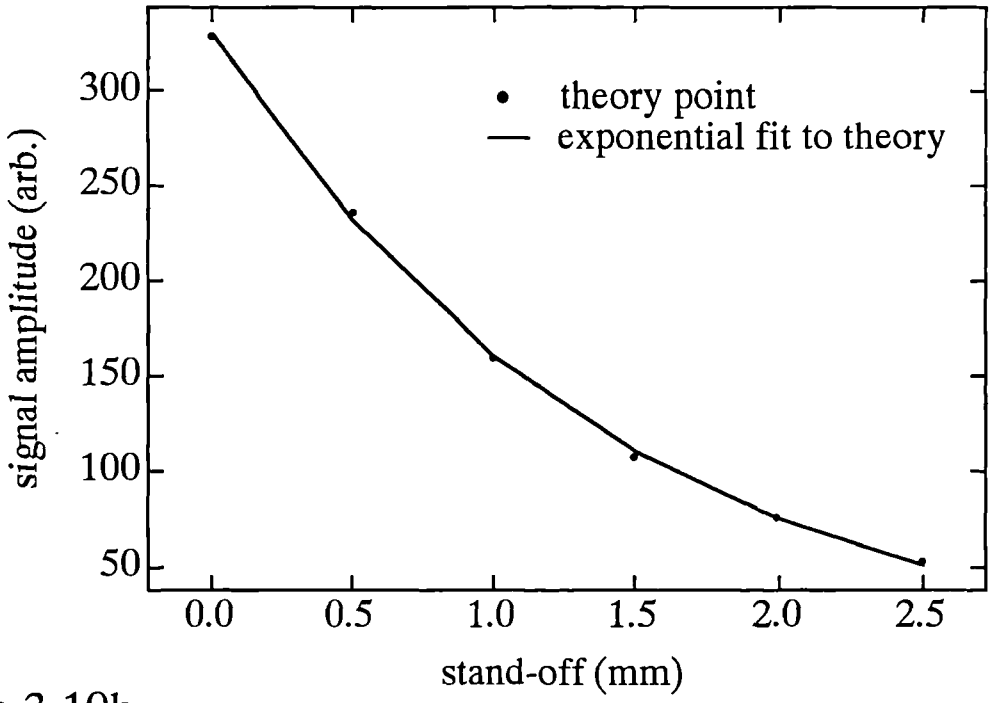

Fig 3.10b

Predicted variation in signal amplitude with EMAT-sample stand-off.

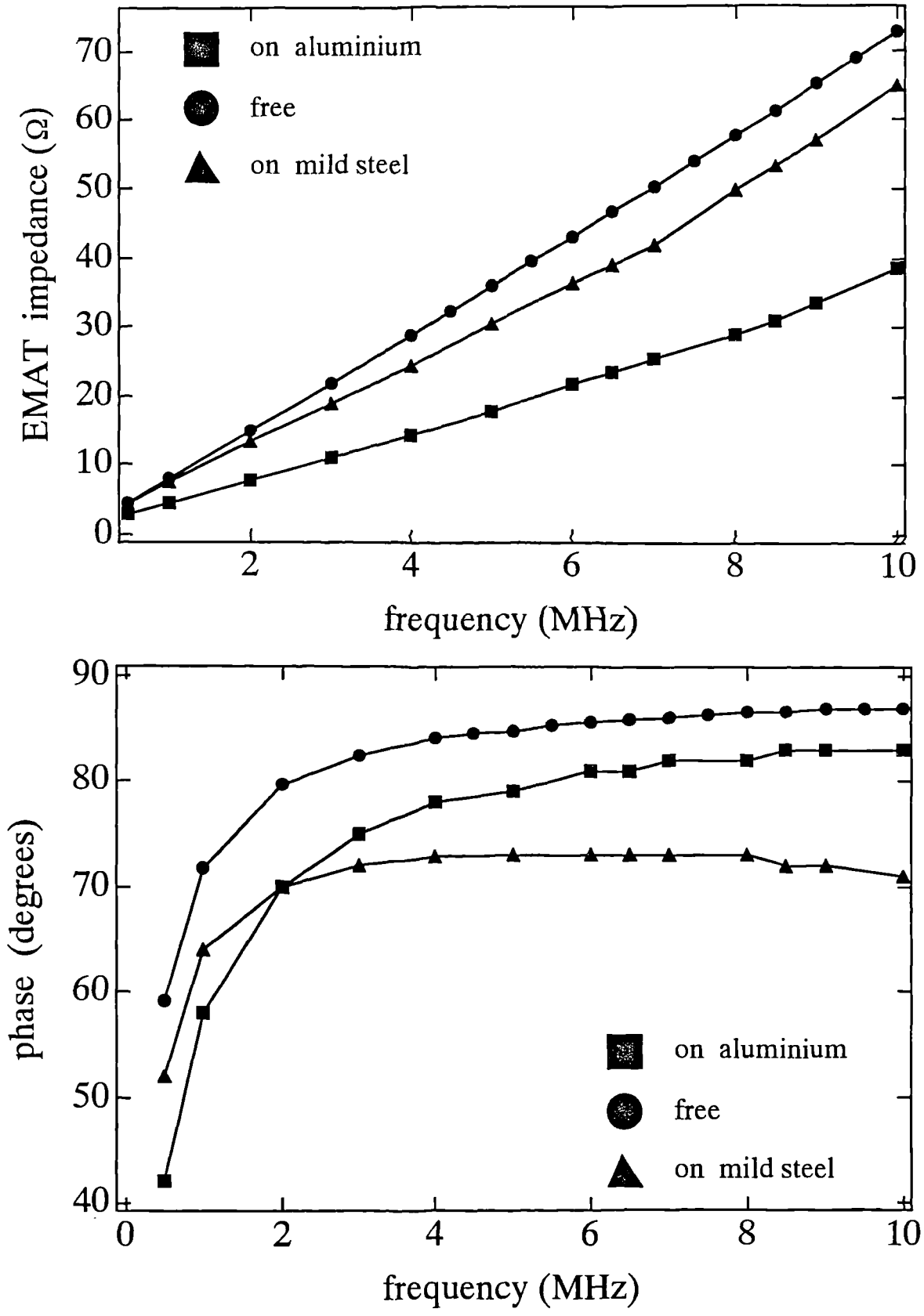

Fig 3.11

Electrical impedance and phase shifting characteristics of the radially polarised EMAT used in this project operating on aluminium, mild steel and in the absence of any sample.

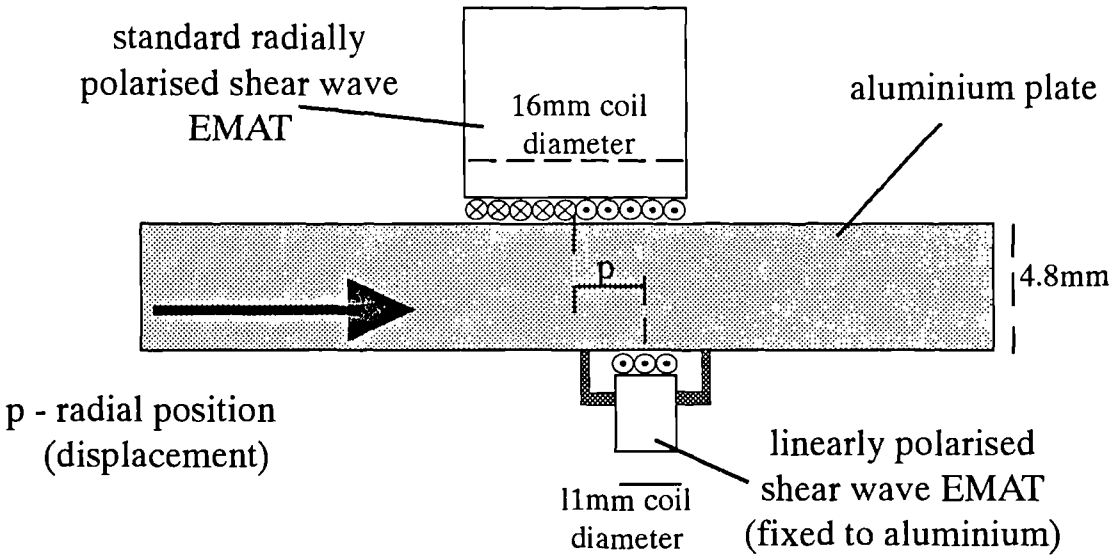

Fig 3.12

Experimental setup of the EMATs used in investigating the ultrasonic field generated by the radially polarised EMATs.

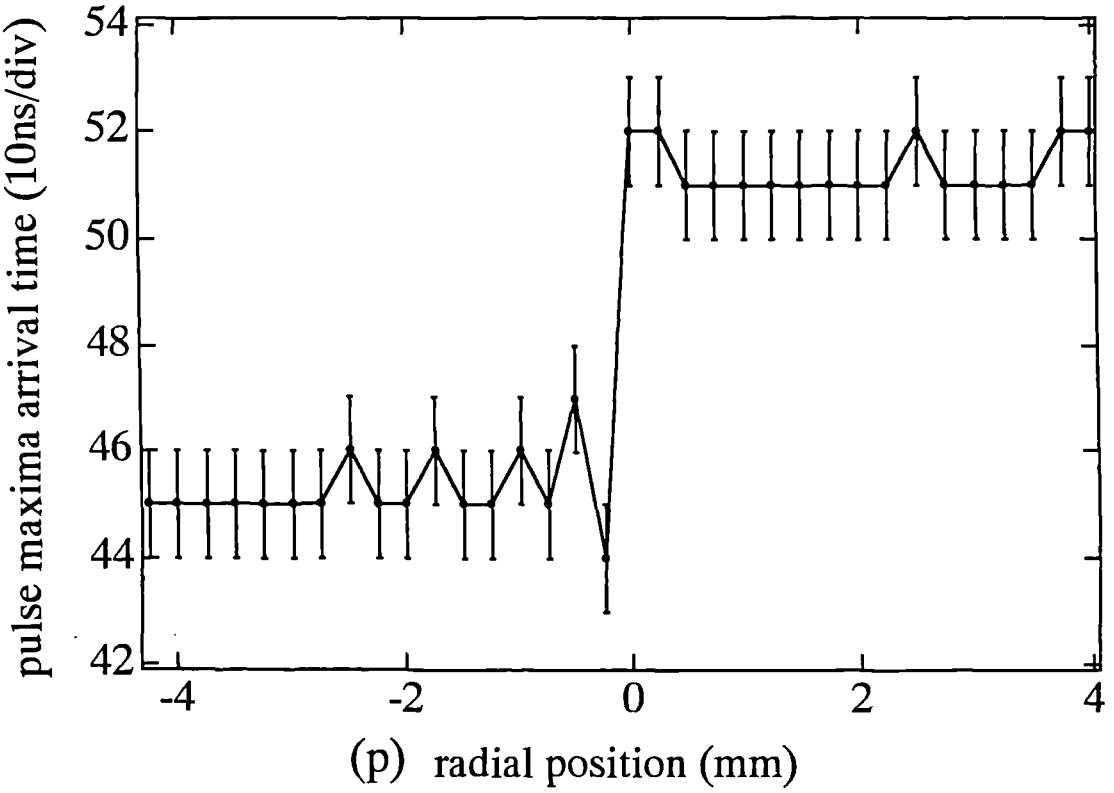

Fig 3.13a

Arrival time of the shear wave pulse maxima generated by the radially polarised EMAT and observed by a linearly polarised in-plane-motion EMAT.

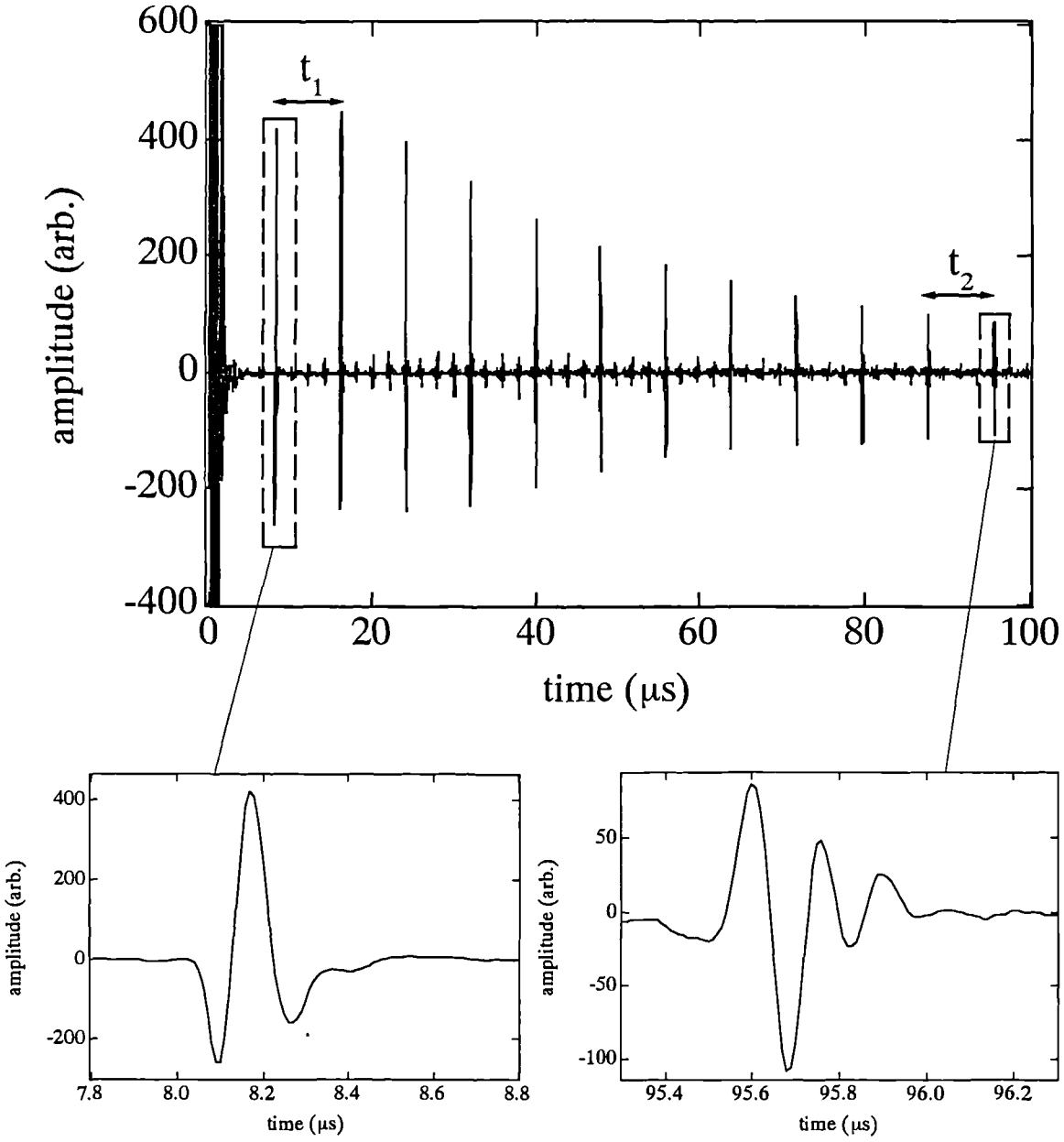

Fig 3.13b

Waveform demonstrating that the shear wave pulse peak-peak reverberation separation is constant over a long total transit distance in a polycrystalline sample (b) and a single crystal sample (c).

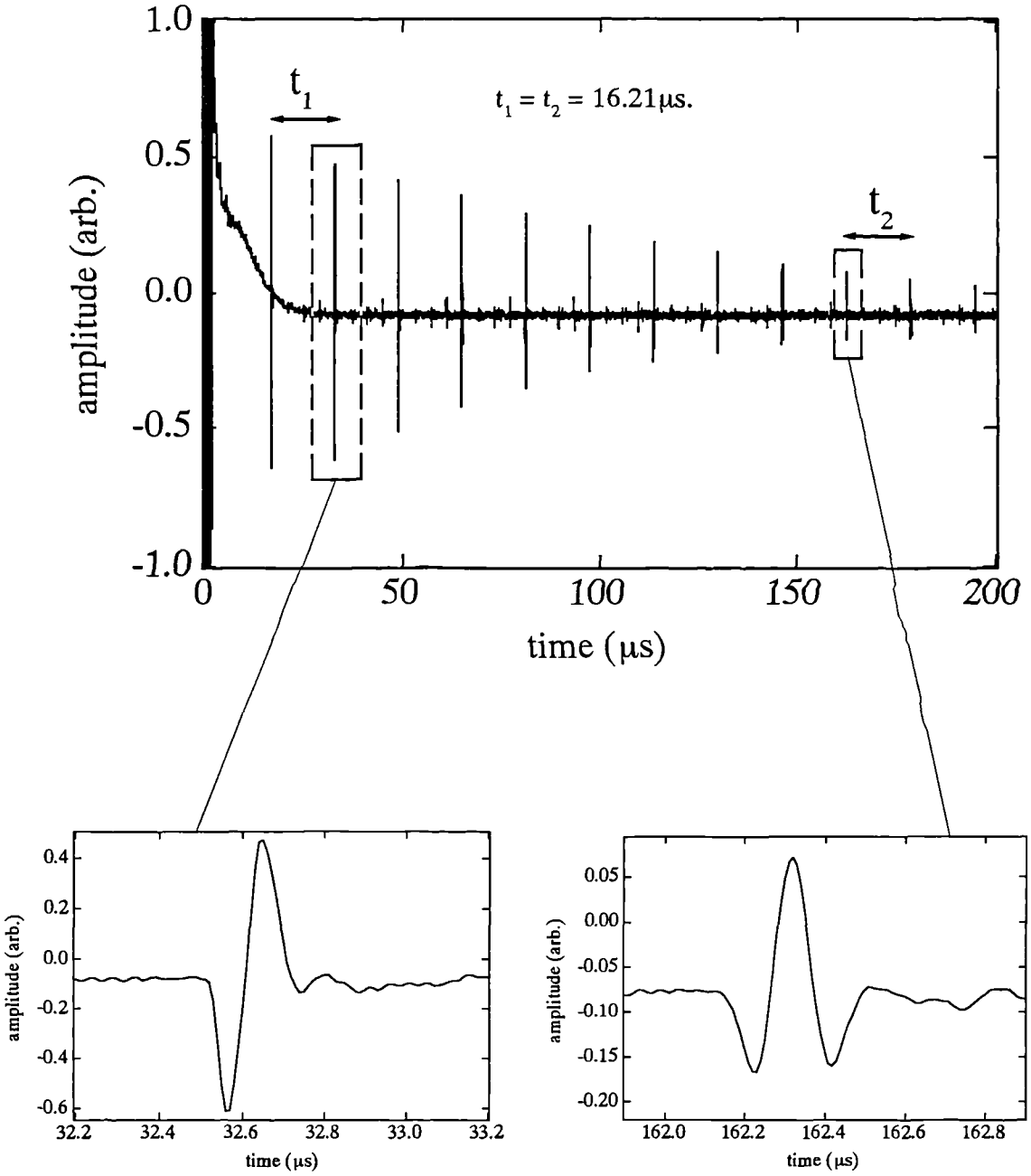

Fig 3.13c

Waveform demonstrating that the shear wave pulse peak-peak reverberation separation is constant over a long total transit distance in a single crystal sample.

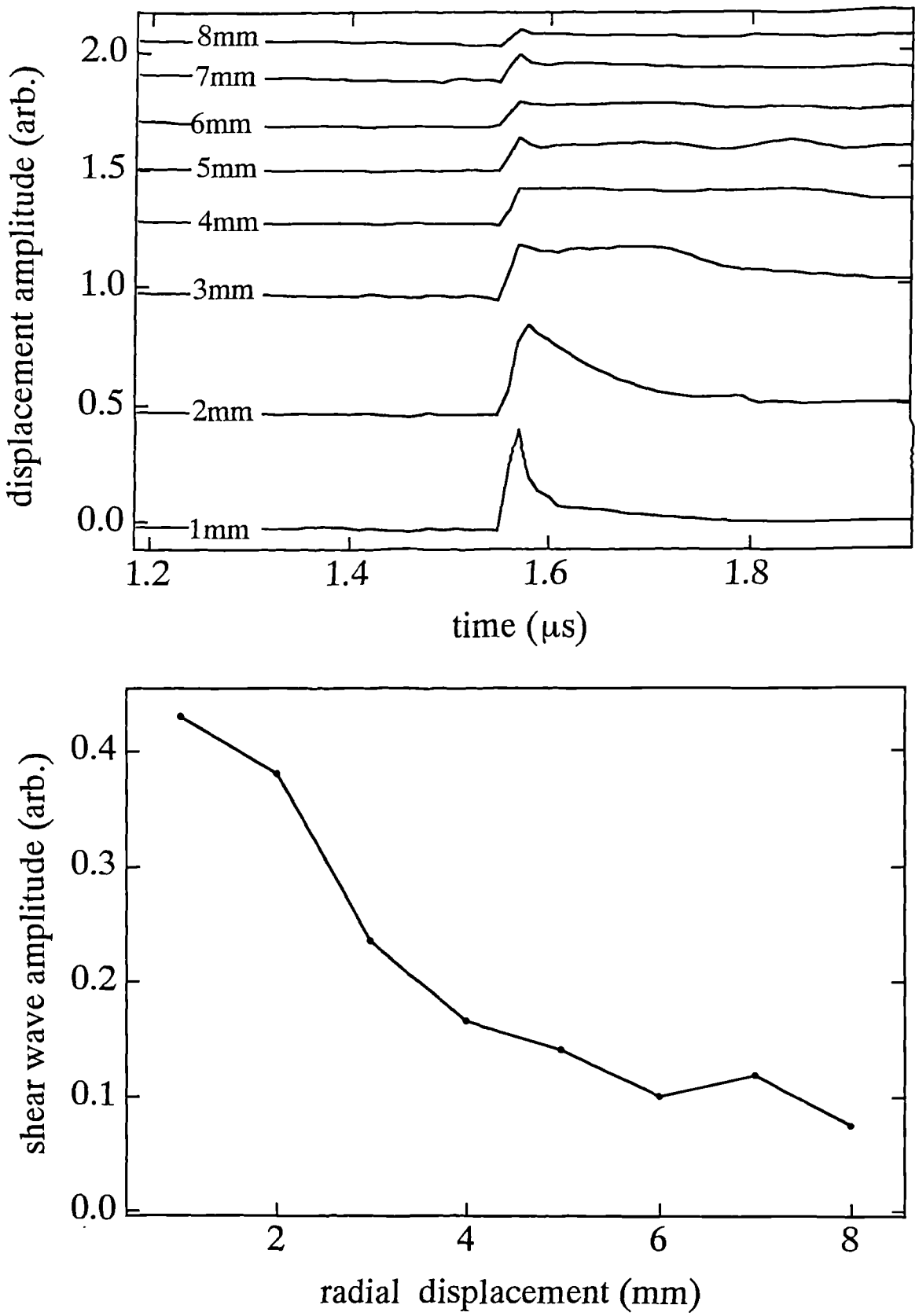

Fig 3.14

Calculations of the shear wave amplitude generated by the radially polarised EMAT for various radial positions from the coil axis in a plane 5mm away from the plane of the coil.

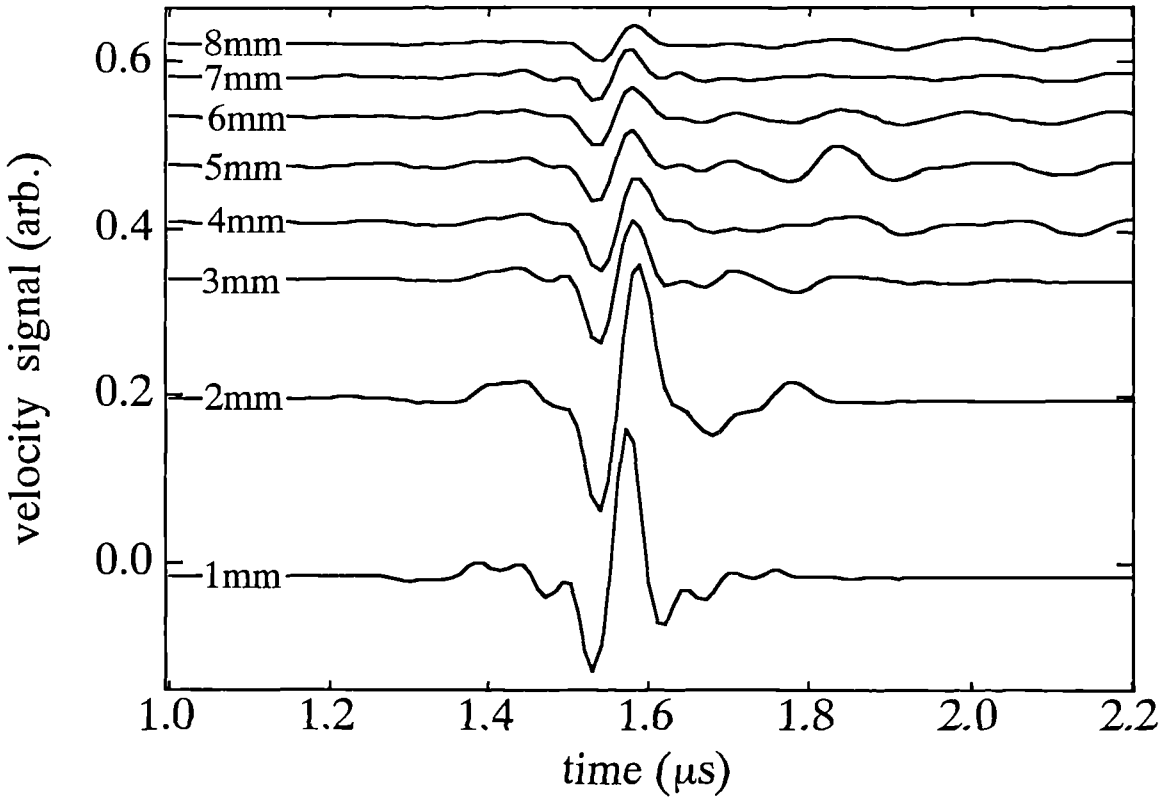

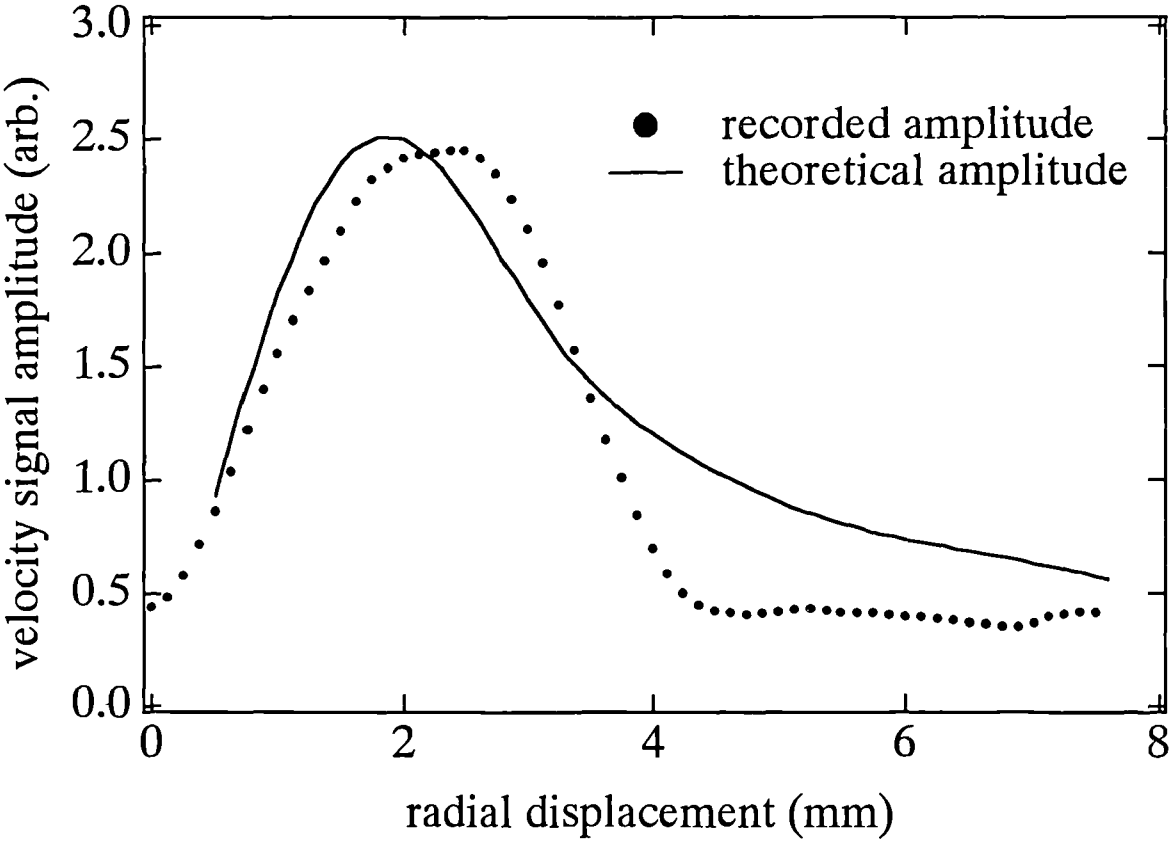

Fig 3.15

Calculations of the shear wave displacement velocity associated with the shear waves generated by the radially polarised EMAT for various radial positions from the coil axis in a plane 5mm away from the plane of the coil.

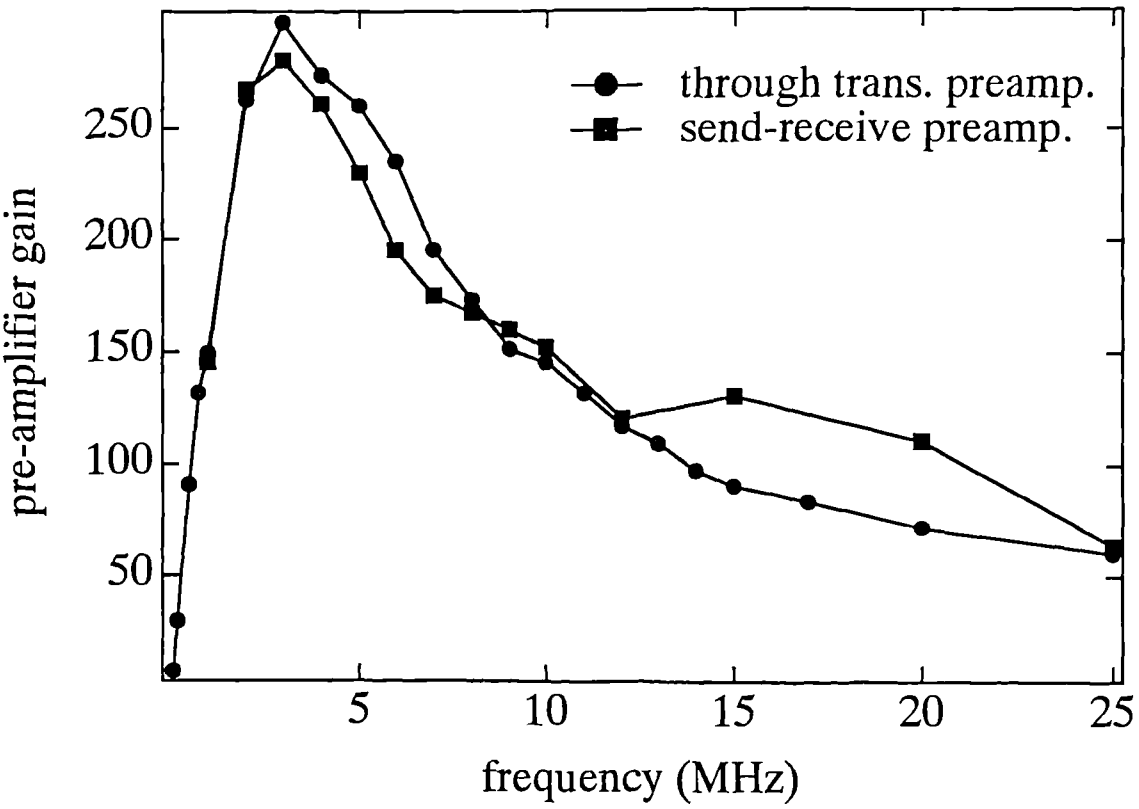

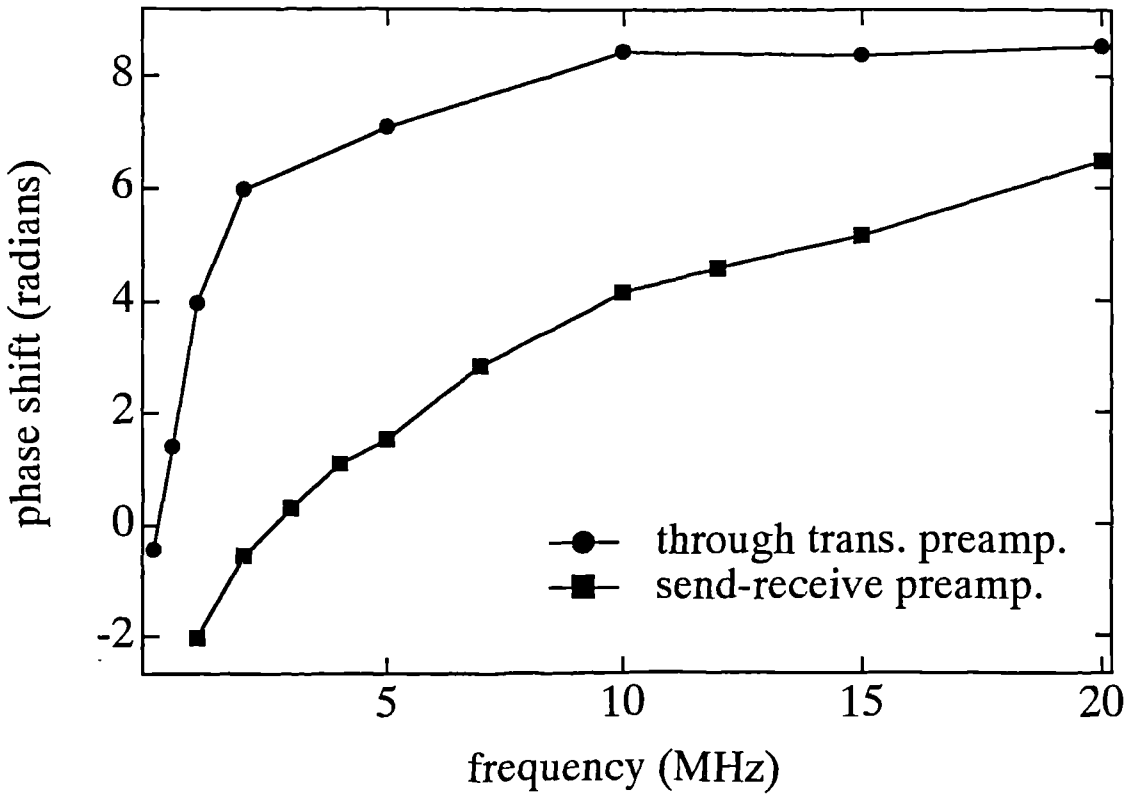

Fig 3.16

EMAT preamplifier phase and gain response for circuit designs used in send-receive and through transmission.

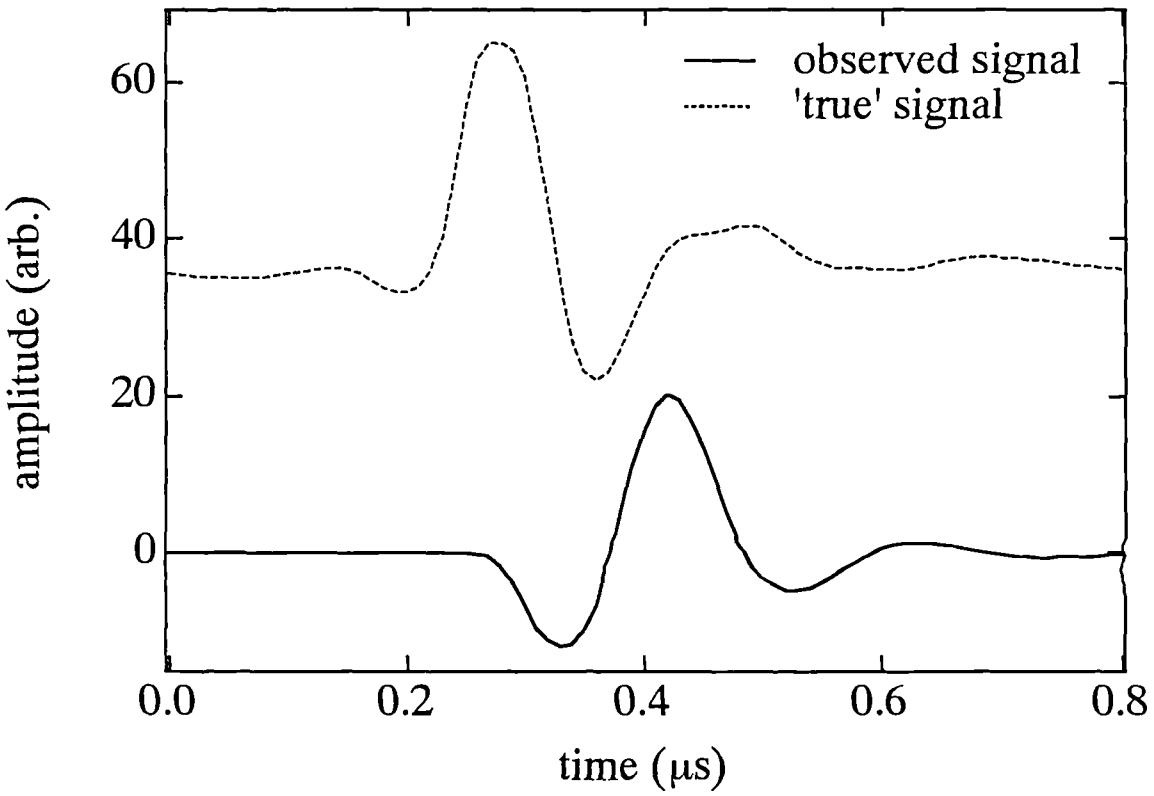

Fig 3.17

Observed and calculated EMAT signals generated and detected in through transmission.

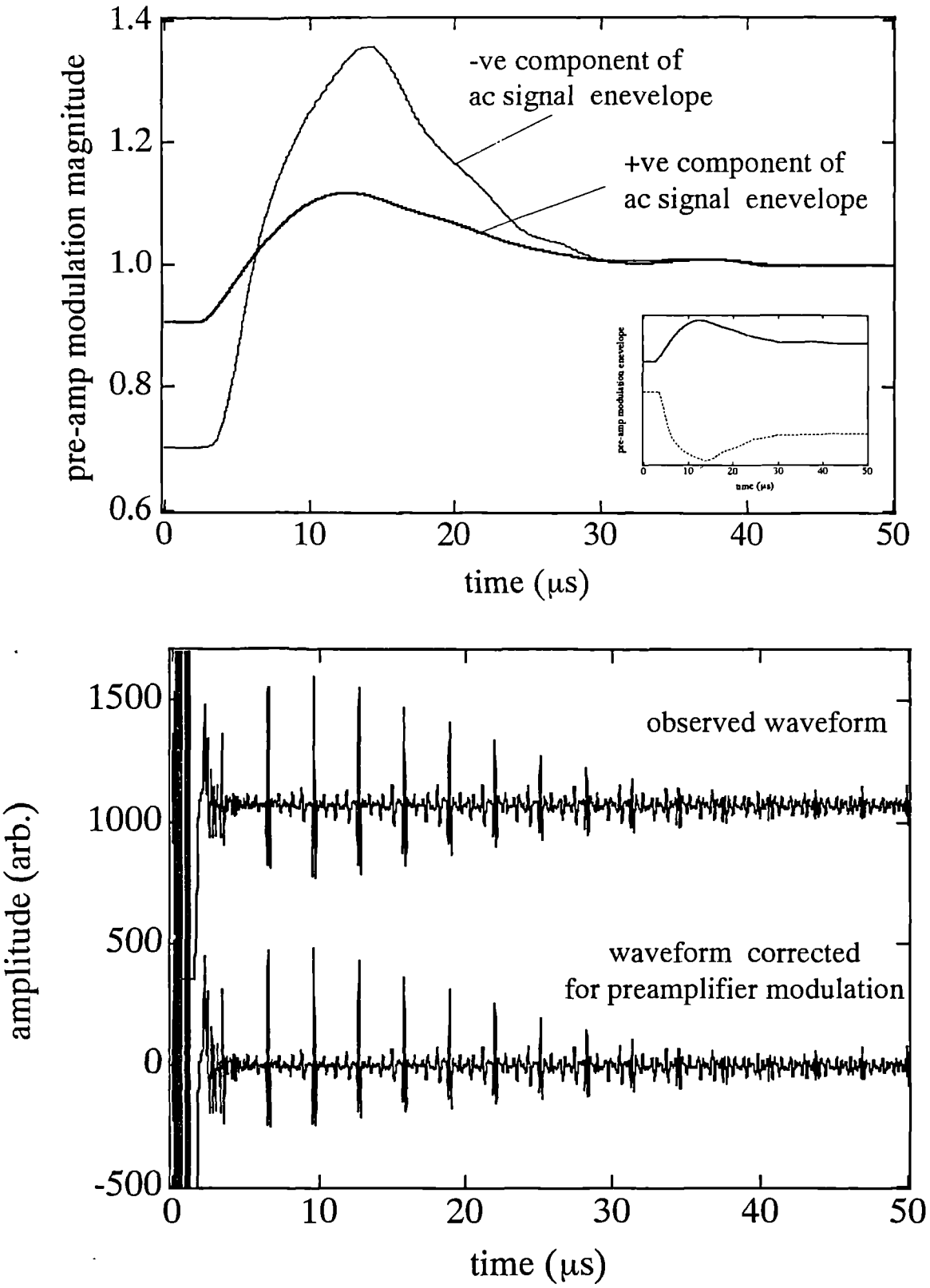

Fig 3.18

Modulation envelope in a send-receive waveform due to partial paralysis of the preamplifier.

Chapter 4

EMAT operation on aluminium plates

4.0 Introduction

The simple theory for acoustic propagation presented in chapter 2 dealt with propagation in isotropic media. In general a metal sample that has been worked is not an isotropic system. It will usually have a degree of inhomogeneity and some type of preferential grain alignment. An isotropic metal would have all the small single crystals (or grains) within it randomly aligned, resultsing in its physical properties being independent of direction within the material. In an anisotropic metal sample, grain alignment gives the aggregate of the grains in the metal a particular symmetry. It arises because there exist particular crystallographic directions in the single crystal where the planes can easily 'slide' over each other and are thus termed easy slip directions. This effect will occur in most aluminium alloys when rolled into sheet plate. The symmetry of the individual crystals are cubic, but the worked (or preferentially aligned), rolled aluminium plate will have an orthorhombic symmetry. This anisotropy is an important consideration in the propagation of ultrasonic waves in the medium, and the present chapter describes some of the experiments that have been performed on aluminium plates where the anisotropy has played an important role. It should be pointed out that in the adhesively bonded aluminium plates provided by DRA Farnborough had only an insignificantly small degree of anisotropy. All the other aluminum plates encountered in this project possessed a significant degree of anisotropy which would certainly complicate the analytical approach presented later if the plates were constructed into an adhesive bond.

4.1 EMAT operation on isotropic and anisotropic polycrystalline metals

So far the discussion has been limited to shear waves propagating in an isotropic material. In most cases however materials will exhibit some degree of anisotropy. The literature concerning the anisotropy considerations within adhesive bonds (such as those investigated in this project), usually highlights the anisotropy of the thin oxide layer on the aluminium adherent, and the anisotropy within the adhesive. The adhesive will often contain a fabric carrier, with a hexagonal weave, and measurements have been reported, demonstrating the existence of stress gradients within the bondline which manifest themselves as some type of acoustic anisotropy or inhomogeneity. In many cases the anisotropy of the aluminium plate is ignored. The degree of anisotropy in some aluminium plate may be too small to effect the acoustic measurements, so that the assumption of an isotropic media is valid, although in general, the anisotropy in rolled aluminium plate is easily observable using EMATs as two distinct shear waves with different velocities.

Anisotropy in aluminium plates arises as a result of the working processes that have been performed on the aluminium. The plate consists of an aggregate of metallic grains, preferentially orientated in a specific direction. There will also be a concentration of impurities at the grain boundaries and it is the combination of the mechanical history and the composition of the aluminium that gives it its mechanical properties. If a radially polarised shear wave is generated on the surface of such a plate then the resulting wave propagating through the bulk cannot really be considered as a radially polarised SH wave. This is because there will be waveguiding within the aluminium due to the propagation velocity having a functional dependance on propagation direction and wave polarisation [1,2,3]. On an anisotropic metal plate, the radially polarised shear wave EMAT will generate a radial stress, which will result in a non-homogeneous radial strain. In the case of an anisotropic aluminium plate, the vibrations associated with wave propagation will fall into two orthogonal directions, along and perpendicular to the direction of grain alignment. The propagation velocity will be different for each of these polarisation directions. This effect is termed 'acoustic birefringence', and in some ways is analogous to optical birefringence.

Thus the observed EMAT waveform will consist of two orthogonally polarised shear waves of slightly different velocity. The difference in the shear velocities in aluminium is typically a few tenths of a percent, but this can vary significantly in different grades of plate from 1% to <.01% . The birefringence is also affected by residual and applied stress. Separating the effect of residual stress from texture is an experimentally difficult problem, requiring very accurate measurements of shear and longitudinal wave velocities simultaneously.

Previous workers have also used EMATs to monitor stress within a metal sample [4,5], but these tend to be narrowband devices requiring analysis of the phase of the observed signals. The general principle of using acoustic birefringence to measure stresses within a slightly anisotropic medium has been examined by many workers [6 - 14].

4.2 Theory of acoustic birefringence of grain aggregates

A polycrystalline aggregate can be ascribed to a macroscopic symmetry as far as ultrasonic properties are concerned. In general, the physical properties of an aggregate will depend on the aeolotropy of the basic unit cell of the pre-deformed material, coupled with the distribution of the alignment of individual grains. In the case of rolled aluminium plate, the symmetry function that describes grain alignment dominates the overall physical properties of the aggregate, rather than the cubic crystallographic symmetry of individual grains. Experimental techniques can yield the effective elastic moduli of the media. An outline of the mathematical method used by Roe [2], in describing such a system is presented below.

The notation used in the Euler co-ordinate system (angles ε, ψ, ϕ), will be adapted to relate the axes of the crystallite to the axes of the polycrystalline sample.

Roe set up a crystalline orientation distribution (COD) function, $W(\varepsilon, \psi, \phi)$ such that the number of crystallites oriented between angles $\varepsilon + \delta\varepsilon$, $\psi + \delta\psi$, and $\phi + \delta\phi$, is given by,

$$W(\varepsilon, \psi, \phi)\, d\varepsilon\, d\psi\, d\phi \qquad 4.1$$

and

$$\int_0^{2\pi}\int_0^{2\pi}\int_{-1}^{1} W(\varepsilon,\psi,\phi)\, d\varepsilon\, d\psi\, d\phi = 1 \qquad 4.2$$

where

$$W(\varepsilon,\psi,\phi) = \sum_{l=0}^{\infty}\sum_{m=-l}^{l}\sum_{n=-l}^{l} W_{lmn}\, Z_{lmn}(\varepsilon)\, e^{-im\psi}\, e^{-in\phi} \qquad 4.3$$

From the above calculations Roe obtained the crystalline orientation distribution (COD) functions. In rolled aluminium plate the effective symmetry is orthorhombic. The elastic constant tensor for the 'orthorhombic' aggregate is given by,

$$\begin{pmatrix}\sigma_1\\ \sigma_2\\ \sigma_3\\ \sigma_4\\ \sigma_5\\ \sigma_6\end{pmatrix} = \begin{pmatrix} C'_{11} & C'_{12} & C'_{13} & 0 & 0 & 0\\ C'_{21} & C'_{22} & C'_{23} & 0 & 0 & 0\\ C'_{13} & C'_{23} & C'_{33} & 0 & 0 & 0\\ 0 & 0 & 0 & C'_{44} & 0 & 0\\ 0 & 0 & 0 & 0 & C'_{55} & 0\\ 0 & 0 & 0 & 0 & 0 & C'_{66}\end{pmatrix} \cdot \begin{pmatrix}e_1\\ e_2\\ e_3\\ e_4\\ e_5\\ e_6\end{pmatrix} \qquad 4.4$$

Taking the COD functions in a stress free aggregate [3], the effects of residual stress and texture can be separated if the elastic constants could be measured as a function of applied stress. This is equivalent to measuring the two shear velocities and the longitudinal velocity simultaneously as stated earlier. Thus for cubic crystallites in an orthorhombic symmetry the longitudinal velocity V_L and the two shear wave velocities V_{T1} and V_{T2} are given by,

$$\rho V_L = c_{11} - 2c\left[\frac{1}{5} - \frac{16\pi^2\sqrt{2}}{35} W_{400}\right] \qquad 4.5$$

$$\rho V_{T1} = c_{44} - c\left[\frac{1}{5} - \frac{16\pi^2\sqrt{2}}{35}\left(W_{400} - \sqrt{\frac{5}{2}}\,W_{420}\right)\right] \qquad 4.6$$

$$\rho V_{T2} = c_{44} - c\left[\frac{1}{5} - \frac{16\pi^2\sqrt{2}}{35}\left(W_{400} + \sqrt{\frac{5}{2}}\,W_{420}\right)\right] \qquad 4.7$$

where cij are the elastic constants of the cubic crystallite and,

$$c = c_{11} - c_{12} - 2c_{44} \qquad 4.8$$

the sum of the velocities can be written as a function of the elastic constants only, independent of texture by -

$$\rho V_L^2 + \rho V_{T1}^2 + \rho V_{T2}^2 = c_{11} + 2c_{44} \qquad 4.9$$

thus, by measuring the velocity of the two shear wave polarisations and the longitudinal velocity simultaneously, the effects of residual stress can be separated from applied stress [6].

The anisotropy giving rise to a difference in the shear velocities in aluminum plates is a very small effect, and requires sharp ultrasonic pulses to be observed directly. The birefringence can also be measured by an ultrasonic interferometry technique by examining beats of resonant toneburst shear waves. In adhesively bonded samples, the main cause for concern is whether the birefringence will invalidate or just confuse the measurements of the physical properties of the bond. The splitting of the shear waves could possibly cause problems in the analysis. The observed effect would be that of superimposing two echo trains with isotropic adherents of slightly different adherent thicknesses. The aluminium plates used in the bonded samples specifically constructed for this project were found to be very weakly birefringent, with differences in the two shear velocities of approximately less than 0.1 %. For such a small anisotropic effect, this particular grade of aluminium plate can

be considered isotropic as far as the shear wave is concerned and thus the analysis is considerably simplified. However, birefringence is in general an important consideration where aluminium plates are to be adhesively bonded.

4.3 Modulation of birefringent waveforms

An interesting feature of the shear waveforms obtained in birefringent samples is the modulation that may arise. As the two pulses progressively separate with increasing time, they interfere and the resulting echo train of the combined pulses does not display the classical exponential decay. The resulting maxima-minima modulation is shown in fig 4.1, neglecting the normal contribution that would lead to exponential decay. This was calculated by progressively shifting two identical pulses and adding them together, while monitoring the resulting interference amplitude.

4.4 Variation in acoustic birefringence in aluminium plate with applied stress

Although bireferingence effects are negligible in the adhesively bonded samples used in this project, in general this may not be so. In order to assess the EMAT performance birefringent plate and compare the technique to existing methods it was decided that some experiments would be perfromed on such plates. These experiments involved scanning flat bottomed holes in different plates, and studying the effects of applying tensile stress to the bireferingence in such a plate.

The aerospace alloy (BL156) used in the DRA adhesive bonds has been the only aluminium plate encountered in this project which could be confidently treated as isotropic. Most aluminium plate will in fact be significantly birefringent. The birefringence experiments presented here performed on aluminium plate have been carried out on 13mm thick rolled aluminium plate. There is extensive literature [4-14] on the birefringence of aluminium plates and the basic ideas behind the experiments described below are only original when taken in the context of the EMATs used.

The birefringence of aluminium plate depends on texture, residual stress and applied stress. Pao et al [15], present a review of the subject and a derivation of the following approximate empirical equation for the birefringent shear wave 'splitting' with applied stress.

VT1 and VT2 are the stress dependant shear wave velocities, and V_1 and V_2 are the two shear wave velocities at zero applied stress.

$$\left(\frac{1}{V_{T1}}-\frac{1}{V_{T2}}\right)^2 = \left[\left(\frac{1}{V_1}-\frac{1}{V_2}\right) + m_1(t_1^i+t_2^i) + m_2(t_1^i-t_2^i)\cos 2\theta\right]^2 + \left[m_3(t_1^i+t_2^i)\sin 2\theta\right]^2 \qquad 4.10$$

where t_1^i, t_2^i are principal stresses in two orthogonal directions 1 and 2, at an angle θ to an axes of symmetry, and the constants m_1,m_2 and m_3 can only be determined empirically. In the experiment here, the stress was applied both parallel and perpendicular to the rolling direction axis which was an axis of symmetry. As tensile stress was applied along one specific direction it can be taken that one of the stresses is zero. Taking $t_2^i = 0$ to be zero, and rewriting the above expression yields,

$$\left(\frac{1}{V_{T1}}-\frac{1}{V_{T2}}\right)^2 = \left[\left(\frac{1}{V_1}-\frac{1}{V_2}\right) + m_1(t_1^i) + m_2(t_1^i)\right]^2 \qquad 4.11$$

or in terms of the arrival times, t_{T1} and t_{T2},

$$(t_{T1}-t_{T2}) = [A + B\cdot S] \qquad 4.12$$

where S is the applied tensile stress, and A and B are constants which dependant on texture and residual stress and must be determined empirically. This assumption of a linear dependance of birefringence on applied stress prediction concurs with the results obtained experimentally.

The exact values of A and B are specific to working, composition and internal structure, and can therefore only be determined empirically. This type of experiment has been performed by other workers, yielding similar results, but normally being performed in a contact regime. Experiments performed using shear contact transducers will use polarised transducers. If this is the case, then it is only the actual time domain measurements that can be described with confidence. The relative amplitudes and decay rates of the shear waves may be influenced by transducer alignment and the presence of acoustic couplant. The decay of each of the two distinct SH waves is shown in fig 4.2, for shear pulses outside the region where the two polarsiations will interfere. The results clearly show that the decay rates for each shear wave polarsation are identical. Thus the difference in amplitude of the different polarisation pulses must occur at the initial generation of the shear waves.

Simple acoustic theory indicates that one factor affecting bulk wave velocity is interatomic separation. If a tensile test sample is stressed in tension then the interatomic separation increases in the direction of applied stress. Orthogonal to the applied tensile stress, a compressive stress develops, and the interatomic separation in this direction decreases - this effect manifests itself as Poisson's ratio. In tensile stress, the propagation velocity of the shear wave with its polarisation in the direction of the stress increases. The observed splitting in the shear waves can thus increase, or decrease depending in which direction the tensile stress is applied.

The data recorded was the observed splitting of the 12th ultrasonic echo within the aluminium plate sample, as shown in fig 4.3. This was done to increase the temporal resolution of the measurement. The temporal separation between succesive echo peaks for an EMAT generated/detected shear wave of a particular polarisation is constant across the entire wavetrain. This indicates that any divergence of the ultrasonic field generated by the EMAT will not corrupt the time splitting measurement of the 12th peak. Tensile stress was

applied to the sample using an Instron tensile test machine, capable of an applied tensile load of up to 5000 kg. Samples were prepared and analysed as shown in fig 4.4. One sample was cut so that its long axis was in the direction of the rolling marks on the aluminium surface, and the other perpendicular to the rolling marks. The results for the time splitting of the two orthogonally polarised shear wave pulses, associated with the 12th echo as a function of applied stress are shown in figs 4.5. As the absolute arrival time of these pulses was also recorded then a velocity variation with applied tensile stress could be calculated, and these results are shown in fig 4.6. Note that due to the inaccuracy of the thickness measurement of the sample, there is an uncertainty in the absolute value of calculated velocity of 2%, while the difference between the two calculated velocites for each polarsiation is less than 1%.

The change in transit thickness with applied stress, and thus transit time due to the Poissons ratio effect is of second order (*<1%*) *compared to the change in transit time* brought about by a stress dependant velocity. Thus the change in thickness could have been ignored, but here it was accounted for in the calculations.

4.5 Comparison of single crystal and textured polycrystalline aluminium

As explained in the preceding sections, the elastic constants of the aggregate of grains is determined by both the elastic constants of the single crystal and the orientation of the grains within the polycrystalline sample. The velocities measured in the plate correspond to shear waves polarised in the (100) and the (010) directions. The symmetry of the aggregate is orthorhombic so that the velocities for these polarisations are different, whereas for a cubic system they would be the same. The energy of the shear wave is guided into the (100) and (010) polarisations, as a result of the shape of the slowness surface in both the orthorhombic and cubic symmetry. Thus, the birefringence observed in the aluminium plate is the difference between the (100) and (010) polarisations. It should not be attributed to the much larger difference between the (100) and (110) directions.

Waveforms were obtained in a single crystal of aluminium using a radially polarised SR EMAT, and are shown in fig 4.7 . The crystal was cylindrical in shape with a (100) axis along the length of the cylinder. The upper waveform in fig 4.7a is for propagation in the (100) direction, such that the polarisations are along the (010) and (001) directions which have equal velocities and thus only one pulse is observed. The lower waveform is propagation along a (110) direction. The large shear wave pulse has polarisation in the (010) direction and thus has the same velocity as that observed in the preceding waveform.This is 3236 m/s +/- 0.1%, which is 0.4% less than the value at room temperature of 3248 m/s (C_{44} / ρ), obtained from tables in Musgrave [1]. The next principal feature occuring at 25.79 μs corresponds to a shear wave propagating in the (110) direction with polarisation in a (011) polarisation. This shear wave has a measured velocity of 2930 ms +/- 0.1%, once again 0.6% less than the value obtained from tables [1] of 2947m/s from the relationship ($(C_{11}-C_{12}) / 2\rho$). These waveforms were taken from the curved side of the single crystal cylinder. The shear wave velocity for polarisation in the (100) direction taken via propagation down the cylinder was measured to be 3244 m/s +/- 0.1% (see fig 6.10) , only 0.1% difference to the values taken from the literature. Thus it is proposed that the consistently lower values of velocity obtained via propagation across the cylinder diameter is due to some sort of geometrical effect of propagating the ultrasound through the long axis of the cylinder, or some slight offset in the calculated trigger point where time=0μs.

4.6 C-scan detection of flat bottomed holes in aluminium plate

In order to assess the EMAT performance on birefringent plate, an aluminium sample 13.4mm thick, was prepared from the same batch as the samples used in the tensile stress measurements. The plates measured 150mm X 150mm, and had a range of flat bottomed holes milled into them of varying diameter, but all to a depth of 2.75mm ,as shown in fig 4.8. The edges of the square plate were parallel and orthogonal to the rolling marks visible on the surface. The plate was then scanned taking a square grid of points, the axes of which were along and orthogonal to the rolling direction. Reflection intensity c-scans for this

sample are shown in fig 4.9a and fig 4.9b. This was done by ensuring that the ultrasonic pulse from the full plate thickness (echo corresponding to a transit of 2 X 13.4mm) was outside the time observation window. The directions of symmetry in the reflection intensity pattern correspond to the direction of rolling and at right angles to the rolling direction.

The experiment was repeated for a square plate having edges at 45° to the rolling direction, and thus the square grid of data points had its axes at 45° to the rolling direction. As can be seen, the intensity pattern produced by the c-scan is the same as that previously obtained except rotated by 45° (see fig 4.10).

It was established in fig 4.1 that the attenuation factors for each shear wave polarisation were nominally identical, while the absolute values of amplitude were significantly different. Electromagnetic differences due to the anisotropy of the sample would be expected to slightly affect the amount of energy, but this should be a second order effect compared to the acoustic anisotropy. Thus, the difference in absolute values of signal amplitude were mainly due to acoustic beamsteering. The shape of the c-scan patterns themselves are very complicated. There has been much work on modelling the acoustic field scatter from such flat bottomed holes [16], but a thorough examination would require the scatter theory convolved with the field produced by the EMAT (and of course the size of the active area of the EMAT) in an anisotropic medium.

For comparison, a hole of diameter 20mm and depth 2.75mm was milled in a plate cut from thick extruded aluminium rod transverse to the long axis of the bar. This hole was exactly the same dimentionally as that in the rolled aluminium plate. In the centre of such a plate the structure should be effectively isotropic for an SH wave propagating along the direction of extrusion. The c-scan for the 'isotropic' flat bottomed hole is shown in fig 4.11. The sizes of the defects appear roughly the same, but the effects of radially polarised EMAT scanning on anisotropic plate has been demonstrated.

The smallest hole detectable was 2mm in diameter. The smaller hole scans still produced the characteristic two fold symmetry patterns, but the maxima of these patterns were distinctly off centre, located approximately 2mm from the centre of the pattern.

Examining the amplitude field generated by the EMAT showed the largest ultrasonic amplitude was at a distance of 2mm from the centre of the coil through a thickness of 5mm of aluminium plate.

4.7 Summary

The radially polarised EMAT is a useful tool in investigating the macrostructure of metal plates, in particularly aluminium. The anisotropy in aluminium plate is typically a relatively small effect (as compared to steel), and it is because the shear wave pulses have high temporal resolution that the birefringence measurements are clearly observable. The birefringence effect could complicate the analysis of adhesively bonded aluminium plate and give confusing results if this phenomena is neglected.

Ch.4 References

1. M.J.P. Musgrave , Crystal Acoustics , Holden-Day , 1970

2. R.J. Roe , Description of crystalline orientation in polycrystalline materials , J. Appl. Phys. , 36 , 1965 , pp2024-2027

3. C.M. Sayers , Ultrasonic velocities in anisotropic polycrystalline aggregates , J. Phys. D : Appl. Phys. , **15** , 1982 , pp2157-2167

4. K. Kawashima, Nondestructive charaterisation of textrue and plastic strain ratio of metal sheets with electromagnetic acoustic transducers , J. Soc. Am. , 87 , No.2 , 1990 , pp681-690

5. A.V. Clark, Jr. and J.C. Moulder , Residual stress determination in aluminium using electromagnetic acoustic transducers , Ultrasonics , 23 , 1985 , pp253-259

6. S.E. Pritchard, The use of ultrasonics for residual stress analysis , NDT Int. , Vol 20, no.1, 1987, pp 57-60

7. M. Hirao, K Aoki and H. Fukuoka , Texture of polycrystalline metals characterised by ultrasonic velocity measurements , J. Soc. Am. , 80 , 1987 , pp1432-1440

8. M. Hirao, H. Hara, H. Fukuoka and K. Fujisawa , ultrasonic monitoring of texture in cold rolled steel sheets , J. Soc. Am. , 84 , pp667-672

9. D.R. Allen and C.M. Sayers , The measurement of residual stress in textured steel using an ultrasonic velocity combination technique , Ultrasonics , 22 , 1984 , pp179-188

10. D.R. Allen , R. Langman and C.M. Sayers , Ultrasonic SH wave velocity in textured aluminium plates , Ultrasonics , 23 , 1985 , pp215-222

11. E. Imanishi, M. Sasabe and Y. Iwashimizu , Experiemntal study on acoustical birefringence in stressed and slightly anisotropic materials , J. Acous. Soc. Am. , 71 , 1982, pp565-572

12. R.B. King and C.M. Fortunko , Acoustoelastic evaluation of arbitary plane residual stress states in non-homogeneous, anisotropic plates , Ultrasonics, 21, 1983 , pp256-258

13. A.V. Clark, Jr. , On the use of acoustic birefringence to dtermine components of plane stress, Ultrasonics , 23 , 1985 , pp21-30

14. R.B. King and C.M. Fortunko , Determination of in-plane residual stress states in plates using horizontally polarised shear waves , J. Appl. Phys. , 54 , 1983 , pp3027-3035

15. Y. Poa ,W. Sachse and H. Fukuoka , Acoustoelasticity residual stress measurements, in: Physical Acoustics **XVII** , (Ed. WP Mason and RN Thurston), Academic Press, New York , 1979 , pp61-143

16. J.A.G Temple , Diffration coefficients for flat bottomed holes from 3-D finite difference calculations , Ultrasonics **31** No.1 , 1993 , pp3-11

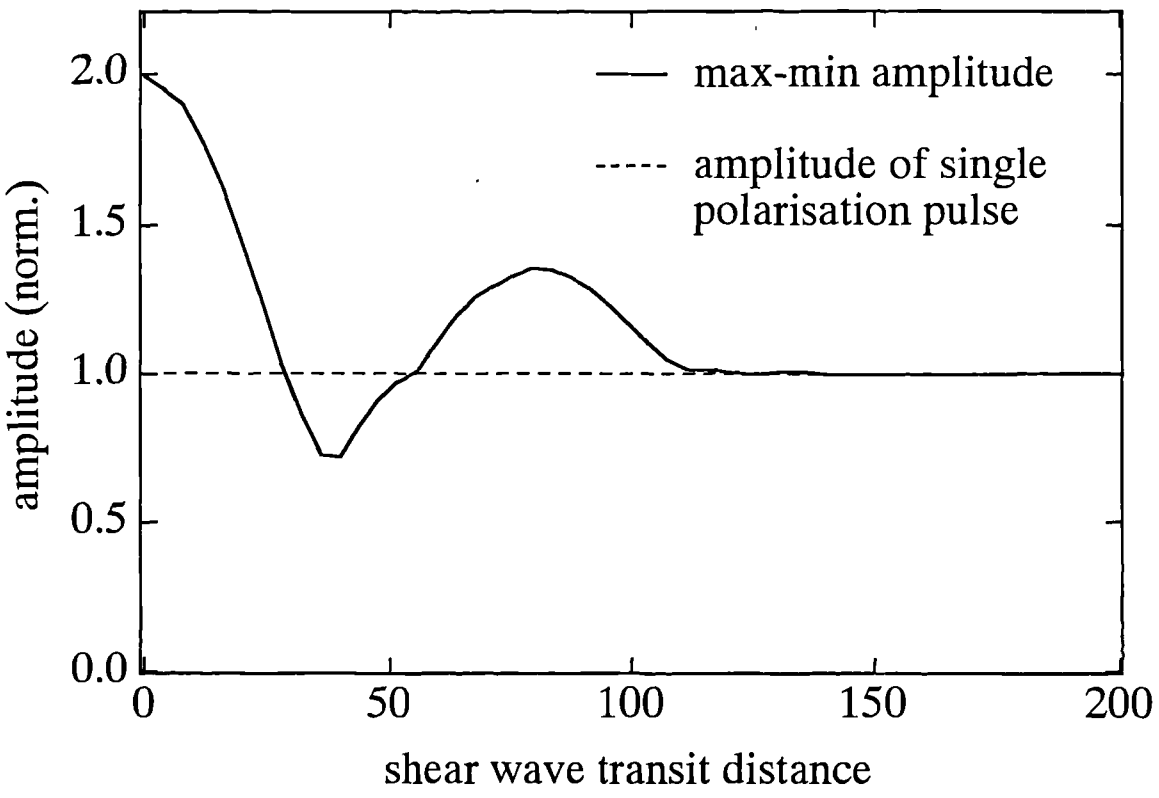

Fig 4.1

Calculated shear pulse minimum-maximum signal amplitude modulation arising due to the birefringent nature of an aluminium sample.

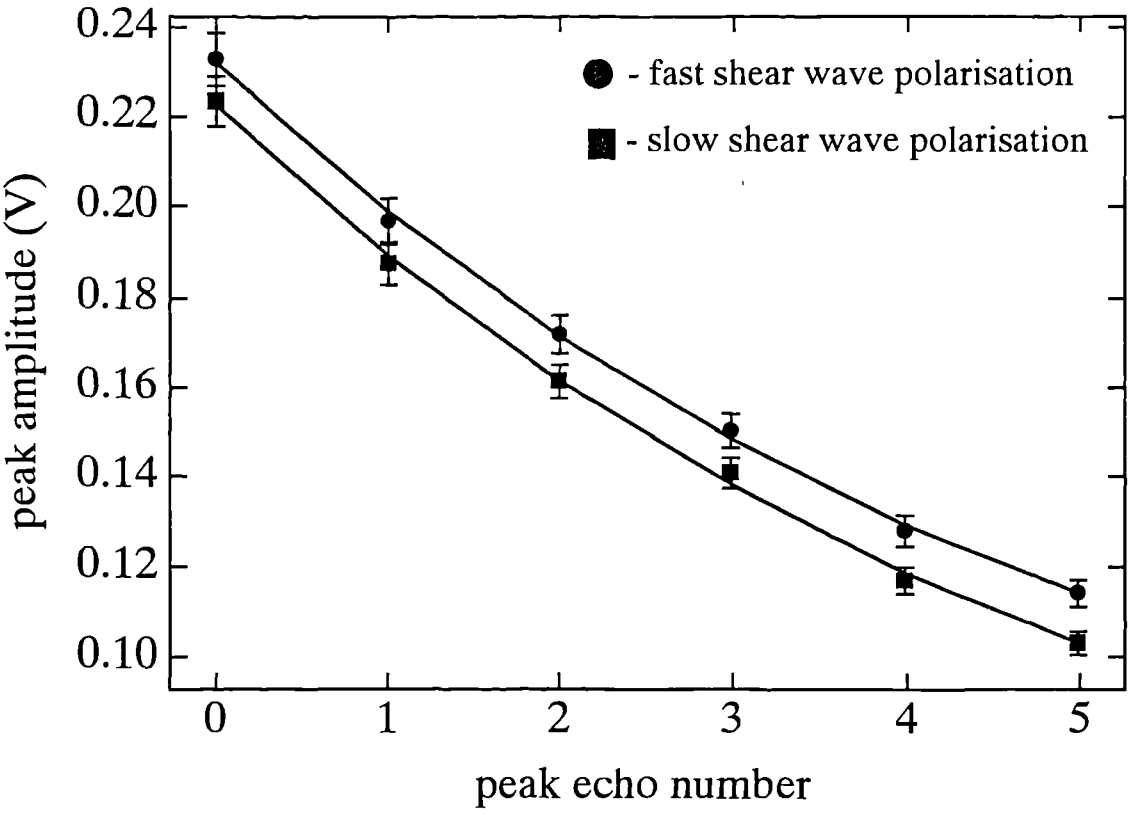

fit to exponential function $a + b \exp[-cx]$

where x is the peak echo number and c the decay factor,
and a and b are constants.

fast polarisation	slow polarisation
a = 0.0258V +/- 0.196V	a = 0.0389V +/- 0.16V
b = 0.197V +/- 0.19V	b = 0.193V +/- 0.16V
c = 0.188 +/- 0.029	c = 0.189 +/- 0.025

Fig 4.2

Amplitude decay of the two horizontally polarised shear wave polarisations observed using the radially polarised EMAT on a birefringent aluminium sample.

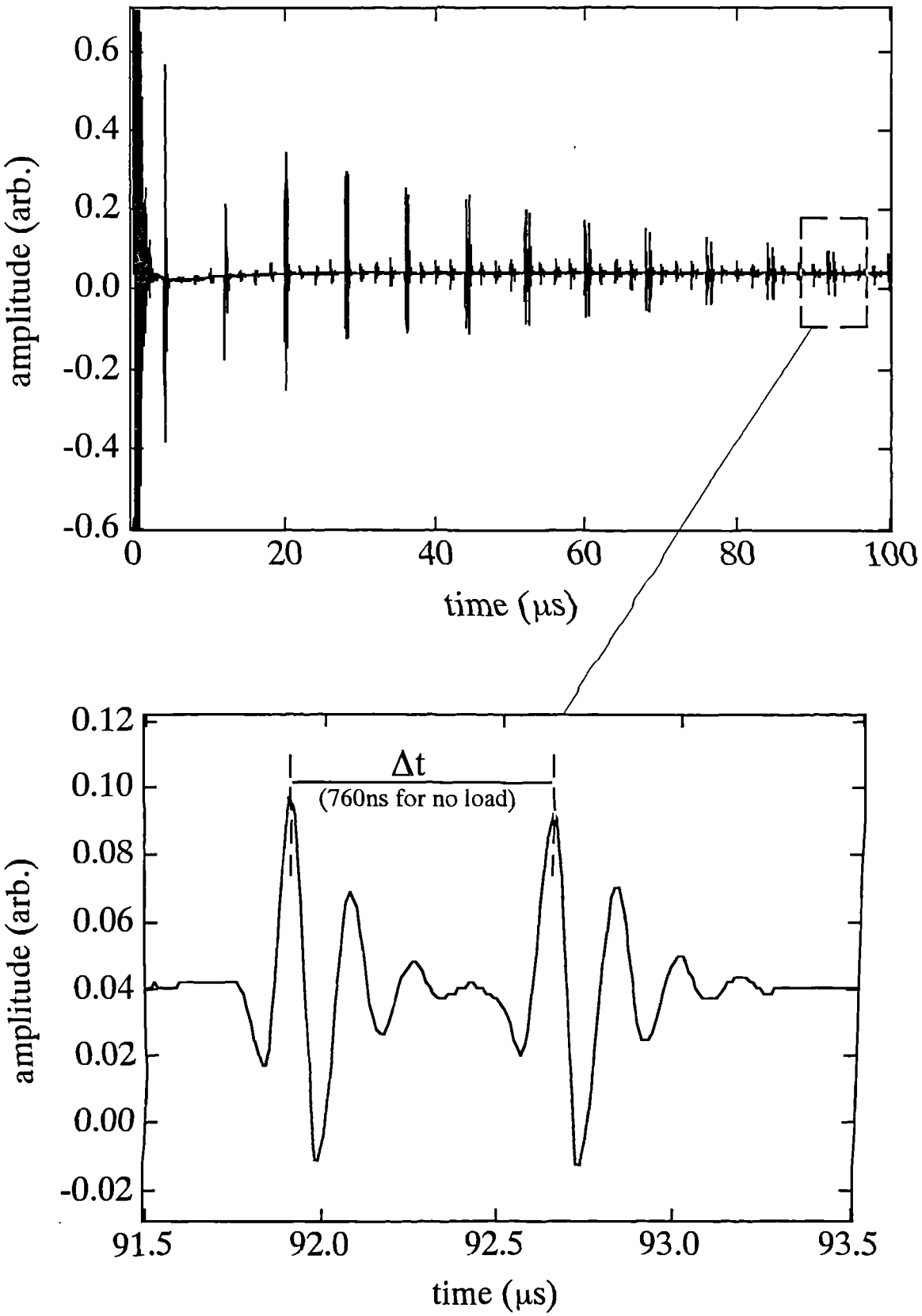

Fig 4.3

EMAT through transmission waveform obtained on a birefringent aluminium sample.

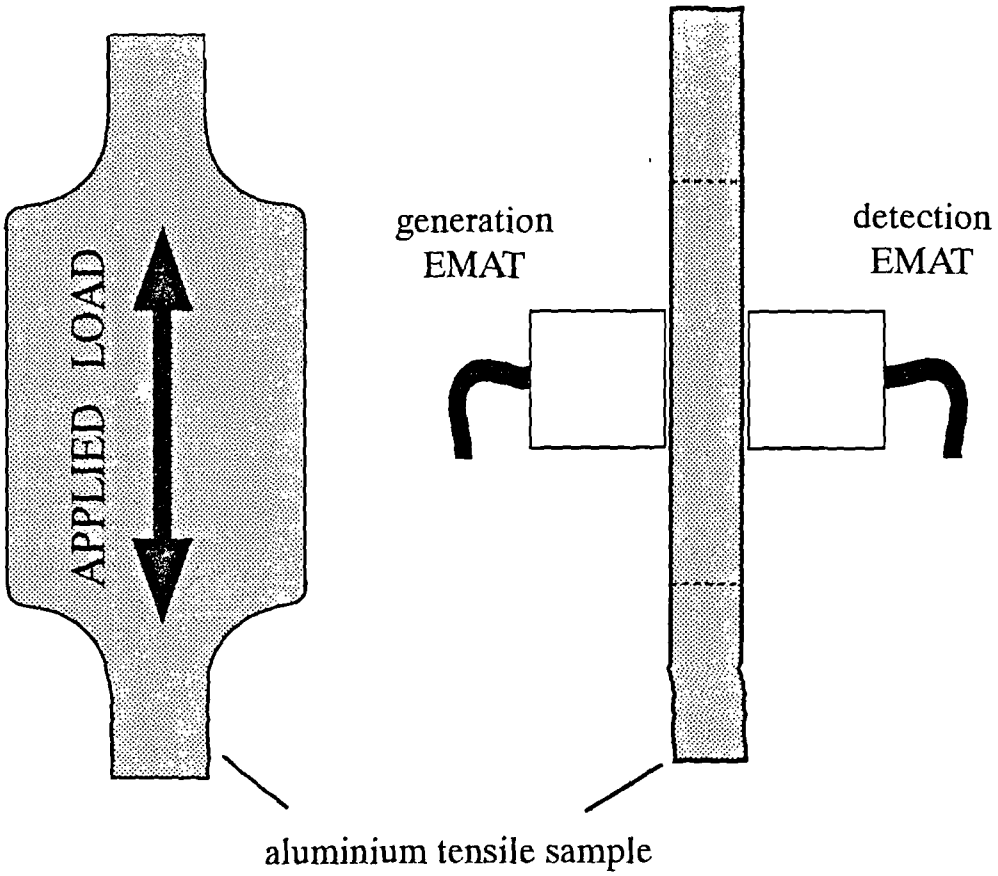

Fig 4.4

Schematic diagram of textured aluminium tensile test samples.

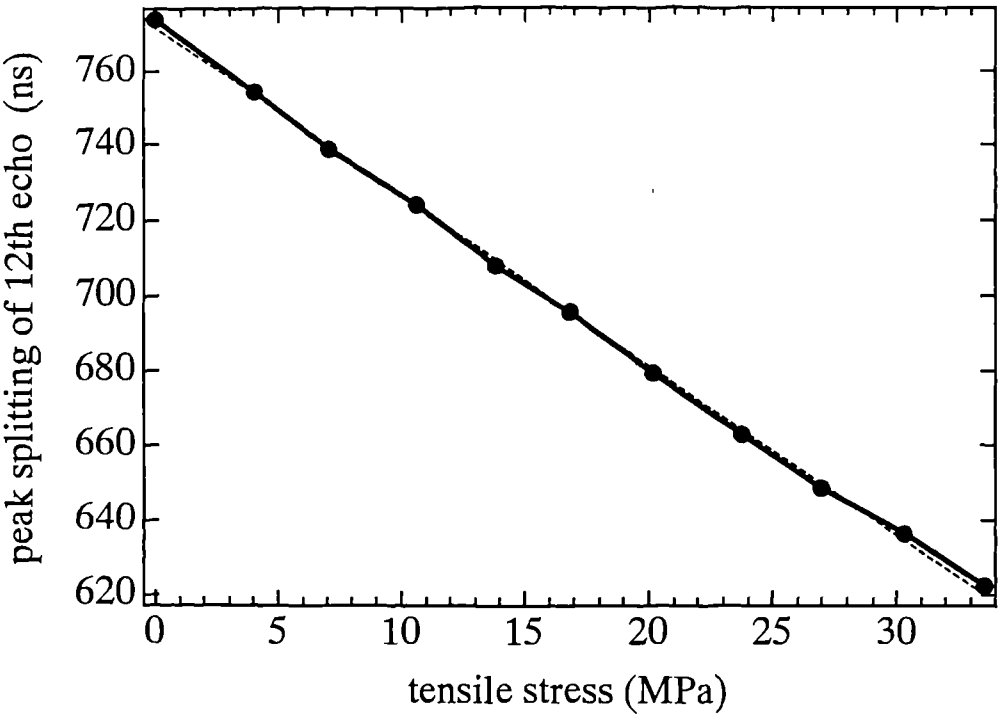

Fig 4.5a

Peak splitting of 12th peak with tensile stress applied along rolling direction.

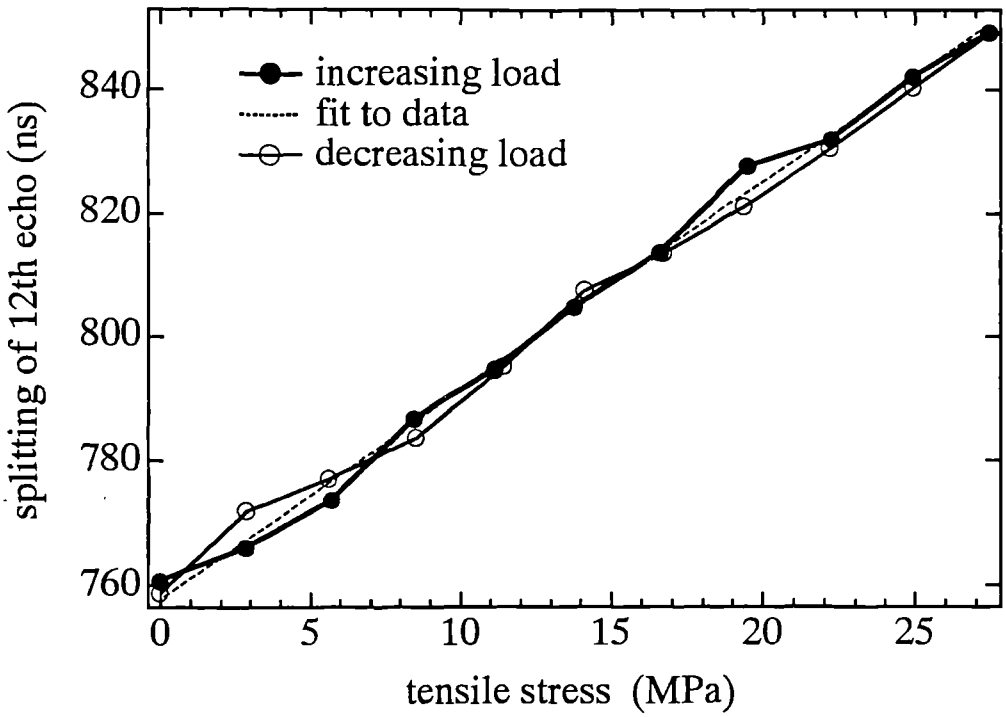

Fig 4.5b

Peak splitting of 12th peak with tensile stress applied orthogonal to the rolling direction.

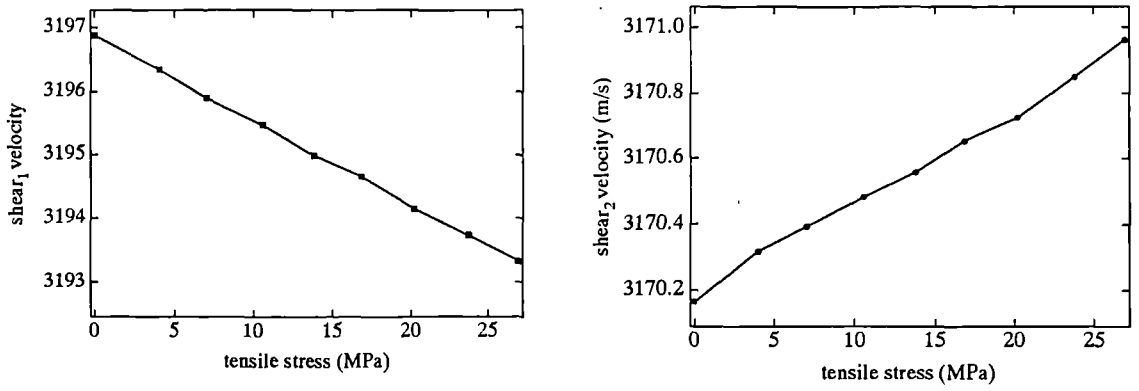

Fig 4.6a

Velocity dependence on applied tensile stress for tensile stress applied along the rolling direction in an aluminium sample for the two shear wave polarisations.

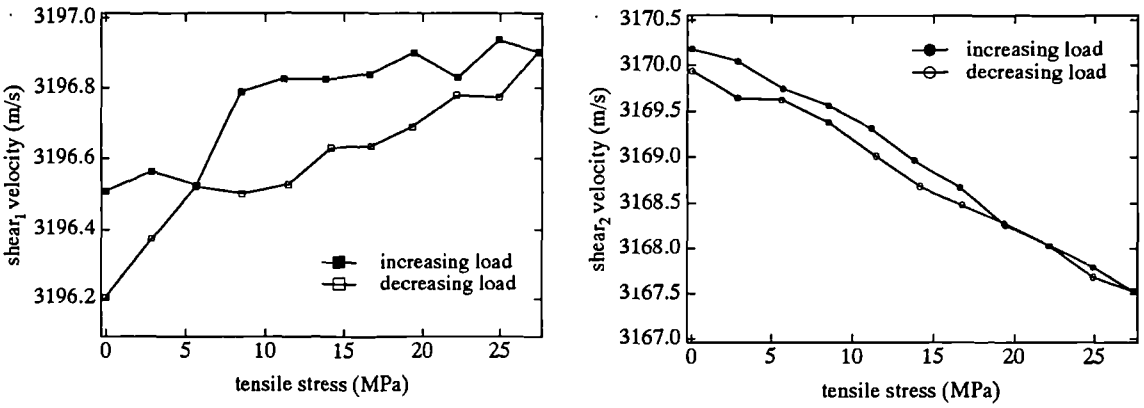

Fig 4.6b

Velocity dependence on applied tensile stress for tensile stress applied orthogonal to the rolling direction in an aluminium sample for the two shear wave polarisations.

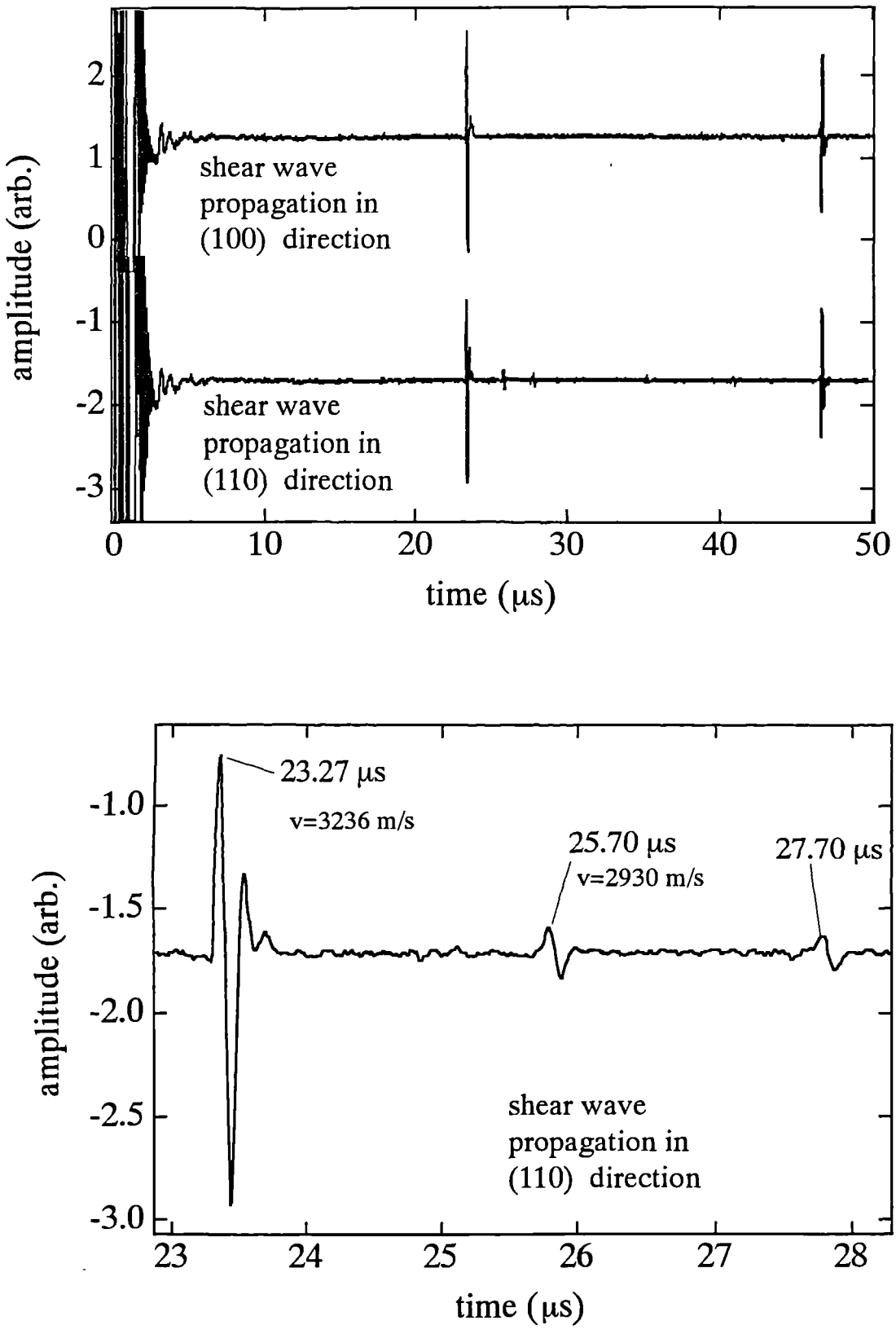

Fig 4.7

EMAT generated raidally polarised shear waveforms in two different crystallographic directions in a single crystal of aluminium.

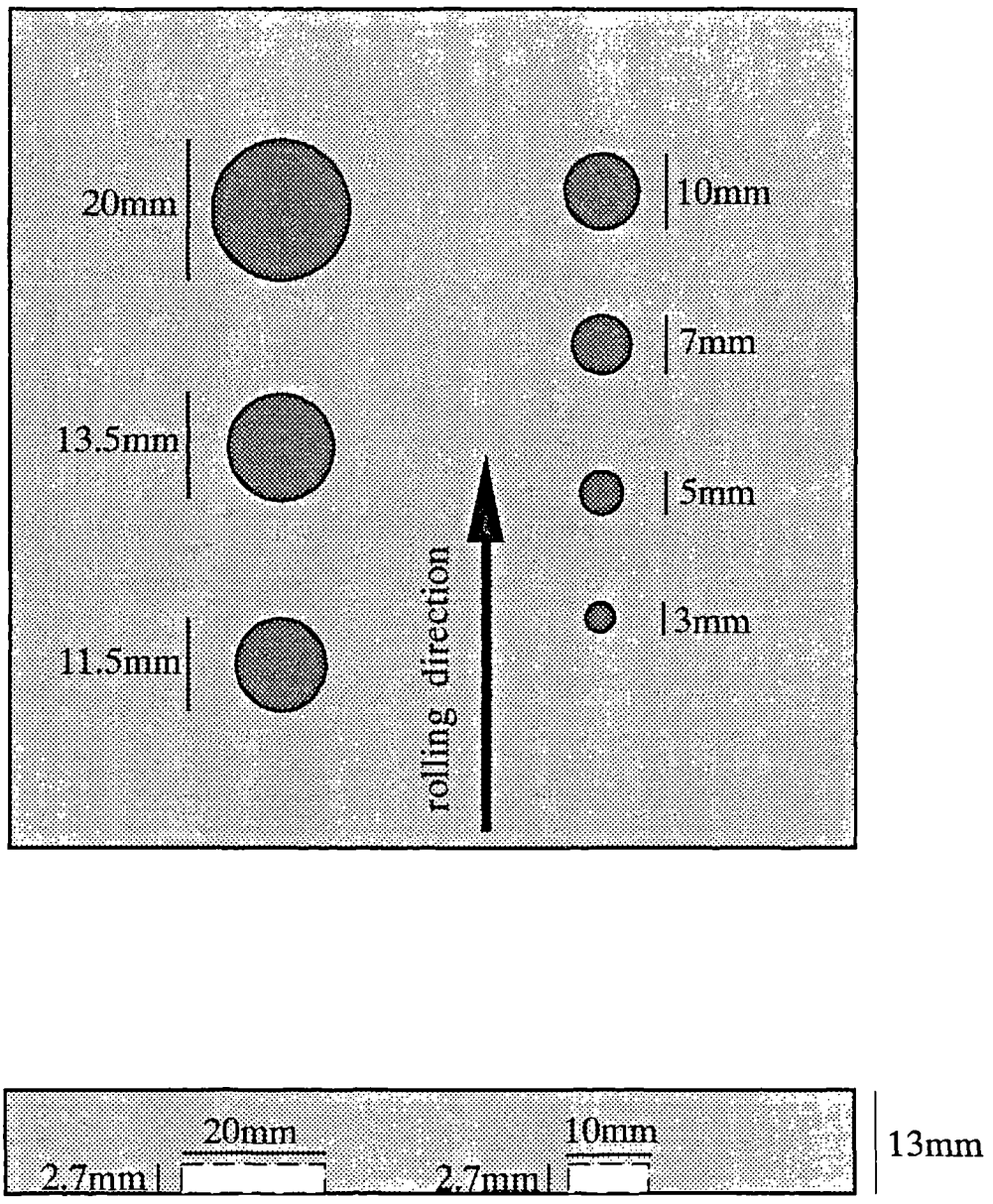

Fig 4.8

Topological and cross sectional view of the range of flat bottomed holes milled into a 13mm thick aluminium plate.

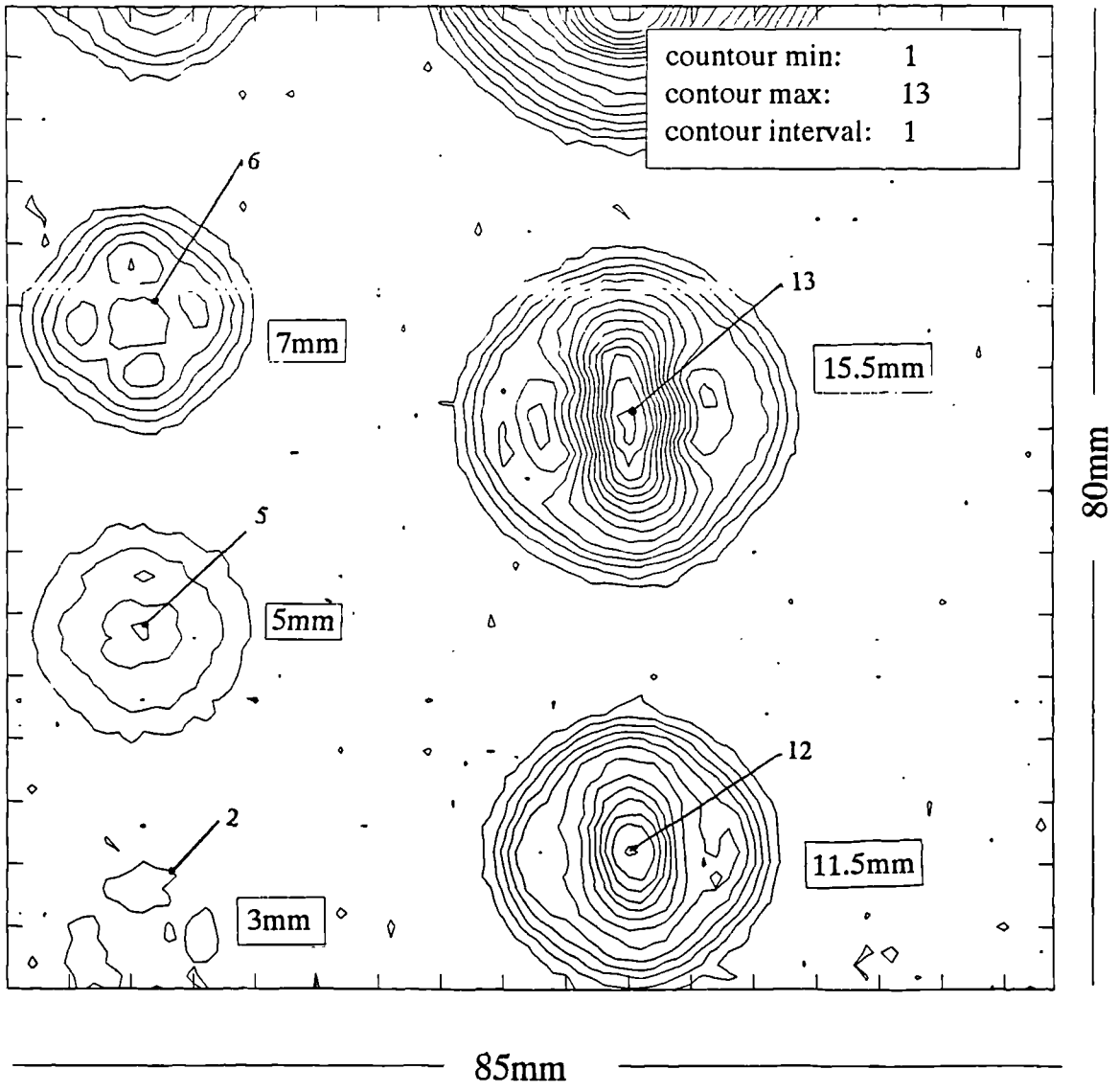

Fig 4.9a

C-scans of a birefringent aluminium plate using an EMAT send-receive system. The scanning grid axes were parallel and perpendicular to the rolling direction. The plate thickness was 13.5mm and the flat bottomed holes were 3mm deep into the plate.

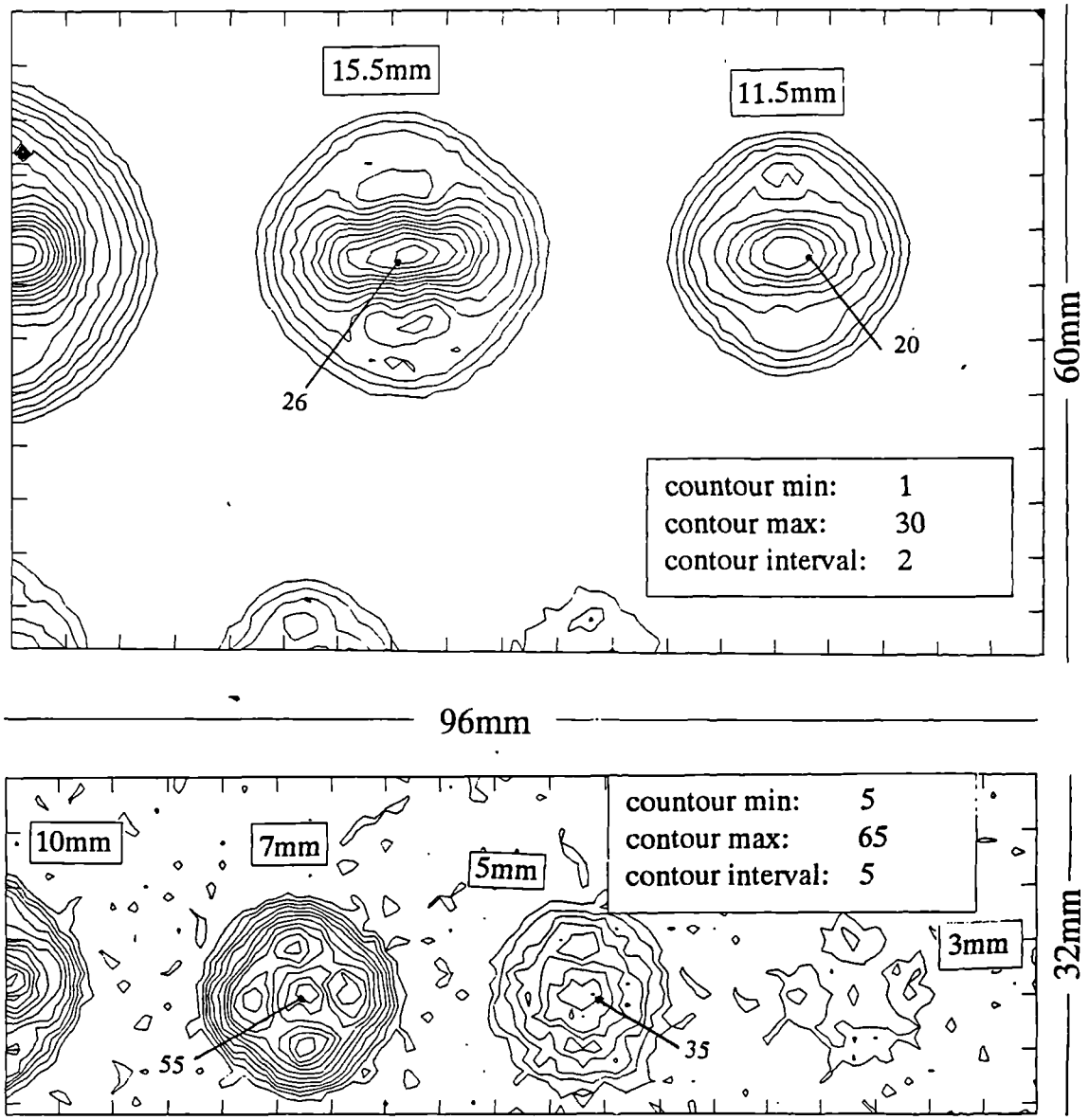

Fig 4.9b

C-scans of a birefringent aluminium plate using an EMAT send-receive system. The scanning grid axes were parallel and perpendicular to the rolling direction. The plate thickness was 13.5mm and the flat bottomed holes were 3mm deep into the plate.

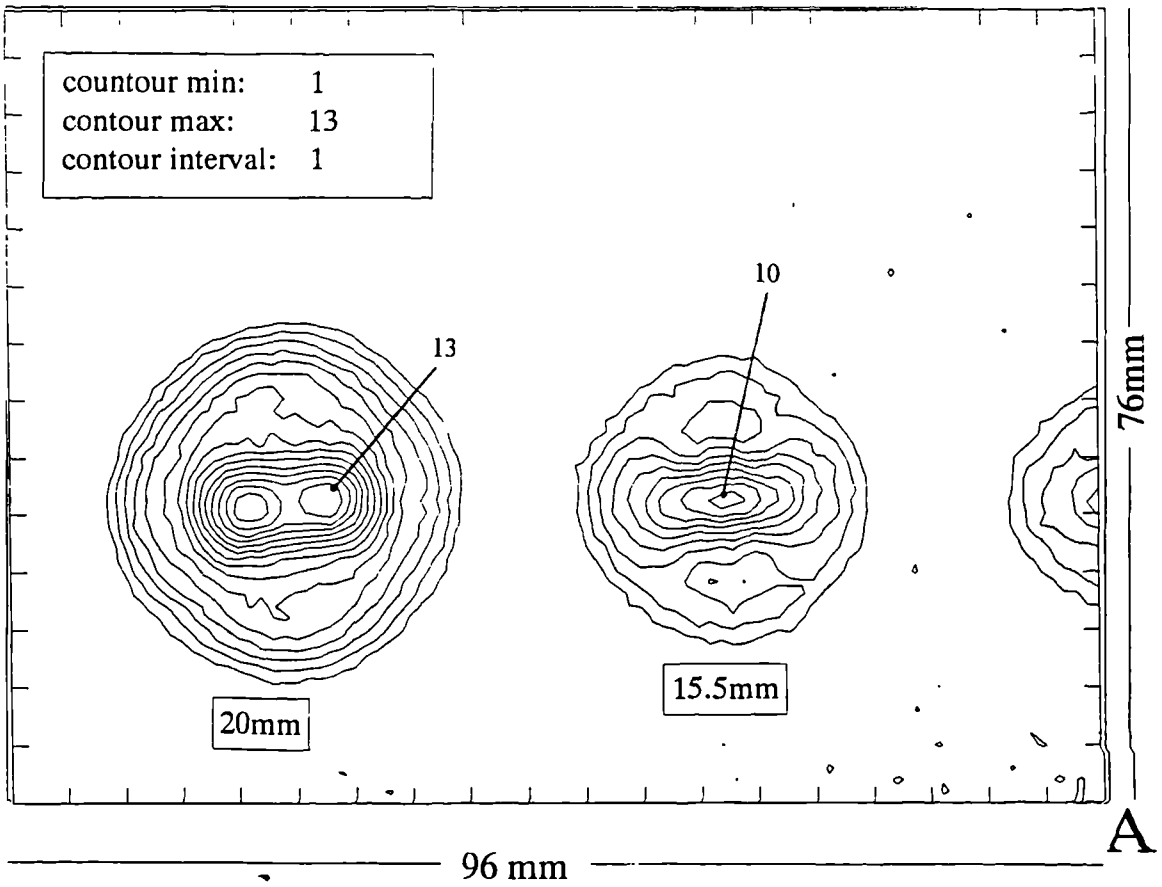

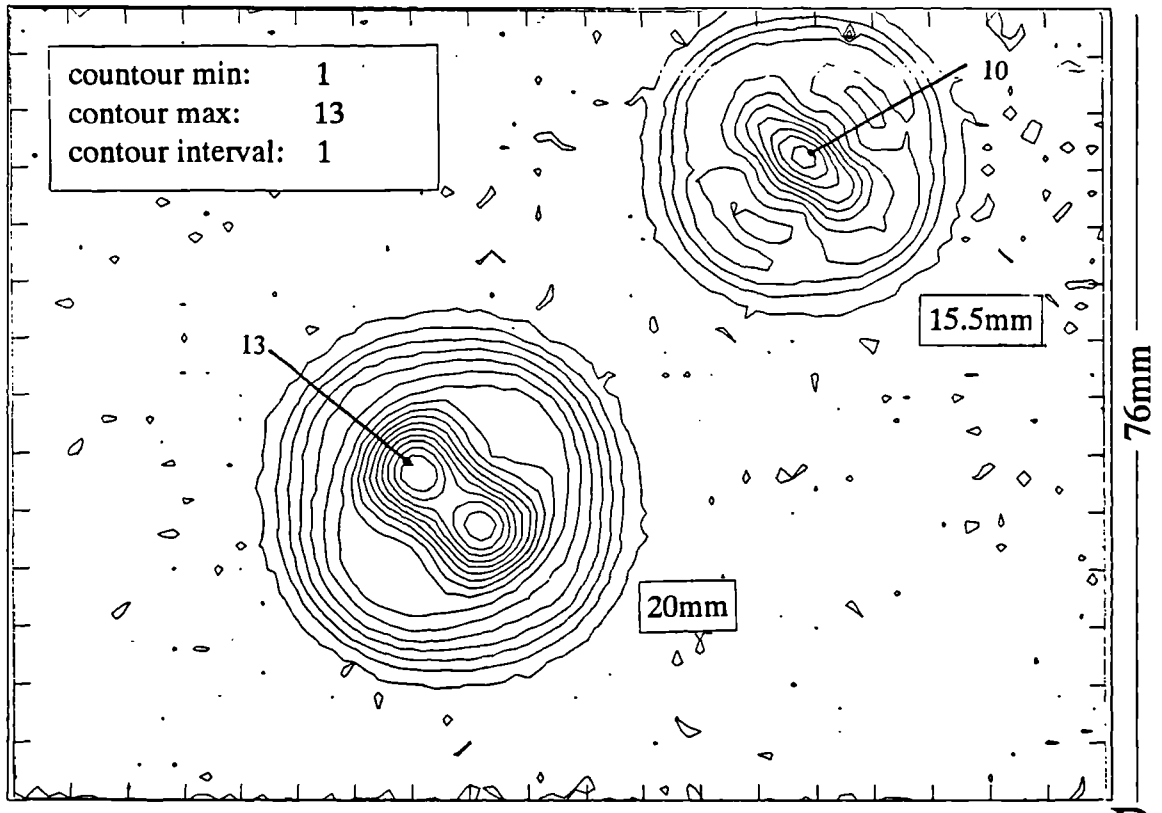

Fig 4.10

C-scans of flat bottomed holes with the scanning grid axes parallel at orthogonal to the rolling direction (A), and at 45^0 to the rolling direction (B). The plate thickness was 13.5mm and the flat bottomed holes were 3mm deep into the plate.

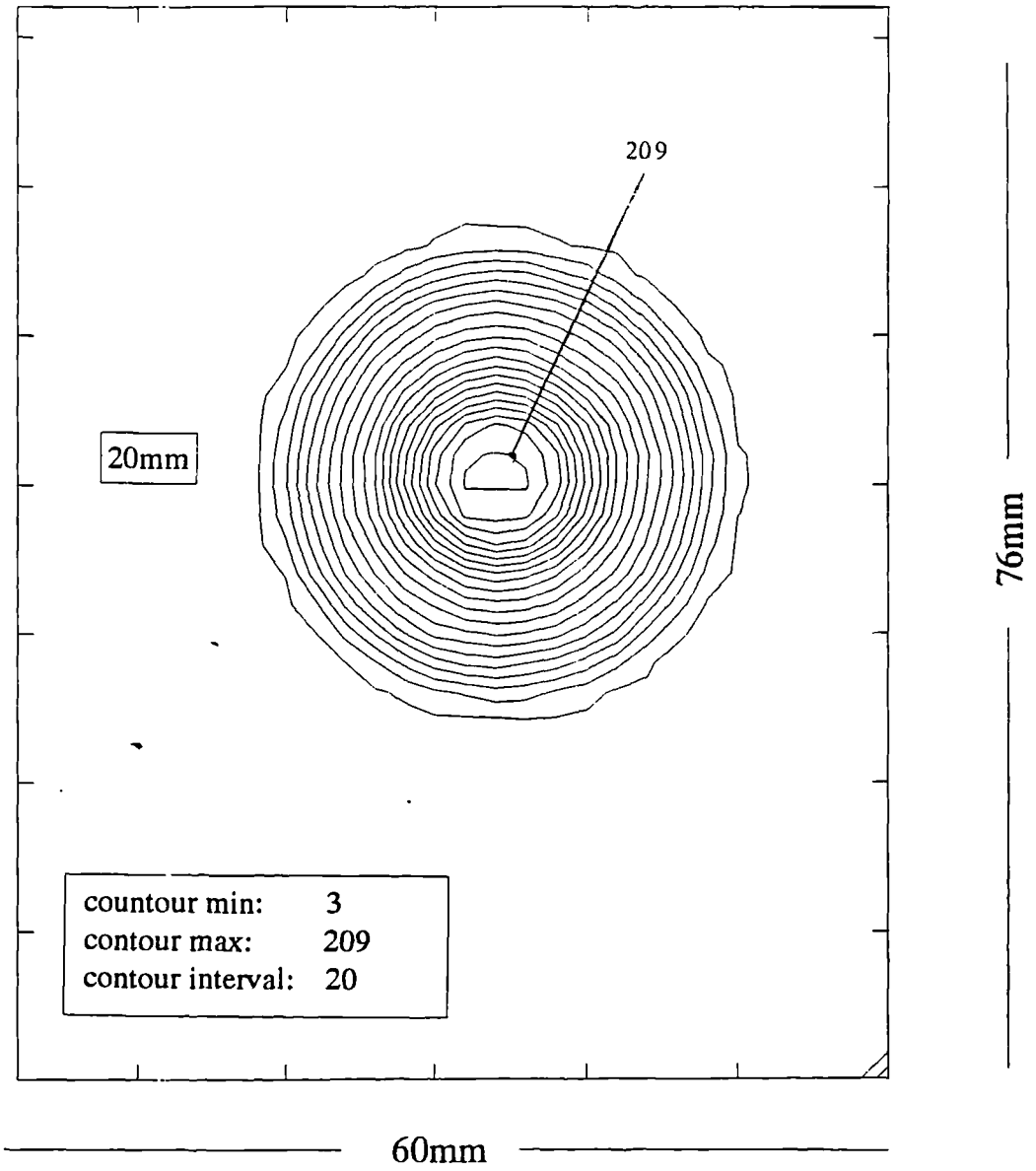

Fig 4.11

C-scans of a transversely isotropic aluminium plate using an EMAT send-receive system. The sample was a cross sectional cut from an extruded aluminium bar of diameter 150mm. The hole was 20mm in diamteter and 3mm in depth into a plate 13.5 mm thick.

Chapter 5

Adhesive bond analysis experiments

5.0. Introduction

In this chapter the basic experimental procedure and results obtained from ultrasonically scanning the adhesive bonds will be discussed. The first part of this section deals with the details of the bond and its isolated components. The relative merits of the through transmission and send receive measurements are explored, and results obtained from these two techniques are explained. Finally, some specific C-scan type results are presented, with an explanation of the ultrasonic measurements resulting from such scans.

5.1 Description of adhesive bonds examined

5.1.1 Geometry of the bonds

One of the most simple types of joint both to construct and test is a lap joint. This bond was chosen because it is commonly used in both experimental studies and the simplest applications of adhesive bonds. The samples were constructed in the form of a 150mm X 150mm sandwich joint where the bonded area completely covers the adherents, strictly speaking not a true lap joint. It essentially consists of a three layered system : adherent - adhesive -adherent. Most simple theoretical models assume that the adhesive layer is completely homogeneous, having little or no thickness variation, and most experimental samples are constructed with this aim. Aerospace adhesive bonds can have large variations in adhesive thickness, typically up to 50% across a joint. The bonded samples used in investigating the technique described here were constructed as shown in fig 5.1 (see Appendix B for description of bond technique). The epoxy adhesive used in the bonds was Redux 312 (Cieba - Giegy), used both with and without a fabric carrier in different samples.

The purpose of the carrier is to prevent excessive adhesive flow and maintain a fairly uniform thickness, typically about 100μm. The aluminium adherents used were 3.3mm and 4.8mm in thickness. The reason for using different adherent thicknesses is that in ultrasonic through transmission measurements the first echoes containing information about the individual interfaces are separated in the time domain. Some samples contained deliberately manufactured defects, nominally 40mm X 40mm square, positioned in the central area of the bond on the surface of the 3mm plate at the adherent-adhesive interface.

5.1.2 Different bond and sample types investigated

A number of different sample types were constructed using the basic bond geometry as described above, containing adhesives with and without the carrier. This was done in order to ascertain whether the carrier had any significant effect on the acoustic properties of the adhesive bond, as the addition of carrier greatly complicates the macro and microstructure features of the adhesive layer. The carrier was a flat fabric of hexagonal structure. The width of the hexagons were about 0.5mm, which was comparable to the range of the ultrasonic wavelengths present in the broadband ultrasound generated by the EMATs. Thus the presence of carrier could potentially have altered the dispersive and attenuative properties of the adhesive, while also introducing a strong anisotropy to the adhesive layer. The presence of carrier was found not to observably affect the ultrasonic signals, as discused later in section 5.3.2.

In addition to the nominally 'perfect' bonds, a range of bonds containing deliberately manufactured defects were prepared. The aim of this exercise was to simulate the physical properties of realistic defect types encountered in bonded aerospace samples. Defect manufacture tends by its very nature to be an imprecise science, and destructive tests must still be employed in examining the exact mechanical conditions that exist within the bond.

A table of sample types is shown in table 5.1. The table gives a brief description of the type of intended sample construction with details of the actual defect revealed by subsequent destructive tests. The size and shape of the adhesively bonded 'DRA' samples

and the location of the defect region is shown in fig 5.2a. The location of the areas of the samples that were slowly milled out to produce strips for tensile testing is also shown in fig 5.2a, with the layout of the results presented in table 5.1. The tensile strips machined from the bonded samples were tested as shown in fig 5.2b, where the aim is to attempt a shear type test on the joint which ultimately fails in a peel type mode.

5.2 Characteristics of isolated bond components

5.2.1 Aluminium plates

An aerospace grade aluminium (BL 156) plates were used for all bonded samples. Prior to adhesion the plates were prepared as described in the appendix. This treatment gives improved protection against environmental attack, by making very thin, porous layers on the aluminium surfaces as shown in fig 5.1. The layers are so thin (total thickness approx 1μm) that there was no observable effect (other than perhaps degree of adhesion) on the ultrasonic properties as investigated using the EMAT systems. The layers were spatially much smaller than even the shortest wavelength component present in the EMAT shear wave pulse. If this layer was to be seen as a gradation in the ultrasonic properties, the frequencies required would be of the order of GHz. In the experiments reported here, the frequency ranges dealt with were well within the limit where the adherent-adhesive interface should behave as a sharp boundary between the aluminium and epoxy. It has been shown [1] that the presence of these layers can effect the mechanical (and thus possibly acoustic) properties of the bonded structure as a whole. During construction of the bond the plates may undergo flexural deformation and thus experience changes of stress within the plate, and other stress effects brought about by shrinkage of the adhesive during cure.

Waveforms obtained using an EMAT-EMAT through transmission (TT) geometry, an EMAT send-receive (SR) geometry and a hybrid laser generation / EMAT detection system are shown in fig 5.3 The EMAT waveforms show the characteristic intermediate peaks due to mode conversions. At longer arrival times the waveform also shows very weak

acoustic birefringence. Acoustic birefringence (chapter 4) is another possible source of complication arising in waveform analysis, but the plates were thin enough and sufficiently isotropic, so that birefringence is not a problem with these particular bonded samples. The modulation of the EMAT waveforms (see chapter 3) requires consideration, even where the faces of the aluminium plate are nominally parallel: we are again dealing with modulation due to the intrinsic properties of the EMAT system.

Billson et al [2] used a similar type of laser-EMAT system and employed shear and longitudinal EMATs to detect the ultrasound, and as in this case the ultrasound was generated by a pulsed Nd:YAG laser. The EMAT was constructed to detect in-plane motion. In general the laser source [3] will generate both longitudinal and shear waves which will be detected by the shear wave EMAT. The EMAT will detect both modes due to the laser source directivity, the tangential components of the EMAT magnetic field and because the longitudinal displacement will have an in-plane component at the surface. Note that the waveform consists of longitudinal and shear waves and longitudinal-shear / shear-longitudinal wave mode conversions. The waveform obtained from the hybrid system is far more complicated than that from the EMAT system and is consequently difficult to analyse in bonded structures. However, the hybrid system is useful for straightforward thickness gauging, especially where the EMAT generated signals are small duefor example, to poor electrical conductivity.

5.2.2 Epoxy adhesive

Epoxy samples were supplied in three different forms; an isolated ingot of cured adhesive, an adhesive layer adhered to an aluminium plate and adhesive within a bonded sandwich. Each of the three cases had the epoxy component under very different physical conditions. A stress gradient would arise at the epoxy at the adherent-adhesive interface during cure, and this effect has been investigated by [4]. The effect of curing an adhesive either adhered to one plate or (to a greater extent) between two plates could possibly give the adhesive very different mechanical and acoustic properties due to the different stress

conditions and different internal structure. By consideration of the acoustic properties of these three cases it may be possible to determine the dominant physical properties that distinguish a free cured epoxy from its behaviour in a bonded structure. However, in all three cases the experiments showed no measurable difference in velocity, or impedance mismatch at the epoxy-aluminium boundary for the bond or single plate with epoxy. The experimental setups and waveforms from these experiments are shown in figs 5.4 and fig 5.5.

As the EMATs cannot directly generate shear waves in the epoxy ingot, ultrasound was generated using a pulsed Nd:YAG laser in a mildly ablative regime, at an energy of approximately 60mJ with a beam diameter of 5mm. The laser generated ultrasound was detected using a stabilised Michelson interferometer as described by Scruby [5], and sufficient reflectivity from the sample surface was achievedby sputtering aluminium onto the surface of the epoxy. The interferometer detects out of plane motion relative to the sample surface corresponding to a longitudinal displacement. Shear waves can also be detected by the interferometer as they have an out of plane component at the sample surface. Using this laser generation/detection technique yields measurements that correspond to the longitudinal and shear wave arrivals (see fig 5.5). Note the longitudinal echo is broader than the preceeding longitudinal arrival, reflecting the viscoelastic properties of the epoxy.

The samples of single aluminium plate with a layer of cured epoxy, and the aluminium plate adhesive bonds were tested using EMATs. Fig 5.4 show the pulse reflected from the aluminium epoxy interface proceeded by the signal from the epoxy-air boundary. This echo is significantly different to the corresponding 'bondline echo' in the adhesively bonded sandwich, as the boundary conditions for epoxy-air are different to that for epoxy-aluminium. The most obvious difference is the pulse inversion in the adhesively bonded plates sample as discussed in chapter 2. As there is a much larger impedance mismatch in going from epoxy-air than from epoxy-aluminium, the adhesive echo in the single plate+epoxy sample is larger in amplitude than the bondline echo in the adhesively bonded sandwich.

5.3 Experimental proceedure

5.3.1 Basic setup

In scanning the bonded samples two basic test geometries were employed, these being a through transmission (TT) and a send-receive (SR) technique. The TT technique required 2 radially polarised shear wave EMATs on opposite sides of the sample on epicentre as shown in fig 5.6. The SR technique (a c-scan method) employed the use of a single EMAT, having either a single or a double coil .

The EMATs were held stationary during a scan, while the sample was moved using an XY table. The transducers were in physical contact with (but not acoustically coupled to) the surface of the plate, to increase signal amplitude by minimising stand-off, and to reduce the radiated electrical noise picked up by the EMAT. The data was taken by positioning the plate, then recording features from the averaged waveform. The waveform itself was not recorded as this would make the process more time consuming and requires much more PC memory. A schematic of the experimental setup is shown in fig 5.7 . By using this method a square grid of points was taken with the relevant experimental values attributed to each point on this grid (amplitude or pulse time separation).

5.3.2 Ultrasonic signals within adhesive bonds

With any acoustic technique the ultrasonic waves must in some way propagate through or within the adhesive layer if the physical properties of the interfaces or the adhesive bulk are to be determined. The adhesive layer within a bond has very different mechanical and acoustic properties to the aluminium adherents. The aluminium is effectively a linear isotropic, homogeneous medium (neglecting anisotropy in this case for reasons outlined earlier), while the epoxy layer is a much less dense viscoelastic medium, with much slower longitudinal and shear wave velocities. This leads to a significant impedance mismatch at the adherent-adhesive boundary, resulting in any SH wave travelling in the adhesive layer having a relatively small amplitude. Therefore the most obvious problem in

investigating possible physical differences at an interface is the fact that the effects will be small changes on an initially small signal. This is further complicated by the presence of other ultrasonic arrivals due to mode conversions and other internal reflections within the layered structure.

The first and most important step was to establish was whether the presence of the fabric carrier was detectable. Two bonded samples of similar thickness were chosen, one with carrier and the other without. An area was found on each where the adhesive thicknesses were identical to within experimental error. Waveforms from these two cases were then captured in the more sensitive through transmission method (see fig 5.8), and found to be nominally identical. This implies that the carrier has no significant impedance mismatch with the epoxy, and that the presence of the carrier does not measurably affect the acoustic properties of the adhesive layer.

5.3.3 The ultrasonic measurement employed

The two fundamental properties of an adhesive bond are the cohesive properties of the adhesive and the adhesion between adherent and adhesive. The cohesion is a measure of the strength of the adhesive, while the adhesion is a measure of the strength of joint between the adhesive layer and aluminium adherent. Cohesion can be measured by examining the ultrasonic dispersive and attenuative nature of the adhesive, while the adhesion can be measured via relative differences in pulse amplitude measurements brought about by an impedance mismatch. Both these areas have been studied using ultrasonics [6], but the main problem still lies in examining subtle variations in adhesion. In a sense, the analysis here has ignored any variation in solely the cohesion or soley the adhesion. The adhesion should only effect the impedance mismatch and thus amplitudes of the ultrasonic pulses. The reflection from an elastic-viscoelastic medium interface will in general be frequency dependant, but over the range of frequencies used here, such effects were unobservable in the samples investigated. As the measurements taken during a scan were pulse amplitude and echo separation, then the measurements are strictly speaking an

indication of both cohesive and adhesive properties. In most real cases it is impossible to separate the effects of adhesion and cohesion, as where one property varies, the other is also likely to change. The mechanical properties and thickness of the adhesive will effect how different ultrasonic frequencies propagate through the adhesive. The thickness measurement of the adhesive layer was made via an echo separation in the time domain. This in itself depends on the velocity in the adhesive, and so on the cohesive nature of the bond.

The amplitude and 'thickness' measurements were made as shown in fig 5.9 for TT and SR. The 'thickness' measurement shown obviously correspond to twice the ultrasonic pulse transit time across the adhesive layer. Some authors suggest that this type of measurement may be flawed [7] as it is affected by the phase velocity within the adhesive (as dispersion could change the pulse shape) and have suggested a technique that measures the area under a broadband monopolar pulse and takes the half area position as the arrival time of the ultrasonic pulse. The bipolar (and non-symmetric) pulses generated by the EMAT were so sharp, and the adhesive so thin that there was little point in trying to locate the central area of the pulse, as the error in the peak measurement (+/- 10ns) is larger than any shift in position from max to half the area position. Also, the magnitude FFT is dominated by a particular frequency, so the ultrasonic properties inferred by analysis of the peak tend to be that of this frequency. The phase velocities of the frequencies present in the pulse differ by approximately 10%. Some workers have also used Fourier techniques [8] to determine both adherent and adhesive thickness. There was no need to perform such a measurement in the experiments described here as the pulses were sharp enough to resolve echoes within the adhesive layer, which varied from approximately 50μm to 800μm in the samples analysed.

5.4 Though Transmission (TT) and Send-Receive (SR)

5.4.1 Detailed explanation and justification of the techniques

The TT technique should be the most sensitive method of investigation using bulk waves at normal incidence, with the EMATs being held on epicentre by use of a bracket. The permanent magnets of the EMATs were oppositely aligned so as to increase the static field within the sample, thus increasing ultrasonic signal generation amplitude and detection sensitivity and also providing a means of maintaining minimum stand-off: The presence of a magnet on each side of the sample not only increases the magnitude of the magnetic flux density, but makes the proportion of the field normal to the surface of the sample larger. The problem with TT measurements is that access is required to both sides of the bond which is not always practically applicable. Also if the adherents are the same thickness then it would not have been possible to distinguish the properties of each interface. By choosing adherents of different thicknesses the echoes that would otherwise be in time coincidence can be separated. The waveform for a sample with identical adherents is shown in fig 5.10 along with the relevant ray diagram. Compare this with a bond waveform for the plate thicknesses used in the experimental samples, shown in figs 5.11a, on the grease contaminated sample provided by the DRA . The usefulness of this approach can be seen by examining the waveforms in figs 5.11b , which show how the amplitudes of the pulses vary for reduced coupling at alternate interfaces (by surface contamination by silicon grease), and for a 'perfect' bond. It can be seen from the ray diagram of fig 5.11a that it is irrelevant on which side of the sample the SH waves are generated as to the resultant TT waveform. Following the notation used in the diagram it can be seen how it is possible in this case to determine which interface contains the defect by straightforward amplitude comparison.

The SR technique offers a more practically viable approach, while not suffering from the potential difficulties encountered with TT when adherent thicknesses are identical. The disadvantage in this technique is the reduced sensitivity to variation in pulse signal amplitudes. The scans were performed as previously described, moving the sample on an

XY table. As only one EMAT is used, force was applied to the EMAT (via a weight) to maintain its 'contact' to the sample to ensure constant stand-off. The signal amplitude will be greatly diminished as compared to the TT technique. The simple principle of examining the first SH wave pulse arrival , and the subsequent echo within the adhesive was also used in this method. The waveform obtained was trivial to analyse within the range of samples investigated. Because the technique examines reflected rather than transmitted pulses, the waveform periodicity is dominated by the near adherent thickness. Examining the more detailed waveform in fig5.9 shows the main pulse reflected from the near interface, proceeded by a smaller pulse that has been reflected from the second interface and has thus travelled 2 adhesive thicknesses. Taking the example of grease contamination outlined above, where one interface was not adhered, the waveforms shown in fig 5.12 were obtained. The sample here was produced by applying a thick smear of grease to one 5mm thick 'isotropic' aluminium adherent and a two part room temperature cure epoxy to a second adherent which was then sandwiched with the first and left to cure in the geometry shown in fig 5.12. This differs to the sample shown in fig 5.11, as here there was a thicker layer (approx 100μm) of grease and a totally different adhesive was used. Note how the echo pulse here is not inverted, as the grease inclusion at the interface gives the boundary condition of effectively zero shear stress at the epoxy-grease interface. The clamped surface boundary condition for longitudinal waves has finite longitudinal stress at the boundary, thus the pulse would be inverted. The ultrasonic evidence indicates a lack of adhesion.

5.4.2 Analysis employed

The first experiments performed on a sample were the TT scans as this was ultrasonically more sensitive than send-receive. TT also avoids some of the potential complications that SR experiences with thicker adhesive layers, and these will be discussed later. In testing for adhesion, the crudest indicator as to whether there is any coupling at the adherent-adhesive interfaces, was to check if there was an observable transmitted SH wave. As the preparation conditions and thicknesses of the bonds can vary, there can be little

meaning in absolute values of transmitted wave amplitudes in any one bond. It is a more reasonable approach to examine any relative changes over the bonded area. There will of course be a variation in amplitude due to thickness variation. In order to calibrate for this and assess the amplitude dependance on glue thickness, samples with a deliberately wedged adhesive layer were prepared. The data from these experiments is discussed in section 5.4.3., as it has a bearing on how some of the later analysis is performed. This data was then be displayed in the form of 2D topological or intensity plots.

As the defective regions were created in a known, well defined area of the plate, specific waveforms were recorded over these regions and over regions that are nominally defect free. This gave a clearer indication of the defect type or cause of the defect, and as to why some defects cannot be detected using this method. Analysing these waveforms gave information on the dispersive nature of the adhesive. By employing Fourier analysis it is possible to calculate both phase velocity and attenuation as a function of frequency through the thickness of adhesive.

In addition to a range of defective bonded samples, a number of defect free bonds were manufactured with different physical construction. These bonds were produced with the aim of keeping them defect free, while maintaining certain specifications of construction. It was discovered that some of these samples contained various defects.

5.4.3 Results derived from EMAT scans of the adhesive bonds

If subtle variations in adhesive coupling were to be resolved, some means of correcting the data for the effects of varying adhesive thickness was required. In order to do this two samples with a deliberately wedged layer of adhesive were examined by scanning in TT. The thickness varied from approximately 50μm to 500μm over the area of a joint. One of the samples was found to be an even wedge, while the other wedge had a slightly curved shape as can be seen from the temporal 'thickness' measurements in figs 5.13. The even wedge contained a defect (top left of scan), thus rendering the data from this region corrupt with regards to using it as some type of thickness-attenuation calibration.

The waveforms obtained from examination of this region are discussed later in section 5.4.4.

Plotting 'thickness' (remembering 'thickness' is defined as the transit time for two adhesive thicknesses) against measured transmitted pulse amplitude yields the graphs shown in fig 5.14. It can be seen that the defect free sample had a linear variation in the transmitted amplitude with 'thickness'. This makes a calibration for other scans possible with the inclusion in the amplitude data of a correction term linear in the 'thickness'. The plot obtained from the defective wedge transmission scan shows that the amplitude in the defective regon is lower than would be expected. The data also shows that the extent of the defective region is perhaps larger than would appear from the topological plot of fig 5.13.

This type of linear dependance of amplitude on thickness traversed would be expected for very thin samples and is described in the proceeding argument. - Assuming exponential decay in the sample (exp[-ax] , where a is a constant and x is distance travelled), the limit of small distance traversed yields a linear relationship (expanding exp[-ax] ~ 1-(ax)). Small distance is a term relative to the wavelength of ultrasound - broadband in this case, but having a particular dominant frequency. It must however be remembered that the pulse is broadband in nature and thus the pulse should disperse on travelling through the adhesive. Linear attenuation of amplitude with adhesive thickness has been observed in the adhesive of adhesively bonded steel plates by [9].

The question now arises whether the fact that the adhesive layer is wedged would have any effect on the transmitted wave. The angle of wedge is typically about 3×10^{-3} deg. In the simple geometry shown in the schematic of fig 5.15 it can be seen that the first expected effect would be a broadening of the pulse due to a variation in transit time across the wavefront. Fig 5.16 shows that the expected pulse broadening is just measurable in the first TT pulse, and clearly visible on the immediately proceeding adhesive layer reverberation. The waveforms were recorded on a wedged adhesive layer bond and a nominally even adhesive thickness bond of identical thickness at the centre of the transducer. The broadening of the first ultrasonic arrival in TT is not observable within the limits set by the digitisation rate (10ns) of the scope used to capture the waveform, but broadening is clearly

revealed in the echo within the adhesive layer. Taking a shear wave velocity of 1000m/s in the epoxy, and the EMAT to be uniformly sensitive across the entire coil yields a difference in max-min arrival time of 240ns in the ultrasonic pulse that has traversed the bond layer 3 times. The observed broadening of the echo corresponds to a min-max arrival time difference of 180ns, significantly less than the simple theory predicts. This is mainly due to the effective coil diameter being much smaller as the sensitivity is not uniform across the coil, peaking approximately half way across the radius. The figure of 180ns was obtained by taking the bond reverberation from the even adhesive layer waveform, then shifting it in time and summing across the EMAT diameter. The result is a broader, lower amplitude signal, closely matched to the observed signal.

Another factor that could affect pulse height is that the wedged nature of a sample gives rise to a Bessel modulation of the echoes with plane longitudinal waves [10]. Also at this point it is useful to note that the EMAT signals on a nominally flat plate also undergo a modulation that is not simply exponential decay (refer to chapter 3 - EMAT system properties, section 3.4). The wedge angle of 3 x 10-3 degrees, would lead to a variation in the amplitude due to Bessel modulation of <0.2% (maximun over the range of frequencies present in the shear wave pulse) , and in the intrinsic EMAT system signal modulation of approximately 0.14% (extrapolatd from modulation observed in a blank aluminium plate). Thus, the wedge angle should be a second order effect compared to thickness variation across the bond.

The Bessel modulation due to the wedged nature of a sample is given by :-

$$\text{Bessel modulation factor} = \frac{2J_1(2k\ \tan n\theta)}{2ka\ \tan n\theta}$$

where 'k' is the wavenumber of the ultrasound (2p/wavelength), 'a' is the radius of the circular ultrasonic transducer, 'n' is the number of times the pulse has bounced within the wedge and 'q' is the angle of the wedge.

As previously stated, the measurement of pulse-echo separation to determine bond layer thickness is taken from positions of the maxima or minima on signal pulses. If the measurement of thickness in the time domain is a valid one, then the real bond thickness should vary linearly with the time domain 'thickness'. In order to measure the 'true' thickness, the total bond thickness was measured across a strip of a wedged sample using a micrometer. The variations in the aluminium thickness are of second order compared to the variation in the adhesive thickness. As the aluminium plate thicknesses were known, calculation of the true adhesive layer thicknesses was trivial. The time domain 'thickness' and the micrometer thickness measurements are shown in figs 5.17 as a function of position. These two results can be combined to give the relationship between effective time 'thickness' and real thickness. This is akin to assuming that there is only one frequency present, thus the position of the echo peak is just a measure of the velocity of this frequency. An important factor to note is that the wedge angle causes echo broadening and thus shifts the maxima of the adhesive echo peak. If the wedge angle is roughly constant as in this case, then the shift in the maxima of the bond reverberation is constant (approximately 40ns here) , and thus the gradient of the graph of attenuation with 'thickness' is a valid measurement.

Calculations of shear wave phase and group velocities within the adhesive (see fig 6.11 in next chapter) show a significant, 10% variation as a function of frequency in the range of frequencies 2-10MHz. Thus the dispersion would be expected to diverge the time domain 'thickness' from a linear relation, but for the fact that there is a dominant peak in the frequency content of the pulse. It is therefore approximately the velocity of this frequency which is being measured in the 'thickness' time domain measurements.

5.4.4 General considerations for results obtained in scanning bonded samples

A range of both defective and defect free samples were examined using SR and TT techniques. In TT one of the factors affecting the amplitude of the signals will be static magnetic field, and thus separation of the EMATs. The EMAT driver may also over long

a period of time experience a change in output amplitude. Therefore from one set of scans to the next, the amplitude may not be the same for the same sample types. Thus, there can be no standard calibration for the absolute amplitude and thickness dependance. It is sufficient however to know that the relationship between echo separation and pulse amplitude is linear. A computer algorithm has been used to alter the amplitude data by the addition of a linear term in time 'thickness', and take into account attenuation in the aluminium.

Some of the samples that were supplied as defective (see table 5.1), did not show any defective or significantly different region in the central area of the structure. The sample of most concern was the one that had been treated with a release agent prior to bonding. On tensile testing the strip sample over the defective region, adhesive failure occurred . This left the adhesive rigidly attached to the 4.8mm plate and smooth on the other unbonded side, with the 3.3m plate being completely free from any trace of adhesive material. This was adhesive failure, but the conclusion cannot be drawn that there was no bonding whatsoever. There could be a variety of reasons as to why the defective region was not detected ultrasonically. One possibility is that the bond actually failed in the plastic limit. That is, the small elastic displacements associted with ultrasonic propagation could be coupled across the interface, without there actually being any mechanical frictional coupling across the interface. Even so, it is possible to induce shear wave coupling across an unbonded interface. This was proved in a qualitative fashion by compressing a 5mm thick aluminum disc with an adhered epoxy layer on one face, against a similar blank aluminium disc and propagating shear waves through the entire structure at normal incidence. The setup and recorded TT waveform is shown in fig 5.18. Note that the poorer signal to noise ratio (even after 20 averages) is associated with a low absolute amplitude. The plates were clamped by screws in 4 places around the circumference of the discs, and the total estimated contact area of epoxy-blank disc was 3-4cm^2. This occurs as the applied compression generates a shear stress across the unbonded interface due to frictional coupling between interfaces. When the experimental samples were constructed, they were formed under elevated temperature and pressure. As the unbonded regions were surrounded by well bonded regions, this could have

the effect of leaving the nominally defective bonded region under a compressive stress. This effect could then possibly be compounded by the fact that as the shear wave arrives at the aluminium-epoxy boundary, there is some mode conversion, generating a compressive stress at the boundary while the shear wave is incident on the boundary.

5.5 Some specific sample scan results

5.5.1 Voided samples

Two of the sample range were constructed in such a way so that they contained a void in the centre of the samples. This type of sample is the most crude and easily observed defect type, and conventional ultrasonics can pick these up quite easily. It is however a good demonstration of the practicality of the EMAT, when used to detect such defects in a non-contact regime.

TT scans amplitude and 'thickness' (time domain) of a void containing sample are shown in fig 5.19a. and fig 5.19b respectively Prior to curing, the void region was square shaped, but as can be seen from the amplitude scan, the air trapped in these bonds flowed out of the adhesive layer changing the shape of the void region. The SR back relected amplitude c-scans (fig 5.20a from 4.8mm adherent side and fig 5.20b from 3.3mm adherent side) appear different to the TT scans, as the TT technique probes both interfaces and epoxy bulk simultaneously. During cure, the epoxy partially flowed into the void region, mainly onto the 5mm aluminium plate giving it complete coverage. The scans show that the reflected amplitude on the 4.8mm plate for SR is roughly uniform for the near interface, but show a drop in amplitude in the bond echo from the far interface. It would be expected that the echo from the far epoxy - void interface over the defective region should yield a higher amplitude as detected by the EMAT. This would only occur if the epoxy that has flowed into the voided region was uniform and homogeneous, so consequently the uneven epoxy layer leads to a drop in the bond echo amplitude. The SR reflected amplitude from the 3.3mm plate shows large amplitude over the defective region. Echoes from the far interface mirror the

image obtained from the principal peak amplitude as these echoes originate from the preceding principal echo.

5.5.2 Release film containing samples

The sample that contained a square of release film at the 3mm plate - adhesive interface was also easily detectable using the EMAT. This type of defect can arise where the adhesive's protective film has not been properly removed from the surface of the adhesive prior to bonding. As with the grease contaminated sample, the impedance mismatch between epoxy-contaminant is much less than the impedance mismatch between contaminant-aluminium. In fact, in this case the release film does not couple to the aluminium plate at all, making this defect effectively a void.

The SR data shows that on the 3.3mm side (fig 5.21c) , where there is no coupling across the near interface, the reflected amplitude is high, and thus there is no or little bond shear wave echo. From the 4.8mm side, the principal pulse amplitude scan (5.21a) shows that the reflection coefficient from the near interface does not contain any defect. The bond layer echo amplitude (fig 5.21b) does however show a drop in amplitude over the defective area which is a combination of the ultrasonic attenuation within the film layer, and the fact that the film layer is present at all. The TT amplitude data (fig 5.22a) shows the same features as the SR data, but are perhaps more pronounced as the TT is more sensitive in general. The TT 'thickness' measurement (fig 5.22b) is corrupted due to the extremely small signal level associated with the defective region.

5.5.3 Silicon grease contaminated adherent sample

A thin smear of silicon grease was applied to the 3.3mm aluminium adherent prior to bonding. As the bonding took place at elevated temperature and pressure, then there was the possibility that the grease could spread, diffuse or even dissolve into the epoxy layer. Data was recorded in through transmission and send-receive from either side of the bonded

sample. The through transmission data is shown in fig 5.23a and 5.23b , and the send receive in fig 5.24a,(b),(c) and (d).

Considering the TT amplitude, the first point to note is that even in the defective region of the bond, a proportion of the incident shear wave is coupled across the bond. Thus there was some degree of bonding, or at least a transfer of shear stress across the interface in the sample, even in the defective region. Therefore the silicon grease contaminated sample served to act as a degraded bond, rather than a total disbond or kissing bond. The scans here show raw data, and the data corrected for adhesive layer thickness. There is little difference in the uncorrected and corrected, as the thickness variation is dominated by interface and bulk considerations. The darker regions of the density plots show a lower level in transmitted signal. Considering the cross-sectional diagram of fig 5.25 shows why this is the case. Shear waves generated from either adherent surface will give the same through transmission signal result. The results could be explained from two equally valid view points, firstly that of a 4 layer system (Al-epoxy-grease-Al), or as a 3 layer system (Al-epoxy-Al) with degraded adhesion at the 3.3mm adherent-epoxy interface. Both these geometries would give rise to a drop in TT signal over the defective region, even if the grease layer could be treated as an elastic solid in the first geometry. Thus, in TT, a defect is indicated by a drop in signal amplitude. The defective interface can be directly identified of the waveform due to the different adherent thicknesses as described in 5.3.1.

The SR scans shown in fig 5.24a,(b),(c) and (d) show a similar pattern to the TT scan, but need more explanation. Scans were performed on both sides of the adhesive bond, but the first back reflected ultrasonic arrival when generating on the 3.3mm adherent was corrupted by the front end electrical noise. Thus, the first arrival was not used for the amplitude scan on the 3.3mm side. However, the second principal pulse and bondline echo were clear of the electrical noise, and their amplitude were recoreded. The amplitude data has a maximum reflected principal pulse signal over the area containing the defect on the near interface (fig 5.24a) . This then has the effect of reducing the amplitude of the epoxy layer echo over the defective region, as less energy entered the adhesive in this area. A high reflected amplitude from the defective region indicates the presence of either an increased impedance mismatch in this location, and/or a change in interfacial coupling strength.

Scanning on the 4.8mm adherent side, the first ultrasonic arrival amplitude showed a slight variation in reflected amplitude from the near adhesive-adherent (fig 5.24b) , but no distinct defective region. The c-scan data from the bond echo associated with the first shear wave arrival shows a drop in amplitude over the defective region of the sample fig 5.24c). This bond echo has probed both the near interface, far interface and adhesive layer bulk. The defective region shows up as a drop in amplitude of the bond echo. This result shows that the bonded sample is behaving more like the 4 layer system than the 3 layer system described above. This is because if the defect region was purely a degradation in interface coupling, less of the energy would be coupled across the far adherent-adhesive interface and would be reflected back towards the transducer. Thus, an increase in echo signal amplitude would be expected for a straightforward lack of adhesion on the far interface, rather than the observed decrease in amplitude. This effect can be explained in the 4 layer model by the fact that there is a smaller impedance mismatch from the epoxy-grease interface than the epoxy-aluminium interface. The grease strongly absorbed the ultrasound that was coupled into it and as there is a higher impedance mismatch grease-aluminium compared to epoxy-aluminium, little energy is transmitted into the far adherent. Addition of an extra elastic layer into the adhesive layer would also decrease the back reflected amplitude due to the geometry of the layered system. Thus the data from the TT and SR scans would indicate that the 4 layer model is relevant to this particular sample. The bondline 'thickness' measurements fig 5.23b (TT) and fig 5.24d (SR) appear consistent in both the range of meaured temporal separations and in the general pattern of the scan. Two possible cross sectional respresentations of the bond are shown in fig 5.25a&b.

5.5.4 Defective wedged sample

The c-sans for the wedged samples are shown in fig 5.26a and (b) for the defect free sample in TT, and in fig 5.27a and (b) for the defective samples in TT. Examining the TT data from the defect free wedged sample, it can be seen that the pulse amplitude (fig 5.26a) correlates inversely to the adhesive layer thickness (fig 5.26b). The information obtained from the defect free wedge was used to calculate the attenuation of the shear waves as a

function of epoxy thickness as explained earlier. The defective region of the other wedged sample was examined in detail using the TT geometry, as the opportunity of examining an accidental defect had arose.

Analysing the data from the SR scan from the 4.8mm plate side, the first principal peak could be observed and the c-scan shows a slight variation in shear wave coupling coefficients across the interface, or shear stifness (relative to a tangential spring coupling model between adhesive and adherent - see Ch2) at the near interface (fig 5.28a). The data from the first echo within the adhesive layer is corrupted by interfering with the mode converted signal (fig 5.28b). This is only occurs in samples with extreme variations in adhesive thickness, or where the bond echo coincides with the mode converted signal. Thus, the information from the far adhesive interface is not easily derived from the available data. The amplitude scan of the second principal pulse (fig 5.28c) shows features associated with the adhesive layer, and is a result of higher order reflections within the structure interfering with the pulse trapped in the upper adherent. This phenomena will be demonstrated in the waveform simulations of chapter 6. Consequently, the bondline echo associated with the second principal pulse is also affected by the higher order reflections and once again, the mode converted signal. Thus, the information contained within successive pulses quickly becomes very complicated. The adhesive layer 'thickness' measurement (fig 5.28d) does not appear to be corupted, which is quite surprising considering the degree to which the amplitude data has been corrupted by interference with other siganls.

In scanning the transducer on the 3.3mm adherent side the first ultrasonic arrival was again masked by front end electrical noise. Amplitude c-scans of the second and third principal pulse were recored, and exibited similar features observed in the scans from the 4.8mm side due to interferce with other ultrasoinc signals in the waveform, and were more pronounced than from the 4.8mm side as these were higher order reverberations.

The defective region of one of the wedged samples was examined in detail, waveforms were captured in this location for analysis. The waveforms obtained in TT for the defective region and defect free region of identical thickness on the same bond are shown in fig 5.29a. The amplitude of the first ultrasonic arrival appears reduced in the defective

region. Examination of the next two pulses shows that they are of equal amplitude to within 0.5%, as demonstrated for a different sample in fig 5.11b . This would then imply that the defect is not localised to one particular interface. This left one of two possibilities, that the adhesive bulk was either defective and thus both interfaces were defective, or just that both interfaces were equally defective. The latter situation was of course less likely, as the chances of the interfaces being equally defective was very small. The SR data from both the 3.3mm and 4.8mm adherent sides showed a small increase in the acoustic amplitude reflected back towards the EMAT of a few percent. This in itself would suggest that the defect present here is a predominantly a bulk defect. There will be a drop in shear wave transmission coupling in this area, but the fact that this occurs at both interfaces indicated that the defect went through the thickness of the adhesive layer. The ratios of the magnitude of the first ultrasonic arrival to associated bondline reverberation (fig 5.29b) showed that there was a much stronger frequency dependant attenuation in the defective region. This would again suggest improper cure or a high degree of porosity. Destructive examination of this area revealed that there was extreme porosity in this region, and some of this had concentrated to form small voids of a few millimetres in size.

5.6 Summary

No defects were identified ultrasonically or by tensile testing in the hydrated, the rubbed and in the acid attack samples. Defects were identified ultrasonically in the release film sample and the silicon grease contaminated sample and the tensile test pieces milled from the defective regions fell apart on machining, revealing that the adhesive did not appear to have 'wetted' the adherent. Tensile testing showed that the voided sample and the skin fat and release agent contaminated samples failed at much lower loads over their defective region, while visual examination showed that these three samples had significant areas in the 'defective region' where the adhesive had not 'wetted' the adherent.

A possible explanation as to why the release agent defect was not detected while the grease contamination defect was, may be that the grease was partially dissolved into the epoxy. Another reason may be that the much thinner, stiffer teflon layer of the release agent at the interface may give an effective stiffer interfacial coupling, considering the interfacial coupling model proposed by Baik and Thompson [11]. The quasi-static model ascribes a coupling spring (tangential or normal to the interface) to the interface contaminant, while making the assumption that the 'spring' itself is perfectly coupled to each interface. The stiffness of such a spring is given by $\rho c^2/d$, where ρ is the density of the interfacial contaminant, d is the thickness of the layer and c the ultrasonic velocity (shear or longitudinal). The grease layer was approximately 100 times thicker than the teflon release agent layer which would be the dominant difference in this spring type model, making the teflon layer effectively much stiffer. Thus the thinner teflon layer could allow a higher degree of shear wave coupling across the interface than the grease layer. There will also come a point where if the teflon layer becomes so thin that the difference is shear wave coupling across the interface due to the presence of this layer will be below the variations observed in experimental error. This type of model has been further developed to account for the dynamic situation by Fraisse and Schmit [12].

Many of the important factors that must be considered when performing both experiments and preliminary waveform analysis have been described in this chapter. Experiments have been performed in both through transmission and in a pulse-echo or send-receive geometry. The main factors that supported the analysis used were the sharp broadband nature of the shear wave pulses generated by the EMAT, and perhaps more importantly the fact that some experiments have been carried out in a true C-scan geometry. The specific C-scans presented at the end of this chapter, demonstrated the detection capability of the EMAT system.

Ch.5 References

1. W. Wang, B. Li, S.I. Rokhlin , Ultrasonic refelectivity determination of interfacial properties in adhesive joints of aluminium alloys , Rev. of Prog. in QNDE **10B** , (Ed. by D.O. Thompson and D.E. Chimenti , Plenum Press, NY , 1991 pp1311-1318

2. D.R. Billson and D.A. Hutchins , Laser-EMAT ultrasonic measurements of bonded metals , Nondestr. Test. Eval., vol **10** , 1992 , pp43-53

3 D.A. Hutchins Ultrasonic generattion by pulsed lasers , in: Physical Acoustics **XVIII**, (Ed. WP Mason and RN Thuston), Academic Press, London , 1988 , pp21-123

4 G.C. Knollman and J.J. Hartog, *Shear modulus gradients in adhesive interfaces as* dtermined by means of ultrasonic Rayleigh waves (I & II), J. Appl. Phys. **53**(3) , 1982 , pp1516-1524 and pp5514-5517

5 C.B. Scruby and L.E. Drain , Laser Ultrasonics Techniques and Applications , Adam Hilger , 1990 , pp77-147

6 E. Segal and R.L. Rose , Non-destructive testing techniques for adhesive bonded joints in: Research Techniques in Nondestructive Testing **IV** (Ed. R.S. Sharpe) , Academic Press, 1980 , pp276-316

7 R.E. Challis, T. Apler, R.P. Cocker, A.K. Holmes and J.D.H. White , Ultrasonic absorption and velocity dispersion measurements in thin adhesive layers , Ultrasonics **29**, 1991 , pp 22-28

8 C.C.H. Guyott and P. Cawley , Evaluaion of the cohesive properties of adhesive joints using ultrasonic spectroscopy , NDT International 4211, 1988, pp233-240

9 F. He , S.I. Rokhlin and L. Adler , Application of SH and Lamb wave EMATs for evaluating adhesive joints , Rev. of Prog. in QNDE , (Ed. D.C Thompson and D.E. Chimenti) ,Williamsburg, 1987 , pp911-918

10 R. Truell, C. Elbaum and B.B. Bruce , Ultrasonic Methods in Solid State Physics , Academic Press NY and London , 1969 , pp107-123

11. J.M. Baik and R.B. Thompson , Ultrasonic scattering from imperfect interfaces; a quasi-static approach , J. Nondestructive Evaluation, 4 , 1984 , pp177-196

12. P. Fraisse and F. Schmit , Ultrasonic inspection of very thin layers , J. Appl. Phys. , 1992, vol 72 , pp3264-3271

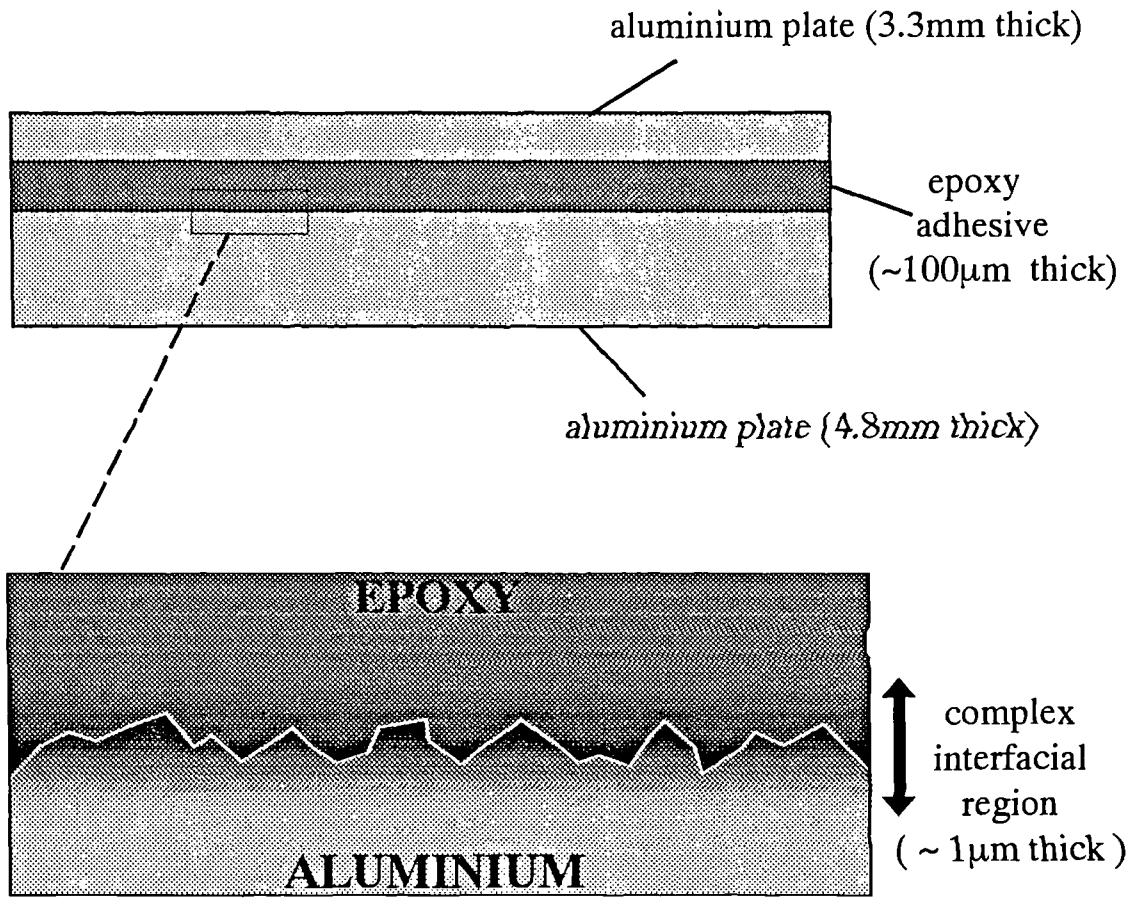

Fig 5.1

Cross-sectional diagram of adhesively bonded samples investigated in this project.

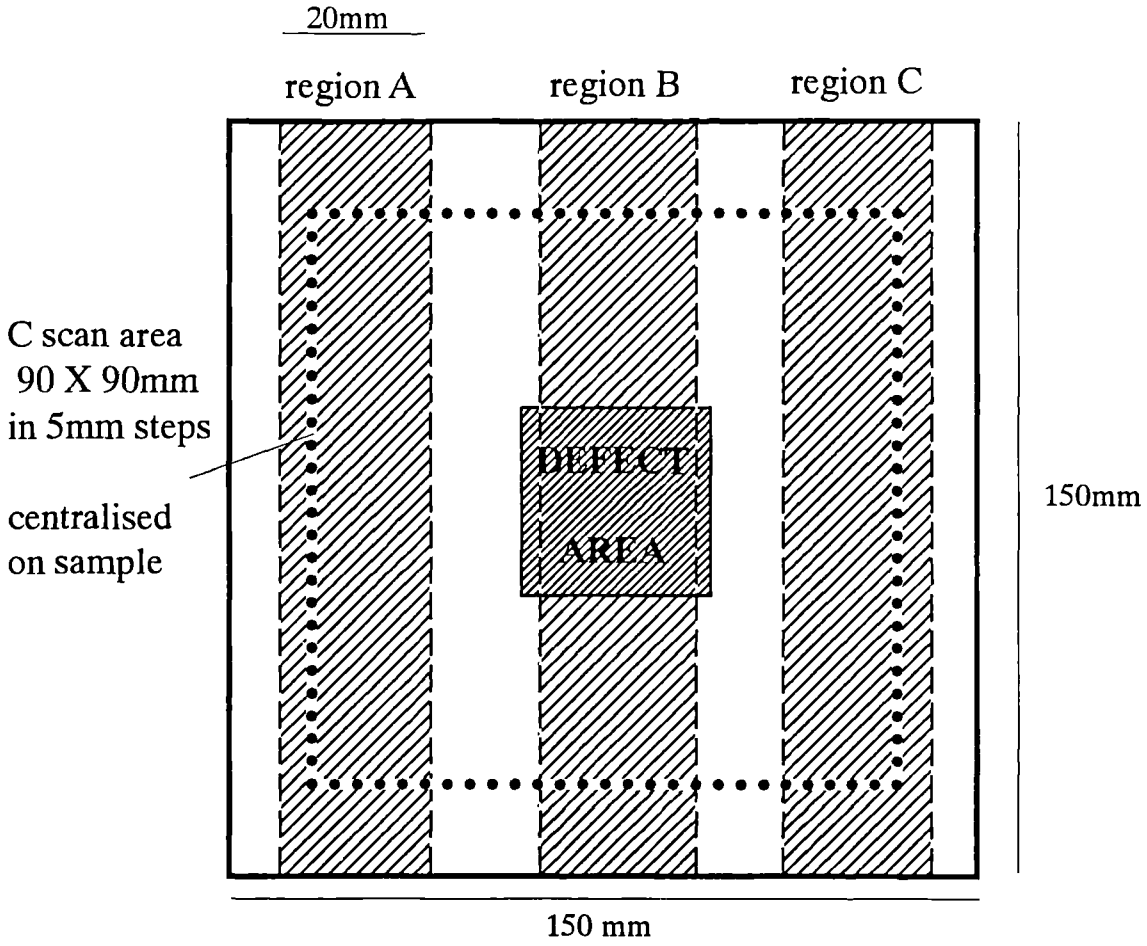

sample type	sample description ultrasonic and mechanical test summary	shear breaking load of test strips region A region B region C

Fig 5.2a

Sample construction, defect location and area from which tensile test strips were prepared from the sample.

Tensile Test Samples

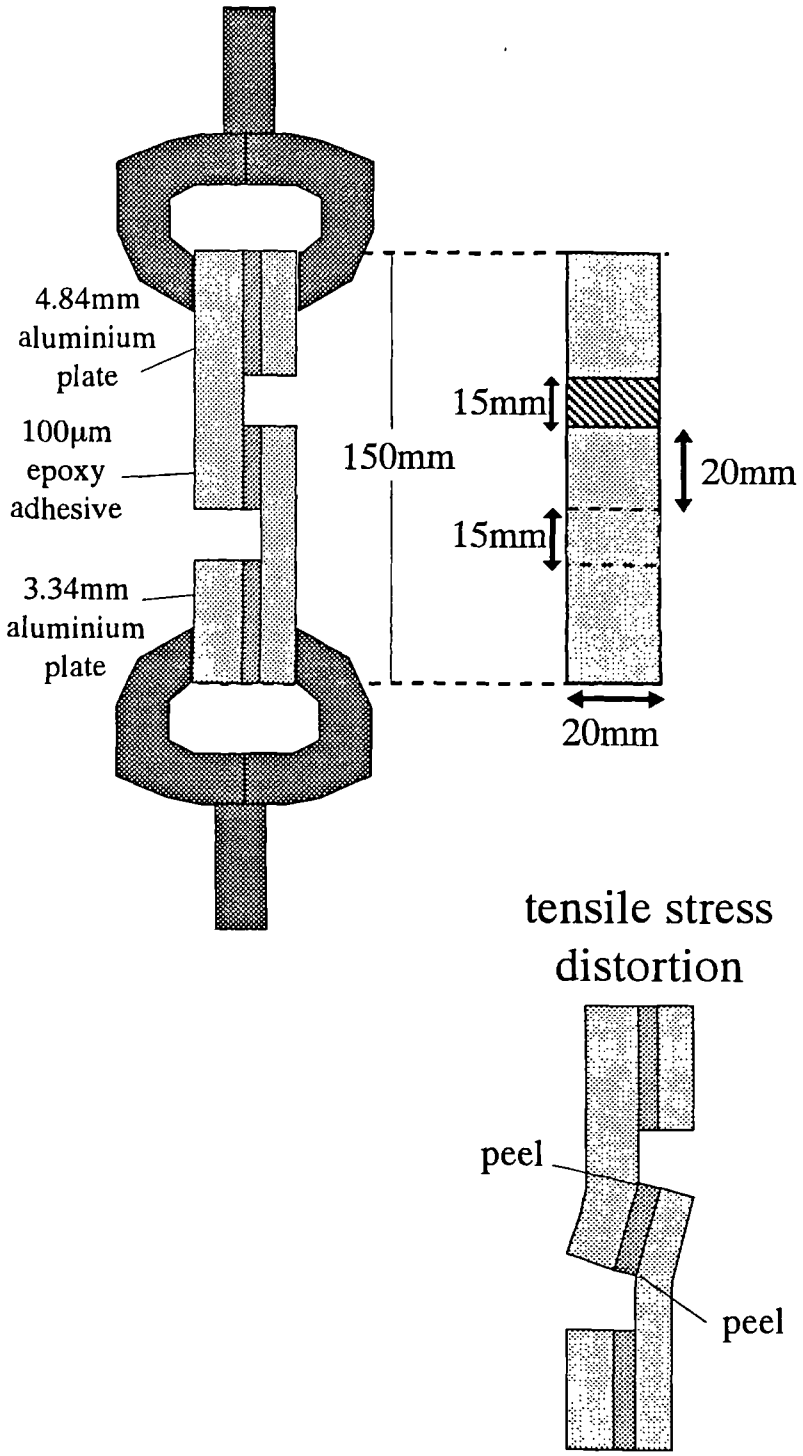

Fig 5.2b

Test geometry for destructively testing regions of bonded samples.

table 5.1

hydrated	hydrated with water prior to bonding	2025
	no defect detected ultrasonically	1810
	no defect found in destructive test	1920
release film	square of release film left on adhesive	2020
	defect detected ultrasonically	fell appart on machining
	defect found in destructive test	2040
skinfat	area treated with grease from constructors hand	2040
	no defect detected ultrasonically	1040
	defect found in destructive test	2060
rubbed	area rubbed with abrasive paper prior to bonding	2045
	no defect detected ultrasonically	2020
	no defect found in destructive test	2000
release agent	area chemically treated with a bonding release agent prior to bonding	2150
	no defect detected ultrasonically	1990
	defect found in destructive test	2100
silicon grease	area treated with thin smear of silicon grease prior to bonding	1980
	defect detected ultrasonically	fell appart on machining
	defect found in destructive test	2000
acid attack	area exposed to attack from phosphoric acid	2050
	no defect detected ultrasonically	2040
	no defect found in destructive test	2000
void	square void area created prior to bonding - the area deforms during bonding as the adhesive flows	2250
	defect detected ultrasonically	140
	defect found in destructive test	2200
defective wedge	deliberately constructed wedged layer contained unintentional defect	2000
	defect detected ultrasonically	1850
	defect found in destructive test (porosity)	no other test sample

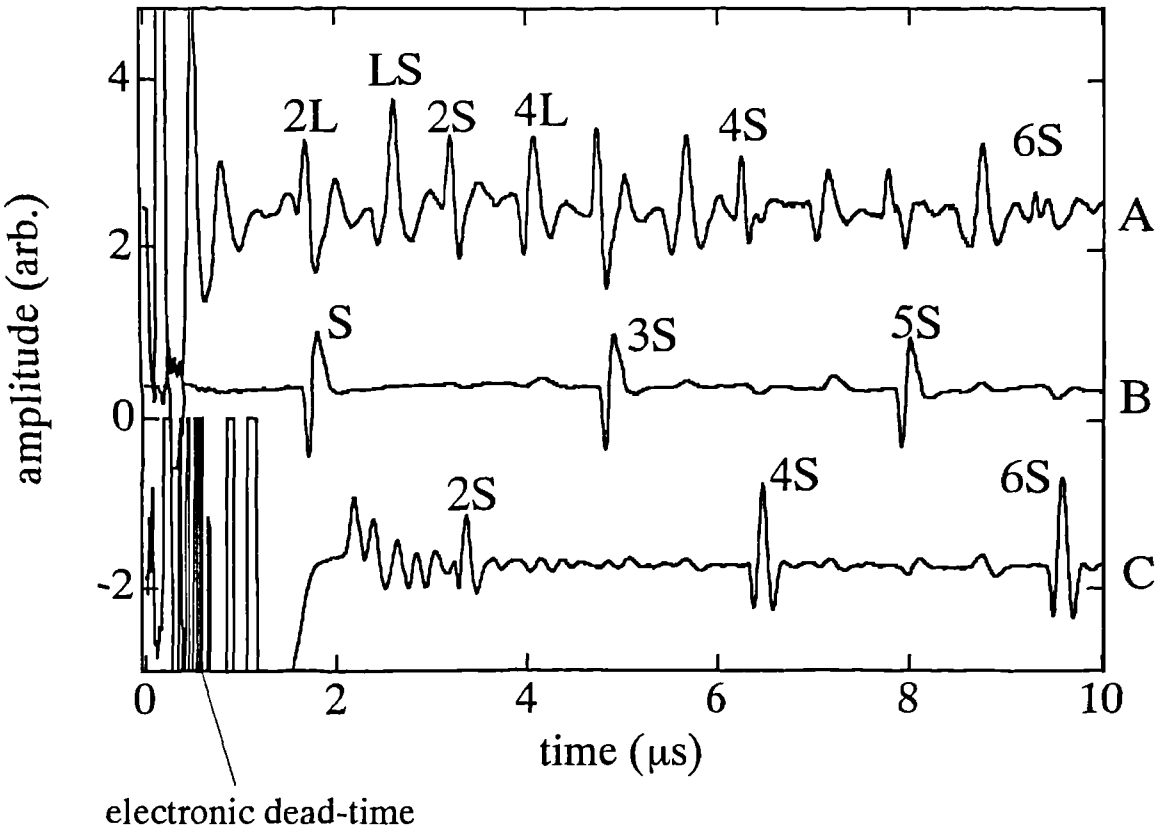

A - laser generation / EMAT detection (same side on epicentre)

B - EMAT generation / EMAT detection (through transmission)

C - EMAT send-receive (pulse echo)

The above waveforms are taken on a 4.8mm thick, blank aluminium adherent, and the amplitudes have been normalised. Waveform A is far more complicated than B or C, as the laser source tends to generate significant longitudinal and shear wave components simultaneously, unless the pulse energy is severly reduced. As the laser ultrasonic source size is also much smaller than the EMAT with a fast rise time (~5ns), the ultrasonic shear wave field from such a source is strongly directed at 60^0 to the surface normal. As a result, the pulses are temporally broadened, and the successive peak-peak echoes are not equally spaced (i.e. 2S-4S is not the same time separation as 4S-6S).

Fig 5.3a

Ultrasonic waveforms obtained using Nd:YAG laser generation/EMAT detection and EMAT send-receive and through transmission geometries.

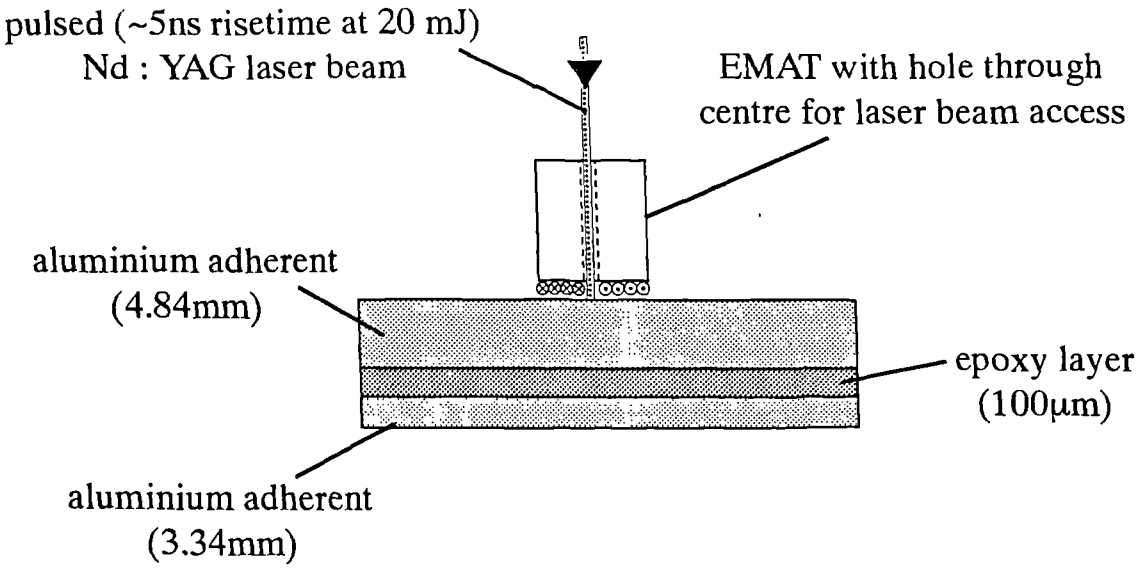

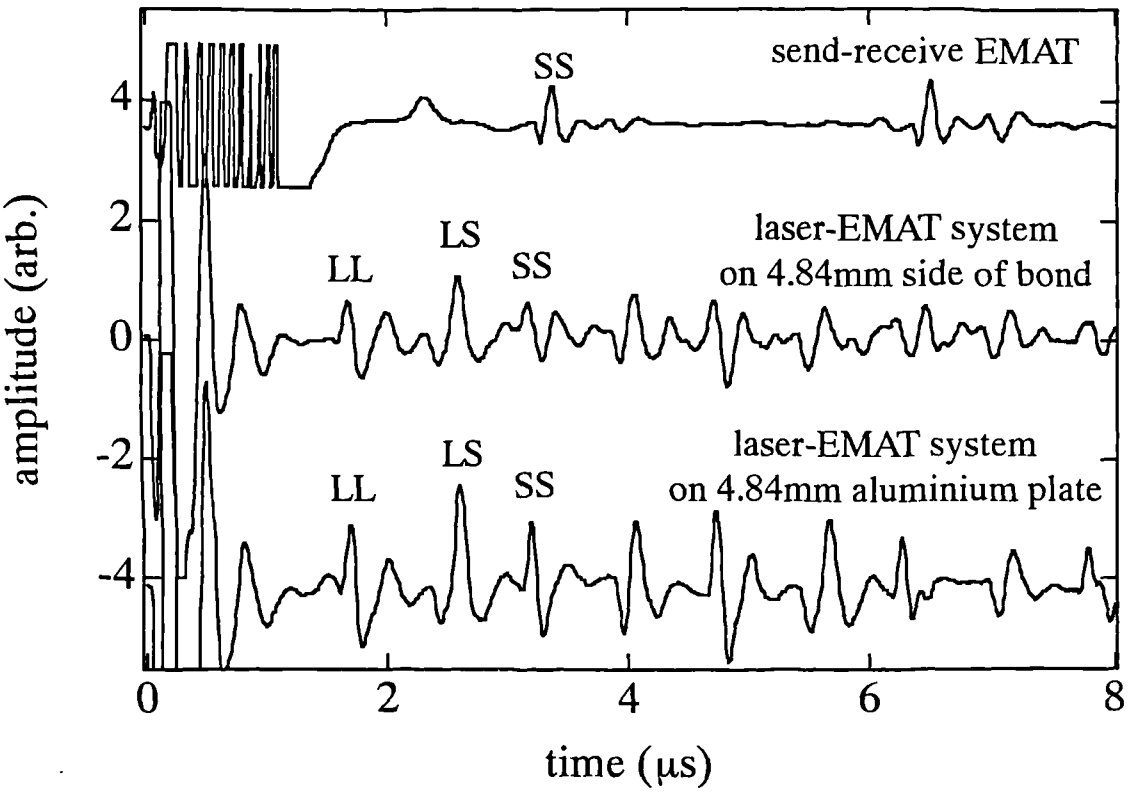

Fig 5.3b

Ultrasonic waveforms obtained using Nd:YAG laser generation / radially polarised EMAT detection and EMAT send-receive.

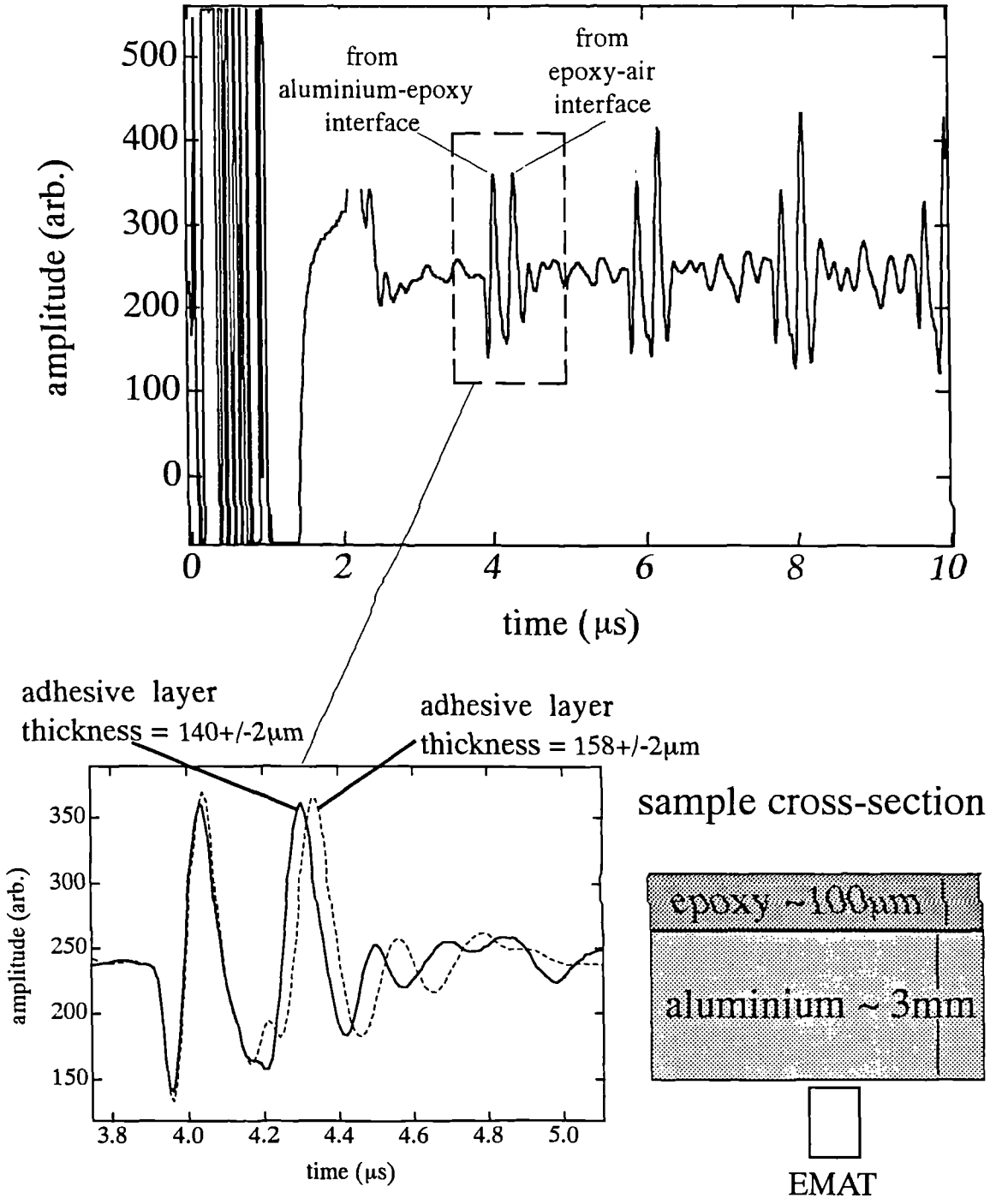

Fig 5.4

EMAT waveforms obtained on a sample of adherent backed by a layer of cured Redux 312 adhesive with carrier.

Schematic for setup for laser generation and detection on the epoxy ingot

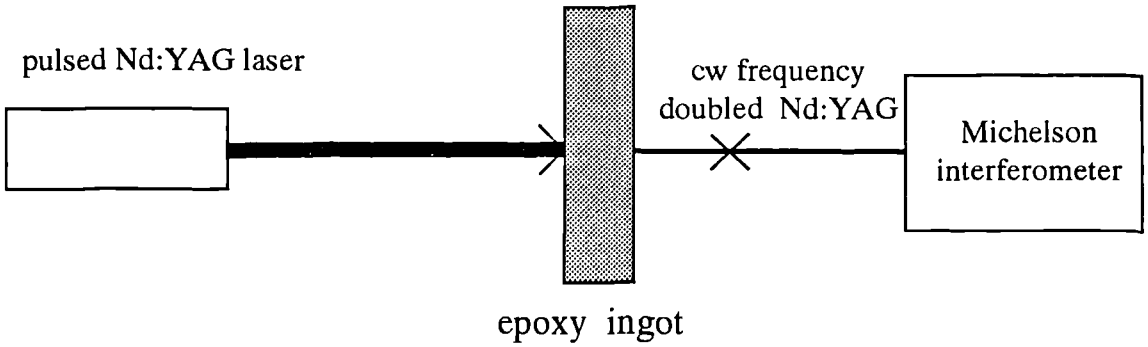

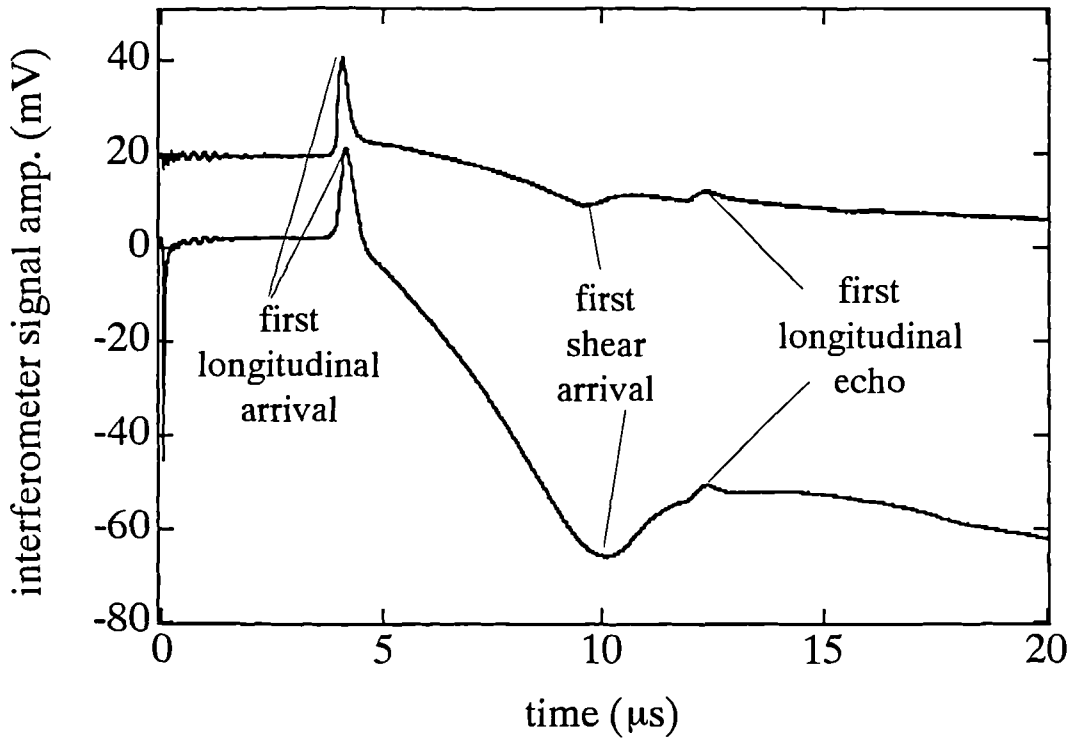

Fig 5.5

Nd:YAG laser generation / Michelson interferometer detection of ultrasound in a cured ingot of Redux 312 epoxy.

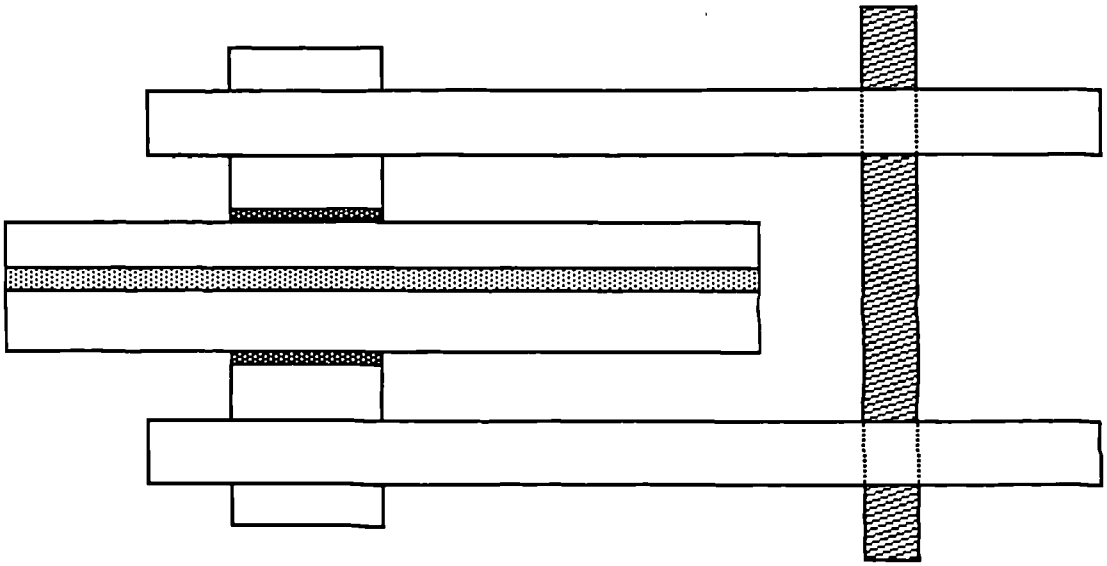

Fig 5.6

Experimental setup of EMATs for scanning adhesive bonds.

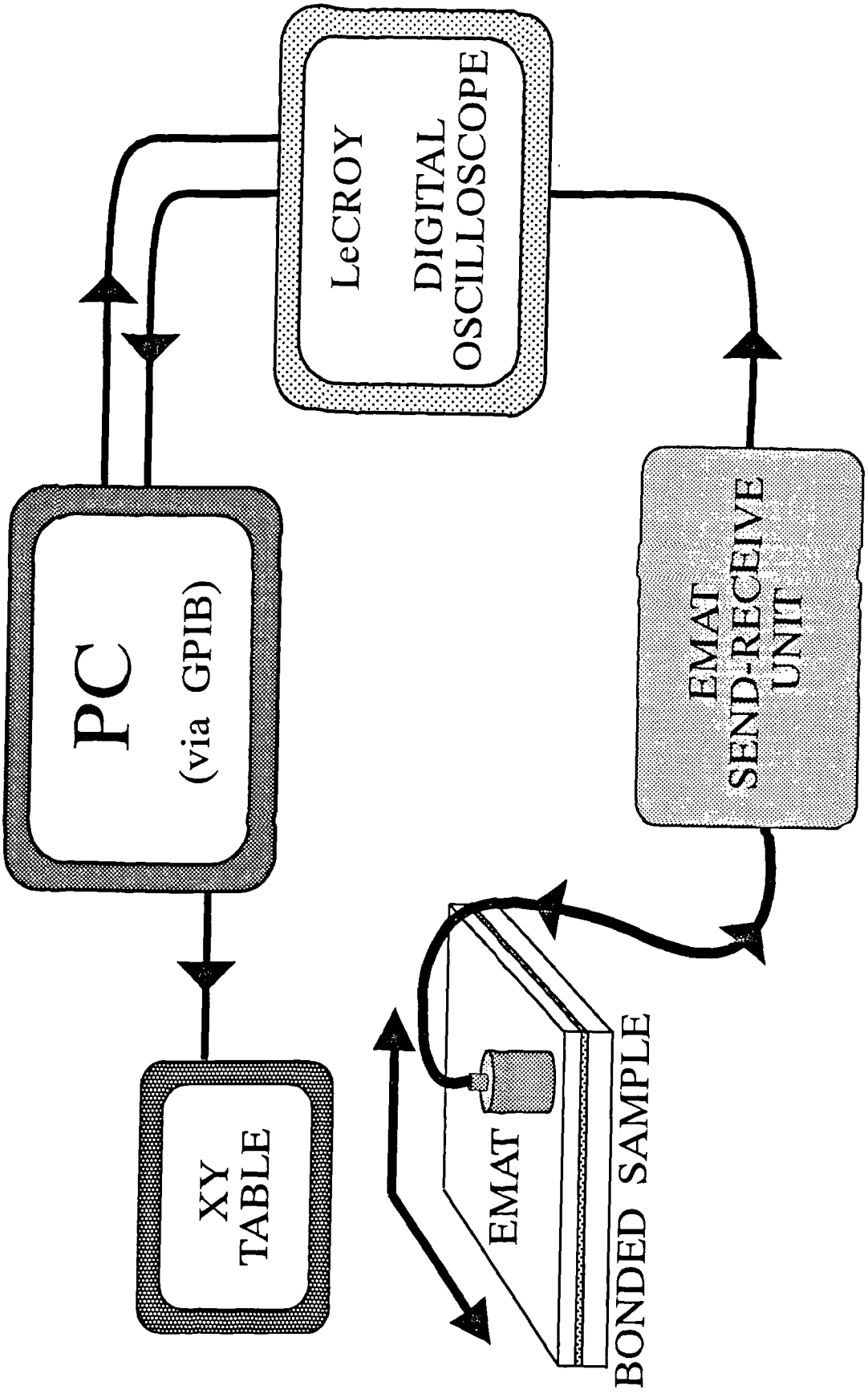

Fig 5.7

Schematic diagram of scanning setup.

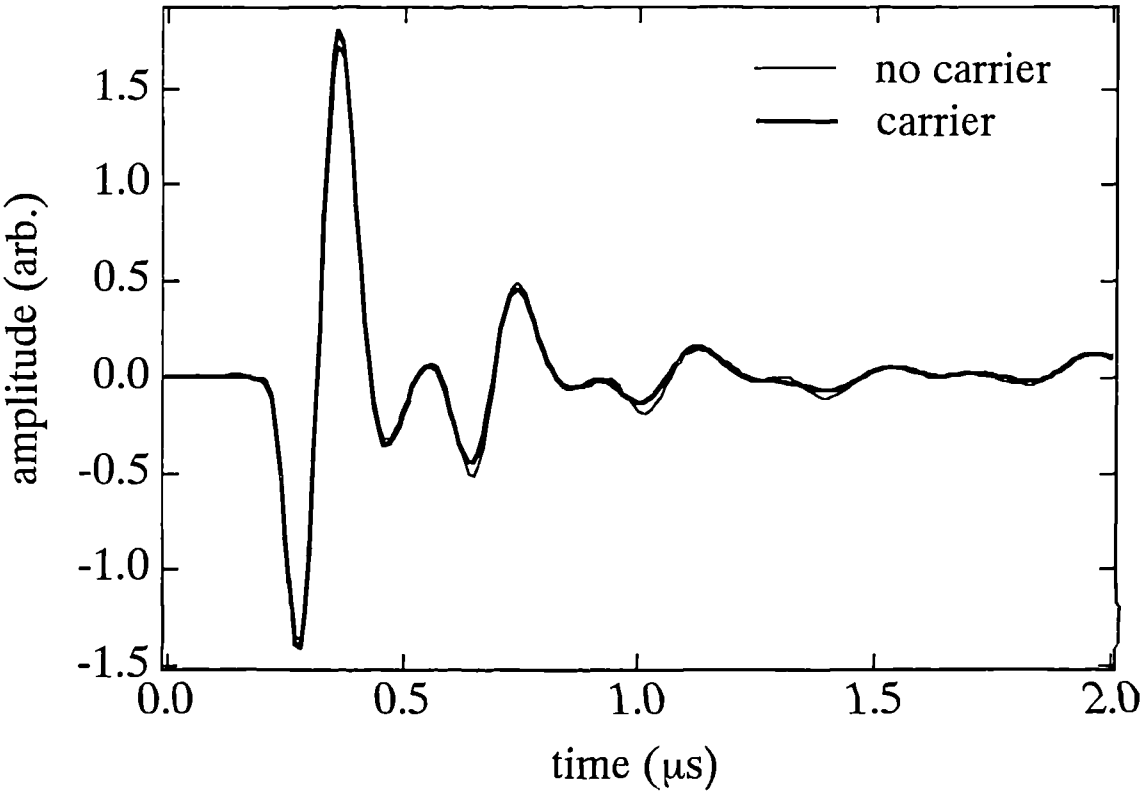

	adhesive layer thickness (μm)	shear velocity in adhesive (ms^{-1})
carrier containing adhesive	154 +/- 8	950 +/- 50
plain adhesive	152 +/- 8	950 +/- 50

Fig 5.8

EMAT waveforms from two adhesive bonds, one plain epoxy adhesive layer, the other bonds' epoxy adhesive layer containing a fabric carrier.

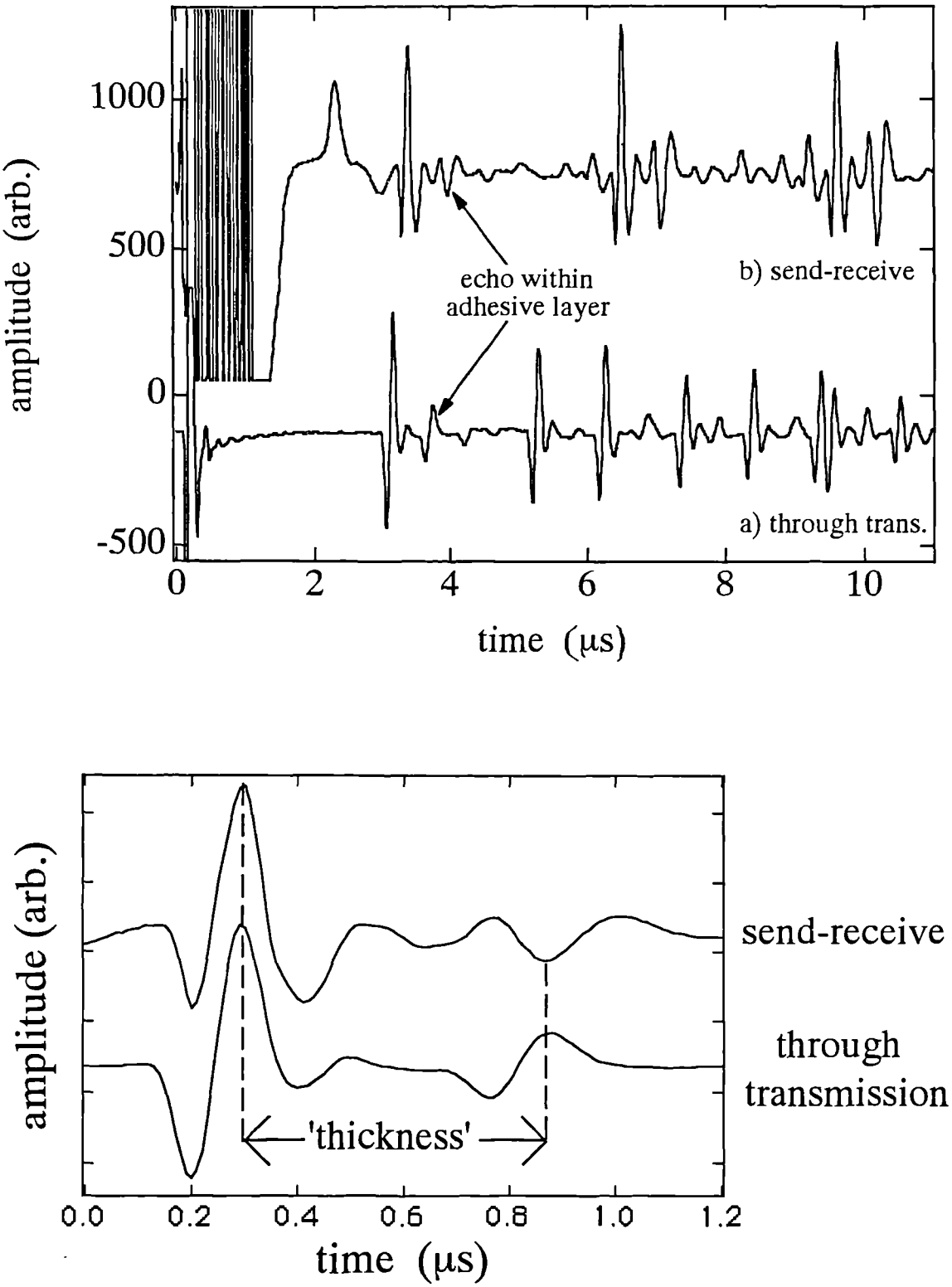

Fig 5.9

EMAT send-receive and through transmission waveforms and measurements on adhesively bonded samples.

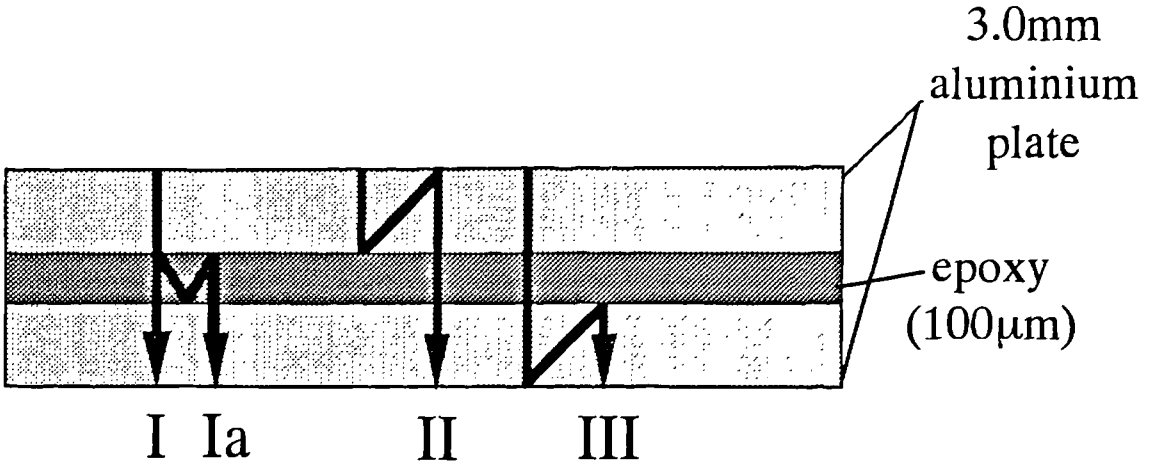

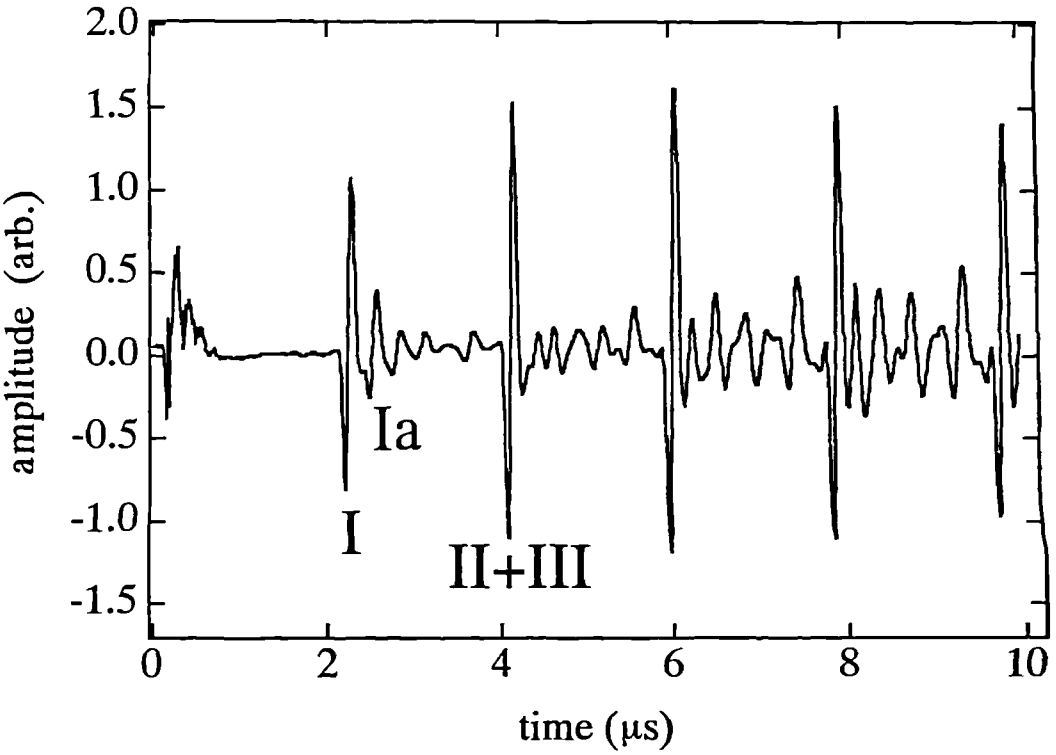

Fig 5.10

EMAT through transmission waveform obtained on an adhesively bonded sample with identical 3.3mm thick aluminium adherents.

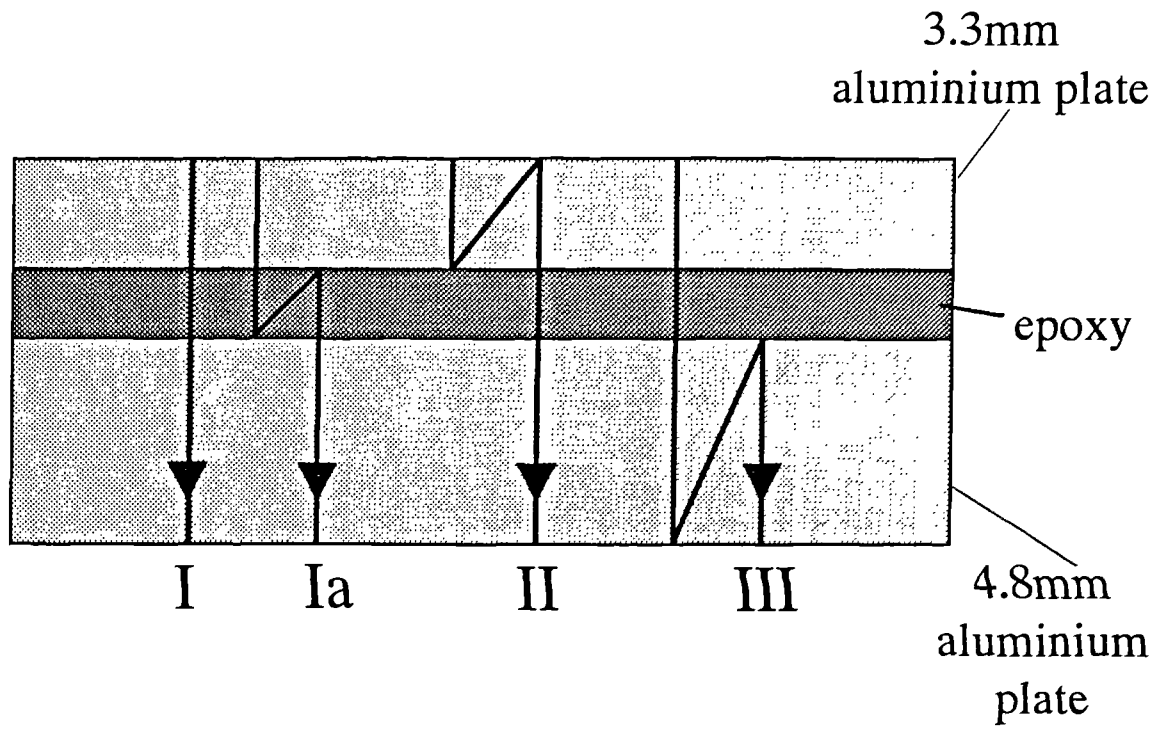

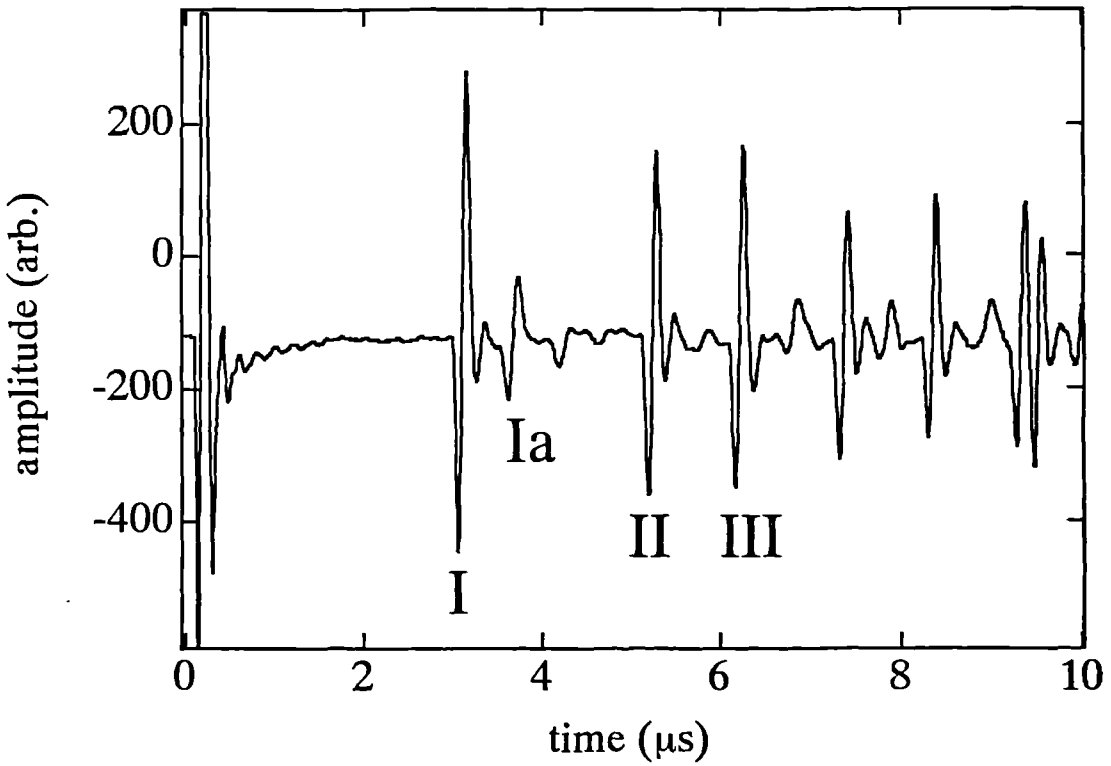

Fig 5.11a

EMAT through transmission waveform obtained on an adhesively bonded sample with adherents of thickness 3.3mm and 4.8mm.

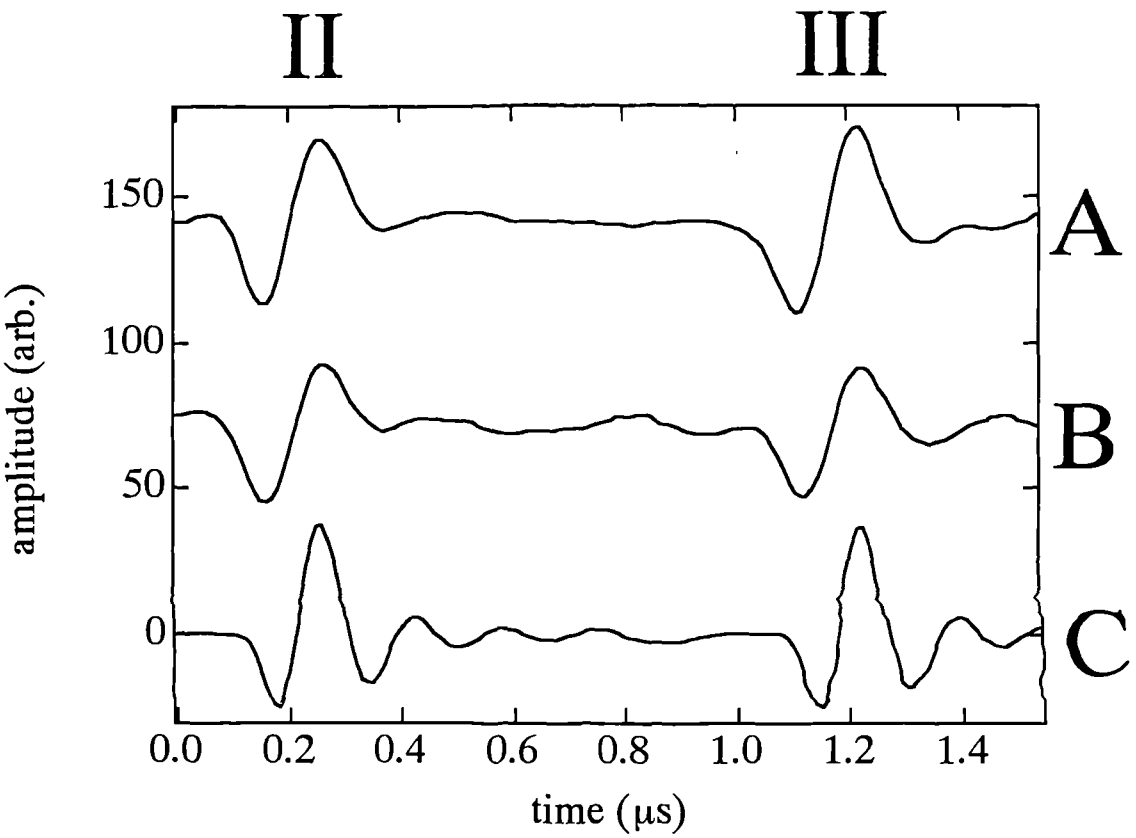

R = ratio of pulse II amplitude : pulse III amplitude

A - defect on 3mm plate	R = 1.00 : 1.13
B - defect on 5mm plate	R = 1.00 : 0.94
C - no defect	R = 1.00 : 1.00

Fig 5.11b

Identification of defective (grease contamination) adherent-adhesive interface by a simple pulse amplitude comparison.

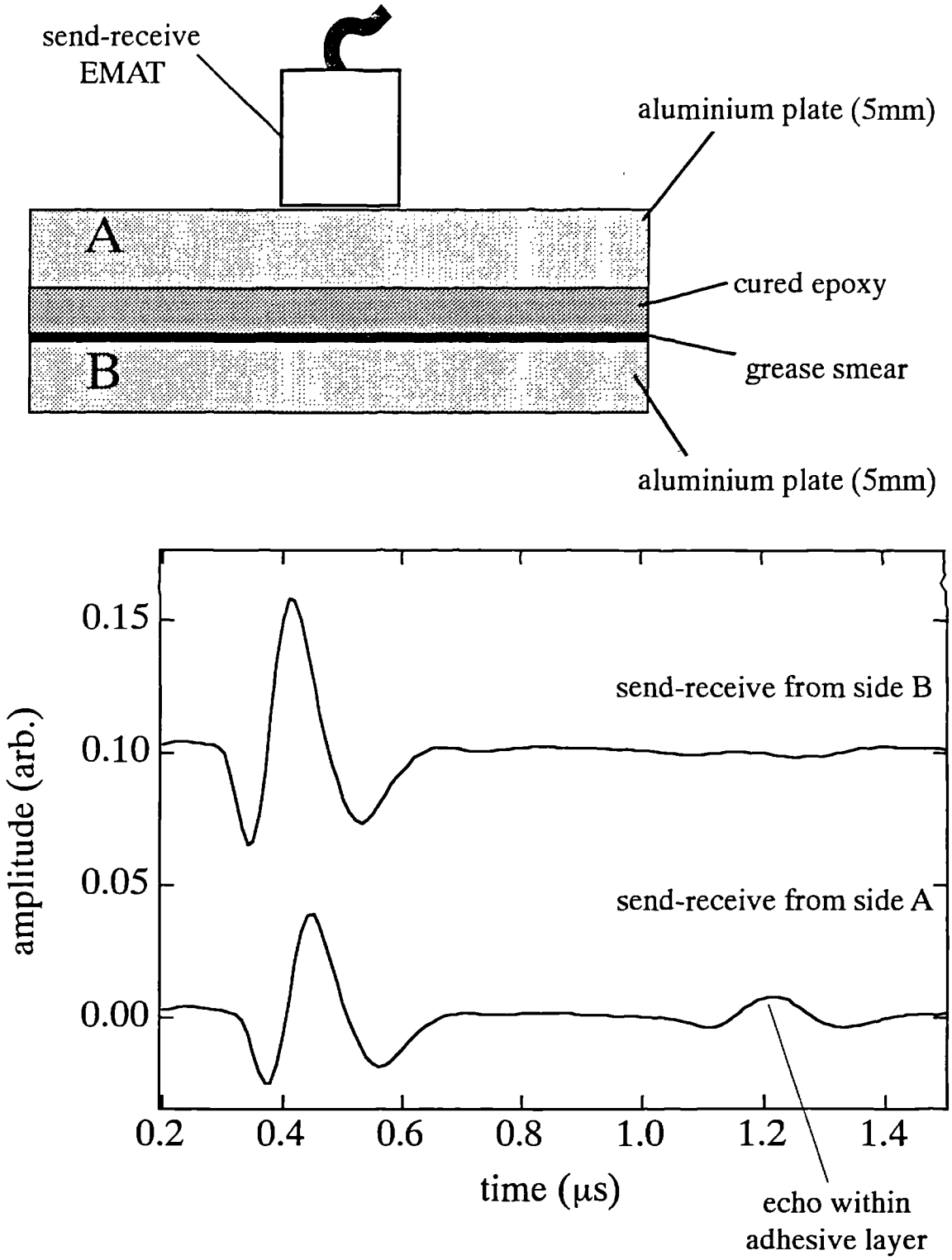

Fig 5.12

EMAT send-receive waveform obtained on an adheisvely bonded sample with one adherent-adhesive interface contaminated by a smear of silicon grease.

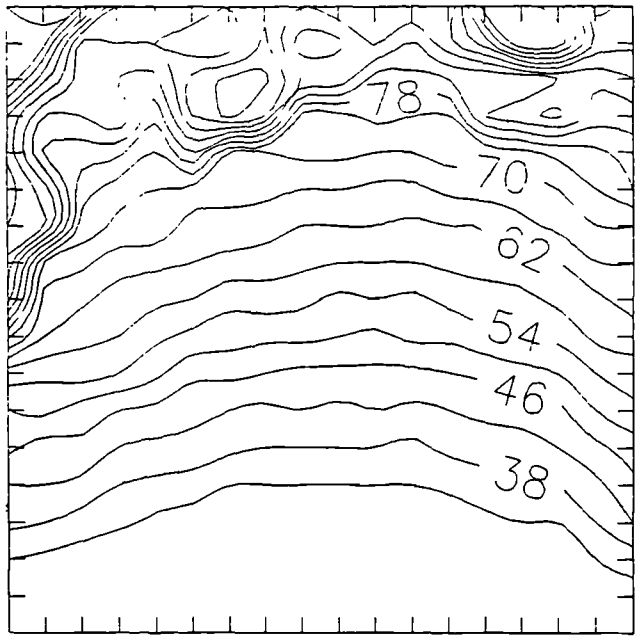

'Thickness'
(10ns/div)

Scan Area
90 X 90 mm

points taken at
steps of 5mm

Fig 5.13a

2D density plot for the 'thickness' data obtained in scanning the defect free wedged sample in through transmission.

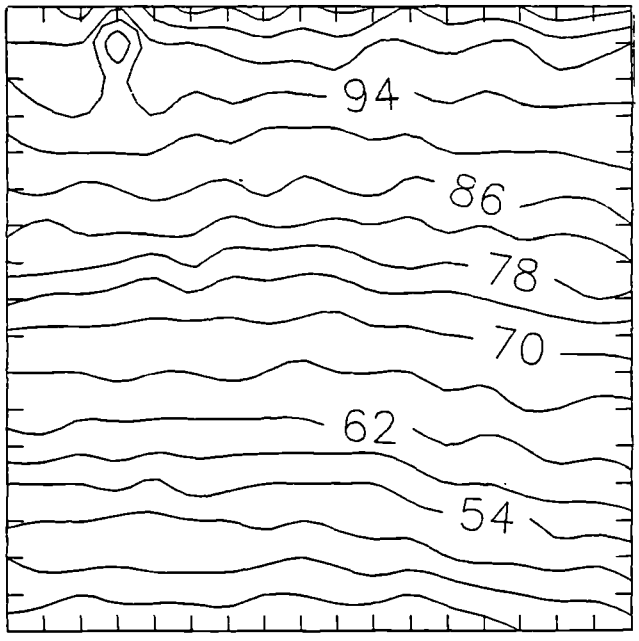

'Thickness'
(10ns/div)

Scan Area
90 X 90 mm

points taken at
steps of 5mm

Fig 5.13b

2D density plot for the 'thickness' data obtained in scanning the defective wedged sample in through transmission.

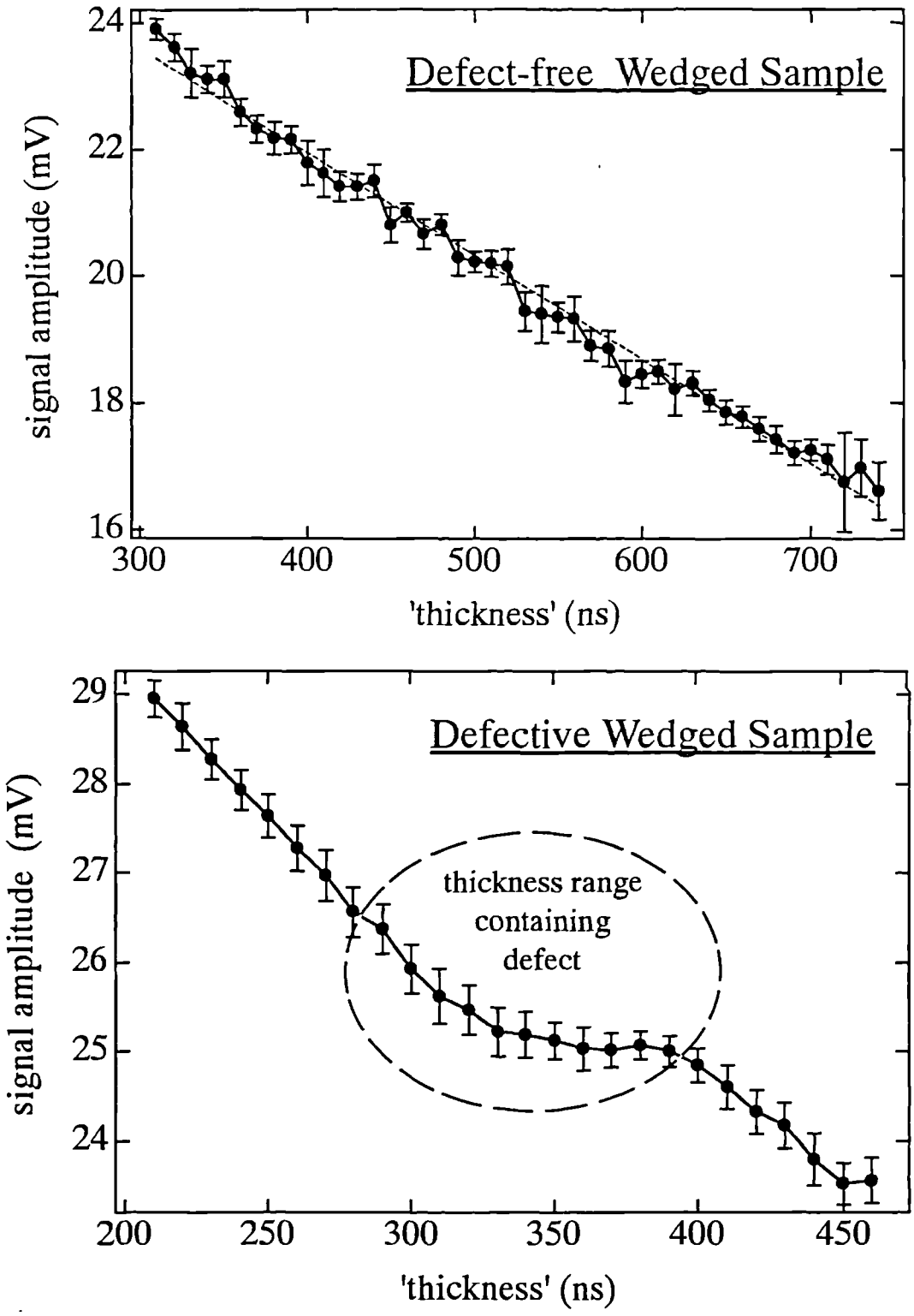

Fig 5.14

Attenuation of shear wave pulse amplitude in the defect free wedged adhesive layer sample and the defective wedged layer sample.

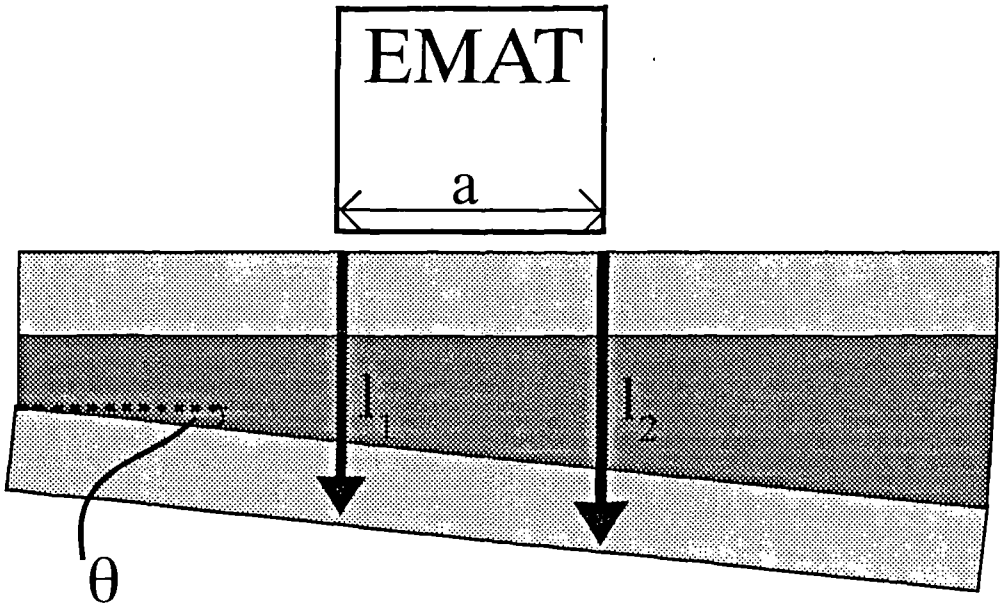

The two extreme acoustic path lenghts are 'l_1' and 'l_2'. The wedge angle is given by 'θ', and the EMAT diameter by 'a'. The difference in transit time Δt is given by :-

$$\Delta t = (l_2 - l_1)/v = a \tan(\theta) / v$$

For the first bondline reverberation in through transmission the above expression needs to be multiplied by 3, as it will have traversed the epoxy 3 times.

Fig 5.15

Schematic diagram of shear wave bond reverberation broadening due to the wedged nature of an adhesive layer.

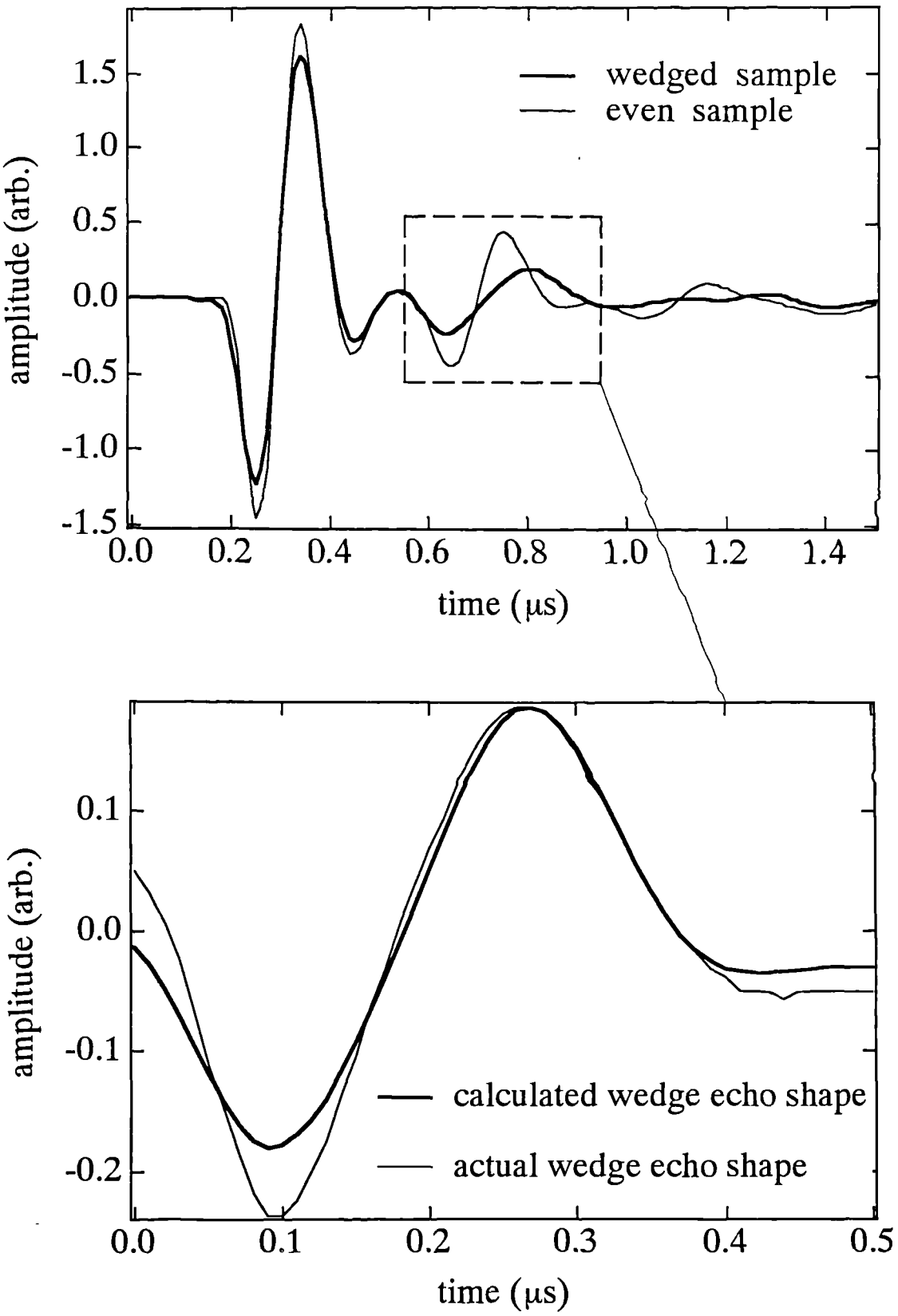

Fig 5.16

EMAT through transmission waveform obtained on two adhesive bonds of identical average adhesive layer thickness over an area of the EMAT face, one a wedged adhesive layer and the other nominally parallel faced.

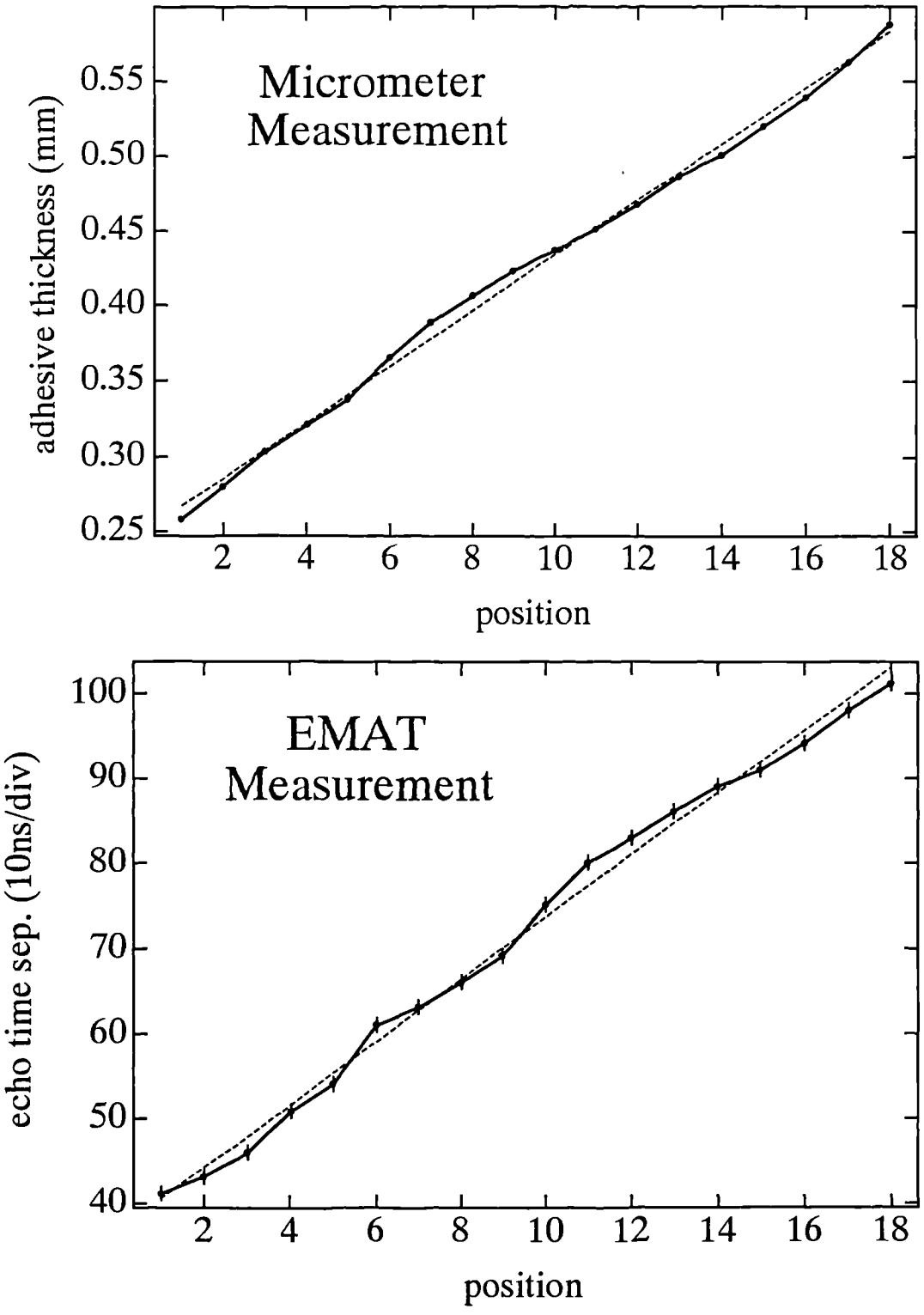

Fig 5.17

Comparison of EMAT generated shear wave transit time (or temporal 'thickness') measurement of an adhesiev layer and a micrometer thickness measurement of that layer as a function of position.

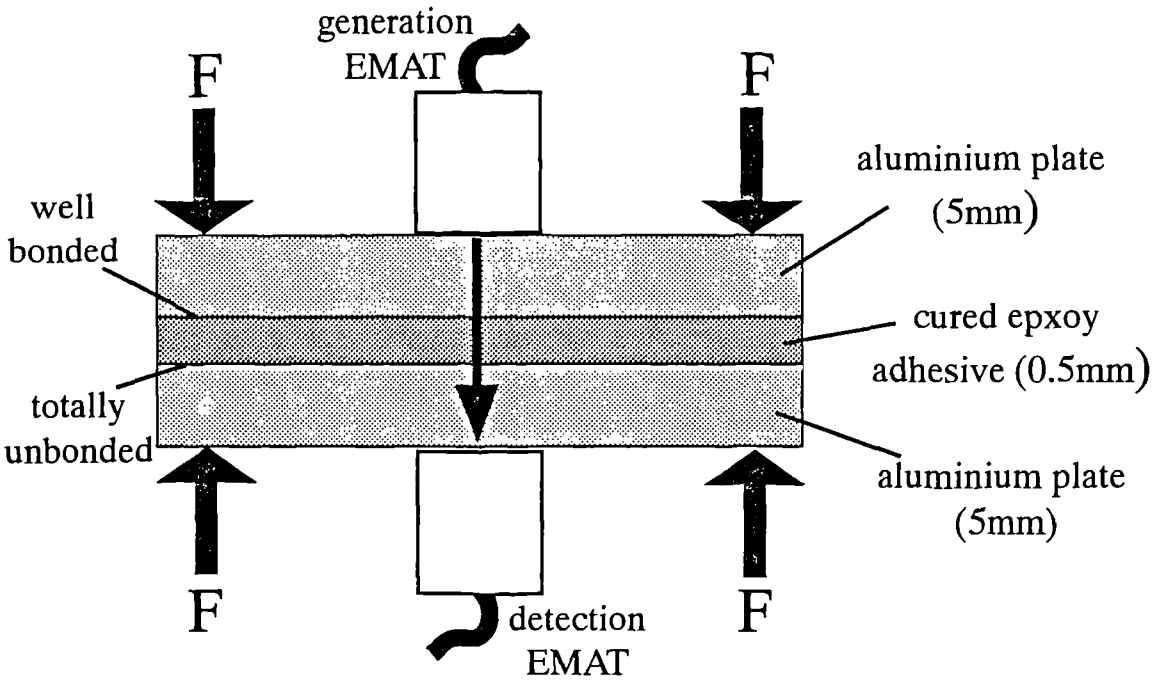

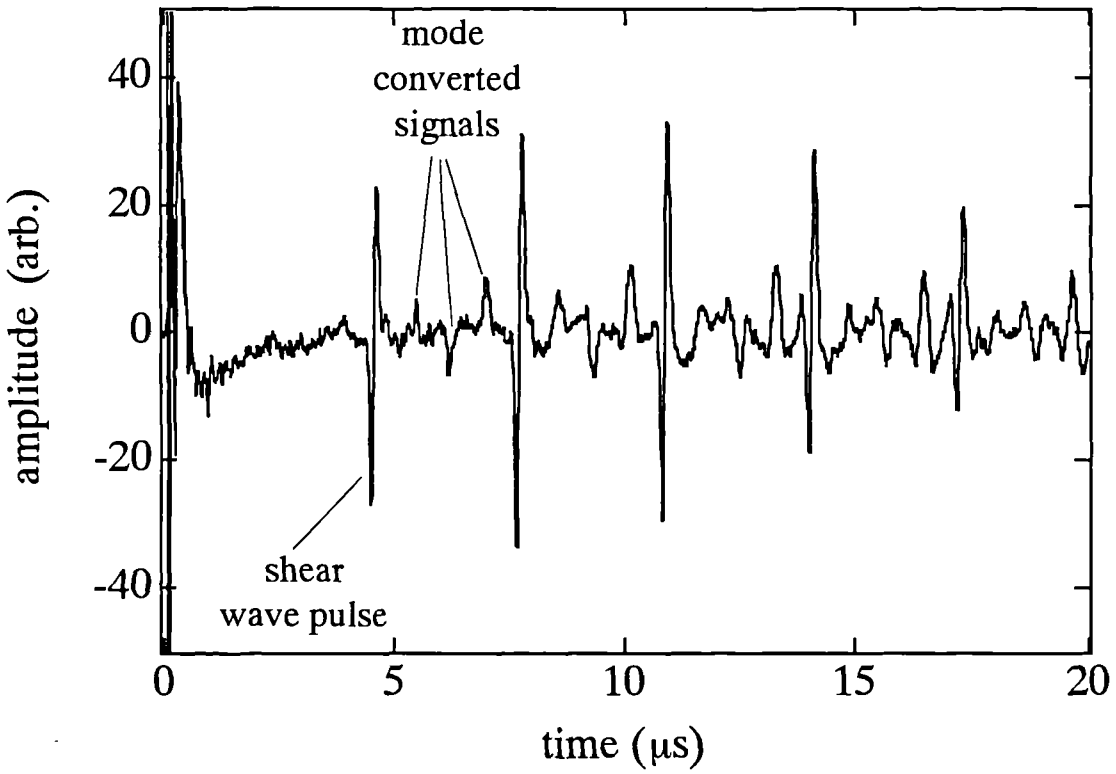

Fig 5.18

Demonstration of shear wave coupling through a totally unbonded adherent-adhesive interface with the application of compressive stress to the interface.

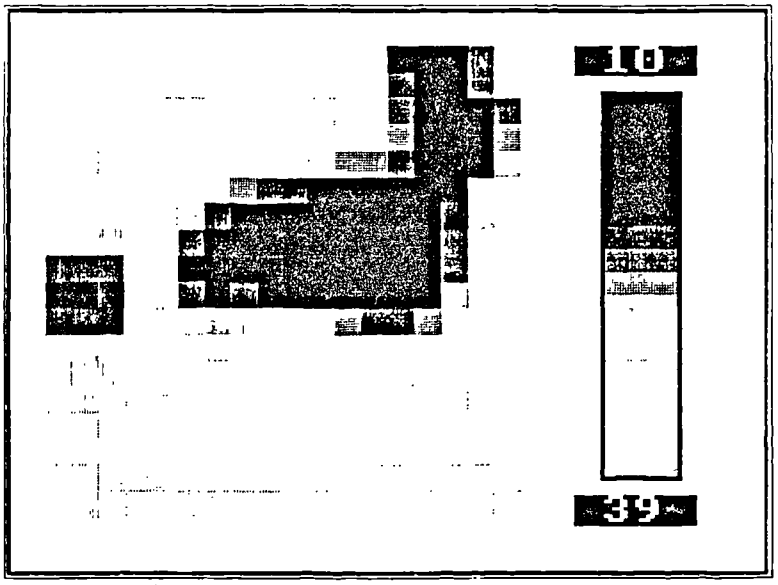

Amp. (arb)

Fig 5.19a

2D density plot for the amplitude data obtained in scanning the voided sample in through transmission.

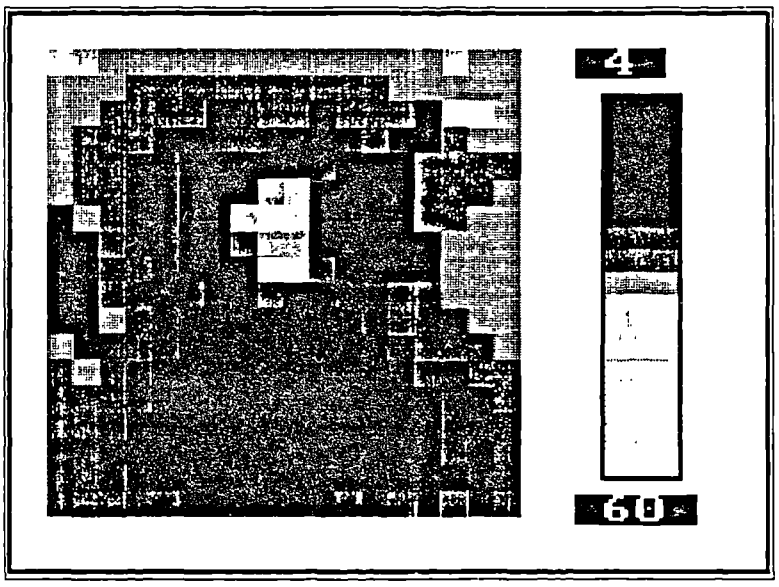

Thickness (10ns/div)

Fig 5.19b

2D density plot for the 'thickness' data obtained in scanning the voided sample sample in through transmission. The data is corrupted in certain regions due to the signal being too small to be measured.

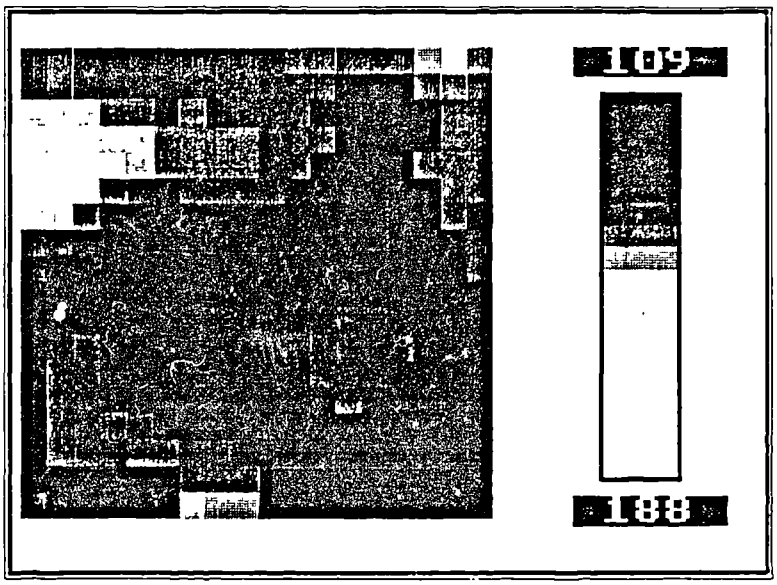

Amp. (arb)

Fig 5.20a

2D density plot for the amplitude data obtained in scanning the voided sample in send-receive from the 4.8mm plate side. The first principal peak amplitude was measured.

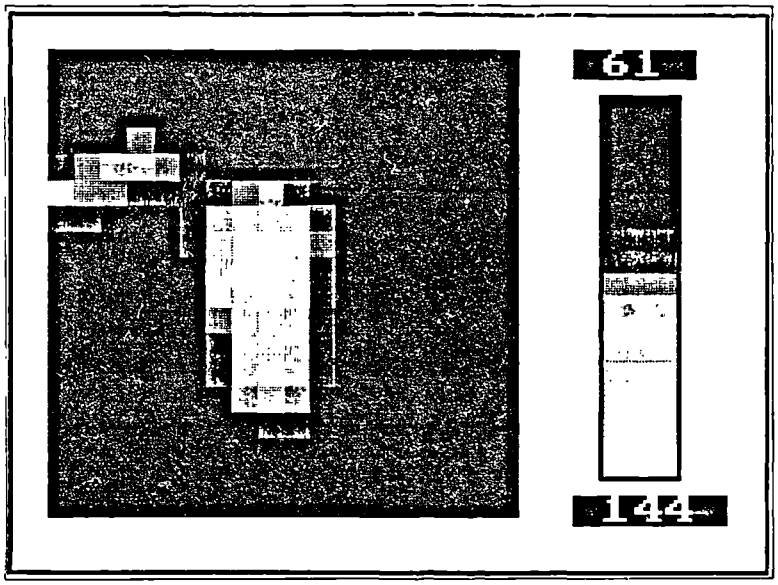

Amp. (arb)

Fig 5.20b

2D density plot for the amplitude data obtained in scanning the voided sample in send-receive from the 3.3mm plate side. The second principal peak amplitude was measured.

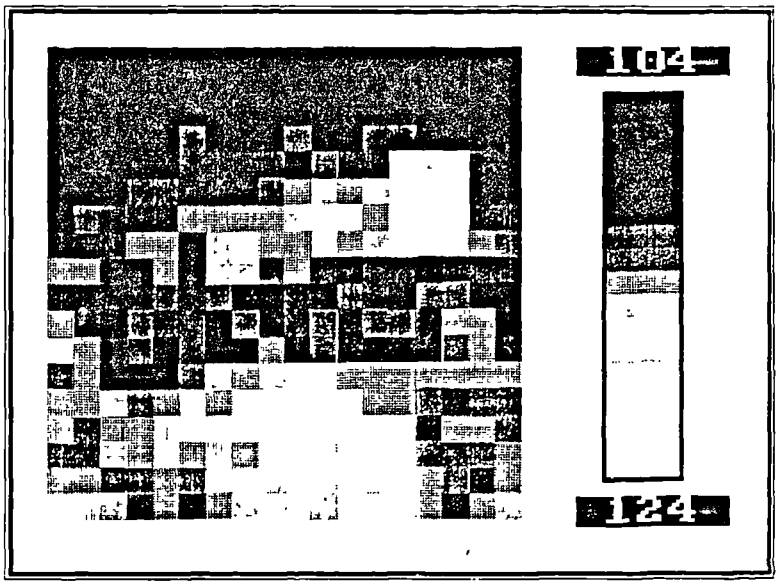

Amp. (arb)

Fig 5.21a

2D density plot for the amplitude data obtained in scanning the 'release film' sample in send-receive from the 4.8mm plate side. The first principal peak amplitude was measured.

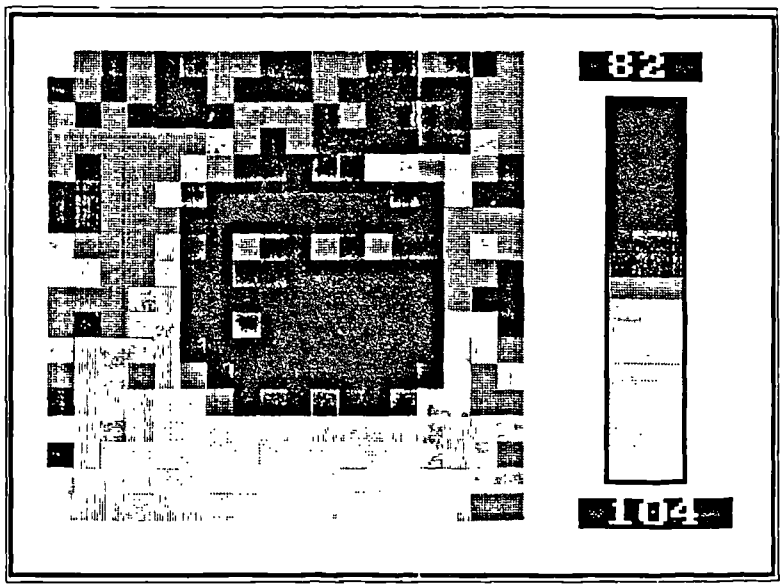

Amp. (arb)

Fig 5.21b

2D density plot for the amplitude data obtained in scanning the 'release film' sample in send-receive from the 4.8mm plate side. The first adhesive echo peak amplitude was measured.

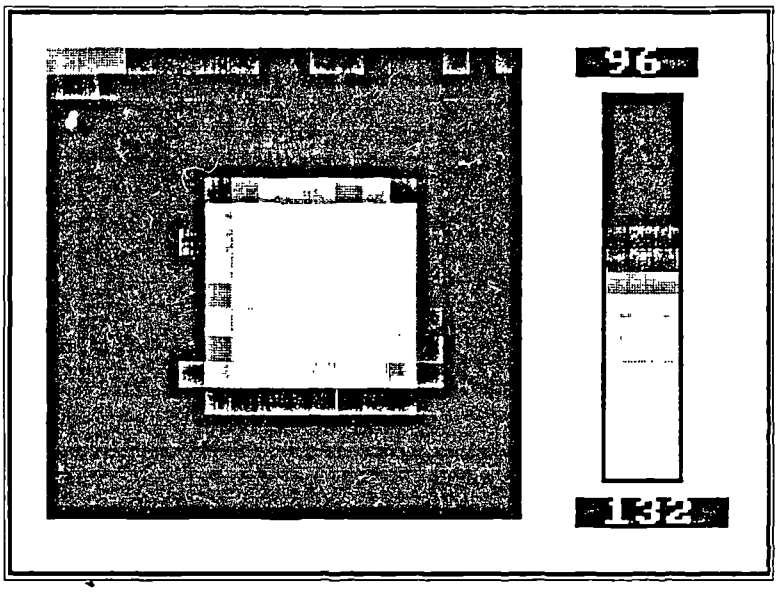

Fig 5.21c

2D density plot for the amplitude data obtained in scanning the'release film' sample in send-receive from the 3.3mm plate side. The second principal peak amplitude was measured.

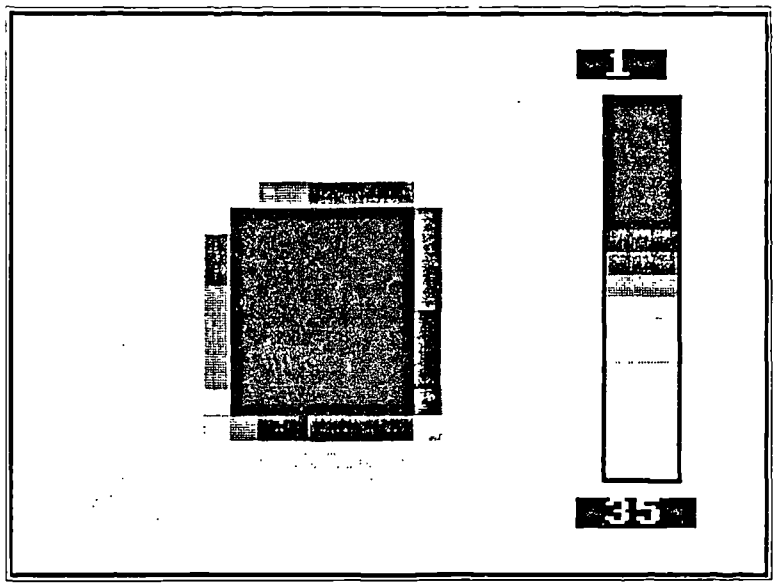

Amp. (arb)

Fig 5.22a

2D density plot for the amplitude data obtained in scanning the'release film' sample in through transmission.

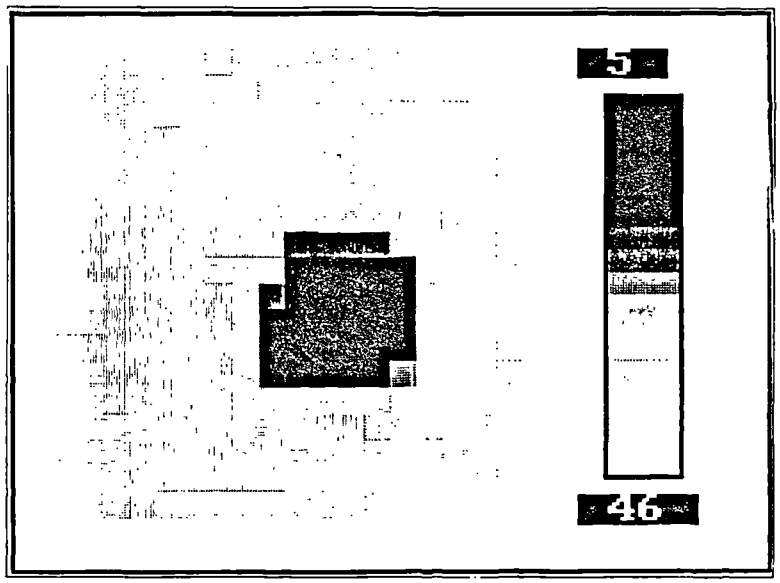

Thickness (10ns/div)

Fig 5.22b

2D density plot for the 'thickness' data obtained in scanning the 'release film' sample in through transmission. Data is corrupted in the region of the defect.

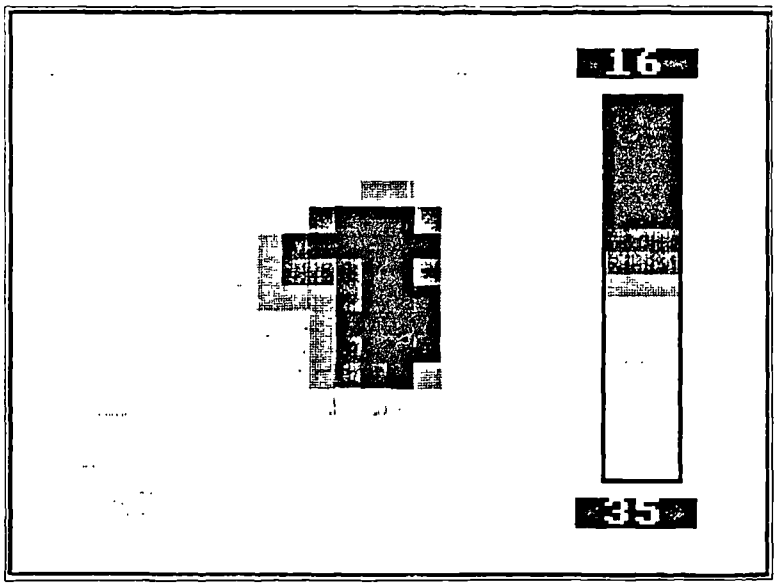

Amp. (arb)

Fig 5.23a

2D density plot for the amplitude data obtained in scanning the 'silicon grease' sample in through transmission.

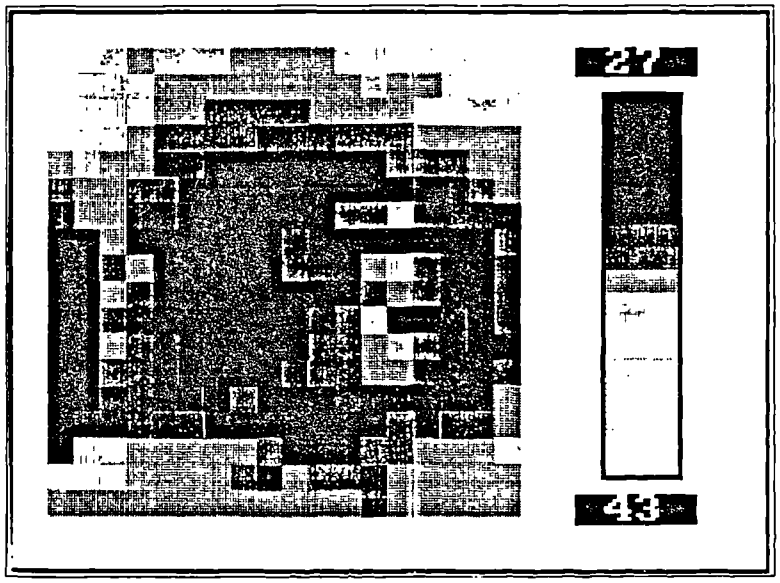

Thickness (10ns/div)

Fig 5.23b

2D density plot for the 'thickness' data obtained in scanning the 'silicon grease' sample in through transmission.

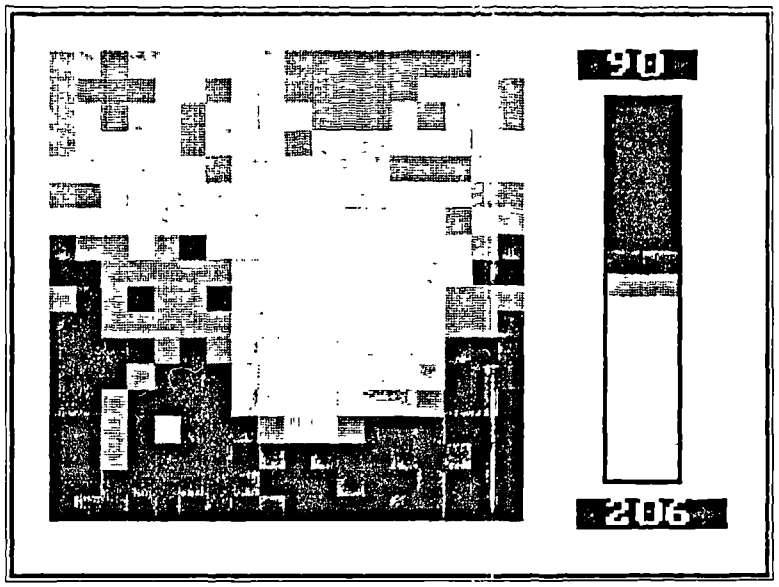

Fig 5.24a

2D density plot for the amplitude data obtained in scanning the'silicon grease' sample in send-receive from the 3.3mm plate side. The second principal peak amplitude was measured.

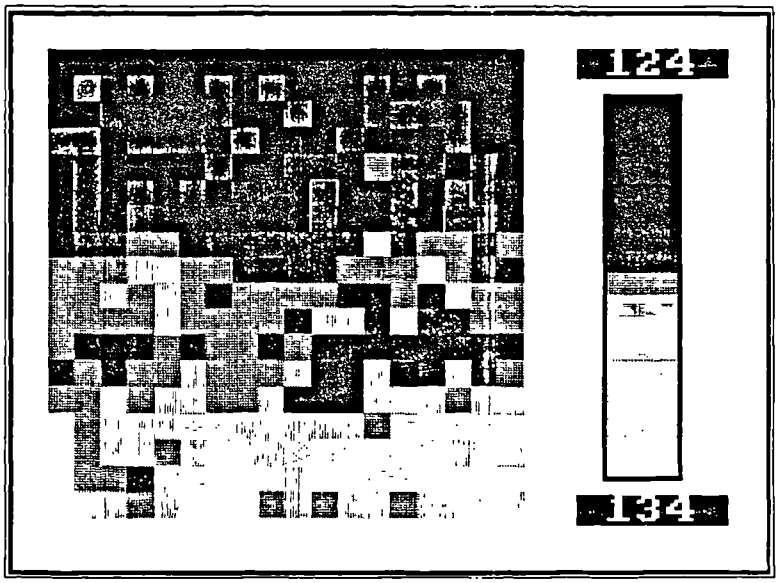

Fig 5.24b

2D density plot for the amplitude data obtained in scanning the 'silicon grease' sample in send-receive from the 4.8mm plate side. The first principal peak amplitude was measured.

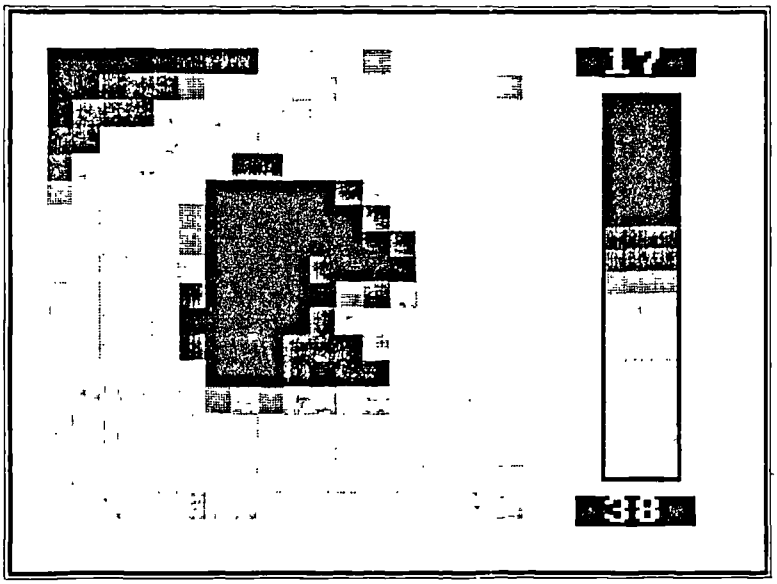

Fig 5.24c

2D density plot for the amplitude data obtained in scanning the 'silicon grease' sample in send-receive from the 4.8mm plate side. The first adhesive echo peak amplitude was measured.

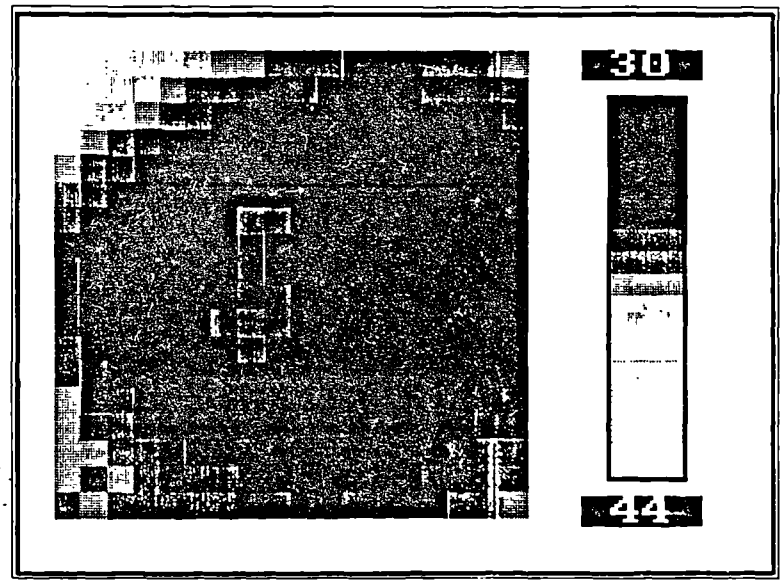

Fig 5.24d

2D density plot for the 'thickness' data obtained in scanning the 'silicon grease' sample in send-receive from the 4.8mm plate side.

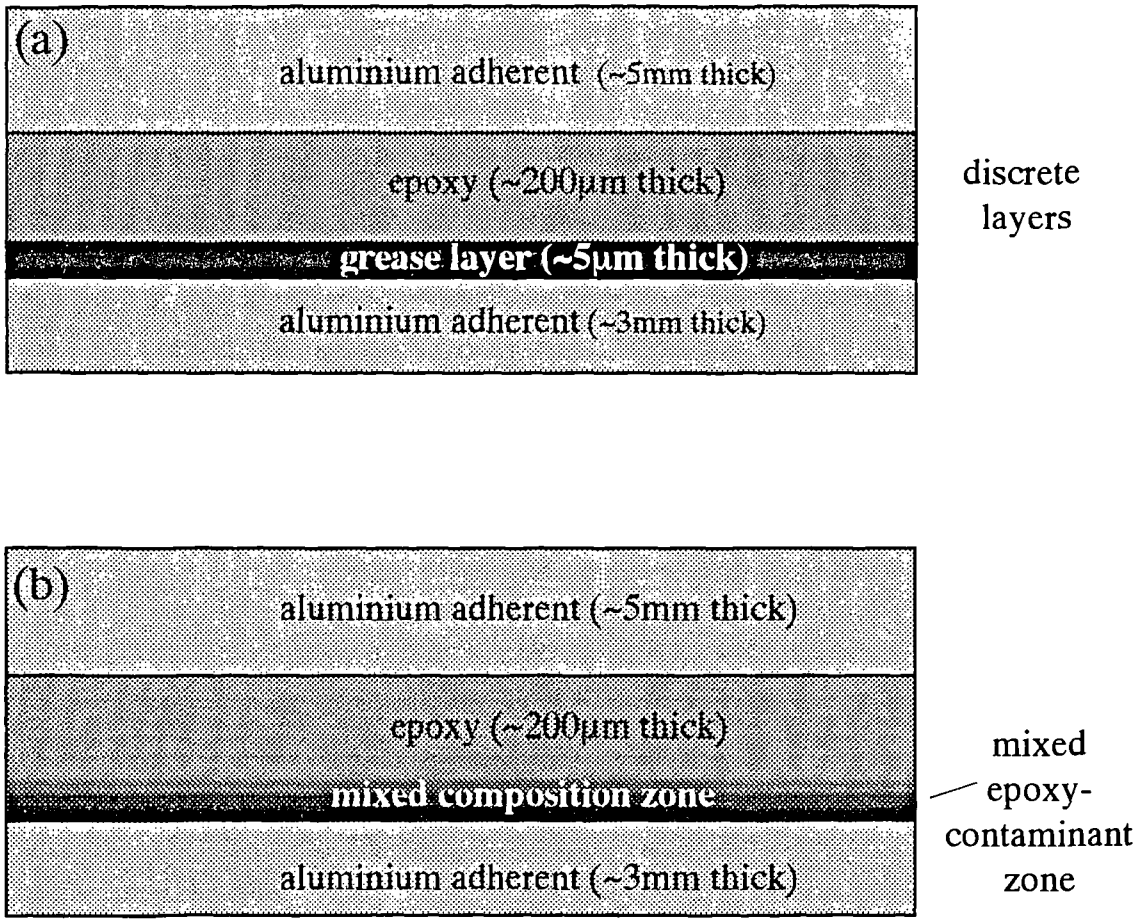

(a) consists of discrete layers which would be a satisfactory explanation for the observed ultrasonic waveforms recorded over the defective region.
(b) shows the more realistic case where the epoxy and grease have mixed to form some indiscrete zone that could be more attenuative to shear waves than the plain epoxy layer.

Fig 5.25

Cross sectional representations of the silicon grease contaminated adhesively bonded sample.

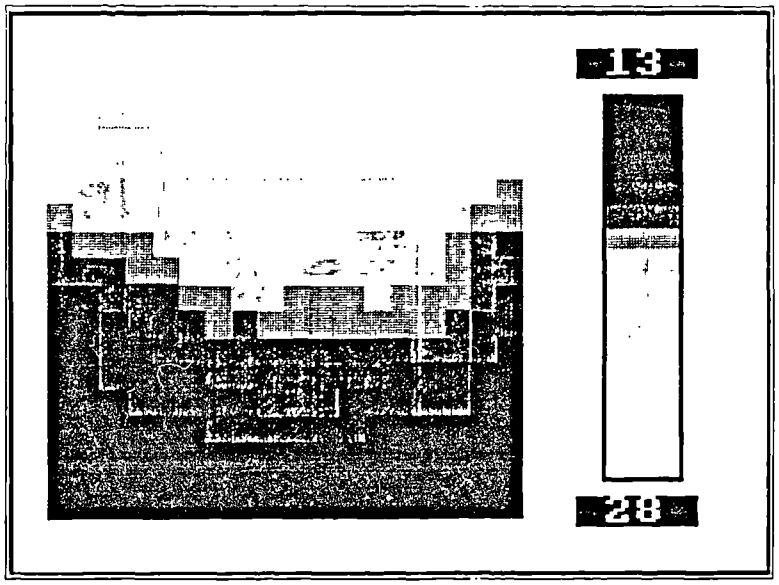

Amp. (arb)

Fig 5.26a

2D density plot for the amplitude data obtained in scanning the defect free wedged sample in through transmission.

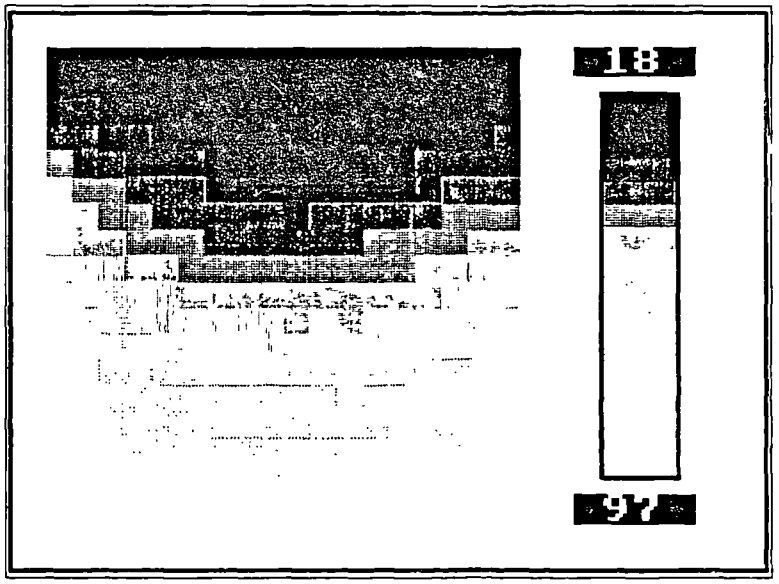

Thickness
(10ns/div)

Fig 5.26b

2D density plot for the 'thickness' data obtained in scanning the defect free wedged sample in through transmission.

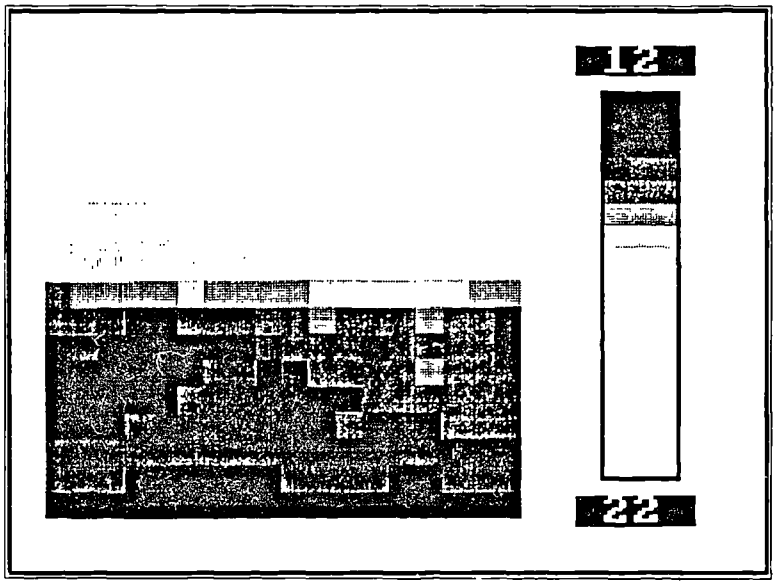

Amp. (arb)

Fig 5.27a

2D density plot for the amplitude data obtained in scanning the defective wedged sample in through transmission.

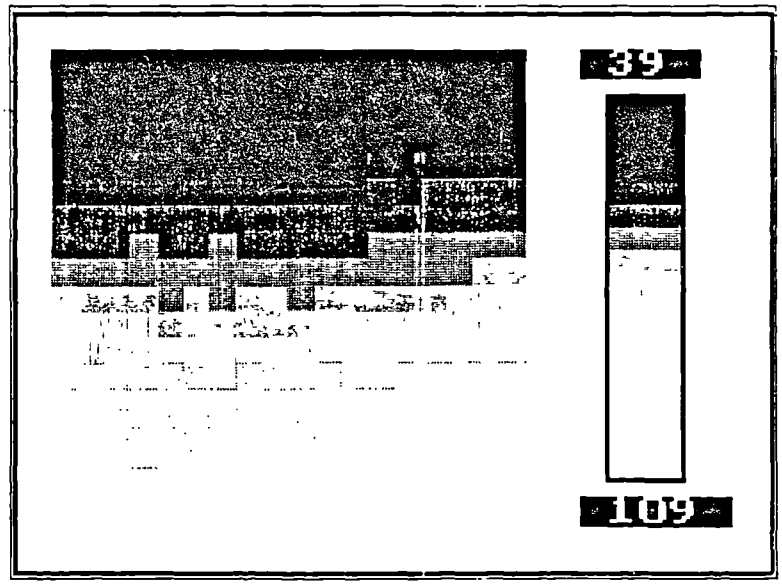

Thickness (10ns/div)

Fig 5.27b

2D density plot for the 'thickness' data obtained in scanning the defective wedged sample in through transmission.

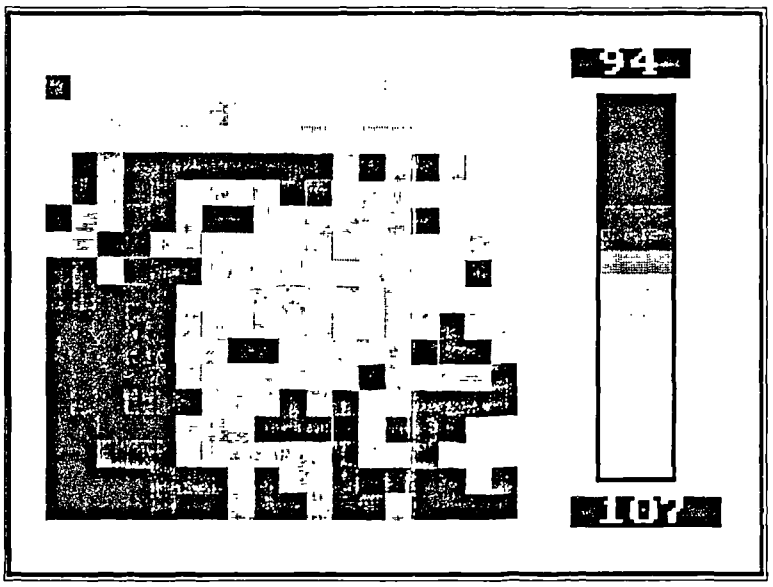

Amp. (arb)

Fig 5.28a

2D density plot for the amplitude data obtained in scanning the defect free wedged sample in send-receive from the 4.8mm plate side. The first principal peak amplitude was measured.

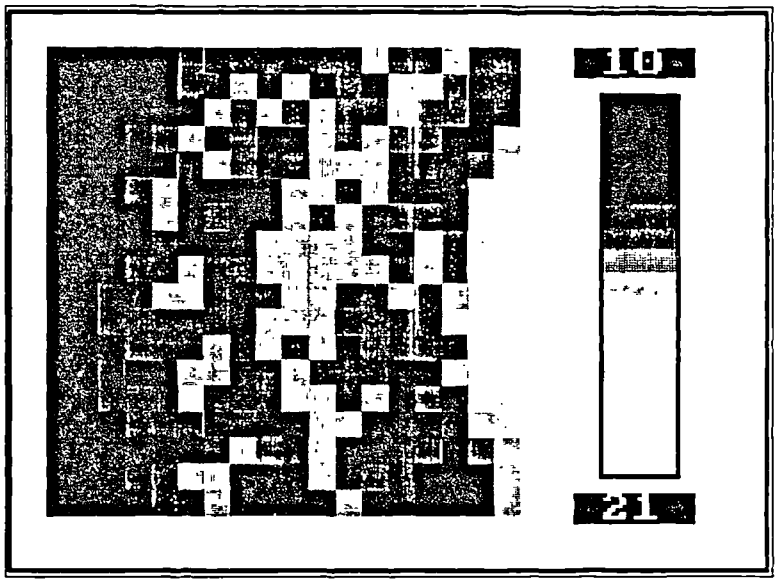

Amp. (arb)

Fig 5.28b

2D density plot for the amplitude data obtained in scanning the defect free wedged sample in send-receive from the 4.8mm plate side.The first adhesive echo peak amplitude was measured.

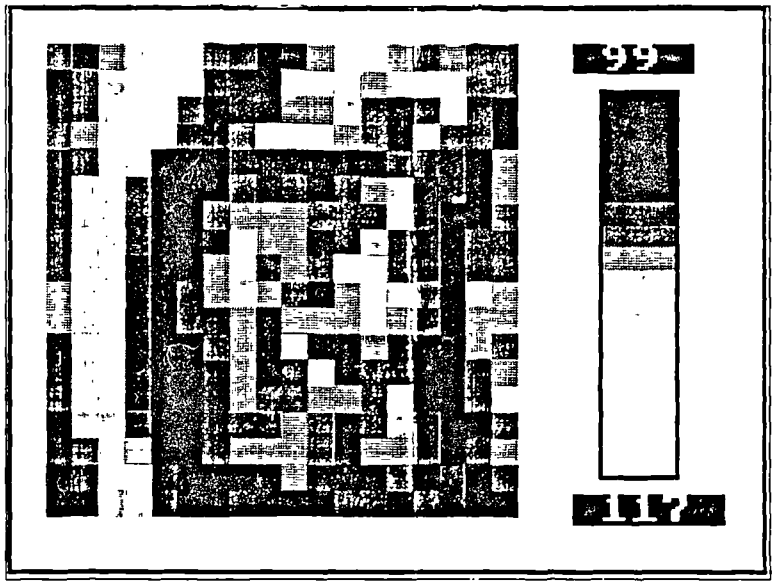

Amp. (arb)

Fig 5.28c

2D density plot for the amplitude data obtained in scanning the *defect free* wedged sample in send-receive from the 4.8mm plate side. The second principal peak amplitude was measured.

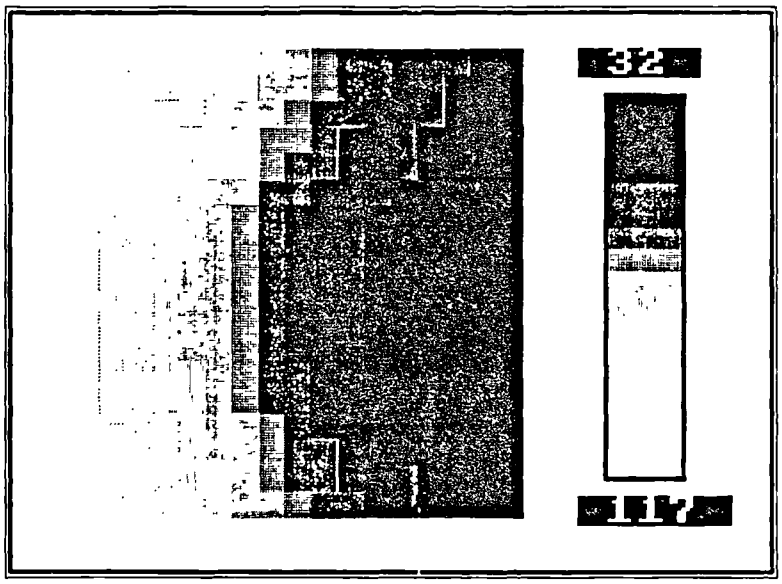

Thickness (10ns/div)

Fig 5.28d

2D density plot for the 'thickness' data obtained in scanning the defect free wedged sample in send-receive from the 4.8mm plate side.

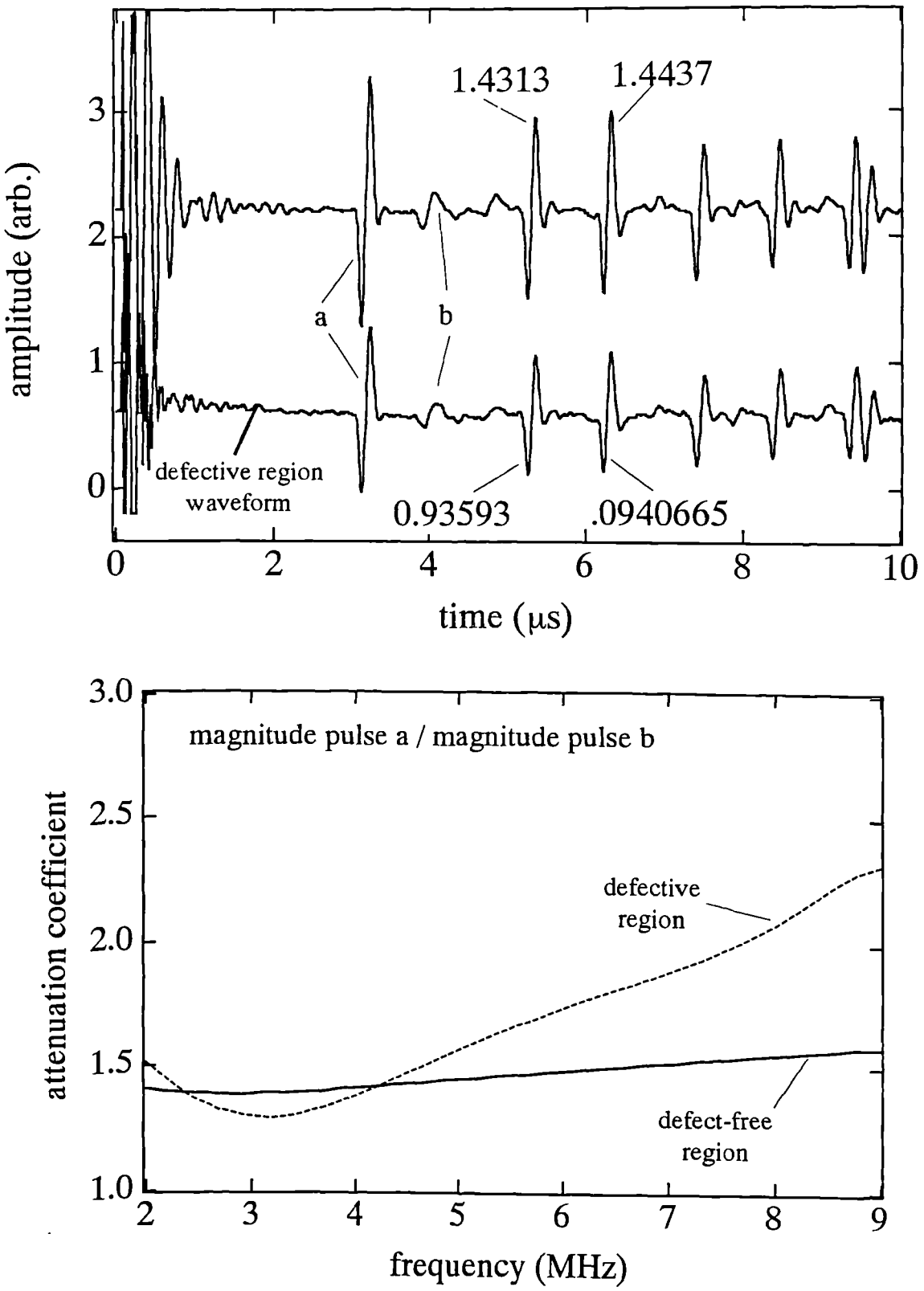

Fig 5.29

Adhesive layer frequency dependent shear wave attenutaion over the defective region of the wedged sample, and over a dfecet free region of the wedged sample of identical wedge angle and thickness.

Chapter 6

Waveform analysis and simulation

6.0 Introduction

The main problem with any scanning transducer technique is obtaining the desired information from the ultrasonic waveform. The last chapter touched upon some of the problems encountered with waveform analysis, and in this chapter, those ideas will be more thoroughly discussed and explored. An important feature of an epoxy adhesive is that it is viscoelastic rather than an elastic medium. This has the result that the ultrasonic velocity is frequency dependant. Calculations of the phase and group velocities, yield information as to the physical properties of the adhesive, and can be used to determine the cohesive strength of the adhesive. Once again, send-receive and through transmission are abbreviated to SR and TT respectively.

6.1 Modelling waveforms

So far the analysis of results has concentrated on the applicability of the EMAT system to examine gross flaws in the interfaces or bulk of the bond. In order to illustrate the types of subtleties that have been encountered, one of the grease contaminated bonds was chosen for a more detailed analysis.

As stated previously, the most useful signal in terms of the analysis of the physical properties of the bond is the first ultrasonic arrival, whether in SR or TT. Initially , the presence of mode conversions within the waveform will be ignored, and the arguments limited to 'pure' shear wave reverberations. The following argument centres on the assumption that the reflection or transmission coefficients are dependant on the degree of adhesion, and on the acoustic impedances of the media that comprise the bond. Basic theory

runs into difficulty as the classical reflection / transmission coefficients at an interface are determined only by the specific acoustic impedances of each medium - i.e. it automatically assumes intimate contact between the adherent-adhesive in this case. Models developed in an attempt to tackle this problem [1,2,3,4,5] but when coupled with experiment have not provided a satisfactory solution to the problem of adhesion monitoring. In the following sections, reflection or transmission just refers to the amount of acoustic energy reflected or transmitted at the interface.

The first most basic property one might want to measure is that of the reflection coefficient at an interface. At first glance, it may be thought that the reflection coefficient is simply the ratio of one principal echo peak amplitude, to the proceeding principal peak amplitude. This will give a reasonable value for the reflection coefficient relative to good/ very poor bond values, but the measurement may be subtly corrupted by the higher order reflections within the whole bonded structure. While other reverberations within the bond are of a much smaller amplitude than the large pulses trapped in the upper adherent, they can still be sufficiently large to cause significant variations in the principal pulse amplitudes (as large as 10% in some cases). This has been demonstrated in the analysis of the grease contaminated sample using a SR EMAT on the (4.8mm) side where the defect is on the far interface. The waveform is shown in fig 6.1. The amplitudes of the first principal pulse and second principal pulse are shown as c-scans in fig 6.2 and fig 6.3 respectively. As can be seen, the general trend in the data for these two scans is very different. The c-scans showing the first echo within the bond and adhesive layer thickness are shown in fig 6.4 and fig 6.5 respectively. It can be clearly seen that the second principal pulse contains information about the bulk and far interface.

The points raised above, show that the measurement of a reflection coefficient by direct amplitude ratio is not valid in general. It also illustrates exactly how important it is to observe the first ultrasonic arrival. The problem gets worse using later pulses, as the waveform becomes even more complicated, as will be shown later. Incidentally, in this case a measurement of the the ratio of the amplitude of the second and first principal pulse amplitude would be totally incorrect, giving values of over 100%, due to the amplifier not

having fully recovered in the time region of the first ultrasonic arrival, and the waveform modulation due to the shape of stress field generated by the EMAT. The modulation caused by this partial pre-amplifier paralysis can, and has been corrected for as described in chapter 3, but the modulation due to the inhomogeneity of the wavefront is a more difficult problem and has not been tackled here.

In general, if precise quantitative values for both reflection coefficients and bulk mechanical properties are to be determined by analysis of the ultrasonic waveform, then the problem cannot be attacked by simple amplitude and time difference measurements. In order to obtain accurate values, some waveform simulation and computational analysis must be performed. As a first step to attempting to obtaining some ideas of how the computation may be tackled, some very simple programs were written. These were not intended to be offered as a complete solution to the problem, but merely a crude approximation to the deconvolutions and analysis that should be employed.

As the shear wave attenuation in both aluminium and epoxy have been measured, a computer program was written to iteratively calculate the relative amplitudes and arrival times of ultrasonic echoes within the bonded sample. In send-receive, the most dominant peak is obviously the principal echo that is trapped in the upper adherent. The next most significant amplitude pulse arises via a direct reflection from the far adhesive adherent interface. There are several other relatively large echoes that have traversed the adhesive layer, and their arrival times relative to the principal pulse is thus also dependant on the adhesive thickness. The main difference in the simulated waveform and real waveform lies within the mode conversions, which are out of the scope of simple plane wave theory. These arise due to the finite size of the transducer and therefore the ultrasonic field and are difficult to simulate as they require the calculation of a Greens type function [6] for the different boundary conditions within the bond. The Greens function calculation in turn, also requires an accurate function (in time and space) to describe the stress field generated by the EMAT. A more detailed description of this effect was discussed in chapter 2 , where a crude model is applied in order to demonstrate the position of peaks within the waveform.

The amplitude of each of the different ultrasonic arrivals was solved iteratively because a fraction of an observed ultrasonic arrival derives from the preceding echo. This explains why the subsidiary echoes actually increase in amplitude rather than decrease, as would be expected for simple exponential decay in a single layer medium. The simulation of this behavior requires the functional dependance of attenuation in both the aluminium and the epoxy layers. Waveform simulation such as that described here is useful in that it shows what magnitude of changes in reflection and transmission coefficients are likely to be detectable. It also illustrates situations where problems may arise in the analysis. This is also clearly demonstrated in the c-scan of a wedged sample, where the principal echoes appear to contain information of the adhesive thickness for certain values of adhesive thicknesses. i.e., where the peak y(i) is coincident with the principal i+1 peak. Also in the wedged sample, the information of the echo within the adhesive is corrupted due to the reverberation within the adhesive layer interfering with one of the mode conversions.

The simple equations used to simulate relative pulse amplitude are shown below. The schematic diagram of the paths these pulses take within a bond are shown in fig 6.6. In the following, 'r' denotes a reflection coefficient, 't' a transmission coefficient: subscripts 1 and 2 and 3 are for the upper adherent (on which ultrasonic generation takes place), adhesive and lower adherent respectively. Thus, subscript 12 in the coefficients indicates that the wave travelling in medium 1 is incident on the interface of medium 1 to medium 2. The symbol 'D' denotes an amplitude decay operator, with subscripts 1,2 or 3 for upper adherent, adhesive and lower adherent respectively.

The nth principal pulse, p_n is given by:-

$$p_n = D_1^n [A\, r_{12}^n] \qquad 6.1$$

The first echo in the adhesive layer associated with the nth principal pulse is denoted e_n, and given by:-

$$e_n = D_1 [D_2 [D_2 [A\, r_{12}^{n-1} t_{12}] r_{23}] t_{21}] + D_1^2 [e_{n-1}] r_{12} \qquad 6.2$$

The first part of this expression is the magnitude of the echo pulse that has derived from the preceding principal pulse.

The second part of the term involving e_{n-1} takes account of the pulse that 'rings' back and forth in the upper plate, for which most of the energy associated with it is trapped in the upper adherent.

The above can be re-written in terms of the nth principal pulse,

$$e_n = D_1 [D_2 [D_2 [D_1^{-1} [p_n] r_{12}^{-1} t_{12}] r_{23}] t_{21}] + D_1^2 [e_{n-1}] r_{12} \quad 6.3$$

The pulses denoted x_n and y_n as shown in fig 6.6, can be written as :-

$$x_n = D_1 [D_2 [D_3^2 [D_2 [A r_{12}^{n-1} t_{12}] t_{23}] t_{32}] t_{21}] + D_1^2 [x_{n-1}] r_{12} \quad 6.4$$

$$y_n = D_1 [D_2 [D_3^2 [D_3^2 [D_2 [A r_{12}^{n-1} t_{12}] t_{23}] r_{32}] t_{32}] t_{21}] + D_1^2 [y_{n-1}]r_{12} \quad 6.5$$

Assuming that the decay operators act linearly on the ultrasound we can write the pulses e_n and x_n, and subsidiary adhesive echoes associated with the x_n pulse as,

$$e_n = D_1 D_2^2 A r^{n-1} t_{12} r_{23} t_{21} + D_1^2 [e_{n-1}] r_{12} \quad 6.6$$

$$x_n = D_1 D_2^2 D_3^2 A r_{12}^{n-1} t_{12} t_{21} t_{23} t_{32} + D_1^2 [x_{n-1}] r_{12} \quad 6.7$$

Thus the first two subsidiary echoes are given by:-

$$x1_n = 2\{ D_1 D_2^4 D_3^2 A r_{12}^{n-1} t_{12} t_{21} t_{23} t_{32} r_{21} r_{23}\} + D_1^2 [x1_{n-1}] r_{12} \quad 6.8$$

and,

$$x2_n = 3\{ D_1 D_2^6 D_3^2 A r^{n-1} t_{12} t_{21} t_{23} t_{32} r_{12} r_{21} r_{23} r_{32}\} + D_1^2 [x2_{n-1}] r_{12} \quad 6.9$$

While these two above echoes have much higher decay factors than the x_n*th pulse, this is* in part compensated for by the fact that there are more combinations of ultrasonic pathlengths that have the same transit time: hence the factors of 2 and 3 in the above equations.

Here, only a few of the pulses present in the waveform have been described, as these demonstrate that the measured amplitudes in the waveform consist in fact of a summation of various pulses. Once again this emphasises the importance of being able to capture the very first shear wave arrival. However the total picture is further complicated by the presence of mode conversions, and other reverberations within the bond that have been ignored above. In general, these reverberations cannot be ignored, and the arguments presented are specific to the experimental geometry in this project.

A program to simulate the echoes described above, was used to generate waveforms, with and without the reverberations from the x_n pulse. The difference in these two waveforms would be the difference in the measured amplitude, and the amplitude of the isolated principal peak, which would be required to calculate the reflection coefficient from the near interface and hence adhesive bulk and far interface properties. The reflection coefficients, decay rates, adhesive adherent thicknesses could be chosen (using values from typical experimentally obtained 'spot' measurements). The simulated waveforms shown in figs 6.7

have reflection coefficients at both interfaces of 0.85 (chosen), and adhesive thicknesses of 150 and 200μm. In the calculations above, dispersion of the shear wave pulse was ignored, and the pulse used in the waveform simulation was a shear wave pulse recorded in the aerospace aluminium plate (4.84mm blank adherent).

6.2 Phase and group velocity

Plane waves in an infinite, purely elastic medium would have phase and group velocities which were equal and independent of frequency. However, as described in chapter 2, the ultrasonic phase and group velocities in a solid medium are in general a function of frequency [7]. The aluminium and epoxy have very different mechanical and thus acoustic properties: the aluminium behaves as an elastic medium while the epoxy is a viscoelastic medium. In order to measure the viscoelasticity, the analysis of the broadband ultrasonic waveforms must be performed in the frequency domain. The magnitude FFT shows that there is very little observed frequency content for frequencies less than 1MHz (limited by the preamplifier) and greater than 10MHz (limited by the frequency content of the drive pulse).

6.2.1. Phase velocity in aluminium

In order to verify that the aluminium behaves as an elastic medium, the phase velocity of an aluminium sample taken from an extruded rod, and one of the thicker adherent plates were examined using EMATs. In addition, a waveform was taken on aluminium single crystal ((100) direction) as this should have very relatively little ultrasonic dispersion over the range of frequencies present in the shear wave pulse, with a predictable velocity when compared to polycrystalline aluminium samples. There will be some dependance on velocity as a function of frequency in aluminium, but it is much smaller effect than in epoxy, and contrary to the behaviour observed in the epoxy, the phonon dispersion relation could be such that the acoustic velocity can be larger for lower frequencies [8].

Fig 6.8a shows the first and twelfth pulse echo (send-receive) in a 12.50mm aluminium disc shaped sample cut from a cross section of extruded rod. Fig 6.8b shows the calculated frequency dependance of phase velocity obtained from this waveform. The window used to capture the pulses was a little over 1μs in width, and thus for frequencies around or below 1MHz, there is insufficient information in the frequency domain to allow a reliable estimate of the velocity. This is why the phase velocity information is not shown below 2MHz. Fig 6.9 shows data from a 4.84mm thick aluminium (blank) adherent. The first and third pulses in TT, and the second and ninth pulses in SR , along with the phase velocity dispersion curves derived from this experimental data are presented.

Dispersion curves obtained in the aluminium disc and the adherent plate exhibit a frequency dependant behaviour, where velocity falls with increasing frequency. Over the range 2-8MHz, the phase velocity from the disc data changes by approximately by 1.3%, while in the plate there is a variation of less than 0.5%. The difference between these two degrees of variation is due to some difference in the internal structure of the disc and the plate such as grain size, composition, orientation and grain boundary scattering characteristics, all of which are unknown parameters for these two particular samples [9]. The phase velocity at 2MHz in the disc sample is 3160 m/s and in the plate 3120 m/s. The absolute error in these values (1% - from micrometer measurement) is greater than the variation in velocity due to dispersion. However, the shape of the dispersion curve should be a reliable indication of the phase velocity frequency dependance.

A SR waveform taken on a single crystal of aluminium was analysed, from which the frequency dependant phase velocity was calculated. The single crystal was 38mm diameter and 26.32mm thickness. The first point to note is that the shape of the second and tenth pulses indicate that while there is some dispersion and non-uniform attenuation of the ultrasound the difference is not as severe as observed in the aluminium disc sample. The difference in the calculated phase velocity over the range 2-10MHz is very small, less than 0.03% (see fig 6.10). The shear wave velocity obtained from the elastic constant C_{44} from the table in Musgrave [10], such that velocity equals $(C_{44}/\rho)^{1/2}$ yields a value of shear wave velocity of 3249 m/s. The apparent frequency dependency from the calculated phase

velocity may be a result of acoustic phonon interaction with electrons and lattice defects , or possibly simply arises as a result of the computation. The effect is so small that it would not be possible to determine its origin using this technique, and it demonstrates that the single crystal behaves as a good elastic medium , especially when compared to the other aluminium samples investigated.

6.2.2 Phase velocity in the epoxy adhesive

Fig 6.11 shows the ultrasonic shear wave attenuation of the epoxy as a function of frequency through a bond of adhesive thickness 300μm. Over the range of frequencies present, the reflection and thus transmission coefficient was found to be constant (effectively frequency independent). In general, the reflection coefficient at the interface of two elastic halfspaces in intimate contact, should be frequency independent. The reflection coefficient at the interface of an elastic and viscoelastic interface should be a function of the frequency of the incident ultrasound. This phenomena should not be confused with the frequency dependance encountered in the model of the three layer media in chapter 2: In this cw model , the frequency dependance is obtained from the FFT of the entire waveform - more of a low frequency measurement. This effect would not be observed in the frequency content of a single pulse through a three layered elastic composite.

Elasticity of a body can be modelled by a spring type representation. Viscoelasticity can be modelled by a suitable choice of dashpot and spring combination [11,12,13]. The first model that will briefly be discussed is the Voigt model for a viscoelastic solid, where a spring is connected in parallel to a damping dashpot and the response of the total system to an applied sinusoidal force is analysed. see fig 6.12a.

The model behaves correctly, in as much as the media becomes stiffer for higher frequencies. This of course assumes that within the media, there is only one type of relaxation process i.e. that every molecular component has the same effective dashpot and spring. A range of relaxation processes can be accounted for [13,14], by essentially integrating a variable relaxation time over some distribution function.

The magnitude of the elastic modulus for the Voigt model can be written as [see Appendix A for calculation],

$$|G^*|^2 = G^2 + \omega^2\eta^2 \qquad 6.10$$

where G is the spring modulus, n is the dashpot damper coefficient and G^* is a complex term representing the modulus of combination of spring and dashpot.

The complex nature of the elasticity (and hence velocity) manifests itself as a frequency dependant property. The main disadvantage of this model is that the elastic modulus of the viscoelastic body tends to infinity as the frequency tends to infinity. Other workers have shown that typical relaxation frequencies are the the order of 40MHz. An improvement to this model is shown in fig 6.12b. It introduces another spring component, whose modulus corresponds to the elastic shear modulus of the epoxy at infinite frequency. The zero frequency or dc shear modulus corresponds to the series combination of the two springs. Over the range of frequencies present in the EMAT waveforms, the models behave nominally identically.

The magnitude of the elastic modulus for such a viscoelastic solid is given by [see appendix for calculation];

$$|G^*|^2 = \left[\frac{G_1 G_2 (G_1 + G_2) + \omega^2 \eta^2 G_1}{(G_1 + G_2)^2 + \omega^2 \eta^2}\right]^2 + \left[\frac{\omega^2 \eta^2 G_1^2}{(G_1 + G_2)^2 + \omega^2 \eta^2}\right]^2 \qquad 6.11$$

The frequency dependance of the elastic moduli for both models are shown in fig 6.13. The modulus tends to infinity for the Voigt model, and for the improved model, it levels off at some frequency (>1GHz). The values of spring stiffnesses and dashpot 'viscosities' used correspond to those determined experimentally for the epoxy adhesive Redux 312, the values being given in fig 6.13.

In order to calculate the phase or group velocities using broadband ultrasound, two ultrasonic pulses are required [15,16]. The analysis detailed below was performed by using a pulse recorded in plain aluminium plate as a reference pulse, and a pulse that had been transmitted through one adhesive layer thickness. Such a procedure required two separate waveform captures, for each pulse. The phase and group velocity calculations for the analysis method described above are shown in fig 6.14a, and 6.14b respectively. A reference shear wave pulse in aluminium plate, and a pulse from the adhesive layer were analysed to preserve the maximum amount of frequency information, as using pulses captured within the same waveform will have pulses that have traversed more than one thickness of epoxy. Taking the necessary pulses from a single waveform will have the result of the pulses being more strongly attenuated via losses within the epoxy, and from ultrasonic transmission at the adhesive-adherent interface/s. Calculations have been performed via analysis of a single waveform obtained in both through transmission and send-receive, using the waveforms shown in fig 5.9 . The phase velocity results from these calculations are shown in fig 6.15, and are consistent with the phase velocity obtained from using two separately recorded ultrasonic pulses.

The models described above predict a frequency dependant reflection coefficient, but there was no observable frequency dependance of the reflection coefficient. The change in phase velocity over the range of frequency shown is approximately 10%. Adhesive layers in the samples are typically 100μm thick giving a difference in arrival times between a 1MHz and 10MHz shear wave of 10ns - the same as the digitisation rate of the scope used to capture the data. Therefore as the adhesive layer is thin, the epoxy may be treated as roughly elastic in some situations: there is a measurable viscoelastic behavior, but this is small. The group velocity shows the expected general trend, and contains small oscillations. The group velocity is effectively derived from the differential of the phase velocity. Closer examination of the phase velocity shows that the oscillations in the group velocity correspond to very small changes in gradient of the phase velocity, or the FFT phase calculation. This is probably due to errors introduced in the computation of the frequency information, rather than being a real effect. The extremely low value and sharp drop in the calculated phase velocity for frequency less than 2MHz is characteristic of all the

calculations done in this project. The value of phase/group velocity should be approximately 1000m/s at zero frequency. Calculated phase velocity sharply decreases below 2MHz as the temporal size of window used in capturing the waveform, did not contain sufficient frequency information less than approximately 2MHz.

Using the improved single relaxation frequency viscoelastic model, a theoretical fit to the phase velocity data was performed (see fig 6.15) using variable parameters for both springs and the dashpot. In order to ensure that the fit converges, it was necessary to initiate the fit with the expected parameters. A damper coefficient of 15 Pa s was used corresponding to a relaxation frequency of 50MHz for a dc shear modulus of 0.9 GPa . The dc shear modulus of the epoxy was given in the technical data as 0.9 GPa , but this value is critical if the fit is to converge properly. In the above model the dc shear modulus is the combination of both spring moduli, so both spring moduli were allowed to be variable parameters in the fit. The model yielded values of dc shear modulus as 1.04 GPa +/- 3%, a shear modulus at infinite frequency of 43.0 GPa +/- 100% and a damping coefficient of 9.57 Pa.s +/- 3% (corresponding to a relaxation frequency of 108.7 MHz +/- 3%). The value of the relaxation coefficient is comparable to the range of values obtained by Challis [17] from the phase velocity for different types of adhesive (from 18MHz to 88MHz - limits include the extremes of the standard deviations on those results) , but is slightly higher than any he reported.

6.3 Summary

The phase and group velocity calculations for the epoxy yield values consistent with those obtained by other workers in the field. There is a very wide range of physical properties for different epoxy compositions and preparations and in the model a single relaxation frequency was assumed, so the discrepancy in the value of the derived relaxation coefficient for the epoxy from those obtained by Challis is not too surprising. The simple waveform simulations show the origin of the most dominant higher order reverberations that corrupt the larger principal pulses, and give an indication of the considerations that must be made when analysing the waveforms.

Ch.6 References

1 P. Cawley , The sensitivity of the mechanical impedance method of non-destructive testing , NDT Int. , vol. 20 , No.4 , 1987 , pp209-215

2 K. Balasubramaniam, C. Issa and R. Sullivan , Quantitative evaluation of adhesive interface layer properties using ultrasonic techniques , Rev. of Prog in QNDE , (Ed. D.C Thompson and D.E. Chimenti), vol.11 , 1992 , pp1229-1236

3 S.I. Rokhlin, and Y.J. Yang , Analysis of boundary condition for elastic wave interaction with an interface between two solids , J. Acoust. Soc. Am. , 89 , 1991 , pp503-515

4 W. Wang , B. Li and S.I. Rokhlin , ultrasonic reflectivity of interfacial properties in adhesive joints of aluminium alloys , Rev. of Prog in QNDE , (Ed. D.C Thompson and D.E. Chimenti), vol.10B , 1991 , pp1311-1318

5 B.S. Wong , T. Cheng Guan and L. Mong King , Mechanical impedance inspection of composite structures , British Jour. NDT , vol. 35 , 1993 , pp3-9

6 W.L. Pilant , Elastic Waves in the Earth , Elesivier, Amsterdam , 1979

7 A.P. French , Vibrations and Waves , Van Nostrand Reinhold , 1972

8 N.W. Ashcroft and N.D. Mermin , Solid State Physics , Holt ,Rinehart and Winston, 1976

9 E.P. Papadakis , Ultrasonic attenuation caused by scattering in polycrystalline materials in: Physical Acoustics IVB , (Ed. W.P. Mason and R.N. Thuston), Academic Press, New York , 1968 , pp269-326

10 M.J.P. Musgrave , Crystal Acoustics , Holden-Day , 1970

11 A.C. Pipkin , Lectures on Viscoelasticity Theory , Springer-Verlag , 1972

12 J.O. Smith and O.M. Sidebottom , Elementray Mechanics of Deformable Bodies , Macmillan , 1969

13 W. Philipoff , Relaxations in polymer solutions, liquids and gels in: Physical Acoustics IIB , (Ed. W.P. Mason and R.N. Thuston), Academic Press, New York , 1965 , pp1-87

14 I.L. Hopkins and C.R. Kurkjian , Relaxations spectra and relaxation processes in solid polymers and glasses in: Physical Acoustics IIB , (Ed. W.P. Mason and R.N. Thuston), Academic Press, New York , 1965 , pp91-164

15 W. Sachse and Y. Poa , On the determination of phase and group velocities of dispersive waves in solids , J. Appl. Phys. **49**(8) 1978

16 T. Ditchi, C. Alquie and J. Lewiner , Broadband determination of ultrasonic attenuation and phase velocity in insulating materials , J. Acoust. Soc. Am. , **94** , 1993 , pp3061-3064

17 R.E. Challis, R.P. Cocker, A.K. Holmes and T. Alper , Viscoelasticity of thin adherent layers as a function of cure and service temperature measured by a novel technique , J. Applied Polymer Science , **44** , 1992 , pp65-81

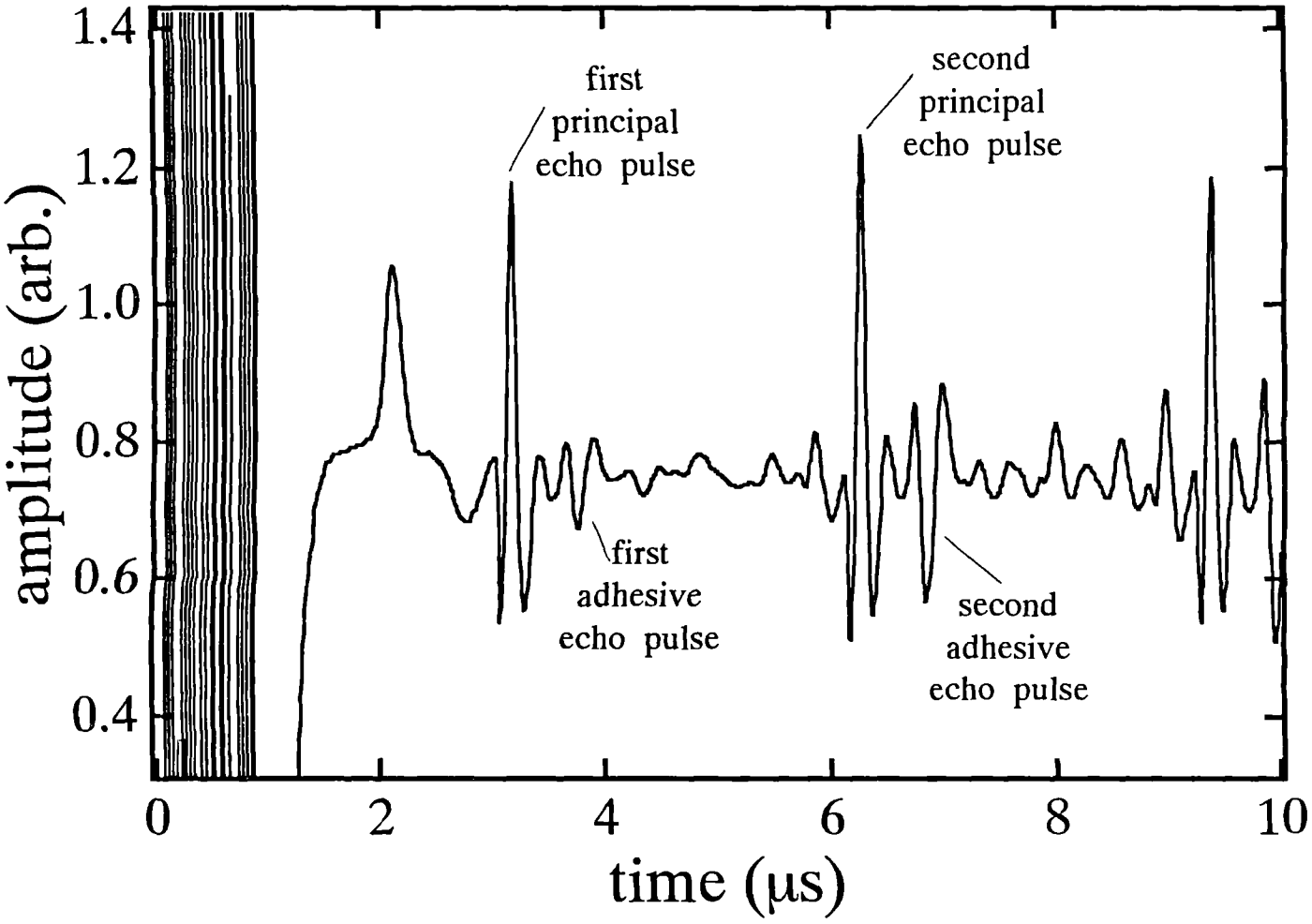

Fig 6.1

Send-receive EMAT waveform taken on an adhesive bonded sample showing where the amplitude and temporal 'thickness' measurements are taken.

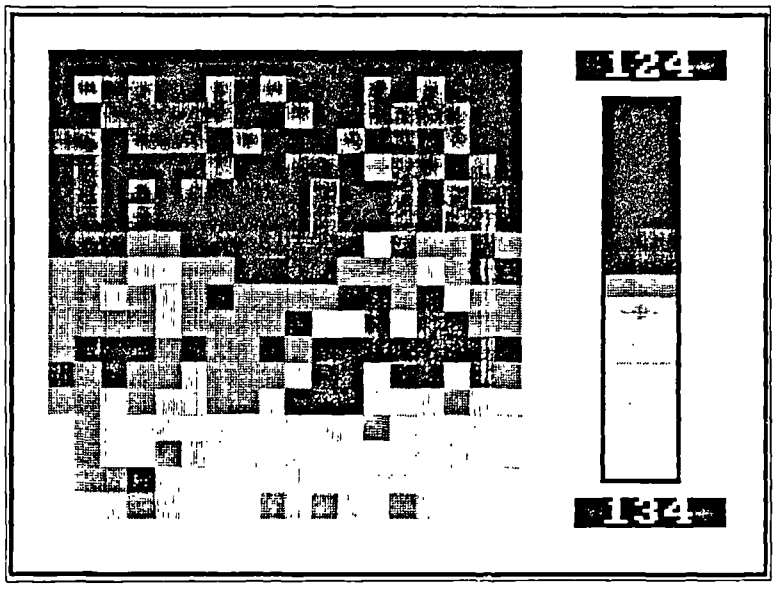

Amp
(arb)

Fig 6.2

2D density plot for the amplitude data obtained in scanning the defect free wedged sample in send-receive from the 4.8mm plate side. The first principal peak amplitude was measured.

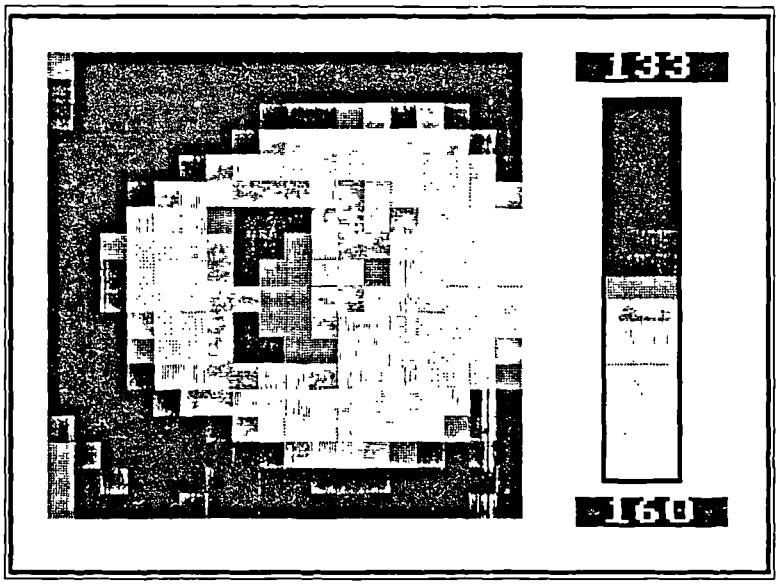

Amp
(arb.)

Fig 6.3

2D density plot for the amplitude data obtained in scanning the defect free wedged sample in send-receive from the 4.8mm plate side. The second principal peak amplitude was measured.

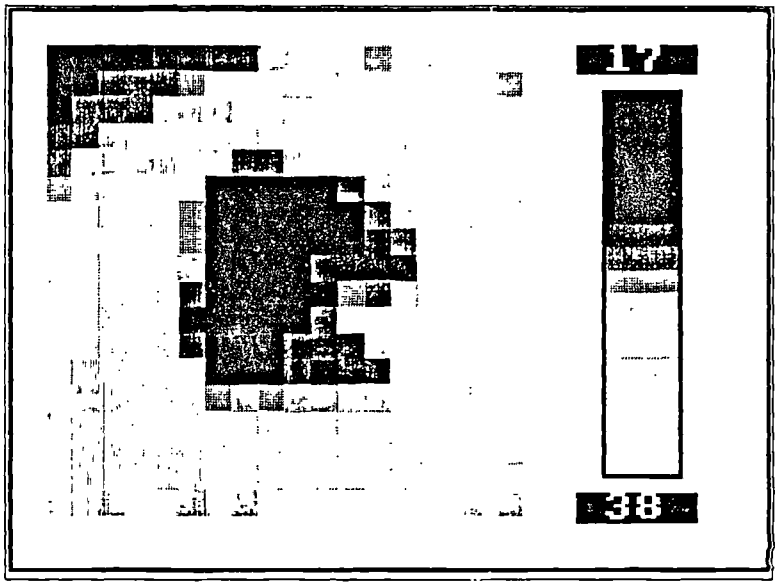

Fig 6.4

2D density plot for the amplitude data obtained in scanning the defect free wedged sample in send-receive from the 4.8mm plate side. The first adhesive echo peak amplitude was measured.

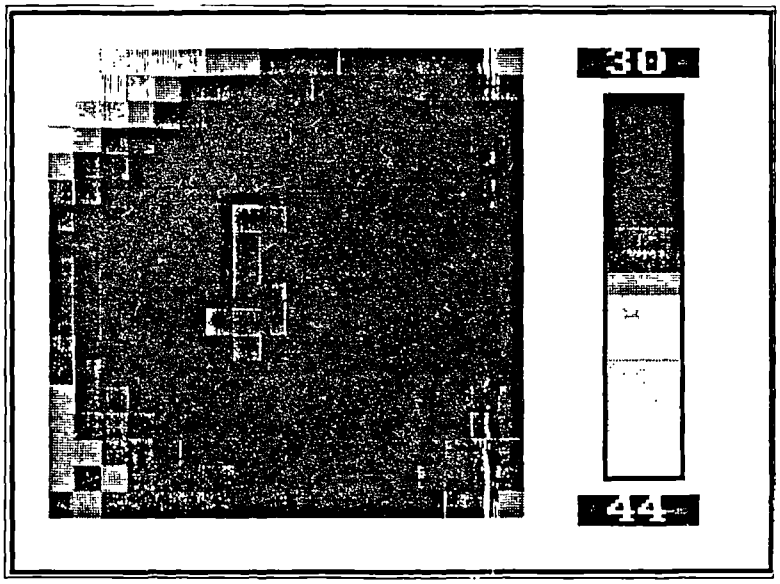

Fig 6.5

2D density plot for the 'thickness' data obtained in scanning the defect free wedged sample in send-receive from the 4.8mm plate side.

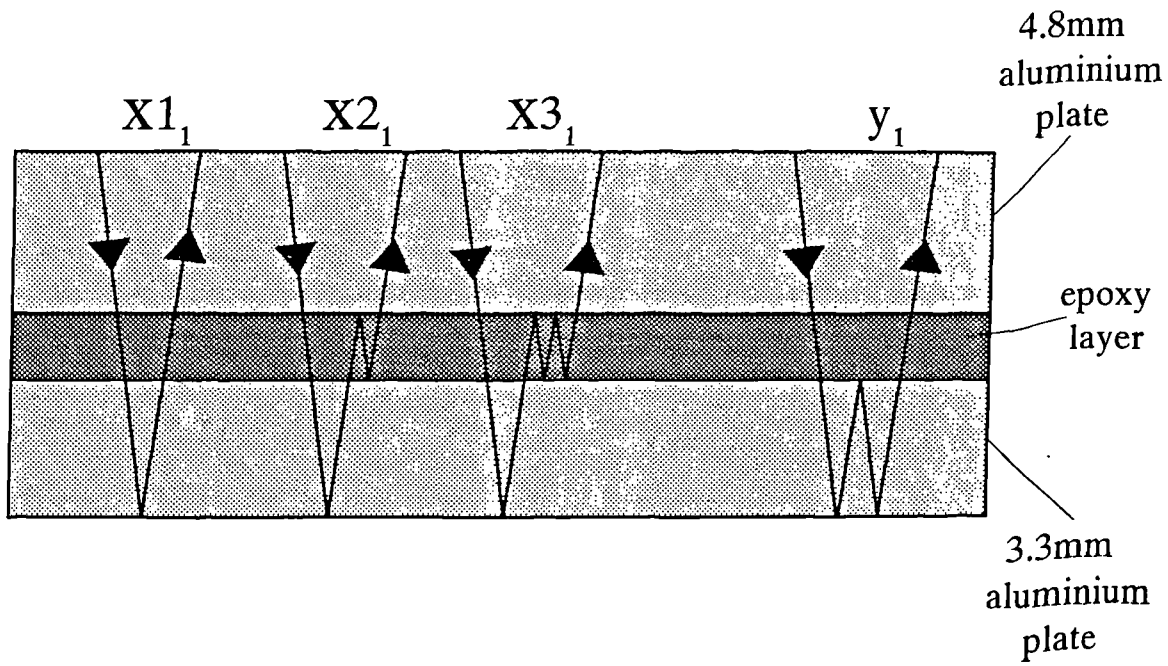

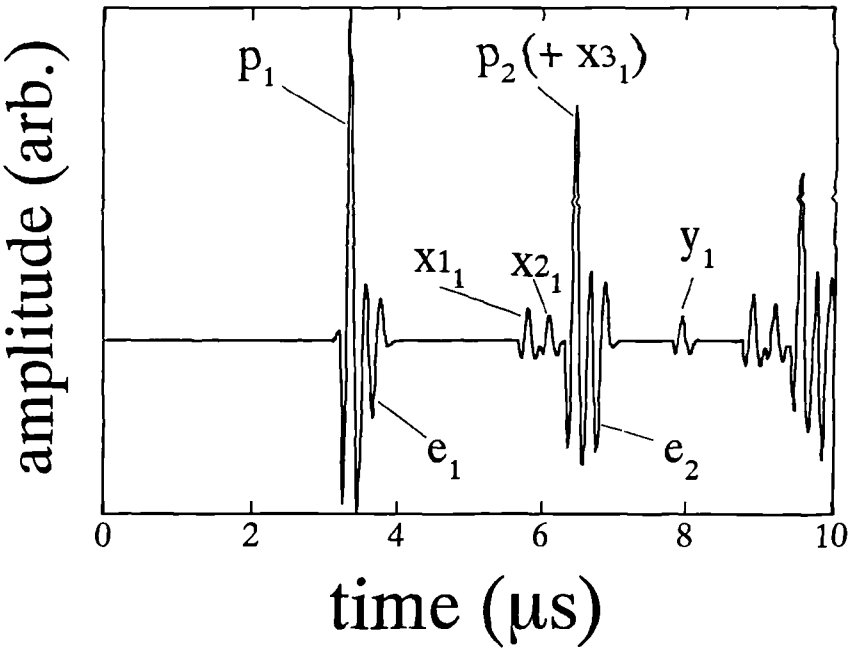

N.B. For the samples investigated, the pulse labelled X3 always lies in the range where it interferes with the peaks p_n and e_n.

The above diagram respresents the acoustic paths taken by the ultrasonic pulses x_n, $x1_n$, $x2_n$, $x3_n$ and y_n. While there is only one solution to the total acoustic path taken by x_n and y_n, there are 2 possible ways to construct the acoustic path of $x2_n$ and 3 possible for $x3_n$. The waveform is computed by convolving the arrival times of the ultrasonic pulses with a pulse obtained in aluminium plate.

Fig 6.6

Illustration of how higher order reverberations within the adhesive structure can significantly interfere with the larger amplitude dominant signals present in the waveform.

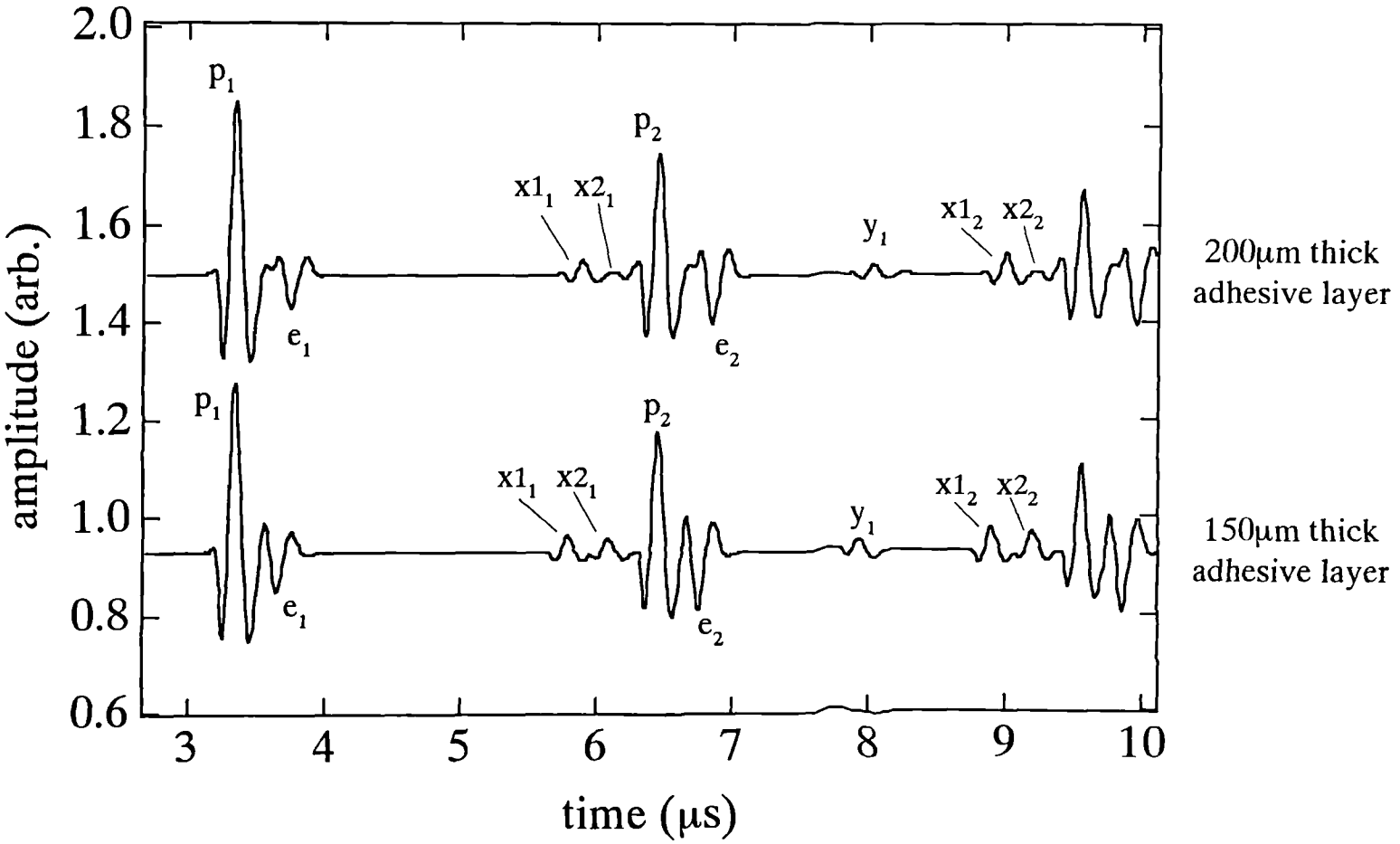

Fig 6.7

The above two send-receive waveforms are simple simulations, showing the higher order reverberations within the structure that corrupt the later bond echoes from the near adherent-adhesive interface.

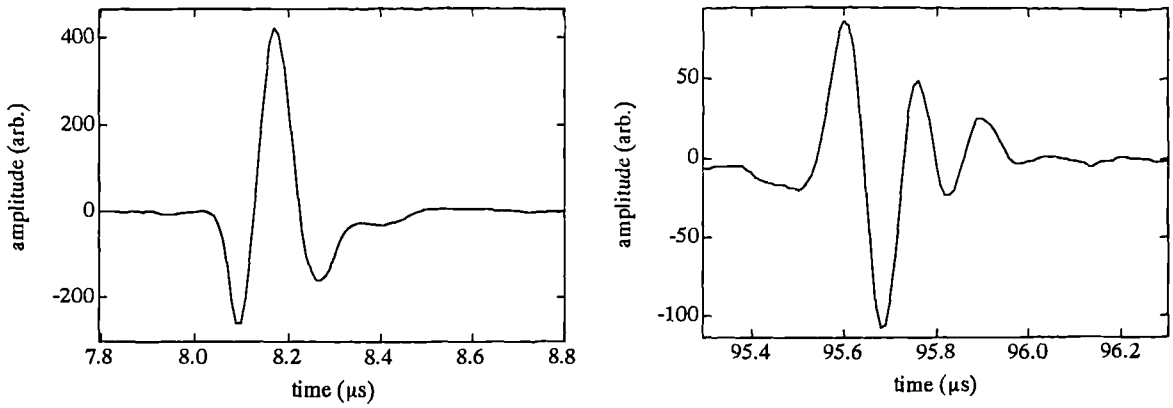

first pulse in aluminium disc

twelfth pulse in aluminium disc

Fig 6.8a

Shear wave pulses taken from a send-receive waveform on a textured 12.50mm thick aluminium disc.

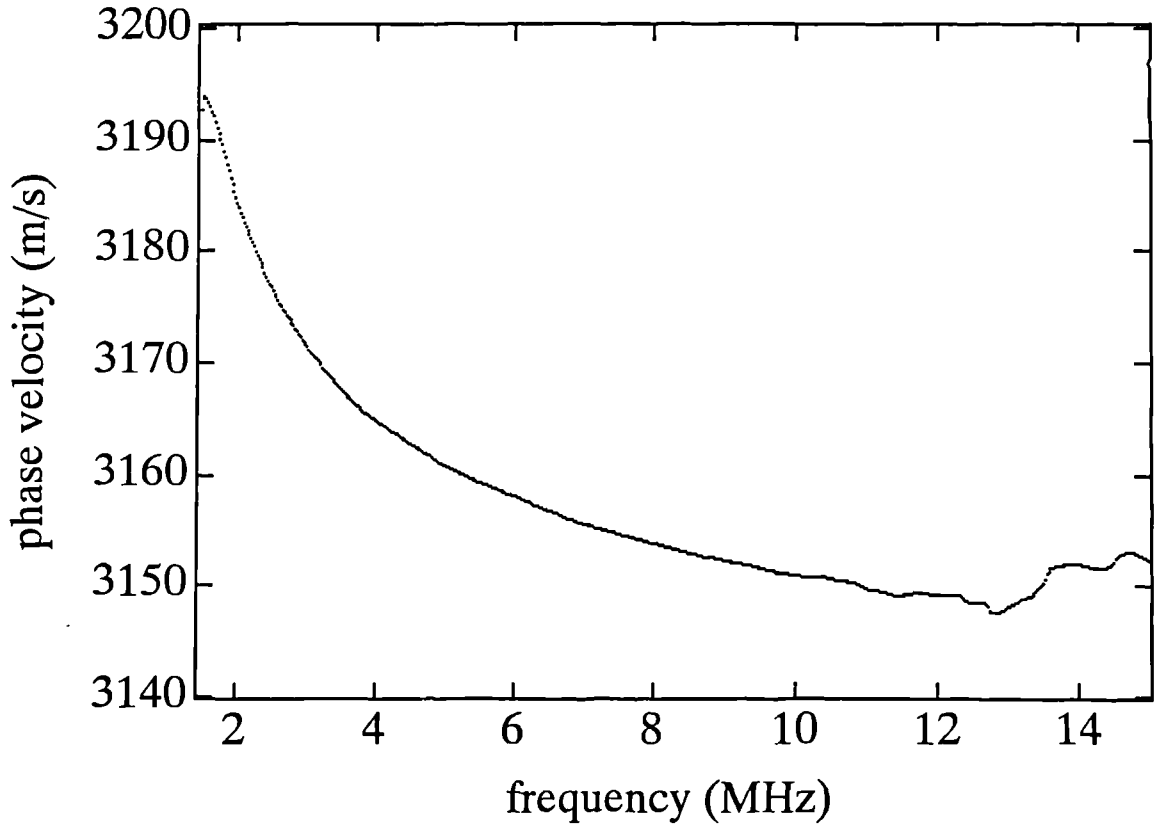

Fig 6.8b

Shear wave phase velocity in 12.50mm thick polycrystalline aluminium disc shaped sample.

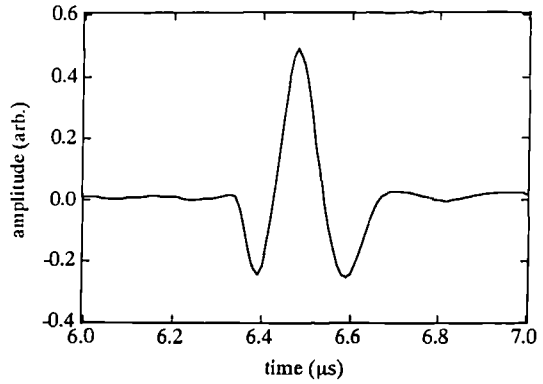

send-receive second pulse
in 5mm aluminium plate

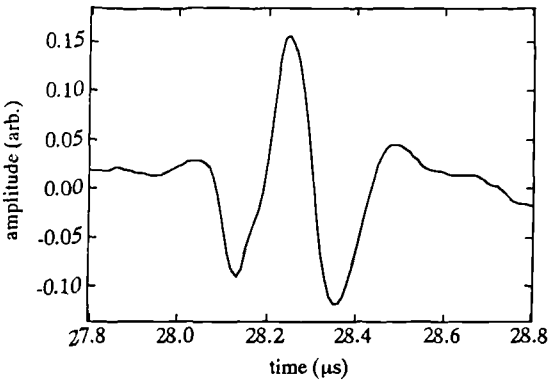

send-receive ninth pulse
in 5mm aluminium plate

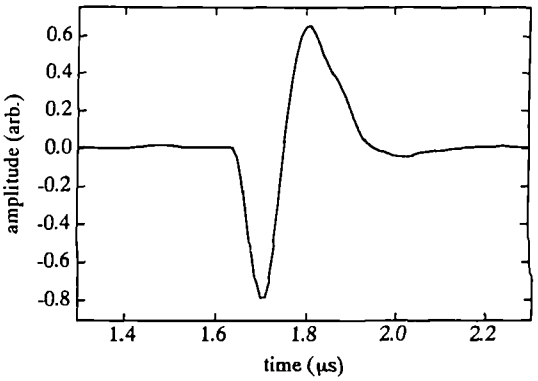

through transmission first pulse
in 5mm aluminium plate

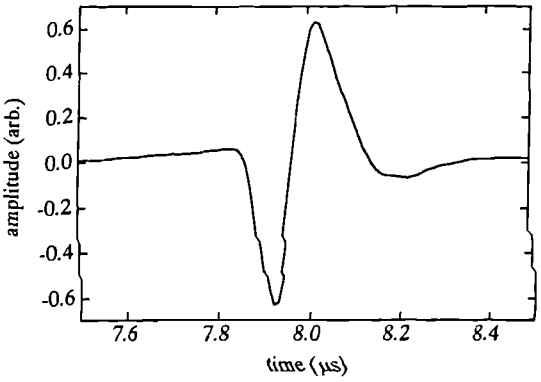

through transmission third pulse
in 5mm aluminium plate

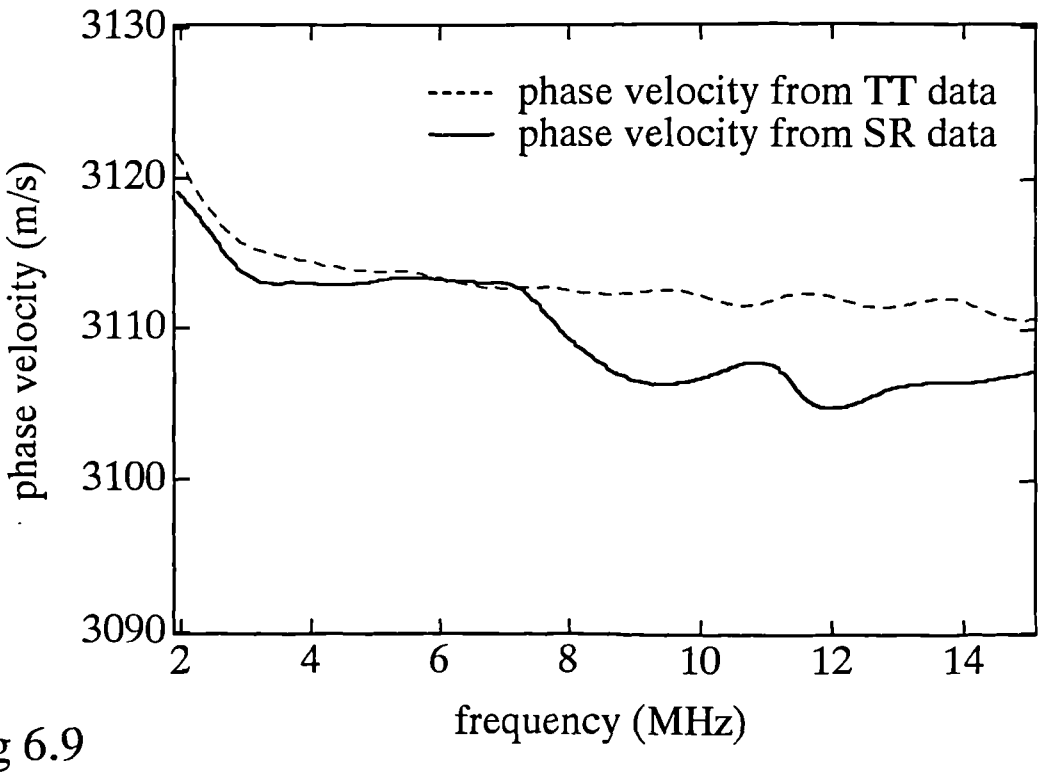

Fig 6.9

Shear wave phase velocity in the aluminium plate adherent used in the adhesively bonded samples (provided by the DRA), using data obtained in both send-receive and through transmission geometries.

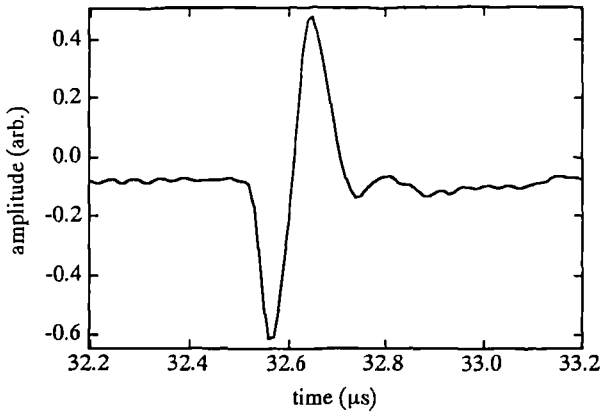

second pulse in
aluminium single crystal

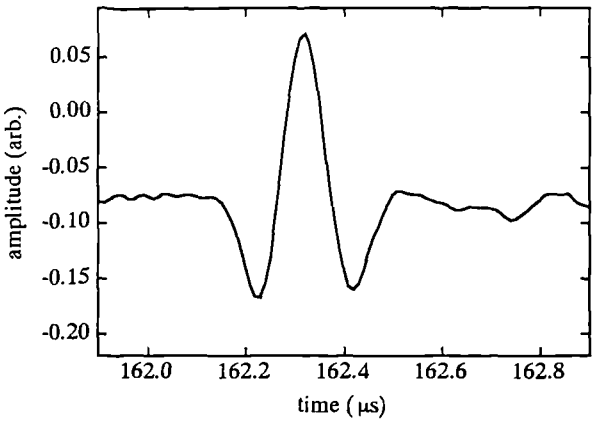

tenth pulse in
aluminium single crystal

The pulse shape has changed, but not as drastically as in fig 6.8 or fig 6.9.

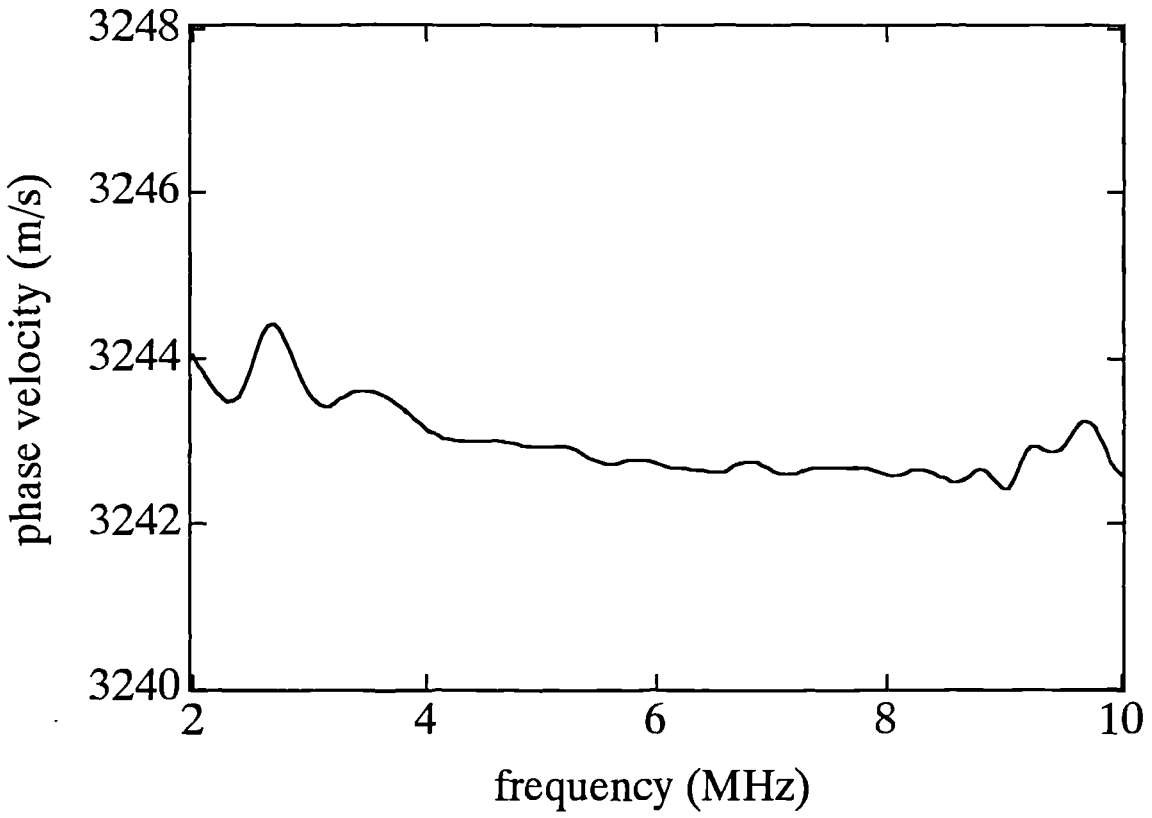

Fig 6.10

Shear wave phase velocity in the (100) direction in a single crystal of aluminium from a waveform obtained using an EMAT.

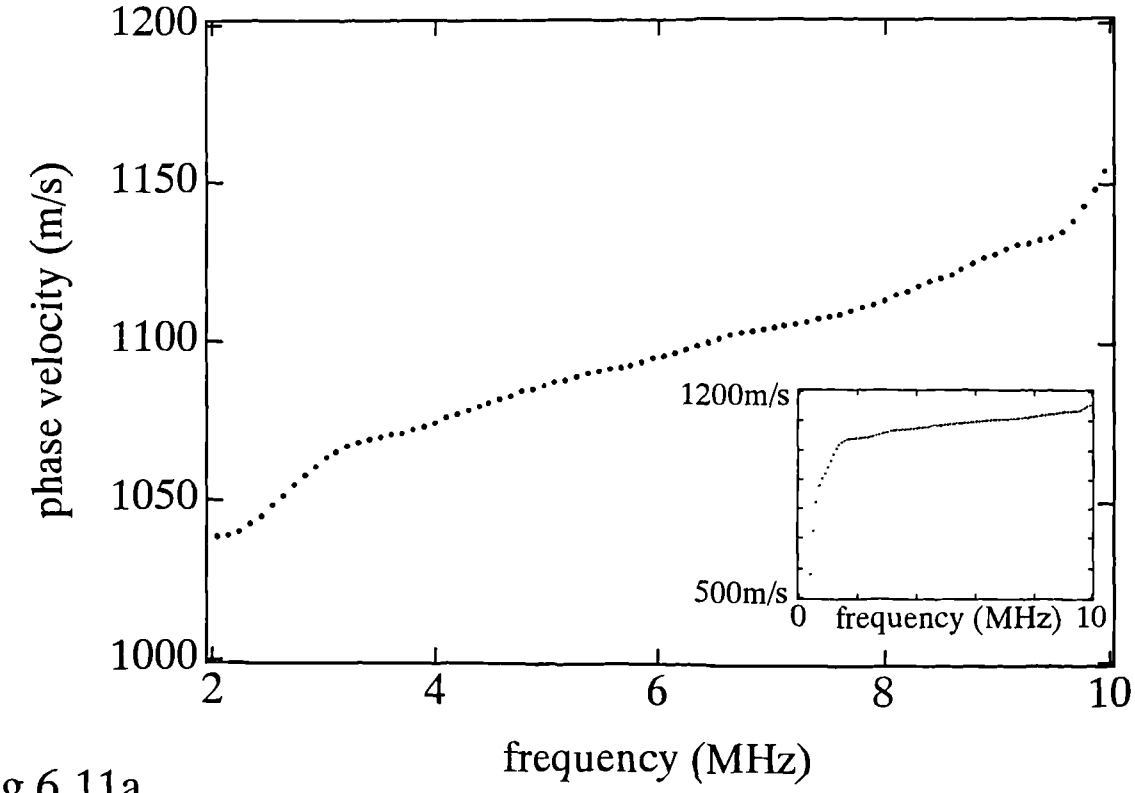

Fig 6.11a

Shear wave phase velocity in the epoxy adhesive layer (calculated from through transmission data).

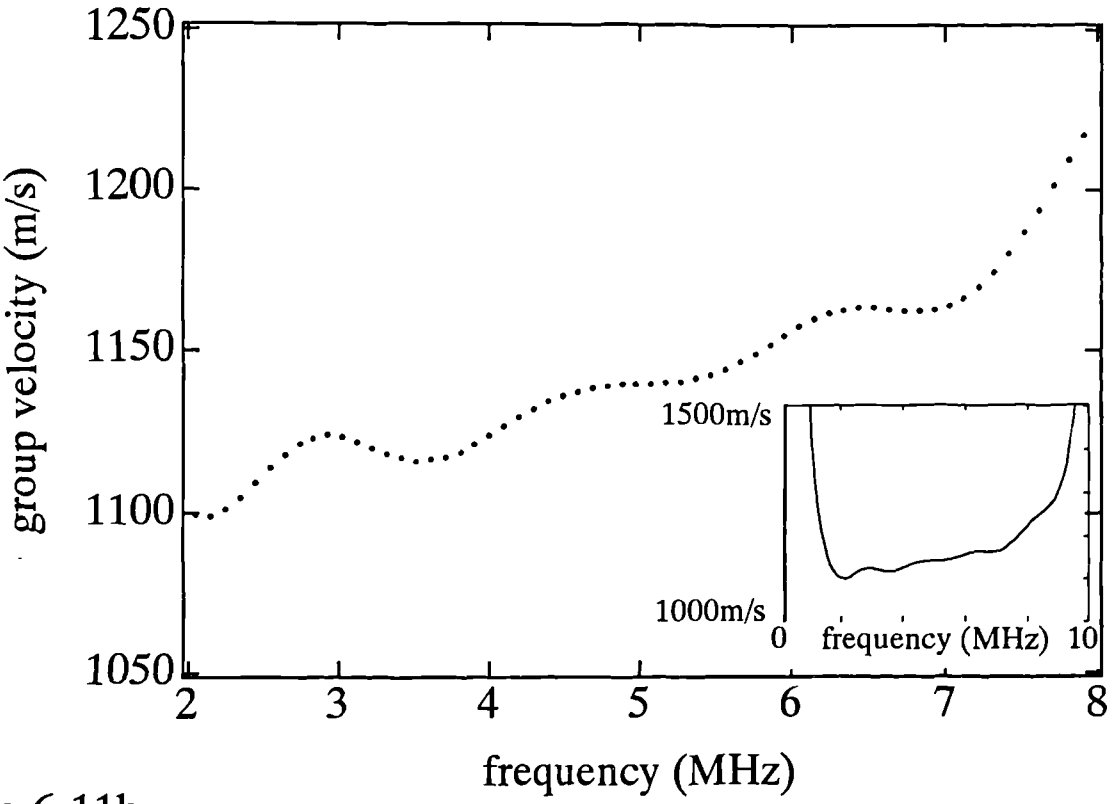

Fig 6.11b

Shear wave group velocity in the epoxy adhesive layer (calculated from through transmission data).

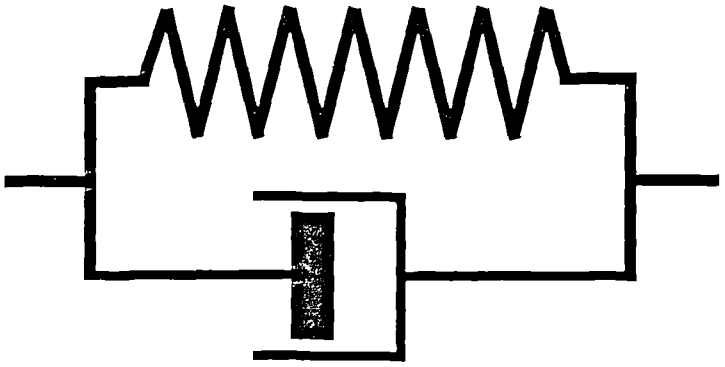

Fig 6.12a

Spring and dashpot representation of the Voigt model for a viscoelastic solid.

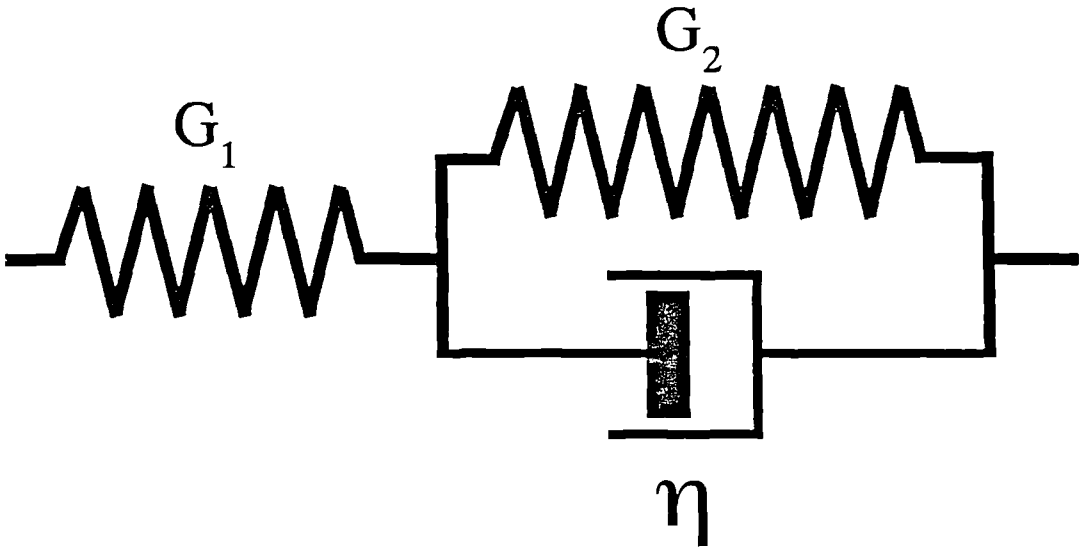

The above model is an improvement on the simple Voigt model. The lower limit (dc) stiffness is the series combination of G_1 and G_2, and the high frequency limit is simply G_1. The dashpot coefficient η is a parameter that corresponds to the relaxation time in the epoxy.

Fig 6.12b

Spring and dashpot representation of the improved Voigt model for a viscoelastic solid.

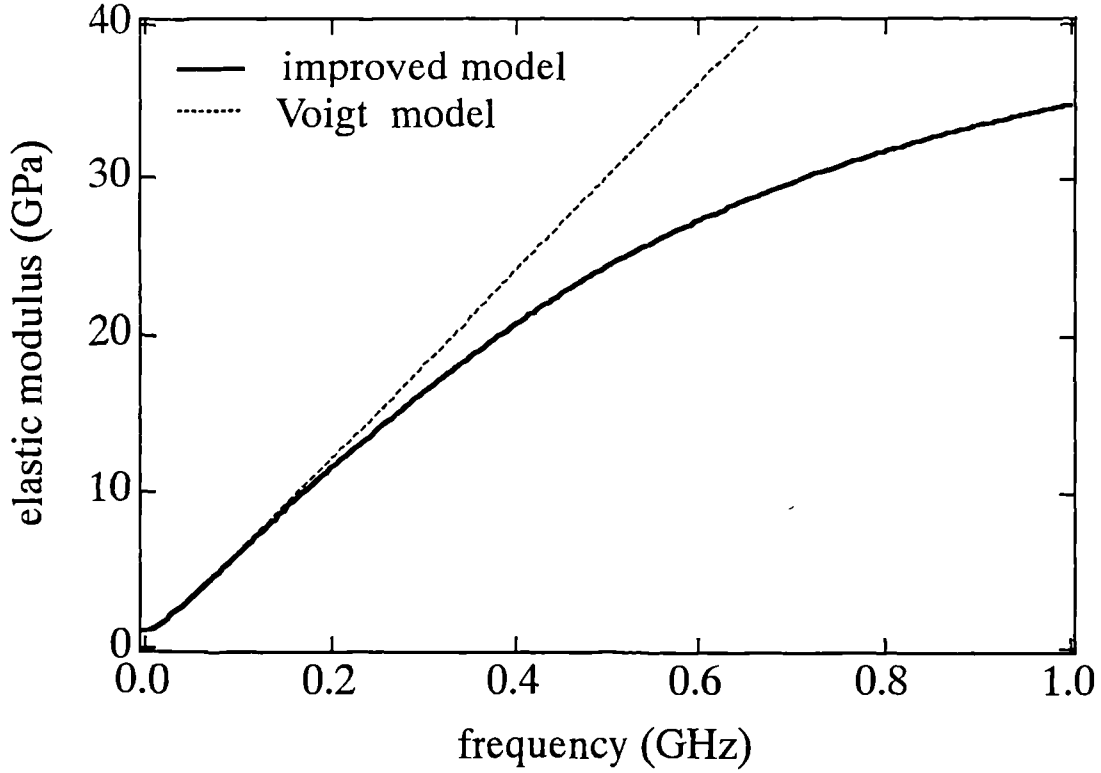

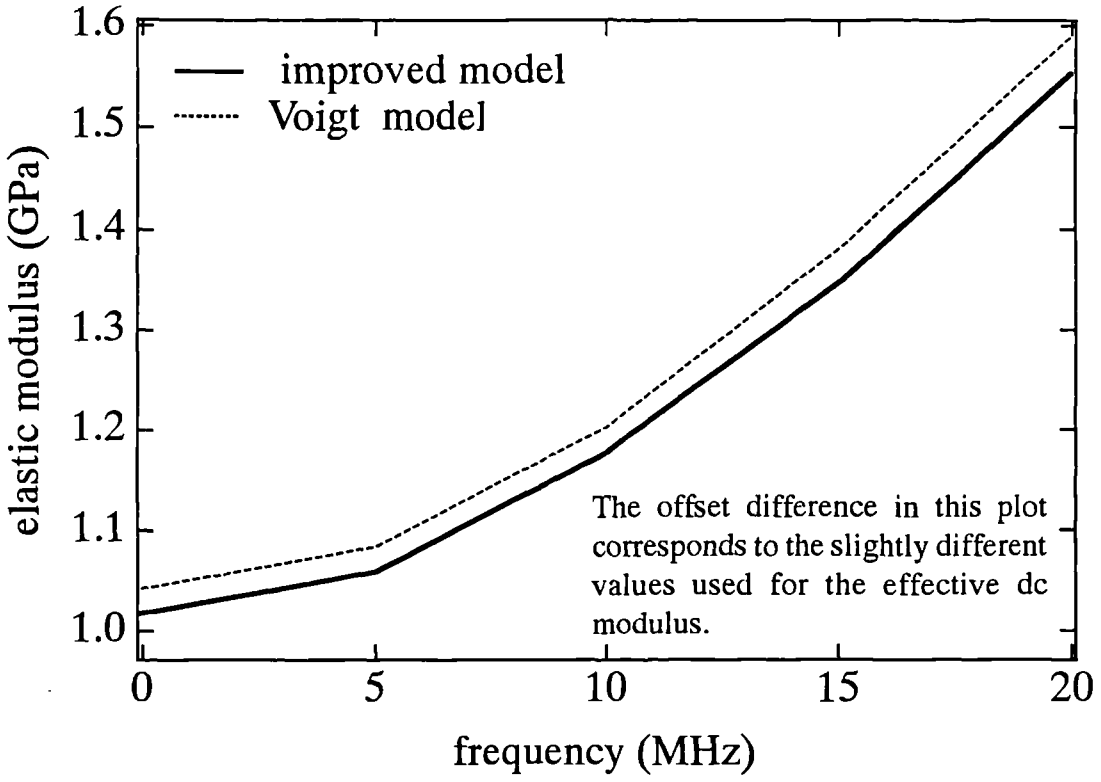

Fig 6.13

Elastic moduli as a function of frequency for the simple Voigt model and the improved viscoelastic model.

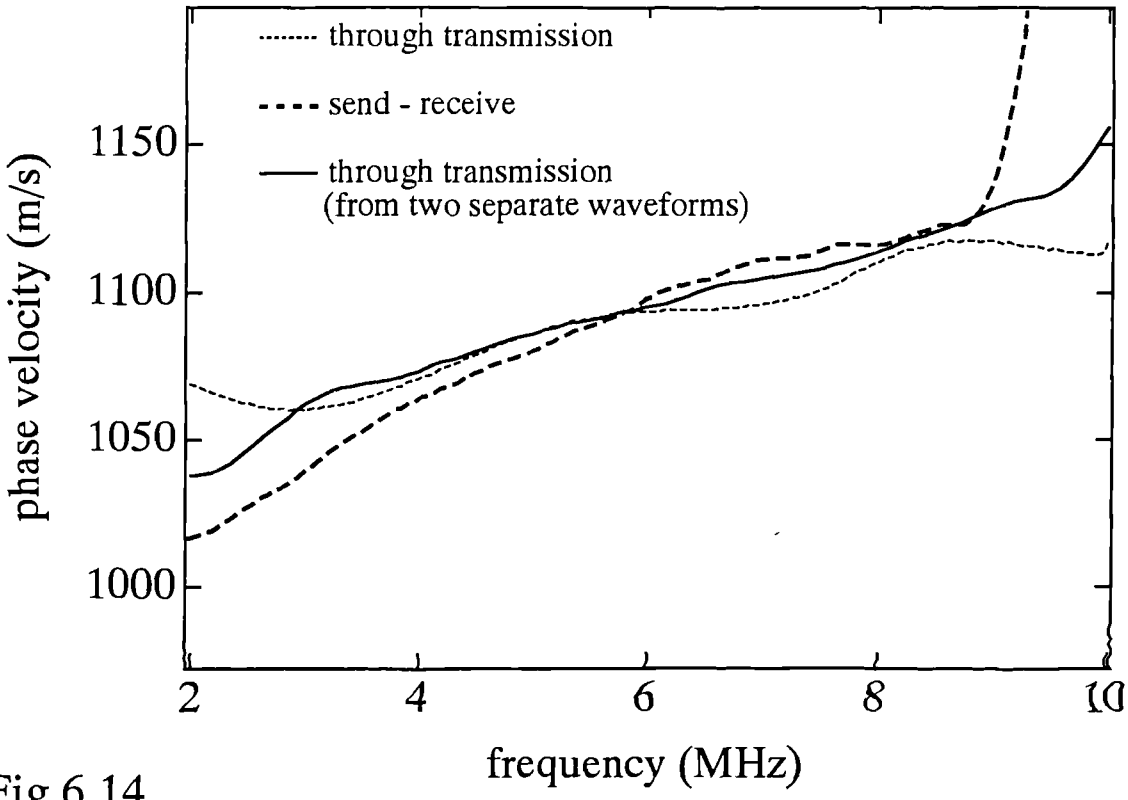

Fig 6.14

Calculated shear wave phase velocity in the epoxy adhesive layer from EMAT send-receive, through transmission and two separate through transmission waveforms.

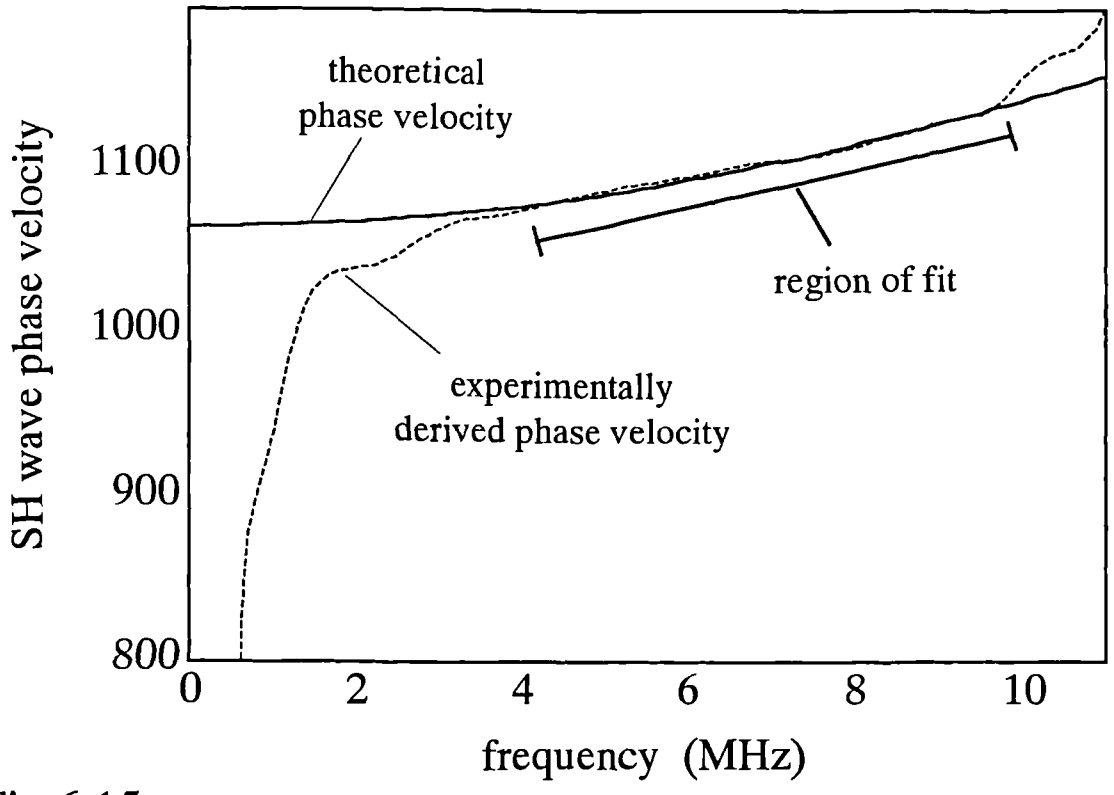

Fig 6.15

Calculated fit to shear wave phase velocity in the epoxy layer from theimproved viscoelastic model.

Chapter 7

Adhesive curing experiments

7.0 Introduction

The study of curing adhesive bonds is a well documented experiment. Classically it is performed by permanently fixing a piezoelectric transducer to the adherent prior to curing. Studying the characteristics of the waveforms in or through the bonded structure yields valuable information concerning the nature of curing in the adhesive. Most of the adhesively bonded samples described in chapters 5 and 6 are from a range of aerospace type bonds prepared using Redux312 adhesive. In this series of experiments, for convenience a two part room temperature epoxy was used to adhesively bond aluminium plates. The aim was to show that the EMAT can not only be a valuable tool in post production, but also has the ability to be practically applied in monitoring the cure of an adhesively bonded sample.

7.1 Justification of the technique

The acoustic theory that is applicable to epoxy resins is that of a viscoelastic medium. This chapter deals with a study of the acoustic properties of a two component free curing epoxy adhesive (Araldite) bond. The use of ultrasonic techniques to monitor cure was first reported by Sofer et al. [1] , and the extension to monitoring phase and group velocity changes during cure was developed by Lindrose [2]. Analysis of the acoustic pulses yielded information concerning the adhesive and cohesive changes during cure. Similar experiment have been done by several workers [5-11], but using different modes of ultrasonic waves and types of transducer. Most of these experiments have employed the use of a contact transducer, which itself usually needs to be 'glued' to an adherent. The presence of this adhesive layer can possibly lead to a loss of information in the experimental data. The

advantage of using SH waves in such an analysis is that the initial state is a viscous fluid, which will not favorably support the propagation of shear waves. The final state (for a properly cured epoxy), should be that of a viscoelastic solid which will support the propagation of shear waves. The SH waves also give a very sensitive indication of what changes are occurring at the interfaces, and in the adhesive bulk. Starting with the theory developed in chapter 2, the ideas can be expanded, to give some indication as to how the mechanical properties of the adhesive change during cure.

7.2 Structural changes within a curing epoxy

Epoxy resins in the uncured state behave like a very viscous liquid, which allows the adhesive to adopt the shape of the cavity between the adherents. On curing, or solidification, they experience little shrinkage which reduces the stresses that could possibly otherwise peel the adhesive (adhesive failure) from the adherent or crack the adhesive itself (cohesive failure). In order to behave as a viscous fluid, the molecules should ideally be monomers, or very short polymers. During polymerisation of the adhesive, the monomers in the adhesive join together to form a polymer chain. A cured resin consisting of many polymer chains would obviously be much stiffer than an uncured resin, but would make a poor adhesive as it would be easy to separate the polymer chains from each other while still being difficult to break an individual chain. In order to obtain a much stiffer cured medium, chemical agents are introduced to the resin that chemically bond one chain to another, becoming part of the cured polymer structure itself. This is termed cross-linkage [3,4]. Different types of cross-linkage agents are used depending on the specific adhesive application and the properties required from the cured adhesive. Quite often, catalysts are also incorporated into the mixture of adhesive and hardener and may be isolated, or part of the cross-linkage hardener.

Thus, when an adhesive is actually curing the two important processes occurring simultaneously are polymer chain growth and polymer chain cross-linkage. If this process was 100% efficient then the resulting cured polymer would be a very strong, but very brittle crystalline medium, whereas ideally both strength and ductility are required. While

crosslinkage is needed to give the adhesive strength, the degree rigidity it gives rise to must be limited. The crystallisation process is inhibited by the growth of the polymer chains themselves, and quite often chemicals are included into the hardener to prevent crystallisation. Thus the adhesive as it cures changes from a viscous liquid to a glassy-like state. Cross linkage is generally a slower chemical reaction than the polymer chain growth itself, thus the polymer chain growth tends to dominate the observed changes in the physical properties of the curing adhesive during the initial stages of cure while the cross-linkage process is indicative of the changes taking place towards the end of the cure cycle.

7.3 Basic experimental setup

As the grade of epoxy used could take up to 48hrs to cure at room temperature, the experiment was automated using a pc (schematic shown in fig 7.1). The bonded sample is shown in fig 7.2. It consisted of two plates 5mm thick machined from the cross section of aluminium extruded rod. Standard aluminium plate was not used so as to avoid any potential complications arising from acoustic birefringence. One of the plates had a recess machined into it to a depth of approx 0.5mm and a diameter of 50mm, as shown in fig 7.2.The two plates could be bolted together, to provide a disc chamber in the cell that contained the epoxy adhesive. This ensured that within the cell there was a flat, uniform thickness adhesive layer. A small hole was drilled into the recessed area to provide a channel for any excess adhesive to escape.

Prior to bonding the plates were degreased using acetone, etched in a dilute sulphuric acid solution (to give some surface roughness and surface treatment), then thoroughly rinsed in water and left to dry. The two components of the epoxy were mixed, then immediately placed in the recess and the whole cell was then bolted together. The cell was then placed within a polystyrene insulation chamber, as rapid changes in the ambient room temperature of a few degrees centigrade were found to greatly effect results introducing sharp discontinuities into the recorded data for shear wave pulse amplitude transmitted

through the adhesive layer and reflected from the adherent-adhesive interface. Temperature effects were studied by Rokhlin at al [6] and found to significantly effect the physical properties of the curing epoxy.

The data was captured on a LeCroy digital oscilloscope controlled by a pc via IEEE GPIB-PC interface. An EMAT SR unit was used to measure the amplitude of the reflected SH wave from the first adherent-adhesive interface. The second peak arrival of the echo train was used as the first peak lay just within the electronic dead time of the equipment for these particular experiments. An EMAT on epicentre on the other side of the cell was used to detect SH wave arrivals in TT. He et al [5] also monitored the arrival of a shear wave using an EMAT obtaining transmitted amplitude data similar to that presented here, but the system used was narrow band and consequently only information for one particular frequency was available. Using the broadband EMATs in this project in the TT geometry, the measured peak was the very first ultrasonic arrival. The peak-peak amplitude of both reflected and transmitted waves were recorded at regular time intervals. Specific SH pulse arrivals were captured and stored at much longer non-equally spaced time intervals. More waveforms were captured during the time when the transmitted wave was observable, and undergoing the most rapid change. A much quicker curing two component epoxy was also examined, but only amplitudes and arrival times were recorded in this instance.

7.4 Shear wave pulse amplitude measurements

The ultrasonic pulses that are generated by the EMAT are broadband, and this should be bourne in mind when any measurements of these pulses are being made. As an epoxy cures, it becomes mechanically stiffer, with relatively little change in volume or total mass. As a result, any acoustic wave that propagates through the bulk will suffer less attenuation and experience an increase in velocity as the adhesive cures. The first types of measurements taken were peak-peak pulse amplitude in both TT and SR. As the temperature of the aluminium plates was constant over the cure cycle, the attenuation coefficient of the aluminium was constant, and thus any changes in the signals can be attributed to the changes

occurring within the adhesive or at the aluminium-epoxy interface. The chemical reaction taking place as the epoxy cured was exothermic, but the thermal mass of the aluminium was large enough to neglect any changes in temperature due to heating from the epoxy.

In SR, the amplitude of the back reflected acoustic pulse depends on the adherent surface coverage, the adhesion of the epoxy to the surface, and on the acoustic impedance of the epoxy. Due to the nature of the cell construction, total surface coverage was achieved and this was verified by destructive examination of the cell after full curing. The remaining factors were the adhesion and cohesion (or stiffness) which are inseparable factors in a the SR geometry. The peak-peak amplitude measurement is a qualitative measurement with respect to any attenuation measurement as the shear wave pulse was broadband. Measuring the reflected amplitude as the adhesive cures yielded the results shown in the graph of fig 7.3a. This is in agreement with results obtained by other workers [6,7]. The changes being monitored here were relatively small, once again high-lighting the fact that SR is not the most sensitive technique for monitoring changes in the physical properties of the adhesive.

The TT results for the transmitted amplitude show the expected increase in amplitude as the adhesive hardens [5,8,9,10,11], and the gradual levelling off as the epoxy approaches its fully cured state (see fig 7.3b). It should be noted that the TT amplitude contains information on the reflection coefficient at both interfaces. Once again, the pulse was broadband, and the attenuation of the epoxy was strongly frequency dependant. As the TT signal traversed the epoxy bulk, the broadband nature is a particularly important consideration.

Bearing in mind the broadband argument stated above, a time dependant epoxy ultrasonic attenuation coefficient (fig 7.3c) was calculated from the SR and TT data. Once again this is a fairly qualitative measurement as it ignores any frequency dependance. The amplitude measurement technique can also be applied to much quicker setting epoxies. The SR reflected pulse (second pulse) amplitude is shown in fig 7.3d, and the TT first pulse arrival amplitude is shown in fig 7.3e. Both of the epoxy TT data show the interesting result that the initial transmitted amplitude shows a gradual increment for the initial 2.5hrs and 0.1hrs for the normal and quickset respectively, then undergo a very rapid change in physical properties. The TT amplitude appears to slightly decrease for the normal cure time

epoxy in the first 2hrs, but this amplitude is the recorded background noise which appears to slightly fall in this time period before the TT shear wave pulse becomes larger than and dominates over the background noise.

At the interface of two elastic halfspaces in perfect intimate contact, the reflection and transmission coefficients are functions of the acoustic impedances of each media only, taking no account of the coupling mechanism or adhesion at the interface. One method of calculating the reflection coefficient, or monitoring a change therein, is to measure the pulse amplitude of a reflected shear wave and compare it to the next echo (taking account of attenuation), or compare it to the pulse amplitude when there is no second medium present. This method, as described above in a real system will not only depend on the acoustic impedance of each medium, but will also be affected by the coupling (adhesion) at the aluminium-epoxy interface.

The measurement described above can be compared to a theoretical reflection coefficient ('r') from the following expression,

$$r = (Z_1 - Z_2) / (Z_1 + Z_2)$$

, where $Z^2 = (\rho c)$, and 'Z' is the acoustic impedance, 'ρ' the density of the medium, and 'c' the ultrasonic wave velocity in that medium.

As the arrival time of the pulse had been measured in TT (fig 7.4) , the ultrasonic velocity in the adhesive has effectively been measured. Care should be taken though as this is not strictly true - once again the pulse is broadband and the arrival time is assumed to be that of a 2.5MHz ultrasonic wave, which was the most dominant frequency present in the TT shear wave pulses. The reflection coefficient obtained from this procedure is shown in fig 7.5 with the reflection coefficient calculated from the amplitude measurement. A value of 1100 Kgm-3 was taken for the density of the epoxy which gave the best fit to the data. The experimentally measured value of density was 1100Kgm-3 +/- 100Kgm-3 , so that the apparently good degree of correlation may be chance but this would only normalise the data. The time dependant form of the two calculated reflection coefficients correlate very closely,

which implies that this ultrasonic technique is not sensitive enough to monitor the change in adhesion during cure for this particular epoxy adhesive.

7.5 Waveform and fourier analysis

In order to obtain more quantitative frequency dependant results, it was necessary to capture specific ultrasonic pulses. The waveforms were captured in both SR and TT, the capture rate concentrating on the lower time scales, where the biggest rate of change occurred.

A selection of the SR signals with time are shown in fig 7.6a. The signals appear to be almost identical, and analysis in the frequency domain shows that the relative frequency content of each pulse is the same: it is only the absolute amplitude that changes, decreasing as the epoxy becomes mechanically stiffer during cure. The magnitude FFTs for the waveforms are shown in fig 7.6b.

The changes in the observed TT signals were totally different to the SR case. The waveforms recorded at various times after mixing are shown in fig 7.7a. It can be seen that there is a significant change in the shape and peak arrival time of the shear wave pulse during the cure cycle. This result was due to frequency dependant changes in attenuation and in the dispersion relation of the epoxy. The magnitude FFTs are shown in fig 7.7b and demonstrating that the higher frequencies are more strongly attenuated, and how all frequencies are less strongly attenuated for a higher degree of cure.

The attenuation as a function of time for certain frequencies are shown in fig 7.8 . In order to perform this calculation a reference pulse through one of the aluminium adherents was required, and the change in 'reflection' coefficient must also be taken into account for the calculations.

7.6 Shear wave phase velocity changes in the curing adhesive

Since the adhesive is viscoelastic, there should be a significant variation in shear wave velocity with frequency - a dispersion relationship. This in turn should also have vary as the glue cures [10] and changes from a more liquid-like state to a more solid-like state. In order to calculate the phase velocity the TT data was analysed, requiring a reference pulse that represented the ultrasonic pulse before it entered the adhesive. This could not be obtained within the experiment as the through transmission EMAT only ever receives ultrasonic pulses that had traversed the epoxy and had therefore been affected by it. The SR pulse could not be used either, as the preamplifiers used in SR and TT have different phase and gain relationships, yielding very different pulse shapes. The reference pulse was generated by recording the ultrasonic SH wave through transmission pulse from one adherent alone. There then remained the problem of obtaining the correct time delay between this pulse and the waveforms that had traversed the whole cell. The time taken for a shear wave to traverse the plates can be measured accurately, so that the theoretical arrival time of the pulse that would have travelled the total path length of aluminium within the cell can be calculated. At this point,we also need to consider the feature of the pulse that gives the time corresponding to the arrival time. The features measured were the peak-trough pulse height (the 'amplitude' measurement) and the position of the pulse maximum (the 'arrival time' measurement). Arrival time measurements are further complicated by the fact that due to the electronics in the EMAT system, the trigger pulse is not necessarily the time at which the ultrasonic wave is generated. Simple measurements showed that the peak of the first SH wave arrival was 270ns delayed to the point that would correspond to the true arrival time. Utilising this information to position the reference pulse, and then taking 2.90 μs (the timebase trigger delay) from the front of the reference TT waveform (the oscilloscope trigger delay), gave the correct arrival time (within the window), of the pulse incident on the adhesive layer. Taking the error in this positioning of the reference pulse to be +/- one digitisation point (10ns digitisation rate), would give an error of approximately 2% in the absolute value of phase velocity. Phase velocity calculations on consecutive waveforms yield differences in

phase velocity of approximately 5% (see fig 7.9), which is obviously significant compared to the absolute error in the calculations. This error would however propagate through all the phase velocity calculations and thus the relative differences in these calculations would remain fairly constant. As is expected, the velocity increases with frequency due to the fact that the 'quicker' particle displacement associated with a higher frequency (for a shear wave) causes the viscoelastic media to respond in such a way that it appears mechanically 'stiffer'.

7. 7 Theoretical fits to phase velocity data

Using the theoretical model shown in fig 6.12b , discussed in section 6.2.2 , the computed phase velocities were fitted to theoretical phase velocity dispersion curves. To recap, the model comprises two springs and a dashpot, and has been treated as the only relaxation mechanism at any particular time - i.e. a single relaxation frequency at any one time during the cure cycle. The theoretical fits were evaluated at specific points on the dispersion curve and are shown overlayed (as dots) on the dispersion curves computed from the experimental data of fig 7.9.

From the fitting parameters, values for the two spring coefficients and their corresponding relaxation frequencies were calculated. The lower spring coefficient 'G_1' and the relaxation frequency are shown in fig 7.10a. The high frequency limit of stiffness had an uncertainty of over 1000% for some values, and these are displayed in the table of fig 7.10b The spring of lower stiffness in the model (approximately the dc stiffness), and the relaxation parameter or dashpot coefficient have a relatively small degree of uncertainty. The relaxation frequency increased from ~90MHz at a time of 5.03hrs, up to a relaxation frequency of ~200MHz at 20.03hrs. The dc shear modulus increased from ~0.4GPa to a maximum value of ~0.8GPa for full curing. Challis et al [10] measured the moduli and relaxation frequencies for an extensive range of adhesives and obtained similar time dependant variation and values and to those described here.

7.8 Shear wave group velocity changes in the curing adhesive

The group velocity of a wave is the velocity of the energy flux associated with that wave. Consequently, the group and phase velocity are not necessarily the same. Once again the time shift within the window and a reference pulse were required for this calculation. The shape of the differential of the FFT phase is independent of the position of the waveform within the window. The time delay correction serves so as to give the differentiated phase a dc offset, which gives the differentiated phase the correct absolute value. The differentiation is carried out by a computer algorithm, which uses a three point differential routine. The differential is susceptible to slight gradient variations in the phase, as the phase consists of discrete points. Thus, the phase velocity calculations appear to contain oscillations which are a result of the computation. The general trend of the data is however, reliable (see fig 7.11). Here once again, the absolute value of group velocity may be affected by an error in the time delay correction, but relative changes of the different waveform group velocities will remain the same. The group velocity increases with frequency for the same reason that the phase velocity increases. As the epoxy cures, the shear wave velocity at a particular frequency also increases.

7.9 Summary

The EMATs were used to study both how adhesive and cohesive properties changed as the bond cured in a broadband non-contact ultrasonic technique. In the range of frequencies studied, it was found that the adhesive properties were frequency independent from the waveforms obtained from the near adhesive-adherent interface in send-receive. This was shown as the relative amplitude of the frequency content of a send-receive pulse remained constant as a function of frequency. It must however be remembered that the back reflected pulse also contains information of the epoxy bulk as the acoustic impedance of the epoxy also affects the amount of acoustic energy reflected at the boundary. The change in the epoxy cohesive properties varied greatly as a function of frequency, resulting in the velocity and attenuation of the shear wave pulse dramatically changing over the cure cycle.

Ch.7 References

1 G.A. Sofer and E.A. Houser, A new tool for determination of the stage of polymerisation of thermosetting polymers , J. Polymer Science , vol. 6 , 1952 , pp611-621

2 A.M. Lindrose , Ultrasonic wave moduli changes in a curing epoxy resin , Exp. Mech, vol.18 , 1978 , pp227-239

3 G. Salomon , Adhesion in:Adhesion and Adhesives Vol 1, (Ed R. Houwink and G. Salomon) , Elsevier , 1995 pp1-140

4 C.A.A. Rayner , Synthetic Organic Adhesives in:Adhesion and Adhesives Vol 1, (Ed R. Houwink and G. Salomon) , Elsevier , 1995 pp186-352

5 F. He , S.I. Rokhlin and L. Adler , Application of SH and Lamb wave EMATs for evaluating adhesive joints , Rev. of Prog. in QNDE , (Ed. D.C Thompson and D.E. Chimenti) ,Williamsburg, 1987 , pp911-918

6 S.I. Rokhlin , Characterisation of composite and adhesive cure by ultrasonic waves , Nondestructive Characterisation of Materials II , (Ed. J.F. Bussiere, J-P, Monchalin, C.O. Rund, R.E. Green Jr.) , pp105-113

7 T. Pilachu and P. Cawley , The detection of a weak adhesive/adherend interface in bonded joints by ultrasonic reflection measurements , Rev. of Prog. in QNDE , (Ed. D.C Thompson and D.E. Chimenti), vol.11 , 1992 , pp1261-1266

8 R.A. Kline, C.P. Hsiao, M.A. Fidaali, Nondestructive evaluation of adhesively bonded joints, J. Eng. Mat. and Tech. , vol 108 , 1986 , pp214-217

9 D.L. Hunston, Cure monitoring of thermosetting polymers by an ultrasonic technique , Rev. Prog. QNDE , 1983 , pp1711-1729

10 R.E. Challis, R.P. Cocker, A.K. Holmes and T. Alper , Viscoelasticity of thin adherent layers as a function of cure and service temperature measured by a novel technique , J. Applied Polymer Science , **44** , 1992 , pp65-81

11 S.I. Rokhlin , Evaluation of curing of structural adhesives by ultrasonic interface waves. Correlation with strength. , J. Composite Materials , vol 17 , 1983 , pp15-25

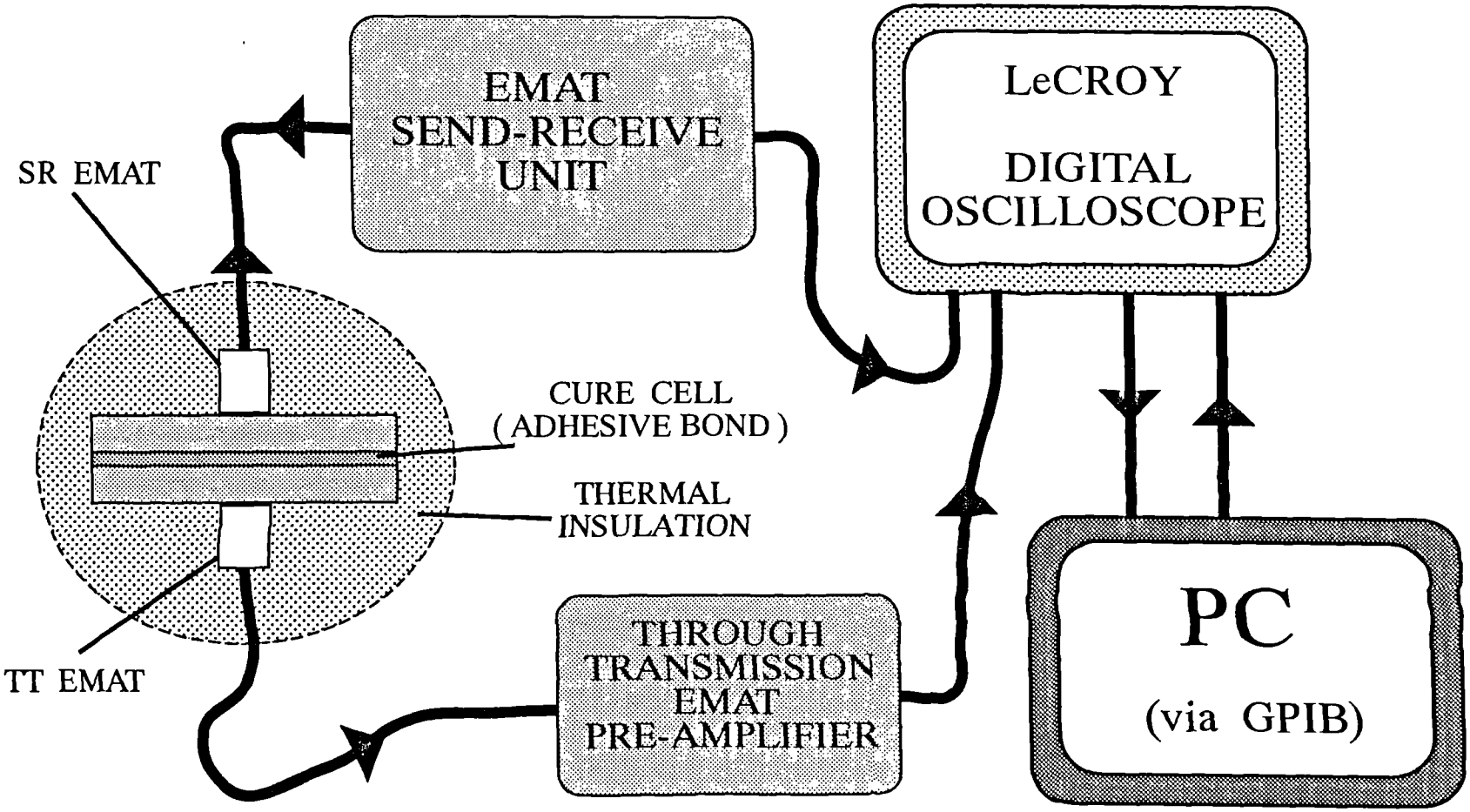

Fig 7.1

Schematic diagram of curing experiment setup.

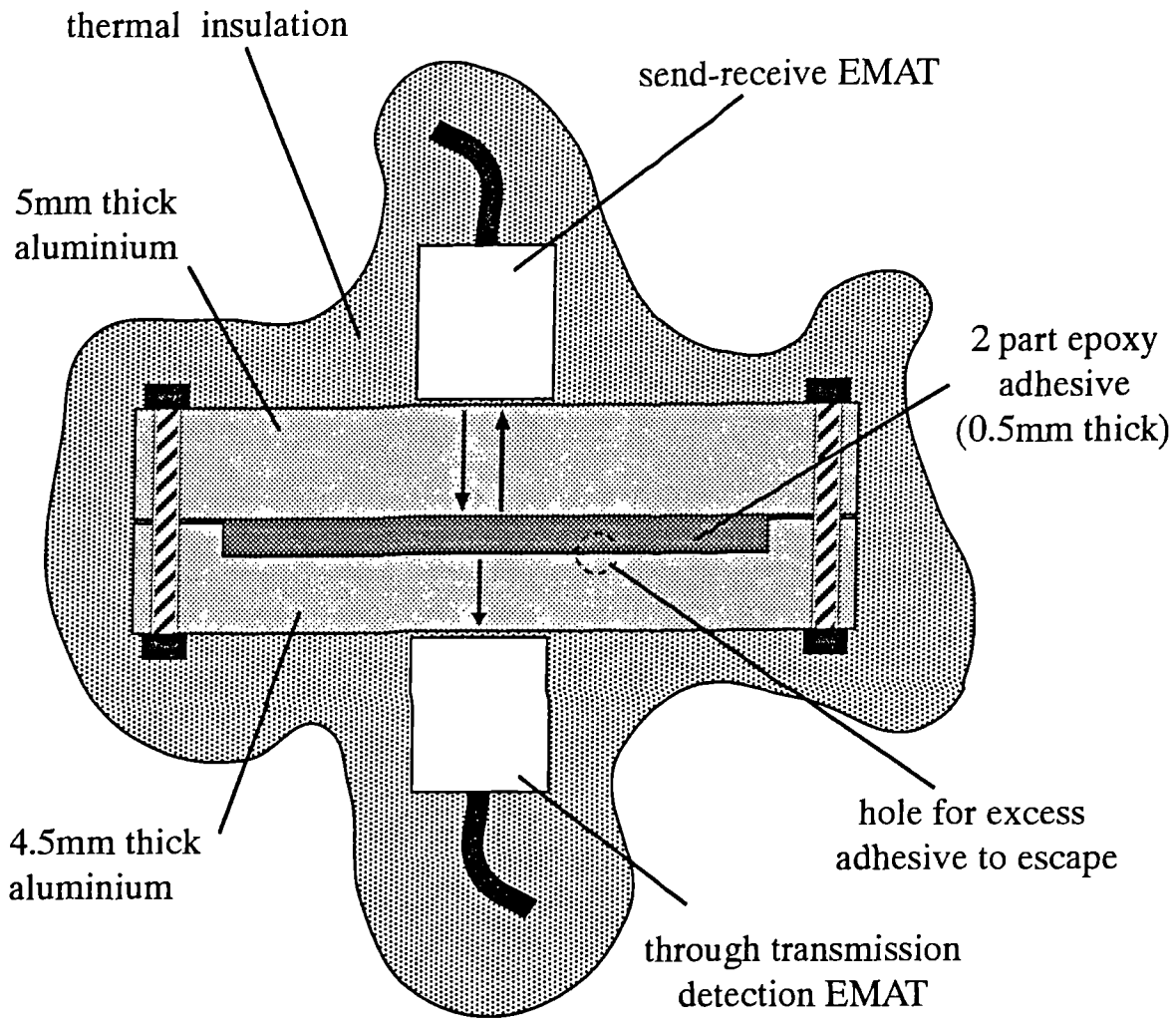

Fig 7.2

Schematic diagram of the experiemntal setup in monitoring the cure of a two component epoxy adhesive.

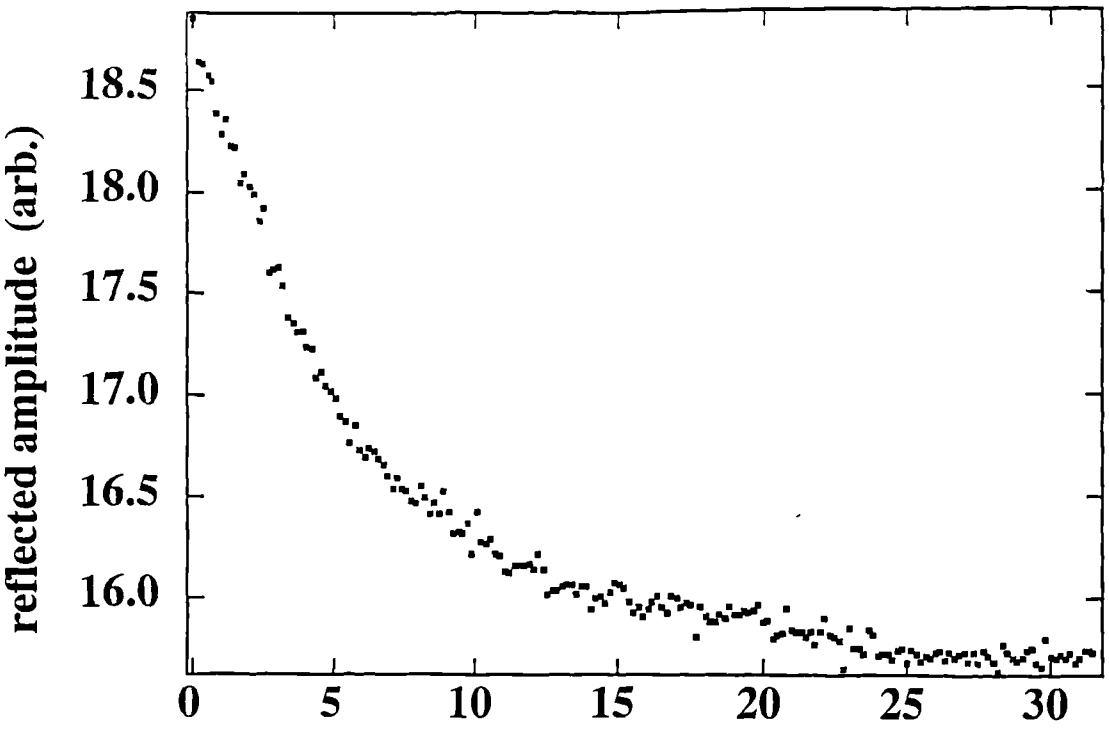

Fig 7.3a

The peak- peak amplitude of the observed reflected shear wave pulse.

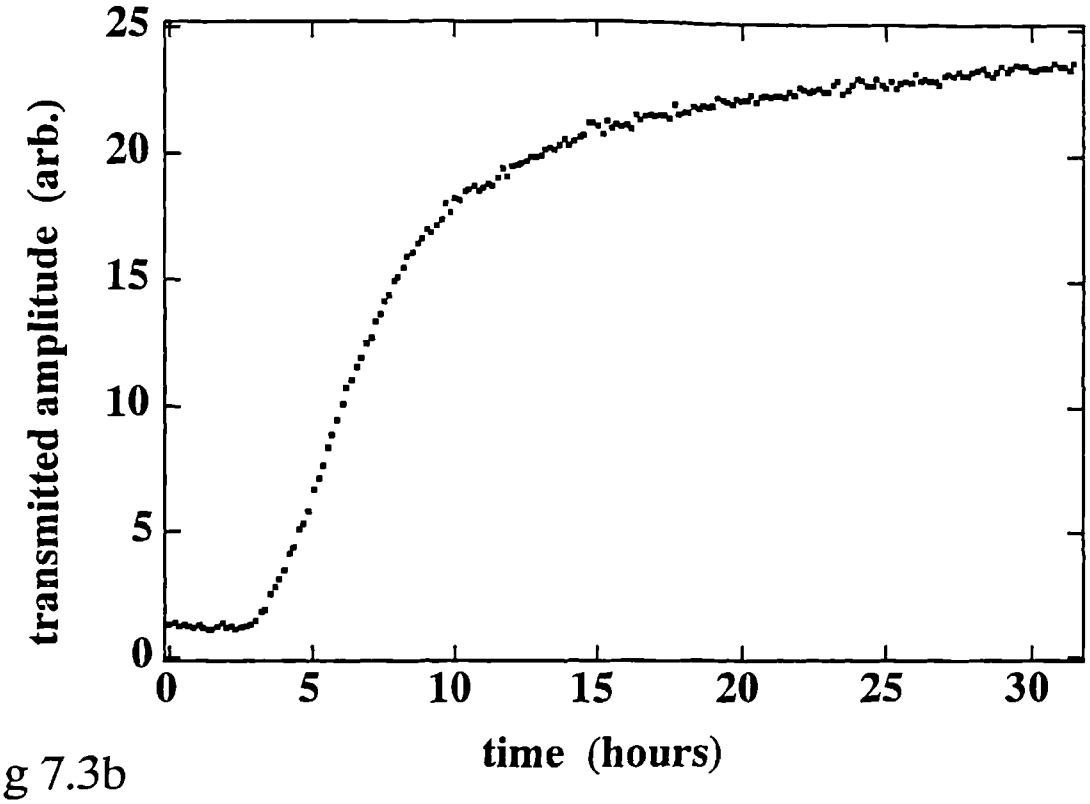

Fig 7.3b

The peak-peak amplitude of the observed transmitted shear wave pulse. For times less than 2.6 hours the transmitted wave amplitude is below the noise level.

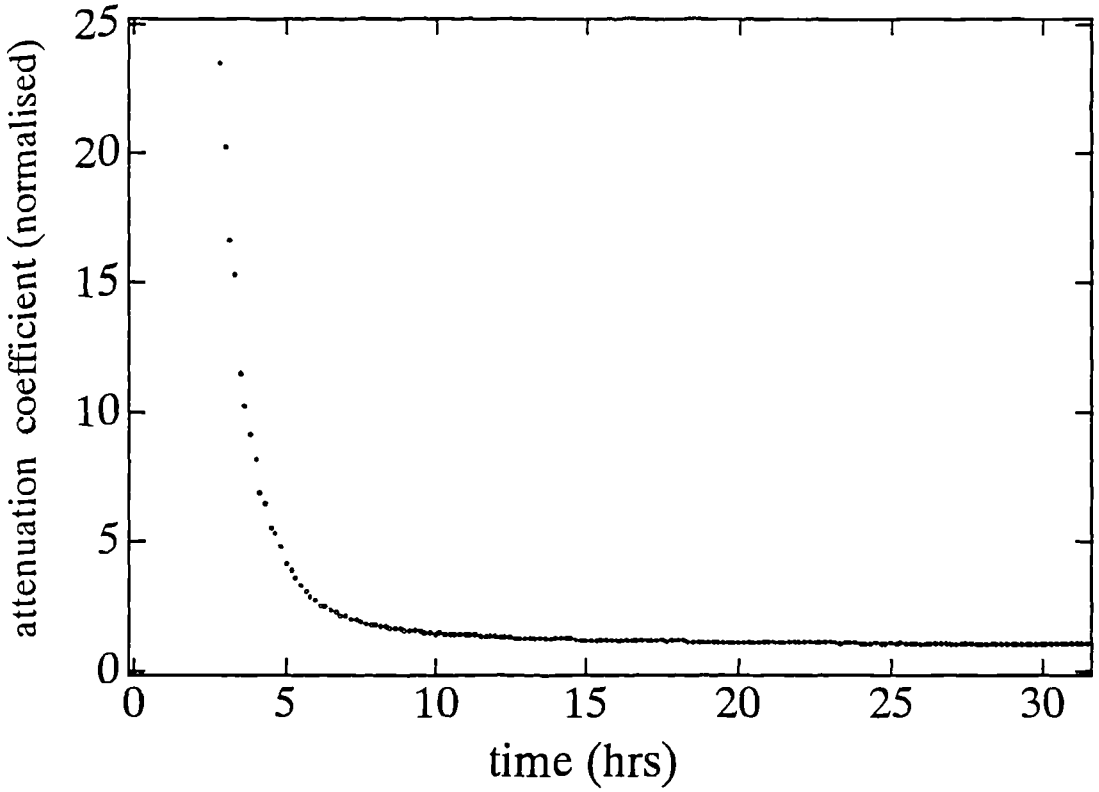

Fig 7.3c

Normalised 'attenuation' coefficient of curing epoxy as a function of time (derived from the reflected and transmitted amplitude data).

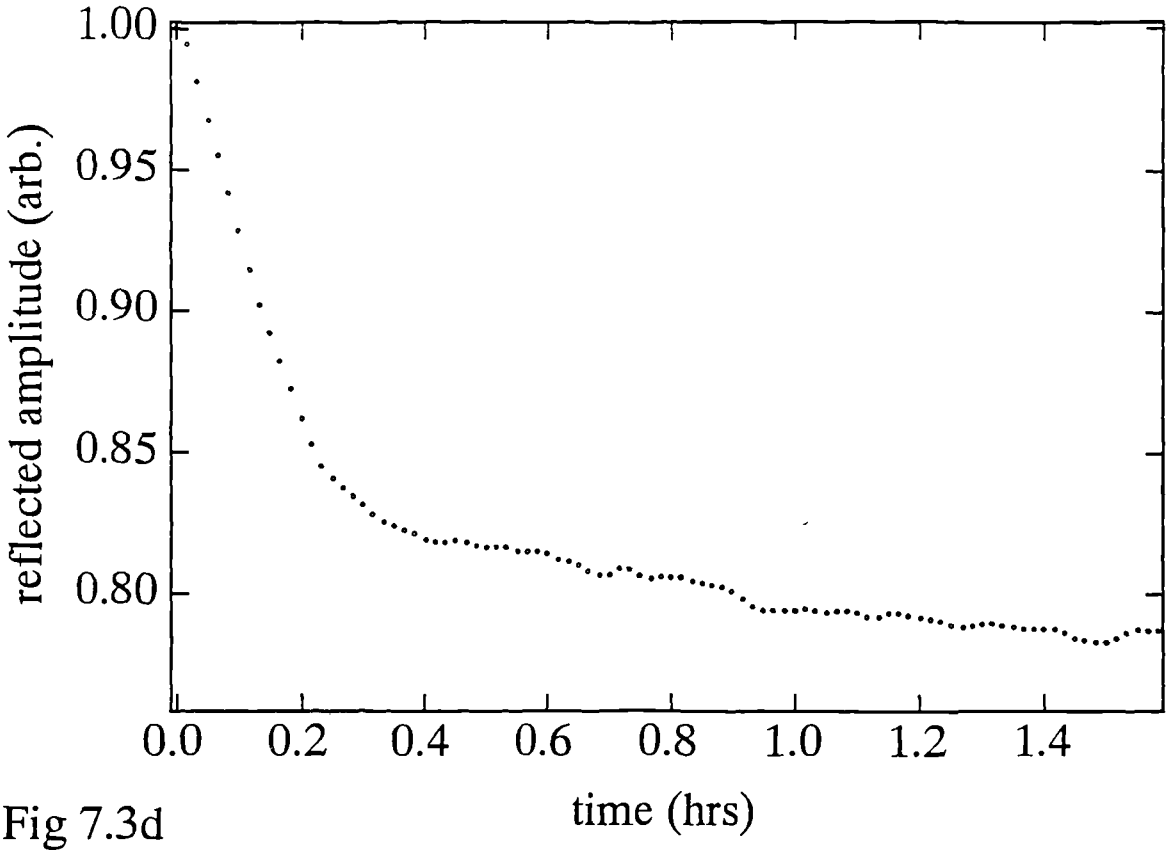

Fig 7.3d

Send-recieve shear wave pulse amplitude for a quicksetting 2 part epoxy adhesive.

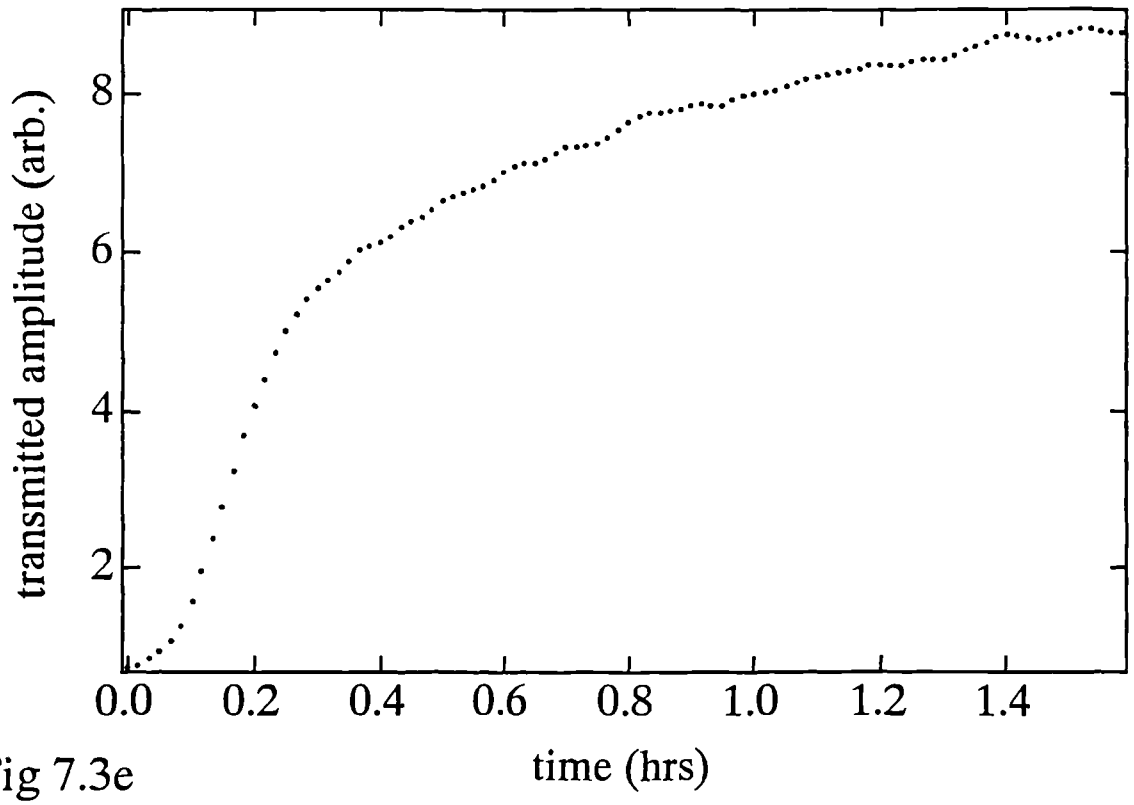

Fig 7.3e

Through transmission shear wave pulse amplitude for a quicksetting 2 part epoxy adhesive.

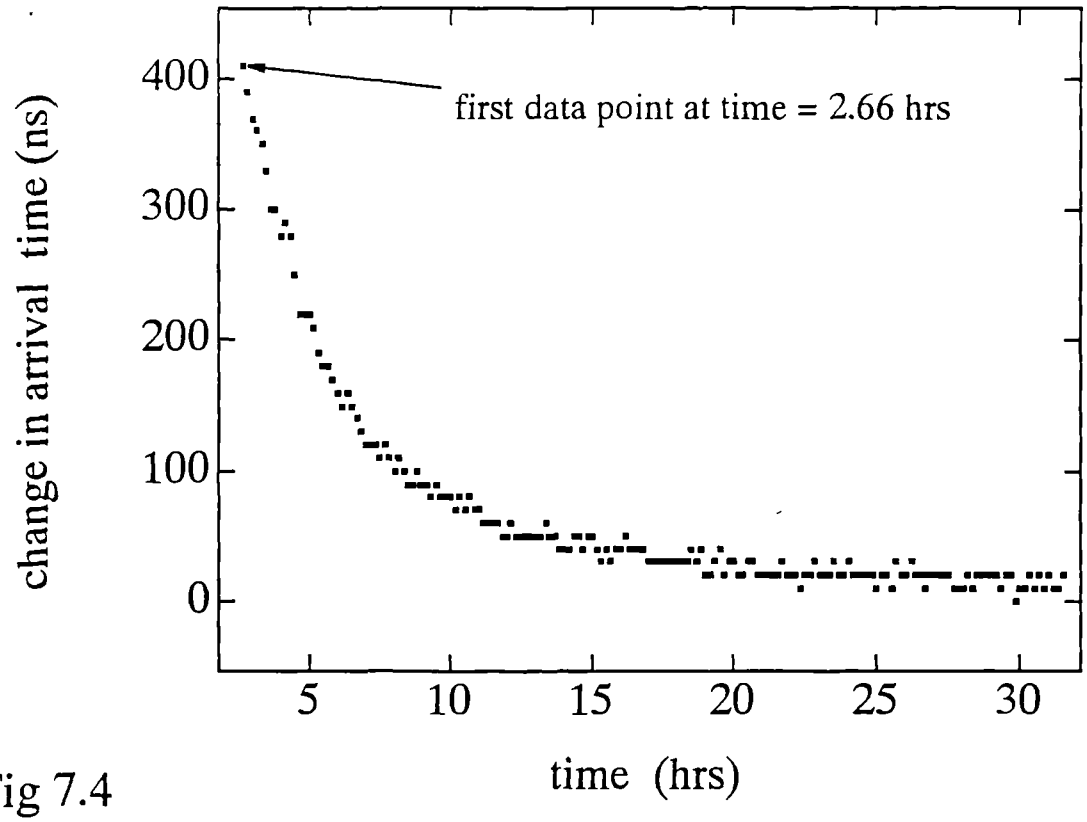

Fig 7.4

The change in pulse maxima arrival time, measured in through transmission.

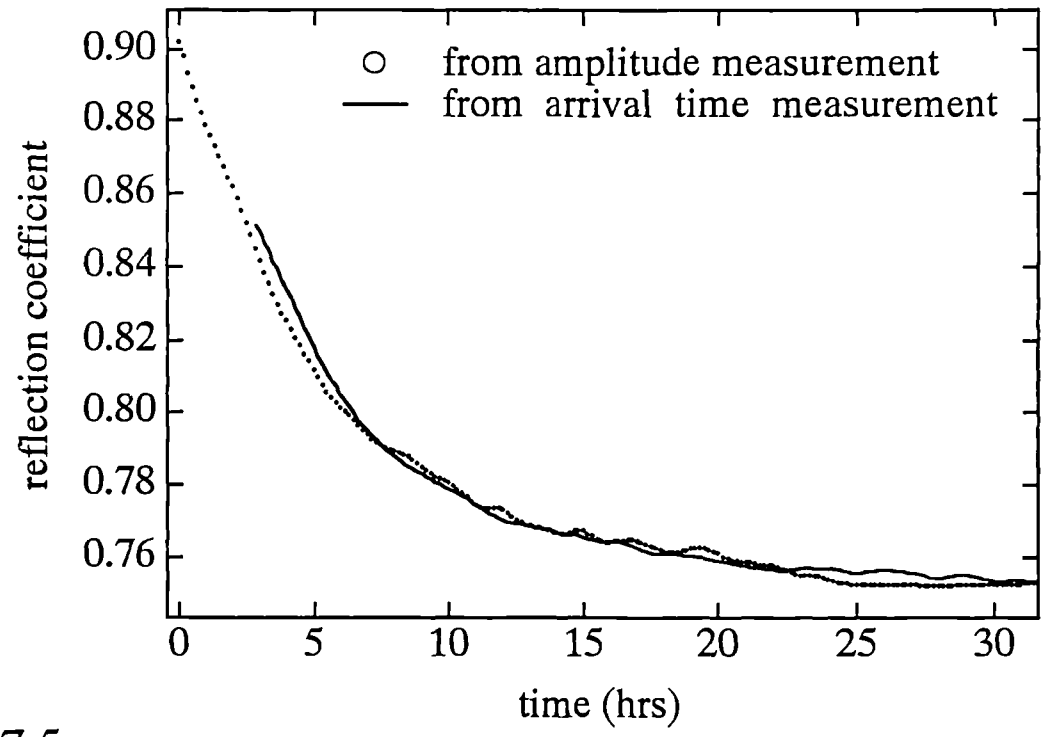

Fig 7.5

The reflection coefficient derived from the amplitude data , and the relection coefficient derived from the change in arrival time (or epoxy velocity).

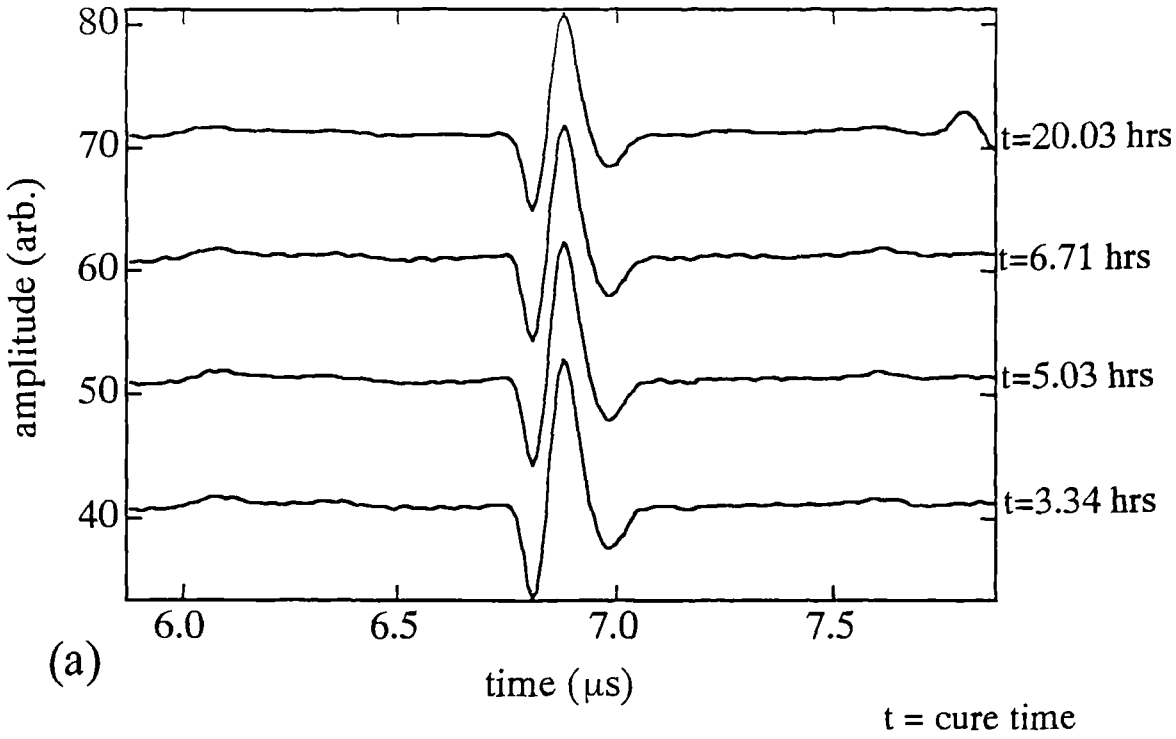

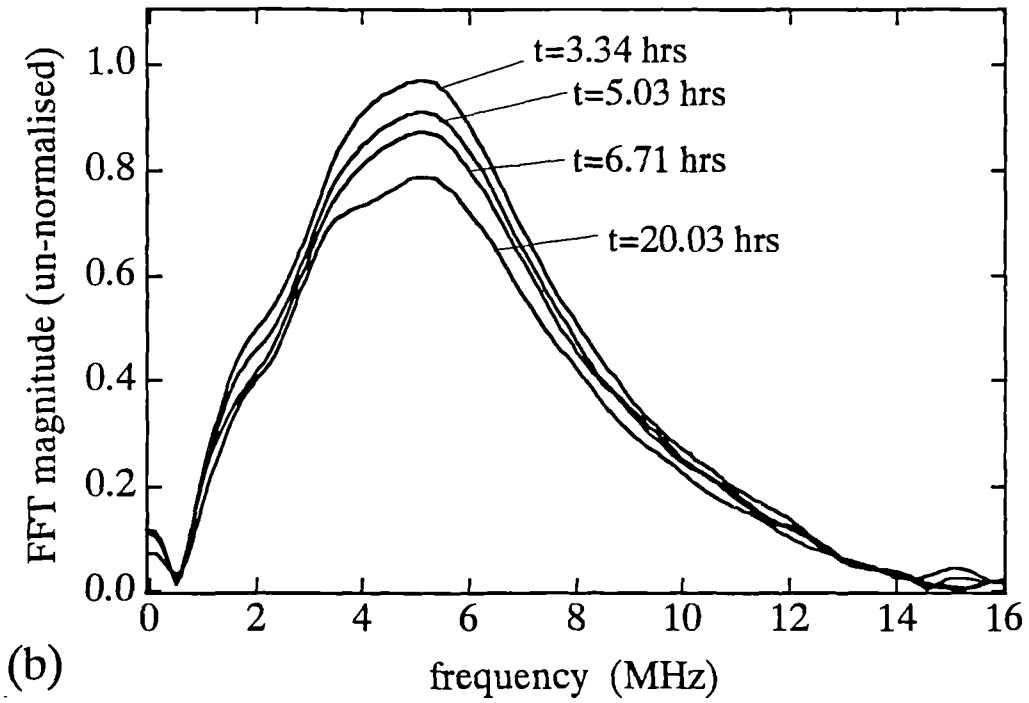

Fig 7.6

Send-receive EMAT shear wave pulses recorded at various cure times (a) with the corresponding magnitude FFTs (b).

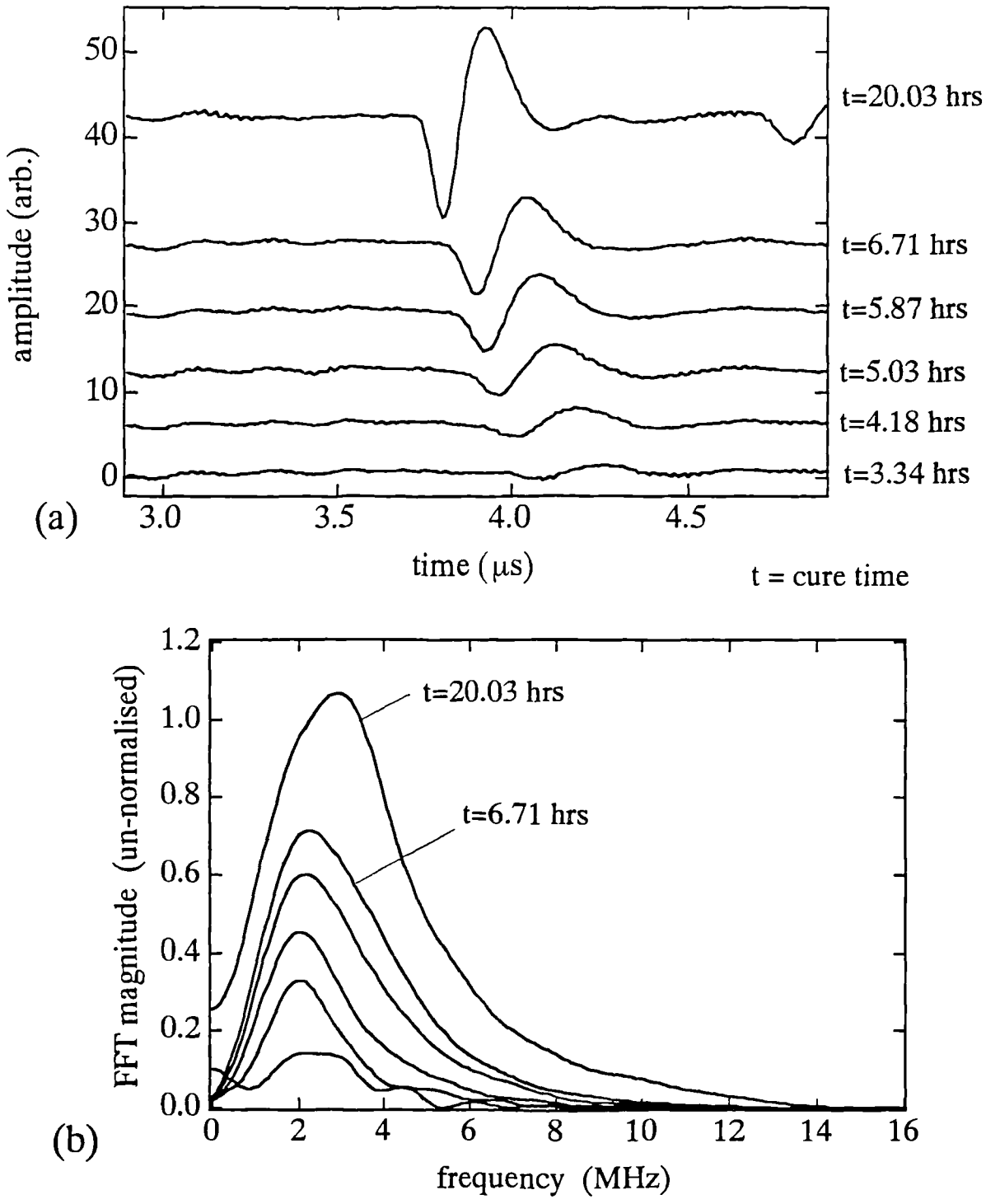

Fig 7.7

Through transmission EMAT shear wave pulses recorded at various cure times (a) with the corresponding magnitude FFTs(b).

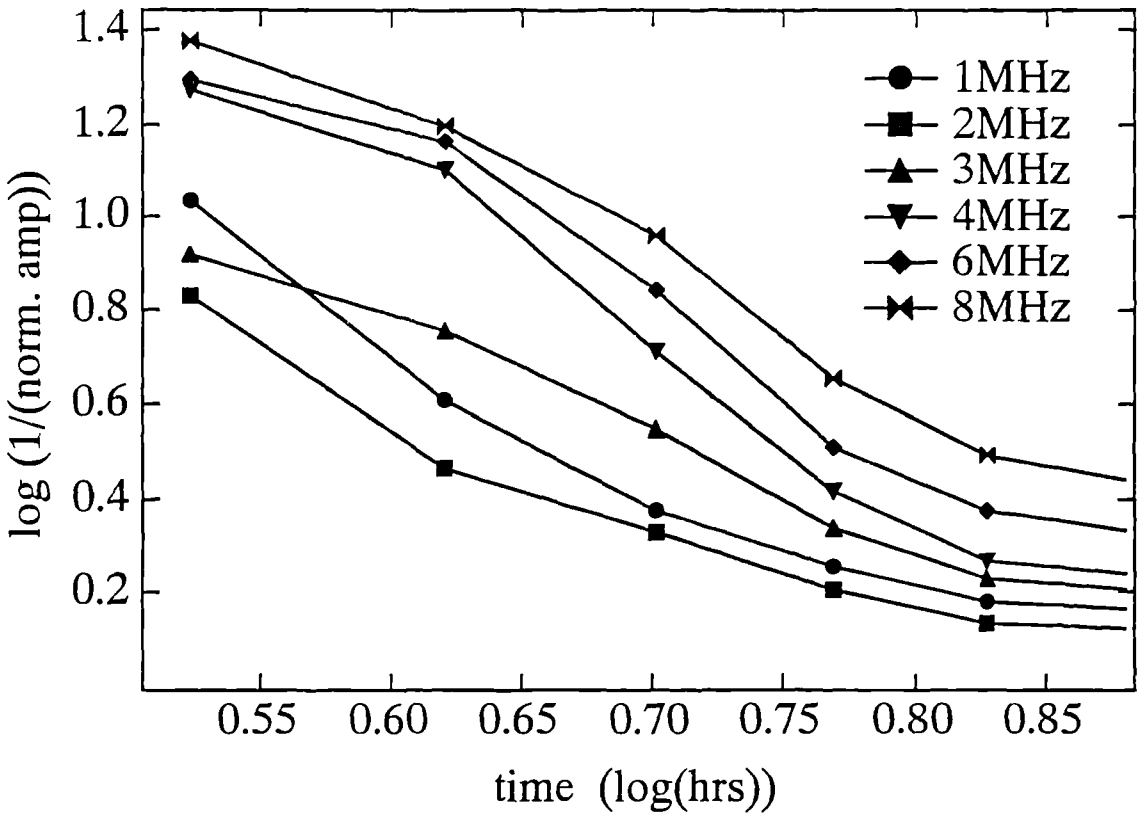

Magnitudes were normalised to the magnitude at time=20.03 hrs for a particular frequency, from which the above log-log plot was derived.

Fig 7.8

Shear wave attenuation in the curing epoxy for a number of specific frequencies as a function of time.

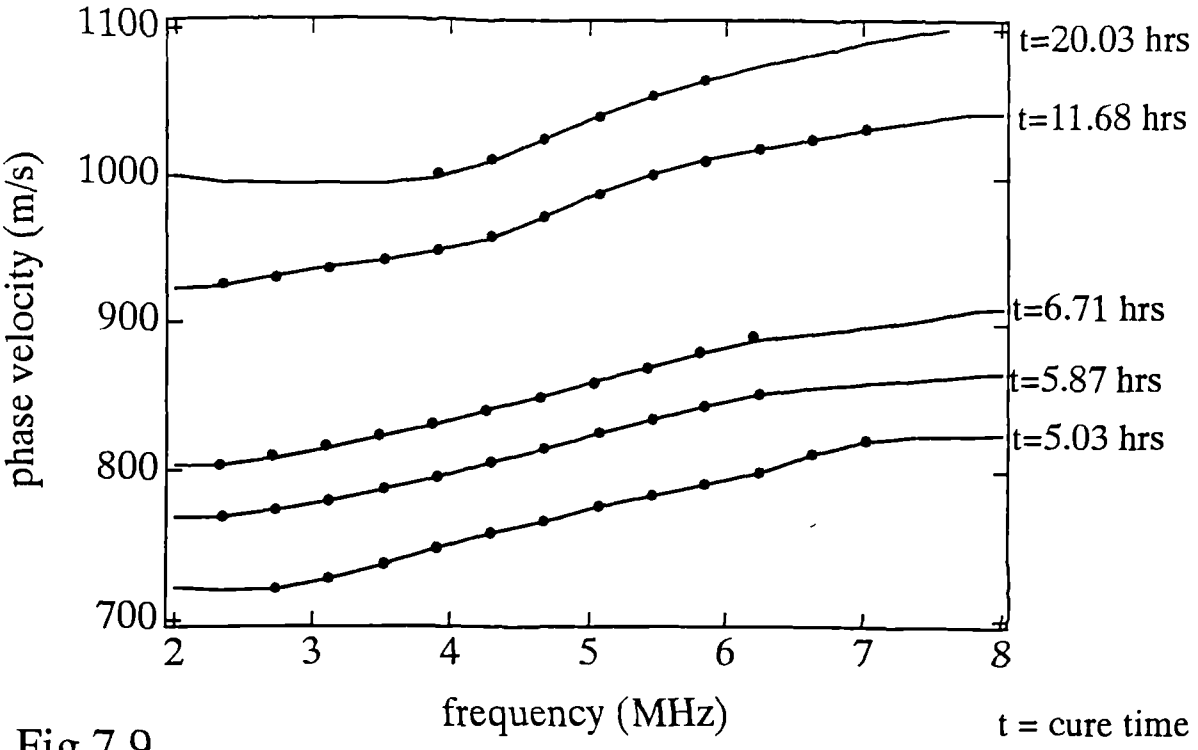

Fig 7.9

Calculated shear wave phase velocity at a number of various times during the adhesiev cure.(obtained from the through transmission data of fig 7.3b. Also indicated on the graph are theoretically fitted points using the model described in section 6.2.2.) .

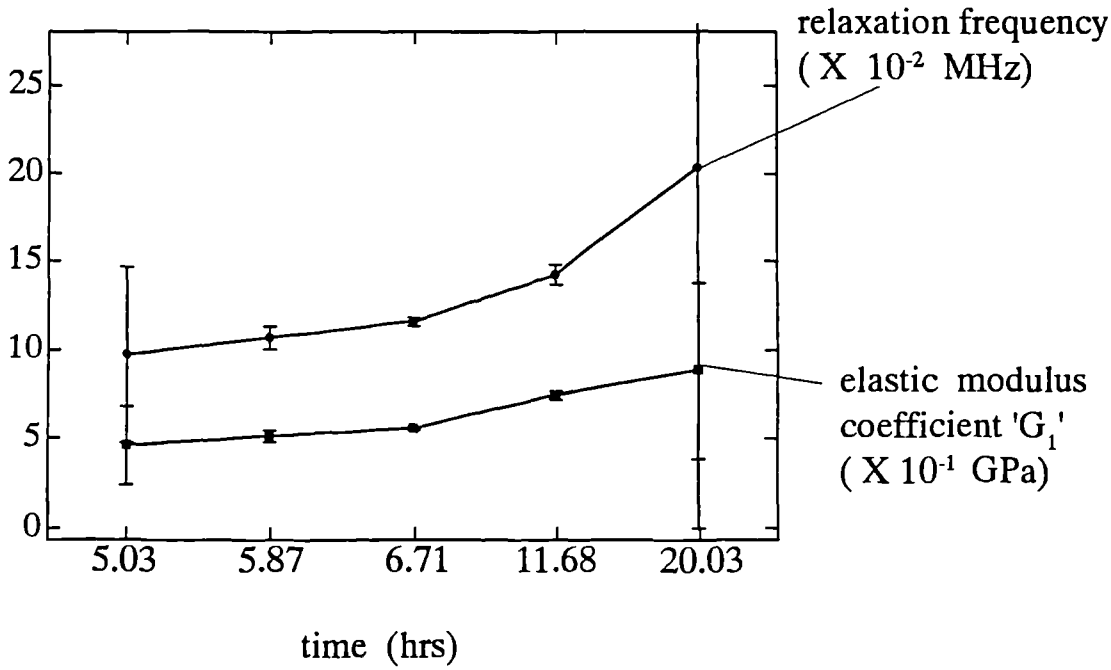

Fig 7.10

Fitting parameters to the improved viscoelastic model for various times during the adhesive cure.

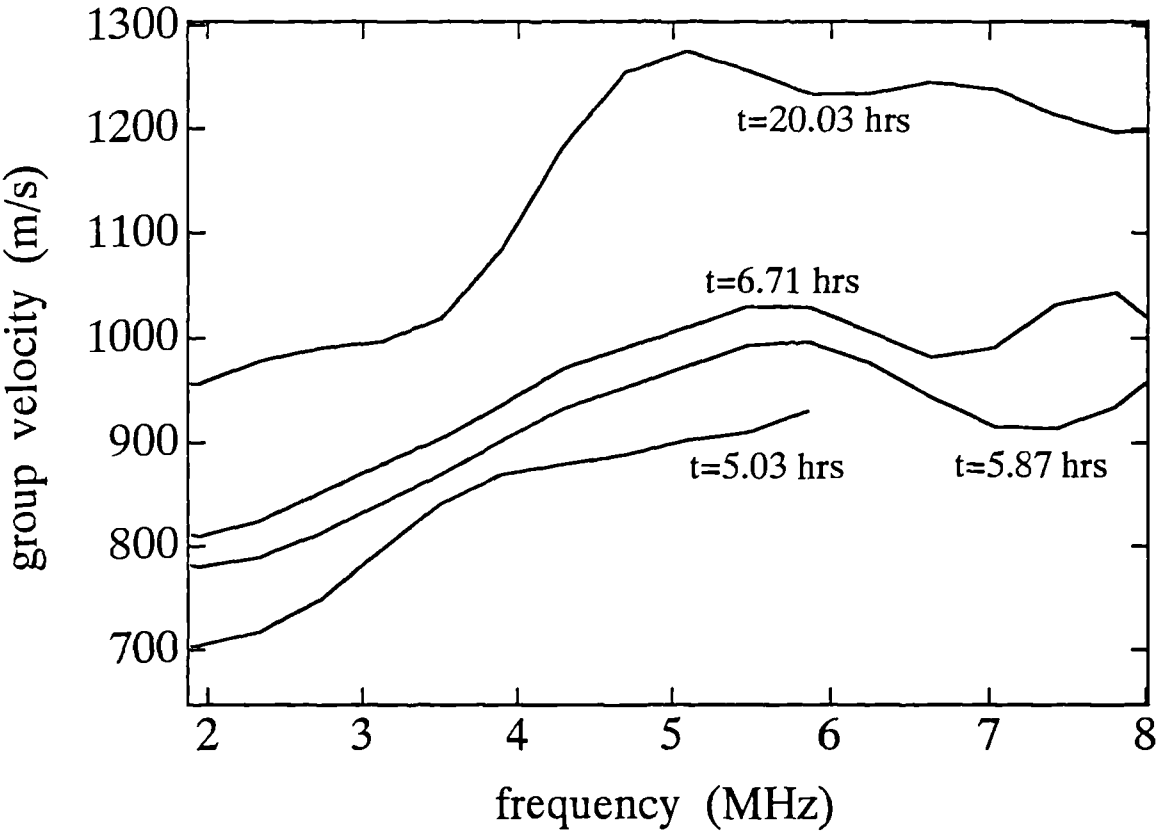

Fig 7.11

Calculated shear wave group velocity at a number of various times during the adhesive cure.

Chapter 8

Conclusion

The work done during the course of this project has demonstrated that the EMAT is a practically viable and inexpensive means of performing nondestructive characterisation of adhesively bonded aluminium plates. The technique is not offered as a complete solution to the problem of examining bond integrity, but rather as a complementary method to the existing techniques already used in both research and industry. This is facilitated by the fact that the equipment is compatible with that already used in the field of NDT. At a less sophisticated level, it has also been shown that the EMAT can replace or be used in areas of testing where conventional ultrasonic transducers would prove problematic. The EMAT system is far less sensitive than a typical PZT piezoelectric based transducer system by around a factor of a thousand, so that there must be special reason to use an EMAT in place of a PZT transducer that outweighs the loss in sensitivity.

The performance of the EMAT system in bond analysis

The EMAT systems used were capable of generating broadband radially polarised shear waves in a totally non-contact regime. The lack of any couplant requirement alone should justify the use of the transducer as oppose to a transducer that requires the application of couplant. The thickness of a couplant may also have to be carefully controlled if amplitude data is being extracted from the waveform. Measuring the relative amplitudes of features within a waveform and gateing out other unwanted acoustic signals would be the ideal type of analysis to persue, but these are difficult to implement and are only ever as accurate as the assumptions used to develop the theory. An outline of some of the considerations that must be made when attempting to use signal processing was described in chapter 6, where it was shown that in order to have confidence in a waveform analysis

technique it must take into consideration every possible acoustic feature that can possibly arise in the waveform and take into account both detailed acoustic properties of adherent and adhesive and the complete response of the transducer system.

It has been suggested that shear waves impinging on the adherent-adhesive interface at normal incidence should be the most sensitive probe of interface quality. Normal incidence shear waves are difficult to couple into a medium using piezoelectric transducers as a viscous couplant is required, and for this reason longitudinal piezoelectric transducers are more commonly used in adhesive bond analysis. A viscous couplant would obviously make most scanning applications using piezoelectric transducers impractical. As the EMAT is totally non-contact scanning is much easier and can be performed through painted layers or non-conductive (electrical) coatings. Obviously, as stand-off from the sample increases the signal will fall and operation on aluminium is usually limited to within a few millimetres. Variations in stand-off could be a cause for concern, but this could be monitored via a variation in the EMAT coil impedance or its phase shifting characteristics as shown in chapter3.

The acoustic signals obtained form the EMAT system are broadband in nature, centred on around 5MHz with a bandwidth of around 6MHz when operating on aluminium at a standoff of approximately 300μm. Normally EMAT systems are operated in a narrow band regime in order to obtain a satisfactory signal to noise ratio, which makes the EMAT signal much more resonant in nature. If the EMAT signal is more resonant in nature it will be temporally broader and thus decrease the temporal resolution in the direction of propagation. Phase analysis of the two overlapping tonebursts could be used but the process of performing the FFT loses resolution in the information compared to the information in the time domain and of course it also takes more time to perform the calculation. The observed frequency content in the EMAT signals from the system used in this project are a result of the characteristics of the drive pulse, the EMAT impedance and the response of the preamplifier. A broadband frequency content makes the shear wave pulse sharper, thus yielding a higher temporal resolution. There is no reason why the EMAT signals cannot be analysed in the frequency domain as was discussed in chapter 2 , but it was considered that

the time domain analysis would be easier to implement and quicker than FFT techniques with the samples investigated.

Most of the defective samples were successfully identified during the course of this project and some that contained unintentional defects were also identified. Defective region were not identified in the fat and release agent contaminated samples, and destructive tests revealed that these had undergone adhesive failure in the defective regions. The temporal 'thickness' of the adhesive layers within the bonds was also successfully monitored - an important measurement if the attenuation in the epoxy is to be accounted for in signal processing. Both through transmission and send-receive (pulse-echo) techniques were demonstrated using the same transducers that have been developed during the course of this project.

Failure to detect adhesion defects

The most striking failure of this technique was that encountered when scanning a sample that had been treated over a certain region with a release agent (Frekote), and a fat contaminated sample. Ultrasonic TT scans (fig 8.1) or SR scans showed no indication of any difference in shear wave impedance mismatch over the treated area of the bond or over the well bonded region of the bond. Shear waves had been coupled across the unbonded adherent-adhesive interface. Modern adhesives can adsorb grease or solvent contaminations from the surface of adherents, and this is usually more effective in the adhesives that cure at elevated temperatures. From the destructive examination results (chapter 5 table 5.1 and fig 5.2) we know that this was not the case - the defective region was a mechanically unbonded area and no adhesive appeared to have wet the adherent surface. In chapter 5 (fig 5.18) it was shown that shear waves could be coupled across an unbonded adhesive-adherent interface if a sufficient compressive stress was applied to the interface. As the samples here were constructed under applied pressure it is possible that a compressive stress developed over the defective region during cure, which could account for the transmission of acoustic energy through the interface. The unbonded adhesive would be a very flat area

and in close proximity to the adherent (a few microns away from the oxide surface depending on thickness of release agent layer) which would make acoustic shear wave coupling across the interface more efficient. There there is also the consideration However, it is unlikely that the compressive stress argument could account for the fact that there was absolutely no observable difference in shear wave coupling across the interface over defective and defect free regions. The explanation behind why the shear wave is actually well coupled across the unbonded interface must lie in the nature of the adhesive bonding mechanisms, which are the interactions that occur at the aluminium oxide surface.

A possible explanation as to why the shear waves couples across the defective release agent coated region follows. It was shown in chapter 5 that the ultrasonic displacements of the EMAT generated shear waves is the order of or less than 10^{-16} m. If the separation of the adhesive adherent surfaces is approximately 1μm then the change in separation of the interacting adhesive-adherent molecules is going to be less than one part in 10^{-10}m. Thus between an infinitely small element of area in the adhesive and the adherent, the forces of attraction do not change. The fact that there was no observable difference in the coupling over a region where the adhesive had not wet the adherent, suggests that the mechanical keying between adhesive and adherent is not necessarily the mechanism that couples shear waves across the adhesive-adherent interface, but it is the factor that will ensure they remain bonded. Therefore if the energy of the incident shear wave was far less than that needed to make the adhesive-adherent interaction significantly change then there would be no change in the shear wave reflection coefficient over the defective region of the bond.

Another possible reason that the Frekote contamination was undetectable may lie in the fact that the very thin teflon layer it leaves on the adherent surface would be mechanically very stiff, as discussed in the summary of chapter 5. This idea of course still relies on the assumption that the teflon layer is weakly bonded to the aluminium and epoxy such that shear waves are coupled across the interfaces without them having sufficient energy to cause any slipping between the planes. If this was the case then this idea could be tested by using very high energy (large amplitude) ultrasound or much higher frequencies (order of GHz), both of which are totally impractical in a real situation.

Suggested future work

The EMAT system used in this project is at least as sensitive and more practical to use than conventional contact transducers or immersion techniques in the analysis of adhesively bonded aluminium plates. The main area for further development of the system would appear to be in the signal processing used to obtain information from the measurements performed using this hardware. In order to do this a detailed analysis must be carried out on the acoustic filed generated by the transducer coupled together with the multi-layered bonded structure. There still also remains the question of why defects such as the release agent defect are not detectable using shear waves at normal incidence, and this may not be possible using ultrasonic techniques alone. This aside, the EMAT system has proved to be a useful tool in assessing bond integrity and as it is also relatively inexpensive technology it appears a promising addition to the techniques and equipment already available for such NDT applications.

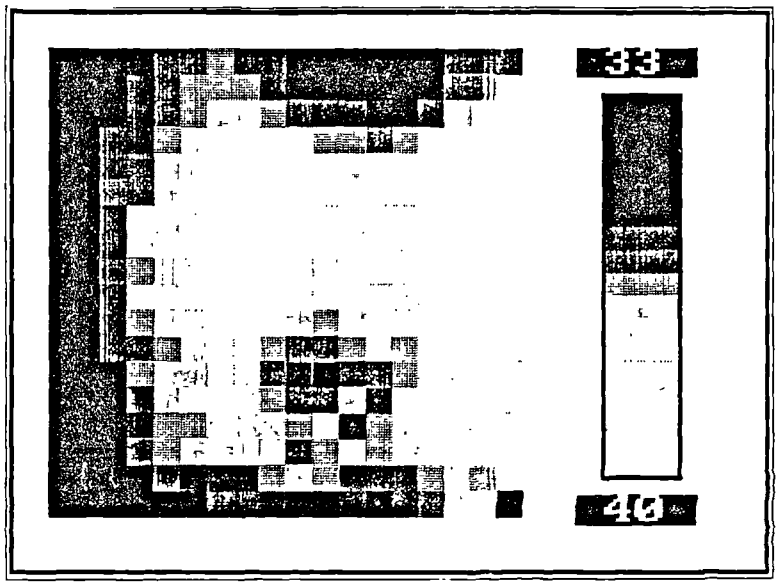

Amp
(arb)

Fig 8.1a

2D density plot for the amplitude data obtained in scanning the release agent treated sample in through transmission.

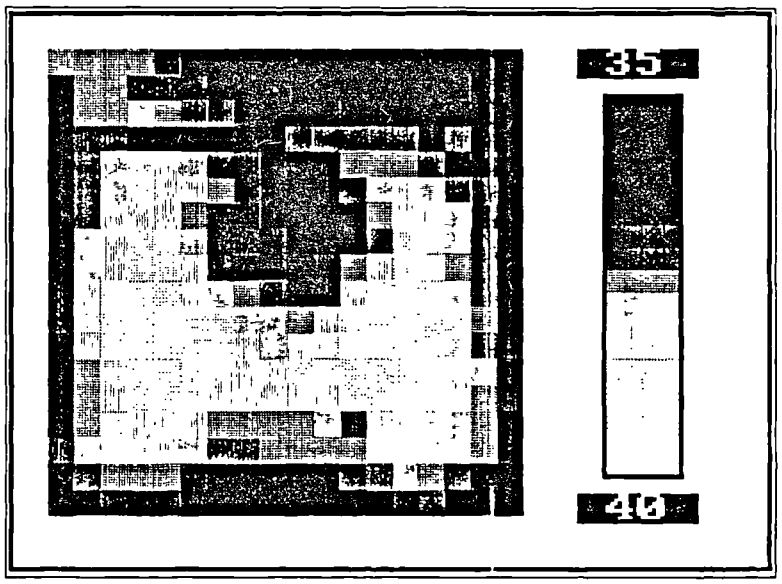

Amp
(arb)

Fig 8.1b

2D density plot for the amplitude data obtained in scanning the release agent treated sample in through transmission.

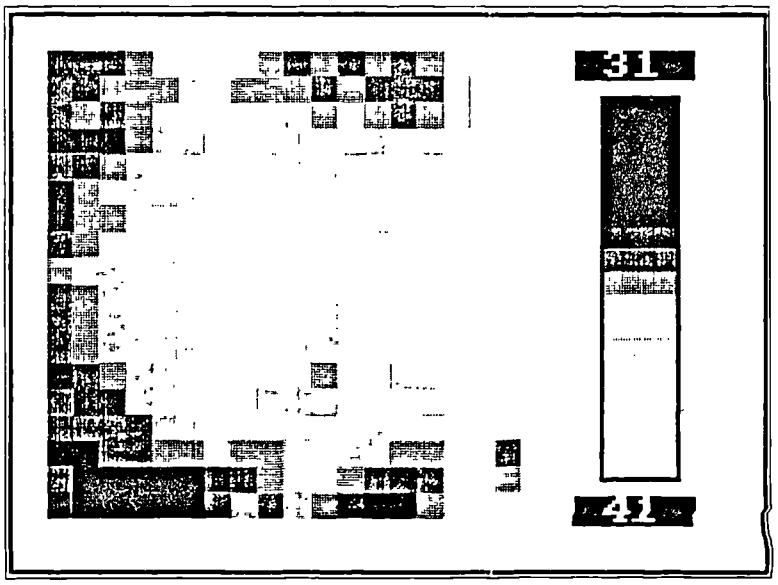

Amp
(arb)

Fig 8.1c

2D density plot for the *amplitude data obtained in scanning the* release agent treated sample in through transmission.

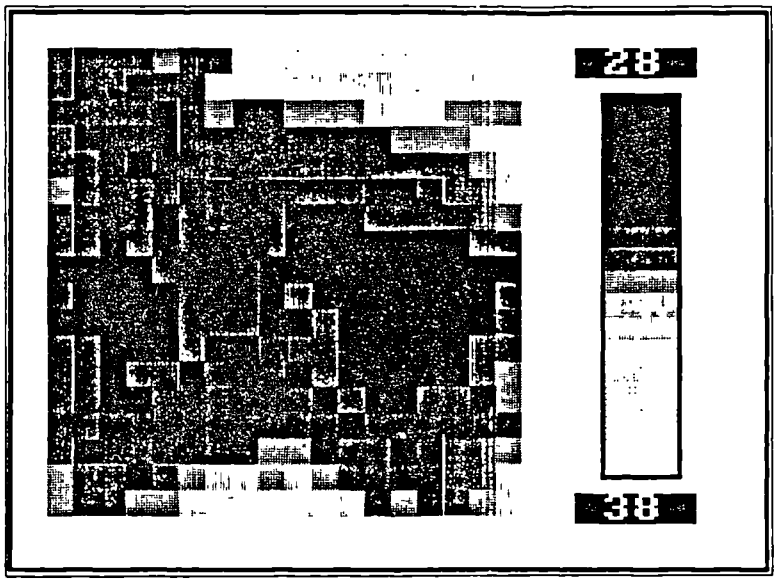

'Thickness'
(10ns/div)

Fig 8.1d

2D density plot for the 'thickness' data obtained in scanning the release agent treated sample in through transmission.

Appendix

Appendix A
Viscoelastic model equation derivation

In the following refer to the viscoelastic model using a spring and dashpot combination if fig 6.11b.

The relaxation time period (1 / relaxation frequency) is given by

$$\tau = \frac{\eta}{G} \tag{1}$$

The stress (T) applied to the network is given by,

$$T = T_1 = T_2 + T_d \tag{2}$$

where T_1 is the stress in the spring of modulus G_1, T_2 is the stress in the spring of modulus T_2 and T_d is the stress in the dashpot branch.

The total displacement (x) of the ends of the network from the equilibrium position is,

$$x = x_1 + x_2 \tag{3}$$

where x_1 is the displacement of spring(1) branch and x_2 is the displacement of the parallel combination of spring(2) and the dashpot from equilibrium.

Stresses in spring(1) and spring(2) are given as T_1 and T_2 respectively by,

$$T_1 = x_1 G_1 \quad \text{and} \quad T_2 = x_2 G_2 \tag{4}$$

Stress in the dashpot (T_d) can be written in terms of a damping coefficient η ,and the differential of x_2 with respect to time,

$$T_d = \frac{d x_2}{d t} \eta \tag{5}$$

The continuity of stress in the network requires that ,

$$T = x_1 G_1 = x_2 G_2 + \frac{d x_2}{d t} \eta \tag{6}$$

Now, take a sinusoidal variation in applied stress and displacements such that,

$$T = T_0 e^{i\omega t} \tag{7}$$

$$x_2 = x_{20} e^{i\omega t} \tag{8}$$

$$x_1 = x_{10} e^{i\omega t} \tag{9}$$

where T_0, x_{10} and x_{20} are constants.

Rewriting equations (2) and (3) yields,

$$T_0 = x_{10} G_1 \tag{10}$$

and

$$x = (x_{10} + x_{20}) e^{i\omega t} \tag{11}$$

Using equation (4) gives,

$$x = T_0 \left(\frac{1}{G_1} + \frac{1}{G_2 + i\omega\eta} \right) e^{i\omega t} \tag{12}$$

leading to,

$$x = T_0 \left(\frac{G_2 + i\omega\eta + G_1}{G_1 (G_2 + i\omega\eta)} \right) e^{i\omega t} \tag{13}$$

The complex modulus of the system is thus given by,

$$G^* = \frac{T}{x} = T_0 e^{i\omega t} \cdot \frac{1}{T_0 e^{i\omega t}} \left(\frac{G_1 (G_2 + i\omega\eta)}{G_2 + i\omega\eta + G_1} \right) \tag{14}$$

Making the denominator real yields

$$G^* = \frac{G_1 (G_2 + i\omega\eta)(G_1 + G_2 - i\omega\eta)}{(G_2 + G_1)^2 + \omega^2\eta^2} \tag{15}$$

And finally as a real and complex part by,

$$G^* = \frac{G_1 G_2 (G_1 + G_2) + \omega^2\eta^2 G_1}{(G_2 + G_1)^2 + \omega^2\eta^2} + \frac{i\omega\eta G_1^2}{(G_2 + G_1)^2 + \omega^2\eta^2} \tag{16}$$

The above equation was used to fit the calculated phase velocity to a simple viscoelastic model, in order to obtain values for the relaxation frequency of the epoxy polymer.

Appendix B

Construction and preparation of adhesively bonded samples obtained from the DRA Farnborough

Aluminium adherent preparation

Samples of 3.3mm thick and 4.8mm thick aluminium BL156 were used in the construction of the adhesive bonds. The adherents were 150mm X 150mm square cut samples.

Preparation steps

1) Aluminium plates undergo vapour degreasing.
2) Aluminium plate cut to required size.
3) Aluminium adherent is degreased in alkaline solution (MINCO 3410) for a few minutes.
4) Adherent is etched in chromic acid at 60°C for 30 minutes.
5) Adherent is rinsed in water.
6) Adherent is anodised in phosphoric acid (BAC 5555) at 25°C . Voltage is increased from 0v to 10V over 30 seconds then held at 10V for 22 minutes.
7) Adherent is rinsed in water.
8) Air dry for 20 minutes. Oven dry for 30 minutes. Store in desiccator.

Construction of bonded sample

Thermosetting epoxy adhesives (Ciba-Geigy Redux 312) were used to bond the 3.3mm aluminium adherent to the 4.8mm aluminium adherent that contained a woven polymer carrier (CG312/5) and a plain sheet of resin (CG312). Samples were cured in a thermal press.

Construction steps

1) Bonded sandwich was formed and pressed under a pressure of around 1MPa. Wire spacers were placed between the adherents in the adhesive layer for the adhesive that did not contain the fabric carrier.

2) Temperature was raised to 120°C at a ramp rate of 8°C per minute.

3) Temperature held at 120°C for 30 minutes.

4) Temperature reduced at a ramp rate of 10°C per minute to room temperature.

5) Applied pressure was released and samples removed from press for storage in a desiccator.

Bibliography

Bibliography

On the Macintosh PC, text and diagrams were presented using Microsoft Word 4.0, and Aldus Pagemaker 4.0. Graphical data was prepared on Igor Pro and Mathematica. Programs used in data analysis elsewhere including the topological density plots were written and run on an IBM compatible PC using BASIC language.

1993 S. Dixon, C. Edwards and S.B. Palmer , A sudy of acoustic birefringence in aluminium plate using broadband electromagnetic acoustic transducers , Ultrasonics International 93 Conference Proceedings , Butterworth-Heinemann , pp213-216

1994 S. Dixon, C. Edwards and S.B. Palmer , The analysis of adhesive bonds using electromagnetic acoustic transducers , to be published in Ultrasonics (accepted June 1994)

1994 S. Dixon, C. Edwards and S.B. Palmer , The analysis of adhesive bonds using electromagnetic acoustic transducers , to be published in Rev. in QNDE Conference Proc., Colorado 1994

As secondary author

1994 C. Edwards, S. Dixon, , A. Idris, J. Reed and S.B. Palmer , Applications of non-contact ultrasonic evaluation , to be published in Rev. in QNDE Conference Proc., Colorado 1994